

DISSERTATION

submitted to the

Combined Faculty of Natural Sciences and Mathematics
of the Ruperto-Carola University of Heidelberg, Germany

for the degree of

Doctor of Natural Sciences

Put forward by

Cristina Benso

Born in Cuneo, Italy

Oral examination : 27th October 2022

Sterile Neutrino Dark Matter in Non-Standard Scenarios

Referees:

Priv.-Doz. Dr. Werner Rodejohann

Prof. Dr. Jörg Jäckel

*A Matteo
il mio più grande compagno di avventura*

Abstract

Sterile neutrino with a mass of $\mathcal{O}(\text{keV})$ is a well-motivated candidate to play the role of dark matter (DM), one of the most abundant constituents of our Universe whose nature remains still unknown. It arises as a natural and straightforward extension of the particle content of the standard model (SM), it is neutral under all SM charges, it can be stable over cosmological time scales, and it can be produced in adequate amount in the early Universe to account for today's DM abundance. In this thesis, we study sterile neutrinos as DM candidates produced in the early Universe through oscillation and collisions induced by their mixing with one of the active neutrino species, i.e. in the framework of the Dodelson-Widrow and the Shi-Fuller mechanisms. In particular, we investigate the parameter space of sterile neutrinos in two non-standard scenarios. The first scenario studied is a non-standard cosmological scenario in which the production of sterile neutrinos is delayed and starts at a critical temperature associated with a low reheating temperature of the Universe or with a dynamical change in the sterile neutrino mass. Here, we show that the discovery potential in terrestrial experiments is considerably enhanced. In the second scenario, the production through the Dodelson-Widrow mechanism is modified by non-standard interactions among active neutrinos. An effective formalism to include such neutrino non-standard self-interactions in the DM production is developed, and the sensitivity of the HUNTER experiment to this specific model is highlighted. At the same time, we demonstrate that the stringent limit on sterile neutrino DM coming from observations in the X-ray band should be considered model-dependent and can be relaxed in different ways, thereby letting open a window in the parameter space of utmost interest for experimental searches.

Zusammenfassung

Sterile Neutrinos im keV-Massenbereich bilden eine Klasse gut motivierter Kandidaten für die Rolle der dunklen Materie (DM), einem der häufigsten Bestandteile unseres Universums, dessen Natur noch immer unbekannt ist. Sie stellen eine natürliche und einfache Erweiterung des Teilcheninhalts des Standardmodells der Teilchenphysik (SM) dar, sind unter allen SM-Ladungen neutral, können über kosmologische Zeitskalen hinweg stabil sein und sowie im frühen Universum in ausreichender Menge produziert werden, um die heutige Menge von DM zu erklären. In dieser Arbeit untersuchen wir sterile Neutrinos im DM-Kontext, die im frühen Universum durch Oszillation und Kollisionen erzeugt wurden und in ihrer Mischung mit einer der aktiven Neutrinoarten begründet ist, d.h. im Rahmen des Dodelson-Widrow- und des Shi-Fuller-Mechanismus. Insbesondere betrachten wir den Parameterraum der sterilen Neutrinos in zwei Nicht-Standard-Szenarien. Im ersten untersuchten Szenario ist die Produktion von sterilen Neutrinos verzögert und beginnt erst bei einer kritischen Temperatur, die mit einer niedrigen Wiedererwärmungstemperatur des Universums oder einer dynamischen Änderung der sterilen Neutrinomasse verbunden ist. Hier zeigen wir, dass das Entdeckungspotenzial in terrestrischen Experimenten erheblich gesteigert wird. Im zweiten Szenario wird die Produktion durch den Dodelson-Widrow-Mechanismus durch Nicht-Standardwechselwirkungen zwischen aktiven Neutrinos modifiziert. Weiter wird ein effektiver Formalismus entwickelt, um solche Neutrino-Selbstwechselwirkungen in die DM-Produktion einzubeziehen, und die Empfindlichkeit des HUNTER-Experiments für dieses spezielle Modell wird hervorgehoben. Gleichzeitig zeigen wir, dass die starke Grenze für sterile Neutrinos als DM-Kandidaten, die sich aus Beobachtungen im Röntgenbereich ergibt, als modellabhängig betrachtet werden sollte und auf verschiedene Weise gelockert werden kann. Hierdurch wird ein Fenster im Parameterraum geöffnet, welches für die experimentelle Suche nach DM von größtem Interesse ist.

Disclaimer

During the course of the doctoral studies the author has undertaken research on a number of topics in the field of particle cosmology. This thesis is based only on the two papers reported in the following that have already been published and underwent peer-review. The original research content of these two papers is at the origin of Chapters 4 and 5 in this thesis and gives significant contribution to the second section of Chapter 2. Each work has been done in collaboration with others.

- 1) C. Benso, V. Brdar, M. Lindner, and W. Rodejohann,
Prospects for Finding Sterile Neutrino Dark Matter at KATRIN,
Phys. Rev. D **100** (2019) 11, 115035, [arXiv:1911.00328 [hep-ph]].
- 2) C. Benso, W. Rodejohann, M. Sen, and A. Ujjayini Ramachandran,
Sterile neutrino dark matter production in presence of NSSI: an EFT approach,
Phys. Rev. D **105** (2022) 5, 055016, [arXiv:2112.00758 [hep-ph]].

Yet unpublished work: Aside from the above mentioned papers, the author spent significant time on three still ongoing research projects:

- a project aiming at the precision calculation of the sphaleron conversion factor (in collaboration with Kohei Kamada, Kyohei Mukaida, and Kai Schmitz),
- a project concerning new dynamical constraints on primordial black hole dark matter (in collaboration with Carlos Jaramillo, Oliver Scholer, and Jakob Stegman),
- a project concerning the use of the 21-cm line from hyperfine transition of neutral hydrogen to set bounds on fundamental physics (in collaboration with Frederik Depta, Christian Döring, Tim Herbermann, and Manfred Lindner).

List of Figures

1.1	Energy-matter content of the Universe	6
1.2	Gravitational lensing phenomenon	7
1.3	Bullet Cluster	8
1.4	Galactic rotation curve of NGC 6503	9
1.5	Simulated evolution of structure formation	10
2.1	Freeze-out and freeze-in mechanisms	14
2.2	Feynman diagrams for the radiative decay $\nu_s \rightarrow \nu_\alpha \gamma$	29
3.1	Energy spectrum of the electron emitted in tritium β -decay	34
3.2	Expected signature of sterile neutrino DM in KATRIN	35
3.3	Engineering drawing of the KATRIN beamline	36
3.4	Sensitivity to sterile neutrino DM of KATRIN/TRISTAN	38
3.5	Spectrum of ^{163}Ho EC	40
3.6	Signature of sterile neutrino DM in ECHo	41
3.7	Expected sensitivity of ECHo to sterile neutrino DM	43
3.8	EC β -decay of ^{131}Cs	44
3.9	Signature of sterile neutrino DM in HUNTER	45
3.10	Experimental setup of the HUNTER experiment	47
3.11	Sensitivity of HUNTER to sterile neutrino DM	48
3.12	K-capture decay of ^7Be	49
3.13	Signature of sterile neutrino DM in BeEST	50
3.14	Representation of the sensor used in BeEST	51
3.15	Sensitivity of BeEST to sterile neutrino DM	52
3.16	First limits on sterile neutrino DM from BeEST	53
3.17	Challenges of the standard Dodelson-Widrow scenario concerning detection in upcoming experiments	54
4.1	Parameter space of sterile neutrino DM produced through "vanilla" Dodelson-Widrow mechanism, in the presence of critical temperature and in the "DM cocktail" scenario	60
4.2	Parameter space of sterile neutrino DM produced through the "vanilla" DW mechanism, in the presence of critical temperature and with relaxation of the X-ray limit by cancellation	63
4.3	Dependence of the abundance of sterile neutrino DM Ω_s on the critical temperature for four benchmark points	64
4.4	Parameter space of sterile neutrino DM produced through standard Shi-Fuller mechanism, in the presence of critical temperature and with X-ray bound relaxed by cancellation	66
4.5	Parameter space of sterile neutrino DM produced through Shi-Fuller mechanism in the presence of CPT violation and with X-ray bound relaxed by cancellation	68

5.1	Parameter space of mediators of neutrino NSSI	73
5.2	Feynman diagrams relevant for the neutrino thermal potential	78
5.3	Sterile neutrino momentum distribution $r^2 f(r)$ where $r = p/T$ in the case of Dodelson-Widrow production in the "vanilla" scenario and in the presence of pseudoscalar NSSI	80
5.4	Evolution with temperature of the production rate of sterile neutrino DM	81
5.5	Parameter space of sterile neutrino DM modified by the presence of pseudoscalar NSSI	83
5.6	Parameter space of sterile neutrino DM modified by the presence of axial-vector NSSI	84
5.7	Free-streaming length of sterile neutrino DM in the presence of pseudoscalar NSSI	87
D.1	Feynman diagram of the effective electron neutrino non-standard self-interaction	108
D.2	Feynman diagrams of the three channels of neutrino self-interactions . .	108
E.1	Feynman diagrams of the contributions to neutrino self-energy from neutrino NSSI	115

List of Tables

5.1	Interaction rates for electron neutrinos subject to scalar pseudoscalar, and axial-vector additional NSSI.	78
5.2	Thermal potential terms for electron neutrinos subject to scalar pseudoscalar, and axial-vector additional NSSI.	78

Abbreviations

ALP	Axion-Like Particle
ARS	Akhmedov Rubakov Smirnov
BBN	Big Bang Nucleosynthesis
BeEST	Beryllium Electron capture in Superconducting Tunnel junctions
BSM	Beyond the Standard Model
C	Charge (symmetry)
CC	Charged Current
CDM	Cold Dark Matter
CMB	Cosmic Microwave Background
CP	Charge Parity (symmetry)
CPT	Charge Parity Time (symmetry)
DAQ	Data Acquisition
DM	Dark Matter
DOF	Degree Of Freedom
DUNE	Deep Underground Neutrino Experiment
DW	Dodelson-Widrow (mechanism)
EC	Electron Capture
ECHo	Electron Capture in ^{163}Ho
EFT	Effective Field Theory
EW	Electroweak
EWPT	Electroweak Phase Transition
FPF	Forward Physics Facility
GUT	Grand Unification Theory
HDM	Hot Dark Matter
HOLMES	Electron Capture Decay of $^{163}\text{Holmium}$ to Measure the Electron Neutrino Mass with sub-eV Sensitivity
HUNTER	Heavy Unseen Neutrinos from Total Energy-momentum Reconstruction
KATRIN	KARlsruhe TRItium Neutrino experiment
LEP	Large Electron-Positron (collider)
LFV	Lepton Flavor Violation
LH	Left Handed
MAC-E	Magnetic Adiabatic Collimation with Electrostatic (filtering)
MCP	Micro-Channel Plate
MMC	Metallic Magnetic Calorimeter
MOT	Magneto-Optical Trap
MSW	Mikheyev-Smirnov-Wolfenstein
MW	Milky Way
NC	Neutral Current
NSI	Non-Standard Interactions
NSSI	Non-Standard Self-Interactions
NuMECS	Neutrino Mass via ^{163}Ho Electron Capture Spectroscopy
νMSM	Minimal extension of the Standard Model by right-handed Neutrinos
PBH	Primordial Black Hole

QCD	Quantum Chromodynamics
RH	Right Handed
RIM	Reaction Ion Momentum
SF	Shi-Fuller (mechanism)
SM	Standard Model
SQUID	Superconducting Quantum Interference Device
STJ	Superconducting Tunnel Junction
TRISTAN	TRitium Beta Decay to Search for STerile Neutrinos
UV	Ultra Violet
VEV	Vacuum Expectation Value
WDM	Warm Dark Matter
WGTS	Windowless Gaseous Tritium Source
WIMP	Weakly Interacting Massive Particle
XRB	X-Ray Background

Contents

List of Figures

List of Tables

Abbreviations

1	Introduction	1
1.1	Massive Neutrinos and the Phenomenon of Oscillation	3
1.2	Baryon Asymmetry through Leptogenesis	4
1.3	Dark Matter	6
1.3.1	Dark Matter Evidence	6
1.3.2	Features of Dark Matter Candidates	10
2	keV Sterile Neutrinos	13
2.1	Production mechanisms	13
2.1.1	Dodelson-Widrow Mechanism	15
2.1.2	Shi-Fuller Mechanism	18
2.1.3	Extra Gauge Interactions	20
2.1.4	Decay of Scalar Field	22
2.2	Existing Bounds on Sterile Neutrino Dark Matter	24
2.2.1	Tremaine-Gunn Bound	24
2.2.2	Limit from Milky Way Satellites	25
2.2.3	Limit from Lyman- α Forest	25
2.2.4	Requirement of Stability over Cosmological Timescale	26
2.2.5	X-ray Bound	26
2.2.6	X-ray Bound Relaxation in "Dark Matter Cocktail" Scenarios	28
2.2.7	X-ray Bound Relaxation due to Cancellation by New Physics	29
2.2.8	X-ray Bound Relaxation by Decoupling of β -Decay from X-ray Decay	31
3	Experimental Searches for Sterile Neutrino Dark Matter	33
3.1	KATRIN/TRISTAN	33
3.2	ECHo	39
3.3	HUNTER	43
3.4	BeEST	49
3.5	Challenges of the "Vanilla" Dodelson-Widrow Scenario in the Perspective of Sterile Neutrino DM Detection	53
4	Sterile Neutrino Dark Matter in Non-Standard Cosmological Scenarios	55
4.1	Details of the Particle Model	55
4.2	Non-Standard Cosmological Scenarios and Critical Temperature T_c	56
4.3	"Dark Matter Cocktail" with Sterile Neutrinos produced through Dodelson-Widrow Mechanism	58

4.4	Reduction of the Decay Rate due to Additional Decay Channel	61
4.4.1	Dodelson-Widrow Mechanism	62
4.4.2	Standard Shi-Fuller Mechanism	64
4.4.3	Shi-Fuller Mechanism in the Presence of CPT Violation	67
5	Sterile Neutrino Dark Matter in the Presence of Neutrino Non-Standard Interactions	71
5.1	Neutrino Non-Standard Interactions	71
5.1.1	Motivation for NSI	71
5.1.2	Motivation for NSSI	72
5.1.3	Details of the Model Including NSSI	74
5.1.4	Specific Constraints on NSSI	76
5.2	Impact of NSSI on Sterile Neutrino Dark Matter	77
5.2.1	Non-Standard Boltzmann Equation, Solution and Evolution of the Distribution Function	77
5.2.2	Impact of NSSI on Sterile Neutrino Dark Matter Production and Detection	82
5.3	Indirect Impact of NSSI on Structure Formation	85
5.4	Outlook	88
6	Summary and Conclusion	89
A	Neutrino Oscillation	93
A.1	In the Vacuum	93
A.1.1	Two-Flavor Picture	95
A.2	In a Medium	95
B	Boltzmann Equation in the Dodelson-Widrow Scenario and its Solution	99
C	Derivation of the Effective Lagrangian of Neutrino Non-Standard Self-Interactions	105
D	Calculation of the Interaction Rate for Neutrino Non-Standard Self-Interactions	107
D.1	Cross Section of NSSI	107
D.2	Interaction Rate of NSSI	111
E	Calculation of the Thermal Potential for Neutrinos with Non-Standard Self-Interactions	113
E.1	Dispersion Relation of Neutrinos	113
E.2	Effective Potential	114
E.3	Self-Energy	115
E.3.1	Scalar NSSI	115
E.3.2	Evaluation of J_n^f	117
E.3.3	Pseudoscalar NSSI	119
E.3.4	Axial-vector NSSI	119
	Acknowledgements	121
	Bibliography	125

Chapter 1

Introduction

Looking at the sky on a starry night and being open to be moved by what is in front of us, we can experience the sense of profound wonder and the sudden feeling of disproportion that for thousands of years raised and inspired common people, philosophers, artists, and poets. In a completely analogous way, as physicists, we have the privilege to experience the same wonder and the impression of how little our knowledge is by looking at the Universe in the shape it has today and at its content through the lenses that mathematics and physics intuition provide us, such as the Friedmann equations and the standard model of particle physics. Despite the extraordinary power of theoretical and observational methods developed and the tremendous progress achieved in the last century regarding the deep understanding of Nature and its mechanisms, the Universe still holds mysteries at small and big scales, which fuel the curiosity and the efforts of researchers. These puzzles include the phenomenon of inflation, the existence of dark energy and dark matter, the weird imbalance between matter and antimatter, and the masses of neutrinos, the lightest matter fields that we know. It is curious to notice that some of these mysteries can be tightly connected to the existence of very elusive particles called sterile neutrinos.

Sterile neutrinos can be defined simply as massive neutral leptons that are not subject to any standard model (SM) interaction.

If neutrinos are Dirac particles (distinct from their antiparticle), the simplest way to introduce sterile neutrinos would be to identify them with the right-handed (RH) component of the SM neutrino field. Indeed, since SM neutrinos are subject only to weak interaction, which couples only to left-handed (LH) fields, RH neutrinos ν_R would be completely neutral with respect to SM interactions. For RH neutrinos, under the hypothesis that they are the only addition to the SM content, the only portal to interact with ordinary matter would be the Dirac mass term

$$\mathcal{L}_\nu^D = -m_D \bar{\nu}_L \nu_R + \text{h.c.} \quad \text{where} \quad m_D = \frac{y_\nu v}{\sqrt{2}} \quad (1.1)$$

that they share with active LH neutrinos. Another possibility would be to have a new massive field ν_s that is a fourth flavor state completely unrelated to the active neutrino fields and just defined by the fact that it is not charged under SM symmetries and is distinct from its antiparticle $\bar{\nu}_s^c$.

If neutrinos are Majorana particles (they coincide with their antiparticle, $\nu^C = \nu^1$), the RH component of neutrino fields is not independent from the LH one and thus it is not sterile. Therefore, to have sterile neutrinos, we need to introduce a fourth neutrino species ν_s , beyond ν_e , ν_μ , and ν_τ , that is not subject to weak interaction and contributes predominantly to a fourth neutrino mass eigenstate ν_4 . If we assume that ν_s mixes with

¹The Majorana condition $\nu^C = \nu$ is explained in detail in chapter 6 of Ref. [1].

one active neutrino species ν_α with mixing angle θ , the fourth mass eigenstate is given by $\nu_4 = \cos(\theta) \nu_s + \sin(\theta) \nu_\alpha$. According to observations of neutrino experiments, the active-sterile mixing angle θ is usually assumed to be very small. Consequently, the fourth mass eigenstate ν_4 almost coincides with the sterile neutrino state ν_s . Therefore, in the following, we will assume that the subscript "4" is interchangeable with the subscript "s".

The sterile neutrinos studied in this thesis are always defined as a fourth neutrino flavor eigenstate ν_s . In Chapter 4, they are assumed to be Dirac particles, while in Chapter 5, they are assumed to be Majorana particles.

Since sterile neutrinos are singlets with respect to the SM symmetries, there is no prediction or limit for their number or the value of their mass. **There could exist more than one species of sterile neutrinos with different mass playing a different role in three of the puzzles mentioned above, namely the generation of active neutrino masses, the baryon asymmetry problem, and the existence and particle nature of dark matter (DM).**

A brief overview of these three mysteries and of the potential of sterile neutrinos to solve them is given in the following sections of this introduction, while the only real protagonist of the rest of this thesis is the sterile neutrino with a mass of $\mathcal{O}(\text{keV})$ that qualifies to play the role of DM.

In **Chapter 2**, we give an overview of the main mechanisms through which sterile neutrino DM can have been produced in the early Universe and of the most significant limits constraining the parameter space of such DM candidates. Moreover, Chapter 2 discusses the relaxation of the X-ray bound that is among the most relevant for the discovery perspective of sterile neutrino DM in terrestrial experiments. This discussion is based on the author's original research work published in Ref. [2].

In **Chapter 3**, the landscape of current and upcoming terrestrial experiments searching sterile neutrino DM is illustrated in a compact way. Chapter 3 is not meant to give a comprehensive overview but rather a summary of must-know for physicists working on sterile neutrino DM from a theoretical point of view.

The purpose of the research work at the origin of Chapters 4 and 5 was to verify whether the discovery potential of such terrestrial experiments increases in the case that sterile neutrino DM production happens in non-standard but minimal scenarios. In **Chapter 4**, based on the author's original research work published in Ref. [2], we consider the production of sterile neutrino DM happening in non-standard cosmological scenarios through oscillation and collisions via the Dodelson-Widrow mechanism, the standard Shi-Fuller mechanism, and the Shi-Fuller mechanism in the presence of CPT violation. The effects of such non-standard cosmological scenarios on the production of sterile neutrino DM and the discovery potential of experiments that look for them are discussed. In **Chapter 5**, we present a modification of the Dodelson-Widrow production mechanism in the presence of non-standard interactions involving only active neutrinos, and we investigate how such interactions vary the accessible parameter space of sterile neutrino DM and the impact of warm sterile neutrinos on structure formation. The content of Chapter 5 originates from the author's original research work published in Ref. [3].

Chapter 6 is devoted to the summary of contents and results presented in this thesis relatively to their relevance to the field and to future outlook.

1.1 Massive Neutrinos and the Phenomenon of Oscillation

Neutrinos are included in the standard model (SM) as massless particles; therefore, a single component, the left-handed one that couples to weak interaction, is enough to describe them. However, contrary to what was assumed in the SM, neutrinos were revealed to be massive particles by oscillation experiments [4, 5]. **The phenomenon of oscillation** explained in detail in Appendix A **requires that neutrinos are massive and that their masses are non-degenerate**, as can be seen clearly in the simplified picture of only two neutrino flavors. The oscillation probability, i.e. the probability that a neutrino produced in the state ν_α with an energy E is detected in a state ν_β after having travelled a distance L , is

$$P_{\nu_\alpha \rightarrow \nu_\beta}(E, L) = \sin^2(2\theta_a) \sin^2\left(\frac{\Delta m^2 L}{4E}\right) \quad (1.2)$$

where $\Delta m^2 = m_2^2 - m_1^2$, $m_{1,2}$ are the eigenvalues of the mass eigenstates $\nu_{1,2}$ and θ_a is the mixing angle between ν_α and ν_β . **The discovery of neutrino oscillation (that corresponds to the discovery of neutrino non-zero masses) made neutrinos the first concrete portal to physics beyond the standard model (BSM)**. In order to give mass to active (weakly interacting) neutrinos, the extension of the SM by introducing a new particle (or at least a new component) or interaction is unavoidable.

The cheapest realization possible, which would be to give mass to active neutrinos through the Higgs mechanism analogously to what happens for the other SM fermions, would require the introduction of the RH component of the neutrino field. This mechanism can work, but it would not explain why neutrinos are so light compared to all other SM fermions.

Neutrino mass models that also respond to the necessity to explain the smallness of active neutrino mass scale can be categorized into two classes: models in which neutrino masses are generated radiatively, and their smallness is explained by the mass scale of fermions running in the loop [6–8]², and seesaw models. In the seesaw mechanisms, the small scale of active neutrino masses is determined by the large scale of new physics introduced to give mass to active neutrinos. There are three types of seesaw mechanisms and they are distinguished by the different heavy particles that are added to the SM content to give mass to active neutrinos. In all three seesaw types, the new degrees of freedom, once integrated out from the Lagrangian, leave the gauge-invariant Weinberg operator [9] leading to the active neutrino mass term at low energies after spontaneous symmetry breaking

$$\mathcal{L}_5 = -\frac{\lambda}{2\Lambda}(LH)(LH) + \text{h.c.} \quad \longrightarrow \quad -\frac{m_\nu}{2}\nu\nu + \text{h.c.} \quad (1.3)$$

where Λ is the effective new physics scale, and λ is a dimensionless coefficient. In particular, in the type-I seesaw mechanism, the UV complete realization beyond the Weinberg operator requires the introduction of at least two sterile neutrinos. Values of mass of these two heavy sterile neutrinos around 10^{15} GeV [1] would naturally justify the two observed non-vanishing mass splittings of active neutrinos and avoid very small values of Yukawa couplings. However, this is not the only possibility. For example, in the ν MSM (Minimal Standard Model extended by the introduction of sterile neutrinos), active neutrino mass generation can occur by type-I seesaw mechanism involving sterile neutrinos with mass below the electroweak phase transition scale [10, 11]. This specific model is extremely interesting because, in it, not only the neutrino mass generation problem but also the baryon asymmetry and the dark matter puzzles find an explanation

²In these models it is not necessary to introduce sterile neutrinos.

relying on the sole introduction of three sterile neutrino species.

The type-II seesaw mechanism works thanks to the introduction of a new scalar field, triplet under $SU(2)_L$ with hypercharge -1.

Instead, in the type-III seesaw mechanism, active neutrinos receive mass based on the introduction of fermions that are part of a $SU(2)_L$ triplet with zero hypercharge. The phenomenology of the latter seesaw type is identical to the one of the type-I, but the triplet Majorana masses need to be $> 10^2$ GeV to evade limits coming from searches of new charged degrees of freedom [12].

1.2 Baryon Asymmetry through Leptogenesis

The matter-antimatter asymmetry problem is the second puzzle in which sterile neutrinos could have played a crucial role. The core of this puzzle resides in the fact that the value of the baryon-to-photon ratio measured in today's Universe $\eta = (n_b - n_{\bar{b}})/n_\gamma = (6.143 \pm 0.190) \times 10^{-10}$ [13] (where n_b , $n_{\bar{b}}$ and n_γ are respectively the number densities of baryons, antibaryons and photons) is extremely small, almost zero but not exactly zero. The fact that $\eta > 0$ is the necessary condition for our world to exist and to be constituted by matter and not by antimatter (the latter being very scarce in the visible Universe), but at the same time, it poses a question. Since today it is impossible to produce matter without also producing antimatter in the same process, how could it have happened that the early Universe had a small surplus of matter over antimatter that survived when particles that had an antimatter partner annihilated into photons? Of course, it is possible that this was an initial condition of our Universe, but this is often considered not to be a good explanation from the theoretical point of view. Instead, what is usually believed is that the asymmetry between matter and antimatter was produced at some point in the evolution of the Universe through a dynamical mechanism in a process called baryogenesis. Any baryogenesis mechanism must satisfy the Sakharov conditions [14]:

- it has to involve baryon number violating processes,
- it has to involve C and CP violating processes,
- it has to include a deviation from thermal equilibrium.

In the past decades, several mechanisms realizing these conditions have been proposed, which include GUT Baryogenesis [15], SuSy Baryogenesis realized through the Affleck-Dine mechanism [16], Electroweak Baryogenesis [17, 18], and other theories summarized in Refs. [19, 20]. A different explanation beyond these theories is the mechanism called **Leptogenesis**, based on the **generation of the primordial asymmetry in the lepton sector and its subsequent transfer into the baryonic sector by means of sphaleron processes** [21]. In this context, heavy sterile neutrinos play a crucial role in generating the primordial lepton asymmetry that can occur via sterile neutrino decay or via oscillation.

On the one hand, a minimal and simplified realization of thermal Leptogenesis **via sterile neutrino decay** is known as **Vanilla Leptogenesis** [22]. In this scenario, three heavy neutrinos N_i with a hierarchical spectrum of masses (in the range $(10^2 \text{ GeV}, 10^{15} \text{ GeV})$) are added to the SM content and can contribute to the active neutrino mass generation in the framework of the type-I seesaw mechanism. The sterile neutrinos are supposed to be thermally produced by Yukawa interactions between leptons and Higgs bosons in the thermal bath. Subsequently, they decay before the electroweak phase transition (EWPT) either into lepton and Higgs doublet, $N \rightarrow l_i + \Phi$, with a decay

rate Γ , or into anti-lepton and conjugate Higgs doublet, $N_i \rightarrow \bar{l}_i + \Phi^\dagger$, with a decay rate $\bar{\Gamma}$. Both inverse processes and decays violate the lepton number ($\Delta L = 1$) since N_i are Majorana particles and do not carry lepton number; they violate also the $B - L$ symmetry ($\Delta(B - L) = 1$) and, in general, CP symmetry. At temperatures much higher than the electroweak scale, the asymmetry produced through these processes is reprocessed by in-equilibrium sphaleron processes. In this way, nearly $\frac{1}{3}$ of the $B - L$ ends up in the form of baryon number while nearly $\frac{2}{3}$ of it results to be in the form of lepton number. Since a fraction of the decays occurs out of equilibrium, part of the asymmetry survives the washout from inverse processes. The final $B - L$ asymmetry is given by the sum of two contributions

$$N_{B-L}^f = N_{B-L}^{\text{pre}} + N_{B-L}^{\text{lep}}. \quad (1.4)$$

N_{B-L}^{pre} encodes the residual value of a possible pre-existing asymmetry generated by some external mechanism prior to the onset of Leptogenesis (that is likely to be negligible). N_{B-L}^{lep} is given by the sum of the products between the total CP asymmetry ϵ_i (determined by the interference of tree level with one loop self-energy and vertex diagrams) and the efficiency factor which depends on the decay parameter for each sterile neutrino species and is defined as

$$K_i = \frac{\Gamma_{D,i}(T=0)}{H(T=M_i)} \quad (1.5)$$

where H is the Hubble expansion rate at the time when the decaying particles became non-relativistic, and $\Gamma_{D,i} = \Gamma_i + \bar{\Gamma}_i$ are the total decay rates.

On the other hand, an example of Leptogenesis occurring **via oscillations of sterile neutrinos** is the **ARS**³ **Leptogenesis** [23]. In this case, the masses of the sterile neutrinos are taken to be of the order of the Higgs VEV, and the smallness of the Yukawa couplings required to explain neutrino masses in this low-scale scenario could be the way to realize the necessary out-of-equilibrium condition before the sphaleron freeze-out. While Vanilla Leptogenesis requires Majorana neutrinos, ARS Leptogenesis could also be realized by Dirac particles, provided that the Dirac phase δ of the mixing matrix violating CP is large enough. Indeed, in ARS Leptogenesis, the generation of the asymmetry does not occur by total lepton number violation or generation but rather by its "separation". Heavy sterile neutrinos are assumed to be produced in the early Universe through their Yukawa couplings in CP-conserving interactions. Once created, sterile neutrinos oscillate and also interact with ordinary matter. None of these processes violates the total lepton number $L^{\text{tot}} = L + L_A + L_B + L_C$, where L is the usual lepton number. However, CP is not conserved due to mixing in the sterile neutrino sector. Therefore, the initially created state with individual lepton numbers $L_A = L_B = L_C = 0$ evolves through the oscillations into a state in which $L_A \neq 0, L_B \neq 0, L_C \neq 0$ but still $L^{\text{tot}} = 0$. That is, the total lepton number gets unevenly distributed between different species of sterile neutrinos [23]. Sterile neutrinos communicate their lepton asymmetry to ordinary neutrinos and charged leptons through their Yukawa couplings, and, by assuming a certain hierarchy among them, not all of them may come into thermal equilibrium before the EWPT when the sphaleron processes become inoperative. If so, not all the lepton number is reprocessed, ensuring the production of the asymmetry.

³Acronym derived from the surnames of the inventors of the mechanism: Akhmedov, Rubakov and Smirnov

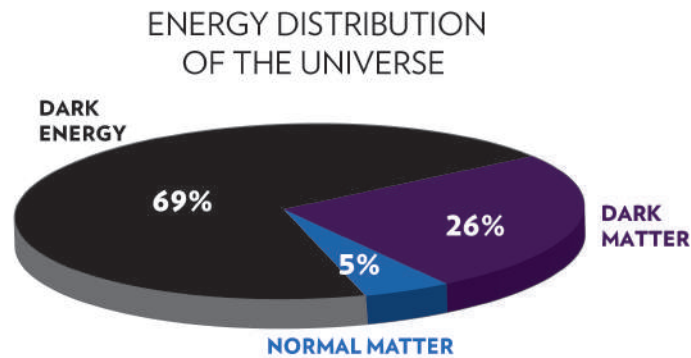


FIGURE 1.1: Energy-matter content of the Universe today based on the data of the Planck mission [24]. What goes under the name of "normal matter" is the baryonic matter that includes photons, neutrinos and atoms that constitute planets, stars, interstellar and intergalactic media, and all other observable celestial objects. We have no clue about the profound nature of the other two components. (Image Credit: NASA/CXC/K.Divona).

1.3 Dark Matter

Finally and most importantly concerning this thesis work, sterile neutrinos are qualified to provide a compelling solution to the DM puzzle. According to the Standard Cosmological Model, the dynamics of the Universe depends on its energy content and can be efficiently described in the setting of the theory of General Relativity by making use of the Friedmann equations. Thanks to measurements regarding the dynamics of our Universe and the observation of some phenomena typically on the galactic scale, it is now well established that just a minimal part of the entire energy content of our Universe is composed of baryonic matter, i.e. ordinary matter accurately described by the SM. The major part of the Universe is composed by constituents whose profound nature is, to date, still not understood, although we unequivocally observe the effects of their presence.

The energy-matter composition of our Universe today is represented in Fig. 1.1 and **the subject of this thesis is the constituent that makes up the 26% of our Universe and is called dark matter**. The denomination "dark matter" originates from the fact that this substance behaves like matter from the point of view of the Friedmann equations, in the sense that it does not apply pressure, but it is not charged under electromagnetic interaction, and therefore it is not observable contrary to ordinary matter. The history of DM is longer than a century, dating back to 1904 when Lord Kelvin first attempted to dynamically estimate the amount of invisible matter in the Milky Way. Since then, several proofs have been found in support of the existence of DM, which are briefly introduced in the following.

1.3.1 Dark Matter Evidence

The first hint of the existence of DM came from observations of galaxy clusters, in particular from the measurement of **velocity dispersion of galaxies** in the Coma Cluster performed by Fritz Zwicky [25]. He estimated the total mass of the Coma Cluster as the product of the number of observed galaxies and the average mass of each galaxy suggested by Hubble. Adopting an estimate for the physical size of the system, he

determined the potential energy of the system and, applying the virial theorem requiring

$$\frac{1}{2} M_{\text{tot}} \langle v^2 \rangle = \frac{1}{4} G \frac{M_{\text{tot}}^2}{R_{\text{tot}}}, \quad (1.6)$$

he calculated the velocity dispersion of galaxies in the cluster. His calculations gave as result a velocity dispersion of ~ 80 km/s, in net contrast with the observed average velocity along the line of sight that was ~ 1000 km/s. This led him to the conclusion that the galaxy cluster composition should be dominated by dark matter present in much greater amount than luminous matter [25].

In the following decades, further and different probes of the existence of DM came from galaxy clusters observations.

For example, the mass profile of galaxy clusters or giant galaxies can be inferred from **observations of X-rays**. The highly ionized gas bound by the gravitational potential well of the cluster or of the galaxy emits X-rays due to thermal bremsstrahlung. The X-ray energy spectrum and flux provide information about the gas temperature and density; from this, the pressure can be calculated and, under the assumption of hydrostatic equilibrium, the mass profile can be obtained. The mass of Coma, Perseus and Virgo clusters have been determined using data of the Einstein X-ray satellite and the results confirmed previous estimates of masses made with the virial method, revealing that the mass of the hot gas itself is only about 0.1 of the total mass of the clusters [26, 27].

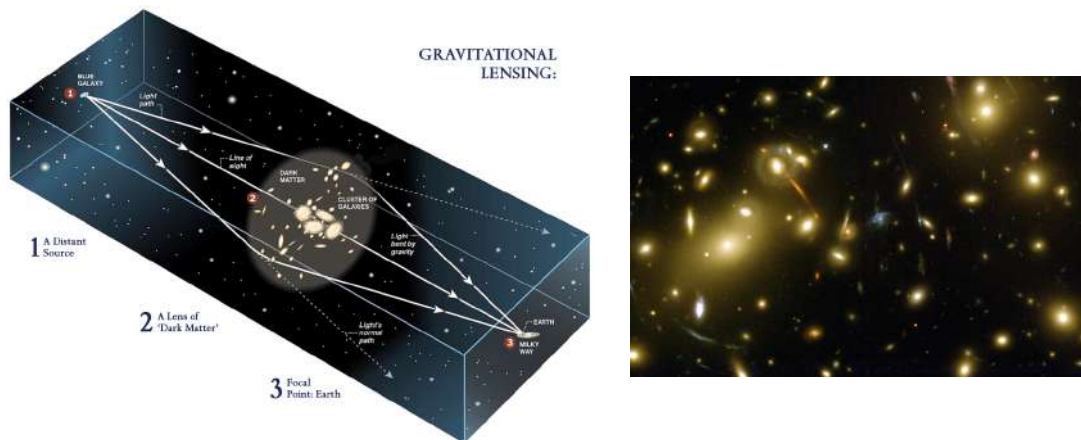


FIGURE 1.2: Left panel: representation of the concept underlying the gravitational lensing phenomenon. Right panel: photograph of the distortion into long arcs and multiplication of the images of stars and galaxies lying behind the core of cluster Abell 2218. (Image Credit: Bell Labs, Lucent Technologies (left panel), NASA/ESA (right panel)).

Another method that can be applied to galaxy clusters in order to infer their mass profile is **gravitational lensing**. The basic idea underlying this method is represented in Fig. 1.2 together with a concrete example captured by the Hubble telescope. If between us and a distant luminous object (such as, for example, a galaxy or a quasar) lies a cluster, a galaxy, or even a star extremely massive, its gravity bends and focuses the light from the distant object we are looking at, as can be done by a sort of odd enormous lens. Therefore, it is possible to use the deformation and/or the position of the image of the object that we receive, to get information on the size and the distribution of the mass that generates

the distortion. A number of observations of this type confirmed the correspondence between the mass-to-light ratios obtained with this method and those resulting from the dynamical DM measurements of clusters [28].

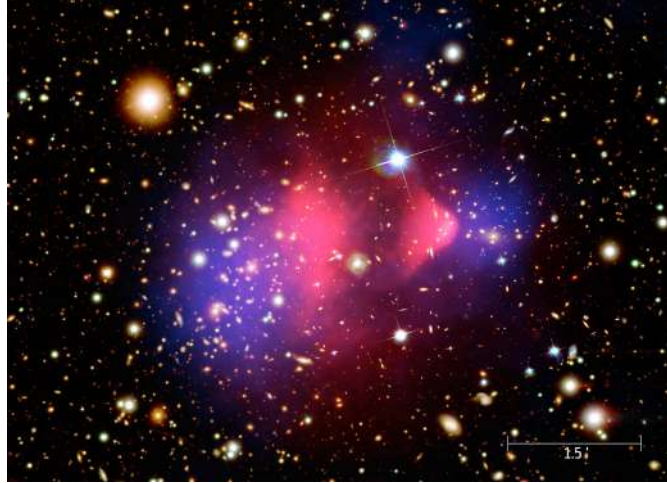


FIGURE 1.3: Bullet Cluster. Composite image showing the galaxy cluster 1E 0657-56. The image in background showing the visible spectrum of light stems from Magellan and Hubble Space Telescope images. The pink overlay shows the X-ray emission (recorded by Chandra Telescope) of the colliding clusters, while the blue one represents the mass distribution of the clusters calculated from gravitational lensing effects. (Image Credit: NASA/CXC/M. Weiss).

Another phenomenon related to galaxy clusters supporting the hypothesis of DM existence, is the so-called **Bullet Cluster**, a subcluster that passed through the center of another cluster 150 million years ago. The result of the collision can be seen in Fig. 1.3. The picture results from the superposition of three images: luminous matter constituting galaxies and stars as we can see it in the optical frequencies, hot gas tracked by the X-rays it emits and represented in pink, and total mass distribution of the clusters tracked by gravitational lensing and represented in blue. If there were no DM, the pink and the blue distribution would overlapped. Instead, there is a clear discrepancy between the two distributions, proving also that the matter different from baryonic gas has a non-collisional nature: when the two clusters collided, the hot gas component was slowed down by its self-interactions while the DM component proceeded in the original direction keeping its distribution unperturbed.

The last evidence of DM on galactic scale that we mention in this section comes from observations of **galactic rotation curves**, that is the circular velocity profile of the stars and gas in a galaxy as a function of distance from the galactic center, and dates back to the work by Vera Rubin and Kent Ford [29]. Based on the distribution of luminous matter in spiral galaxies, it should be possible to model the galaxy as a point mass in the centre surrounded by test masses orbiting around it analogously to what happens in planetary systems. If this were the case, according to Kepler's second law, we would expect the tangential velocity of test masses (stars) and gas to be described by

$$v(r) = \sqrt{\frac{GM(r)}{r}} \quad (1.7)$$

where $M(r) \propto \rho r^3$ is the total galactic mass assumed to be concentrated in the center: we would expect a decrement of velocities inversely proportional to the square root of the distance from the galactic center. However, using signals from hydrogen at different distances from the galactic center of the Andromeda galaxy, Rubin and Ford found out that the tangential velocity remains constant at very large radii, where it was supposed to fall like $r^{-1/2}$, as represented in Fig. 1.4. The simplest explanation for this phenomenon is that the galaxy is embedded in a spherical DM halo that extends far beyond the end of the luminous matter distribution.

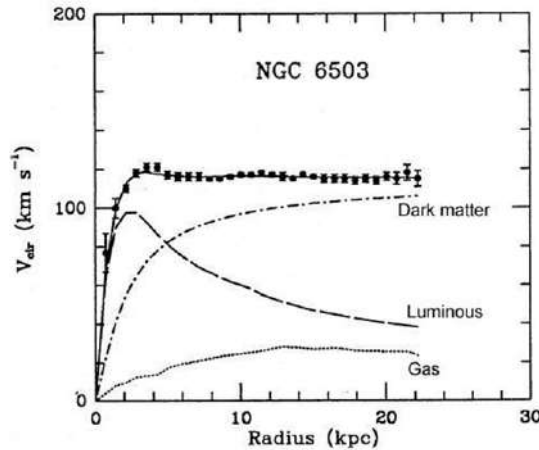


FIGURE 1.4: Rotational curve profile of NGC 6503. The need of the DM halo is evident in order to explain the flat velocity profile in the most remote regions of the galaxy. Figure taken from Ref. [30].

Beyond the astronomical proofs of the existence and abundance of DM listed above, different moments in the evolution of the early Universe provide also powerful cosmological evidence of DM.

Big Bang Nucleosynthesis (**BBN**) [13] and Cosmic Microwave Background (**CMB**) [24] encode the information regarding the baryon content of the Universe respectively at about 1 minute and 380 000 years after the Big Bang. Combining this information with what we know about the scaling of the energy density of matter, radiation, and cosmological constant in the framework of the Standard Cosmological Model as the Universe expands, and with the information on the recent Universe expansion history coming from observations of **supernovae type-Ia** [31], it is evident that ordinary baryonic matter cannot be the only matter present in the Universe. Instead, almost the 85% of the entire matter abundance present in today's Universe must be in the form of DM.

Imprints of DM can be observed also in the CMB power spectrum as a consequence of acoustic oscillations in the photon–baryon fluid of the early Universe (**BAO**) right before recombination and CMB decoupling. Baryonic matter interacts directly with photons via Thomson scattering. On the other hand, DM does not, and it affects CMB only through its gravitational potential and its effects on the density and velocity of ordinary matter. Therefore, baryonic and dark matter perturbations evolve differently with time and leave different imprints on the CMB. Thus, from the study of CMB anisotropies it is possible to obtain the information on the composition of the Universe at the moment of recombination and in particular on the abundances of baryonic matter and DM.

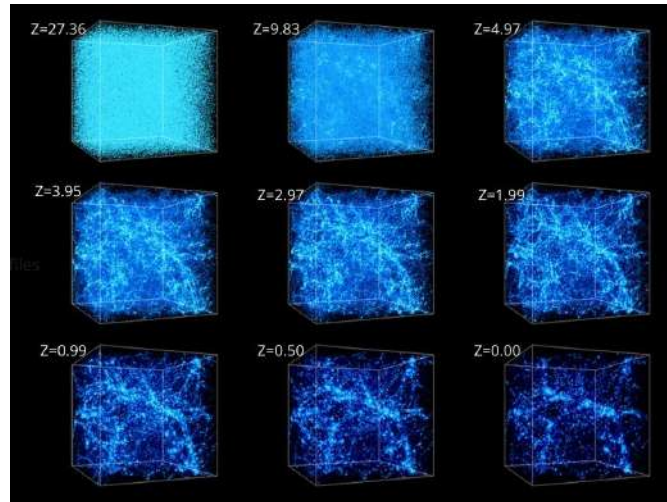


FIGURE 1.5: Subsequent steps in the evolution of clusters and large scale filaments in a model including cold DM and dark energy, marked by different values of redshift z . (Image Credit: Center for Cosmological Physics/A.Kravtsov).

Finally, the presence of DM in the early Universe is crucial for **structure formation and evolution**. The seeds of structures are usually assumed to be quantum fluctuations left after the inflation period. The subsequent growth of structures is considered to happen hierarchically starting from these seeds due to gravitational instability: since matter is subject to gravity, any denser region would draw more matter from its surroundings, gradually becoming denser and more massive. However, during the earliest stages of the evolution of the Universe, baryonic matter was strongly coupled to photons. Their radiation pressure tended to push away any concentration of matter that might be created under the effect of gravity, preventing any fluctuations in the distribution of ordinary matter to grow denser before CMB decoupling. Instead, DM was not coupled to photons and therefore it could go on undisturbed collapsing and growing its fluctuation more and more dense and more massive. The idea is that DM collapsed first and the resulting gravitational potential acted as an attractive potential well for ordinary matter collapsing later speeding up the structure formation process.

The goodness of the cold DM (CDM) scenario (involving non-relativistic and typically heavy DM particles) is confirmed today by means of solid N-body simulations taking advantage of the increasing power of numerical technologies and of an always increasing knowledge of the many factors playing a role in structure formation. Fig. 1.5 represents some steps in the evolution of clusters and large scale filaments in a model including CDM and dark energy.

1.3.2 Features of Dark Matter Candidates

Based on the evidence of DM mentioned in the previous subsection and on the results of past and ongoing searches for DM, it is possible to derive a list of conditions that a particle species must satisfy to be considered a good DM candidate today. Such conditions can be formulated as follows, according to Ref. [32]:

1. Is it neutral under electromagnetic and strong interaction?
2. Is it compatible with constraints on self-interactions?
3. Is it stable over timescale comparable with the age of the Universe?

4. Does it match the appropriate relic density? Does it have an appropriate mass in relation with its produced abundance?
5. Was it produced with momentum distribution compatible with the formation of large scale structures that we observe today?
6. Is it consistent with Big Bang Nucleosynthesis?
7. Does it leave stellar evolution unchanged?
8. Is it in general consistent with direct DM searches?
9. Is it compatible with indirect searches of its annihilation processes (gamma-ray and cosmic-ray constraints)?
10. Is it compatible with the other astrophysical bounds, specific of each type of DM candidate?

Among the SM particles, the species closest to be good DM candidates are neutrinos. Today, at least two of the three neutrino species that we know are non-relativistic and contribute to the matter budget of the Universe, so they can effectively be considered DM. However, they became non-relativistic only at very late times and they certainly contributed to the radiation budget during the period crucial for structures formation, thereby impeding the formation of structures on small scales. This is why they must be considered hot DM (HDM) and it is excluded by observations of structures that they can constitute the entire DM abundance in the Universe, although they make up a small fraction of it.

A good DM candidate has thus to be searched beyond the SM.

In the last decades, a number of proposals for new particles have been formulated to solve the DM problem. They include WIMPs⁴ (such as, for example, Sneutrinos, Neutralinos, and Gravitinos, or first excited states of Kaluza-Kline towers), axions and ALPs⁵, Hidden DM belonging to a dark sector, scalar DM in the Higgs sector, fuzzy DM, PBHs⁶, and sterile neutrinos.

Based on the list of requirements reported above, sterile neutrinos with a mass $m_s \sim \mathcal{O}(\text{keV})$ can be considered good DM candidates. Indeed, by definition they are not charged under any SM interaction and in the simplest possible scenario, they are linked to the SM particles only through weak interaction suppressed by the magnitude of their mixing angle θ with active neutrinos, and they are not subject to self-interactions. If θ is small enough, they can be stable over cosmological timescales and can be still around in the Universe today contributing as matter to its energy budget. They can have been produced in the early Universe through at least four mechanisms, discussed in Section 2.1 in the next chapter, which rely on different assumptions and originate sterile neutrinos with different momentum distributions. These four mechanisms can produce the right amount of sterile neutrino DM for a ranges of values of sterile neutrino mass m_s and coupling parameter broad enough not to be fine tuned. This aspect of production in the early Universe is discussed more in detail in Chapters 4 and 5 of this dissertation. Moreover, the resulting distribution functions are not in tension with observations of structures for wide ranges of values of the parameters. The production of sterile neutrino DM in the early Universe does not spoil BBN and does not affect stellar evolution, since

⁴Weakly Interacting Massive Particles

⁵axion-like-particles

⁶primordial black holes

it happens mainly much earlier than these two events. For what concerns detection, due to the smallness of the sterile neutrino coupling to SM particles, the constraints on sterile neutrino DM from direct detection experiments are extremely loose. The conditions under which sterile neutrino DM is compatible with constraints from indirect detection are discussed in Section 2.2 in the next chapter.

A further point in favor of investigating sterile neutrinos as DM candidates is that a number of experiments, presented in Chapter 3 of this thesis, will be sensitive in a large region of sterile neutrino parameter space in the near future, thereby being able to test different models that predict their existence.

Chapter 2

keV Sterile Neutrinos

2.1 Production mechanisms

For any particle species i produced in the early Universe, the fundamental quantity needed to calculate its abundance is the distribution function f_i . Assuming the cosmological principle to be valid and, as a consequence, assuming that the Universe can be described in terms of the Friedmann-Robertson-Walker metric, f_i is a function only of the particles' momenta p and of time t (or of temperature T , more frequently used to parameterize time in cosmological contexts). The distribution function is the **solution of the Boltzmann equation**, whose general expression is

$$L[f_i(p, t)] = C[f_i(p, t)] \quad (2.1)$$

Here, the l.h.s of the equation is called Liouville operator and tells us how the distribution function evolves with time, based on the background evolution of the Universe and the interactions of the species i with other species in the plasma, information contained in the collision operator $C[f_i(p, t)]$ reported on the r.h.s of Eq. (2.1). The Boltzmann equation encodes all the features and details of particle production, and therefore, it takes different shapes according to different production mechanisms. Once the solution of the Boltzmann equation is obtained, it is integrated over all possible values of momentum p to get the particle number density that is only a function of time t or, better, of temperature T

$$n_i(T) = \frac{g_i}{(2\pi)^3} \int_{-\infty}^{+\infty} d^3p f_i(p, T) \quad (2.2)$$

where g_i is the number of internal degrees of freedom (DOF) of the particle. We can define the total co-moving entropy density of the Universe in the radiation-dominated epoch, receiving contribution only by relativistic degrees of freedom, as

$$s(T) = \frac{S}{V} = \sum_{i=\text{rel}} \left(1 + \frac{1}{3}\right) \frac{\rho_i(T)}{T} = \frac{2\pi}{45} \sum_{i=\text{rel}} g_i \eta'_i T^3 \simeq \frac{2\pi}{45} g_{*s}(T) T^3 \quad (2.3)$$

where the sum runs over all relativistic species in the plasma, $\rho_i(T)$ is the energy density of each species i , η'_i is a quantum statistic factor that can be approximated by the values $\eta'_i = 1$ for bosons and $\eta'_i = 7/8$ for fermions, and in the last step we introduced the approximated formula of the total number of relativistic DOF contributing to the entropy of the Universe

$$g_{*s}(T) \simeq \sum_{i=\text{rel. bosons}} g_i \left(\frac{T_i}{T}\right)^3 + \frac{7}{8} \sum_{i=\text{rel. fermions}} g_i \left(\frac{T_i}{T}\right)^3. \quad (2.4)$$

The number density divided by the co-moving entropy density of the Universe $s(T)$ gives the yield $Y_i = n_i(T)/s(T)$ at any time of the evolution of the Universe. Finally, integrating over T from the beginning of the production to today, one obtains the yield in today's Universe $Y_{i,0}$, that is used to calculate the abundance $\Omega_{i,0}$ of the species i today. The abundance of a species i is defined as $\Omega_i = \rho_i/\rho_c$ that is its energy density divided by the critical energy density of the Universe. The critical density

$$\rho_c = \frac{3 H_0}{8\pi G} = 1.878 \times 10^{-29} h^2 \text{ g cm}^{-3} \quad (2.5)$$

where $G = 6.674 \times 10^{-11} \text{ m}^3 \text{ kg}^{-1} \text{ s}^{-2}$ is the Newton gravitation constant [13], is the energy density for which a flat Universe ($k = 0$) stops expanding. For a non-relativistic species, such as keV sterile neutrinos, the formula giving the abundance is

$$\Omega_{i,0} = \frac{\rho_i}{\rho_c} = \frac{m_i n_{i,0}}{\rho_c} = \frac{m_i Y_{i,0} s_0}{\rho_c}. \quad (2.6)$$

The abundance is usually given in terms of the Hubble reduced constant $h = H_0/100$, and it is the final reference observable to be compared with the data coming from observations. In the following, we will drop the subscript "0" that refers to the value of a quantity $Y_{i,0}$ or $\Omega_{i,0} h^2$ to a measurement or a prediction relative to today's Universe. We will assume that every time $\Omega_i h^2$ appears it is referred to the present time.

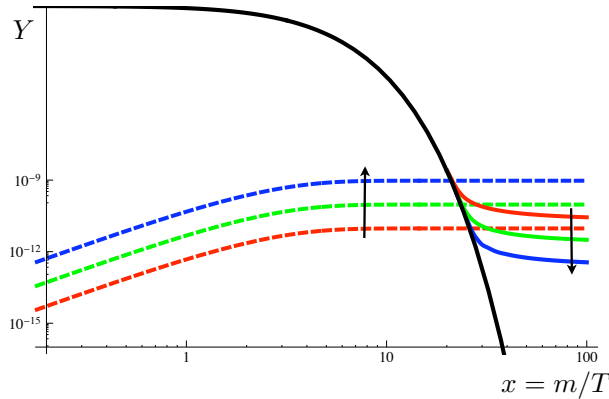


FIGURE 2.1: Freeze-out and freeze-in mechanisms. Log-Log plot of the evolution of the relic yields $Y = n/s$ for conventional freeze-out (solid coloured) and freeze-in (dashed coloured) as a function of $x = m/T$. The black arrows indicate the effect of increasing coupling strength for the two processes. The colored solid lines indicate the yield of a species that reaches thermal equilibrium and decouples once the Hubble expansion wins over the interaction rate. In this case, the abundance decreases if the coupling strength increases because of the Boltzmann suppression factor. The dashed lines represent the evolution of the yield of a species that is produced via freeze-in and never reaches thermal equilibrium. In the freeze-in case, the final abundance is larger for larger couplings. Figure taken from Ref. [33].

Two classes of production mechanisms can be distinguished for a non-specified species of particles χ produced in a standard cosmological scenario in the early Universe: freeze-out mechanisms and freeze-in mechanisms.

In **freeze-out mechanisms** [34], χ is produced abundantly and reaches the thermal

equilibrium thanks to a relatively large coupling with the SM thermal plasma. When, due to the expansion of the Universe, the interactions of the particles χ and the SM particles of the plasma become too rare (approximately when the interaction rate falls below the Hubble rate satisfying the condition $\Gamma_{\chi \leftrightarrow SM}(T) \lesssim H(T)$) its abundance gets "frozen". Particles produced through freeze-out are usually called "thermal relics".

In **freeze-in mechanisms** [33], the coupling of the species χ to the other species in the plasma is much smaller than the typical coupling of a freeze-out scenario. The initial abundance of χ is reasonably assumed to be zero, and the species χ is produced much more inefficiently, never reaching the equilibrium. Its abundance is typically suppressed with respect to that of a thermal relic, and it is dominated by the contribution arising at low temperatures.

In the following subsections, different production mechanisms for sterile neutrino DM are introduced in detail. More emphasis is put on the two mechanisms relying on oscillation and collisions, at the basis of the work carried out in Refs. [2, 3].

2.1.1 Dodelson-Widrow Mechanism

The simplest way how to produce sterile neutrino DM in the early Universe, given that it mixes at least with one active neutrino species, was proposed by Scott Dodelson and Lawrence M. Widrow in Ref. [35] and it is known as Dodelson-Widrow mechanism (DW, from here on).

In the following, we assume for simplicity that sterile neutrinos ν_s mix exclusively with one species of active neutrinos ν_α , so that all the formulas are given in the most simplified and intuitive form possible. The results of the work presented in Chapters 4 and 5 are obtained for ν_s mixing with ν_e . The choice of this mixing is due to the fact that the ongoing and upcoming terrestrial experiments will be sensitive to this mixing and not to the mixing of ν_s with ν_μ or ν_τ . However, in the rest of this chapter we do not fix $\nu_\alpha = \nu_e$ yet and report the formulas in a more general form.

The DW mechanism relies on the only assumption of active-sterile mixing, parameterized by the angle θ , and predicts $\Omega_s = \Omega_{DM}$ to be achieved for values of $\sin^2(2\theta)$ in the range $(10^{-11}, 10^{-7})$ depending on the value of the sterile neutrino mass m_s . Assuming that the mixing with active neutrinos is the only coupling of sterile neutrinos to the SM sector, such values of θ are **insufficient for sterile neutrinos to achieve thermalization**. The DW mechanism can therefore be considered a freeze-in mechanism. **The phenomenon that makes this mechanism possible is neutrino oscillation**, discussed in Appendix A combined with collisions in the plasma, and the concept at the basis of the production is outlined below.

Neutrino fields, while propagating in the plasma, oscillate between the active and the sterile state. The interactions of neutrinos with other particles act as quantum mechanical measurements, and collapse the wave function either into ν_s (with a probability of $\frac{1}{2} \sin^2(2\theta_M)$), or into ν_α (with a probability of $1 - \frac{1}{2} \sin^2(2\theta_M)$). Here, θ_M is the effective active-sterile mixing in the plasma, that corresponds to the mixing angle θ modified by the fact that active neutrinos "feel" the presence of the plasma due to their forward scattering with particles of the plasma that carry weak charge ¹. After the measurement, the oscillation starts again and thus active neutrinos acquire a new ν_s component $\propto \sin^2(2\theta)$ along the oscillation, and sterile neutrinos acquire a ν_α component of the same magnitude. However, while active neutrinos are continuously replenished via pair production or charged current weak interactions, the only existing abundance of

¹The detailed calculation of the form of $\sin^2(2\theta_M)$ can be found in Appendix A

sterile neutrinos comes from this process and it is much smaller than the abundance of active neutrinos. Therefore, the back-conversion from ν_s to ν_α is negligible, and a non-negligible abundance of sterile neutrino DM is produced after many collisions. The sterile neutrino production ends when the active neutrinos decouple from the plasma at $T_{\nu,D} \sim 1.2$ MeV (in standard cosmology) [36], because after that moment neutrinos free-stream and oscillate but there is no way anymore to make the neutrino wave function collapse into the sterile state.

If we wanted to follow properly the evolution of active neutrinos in the primordial plasma taking into account the possibly coherent flavor inter-conversion among them, we should use the density matrix formalism and the quantum kinetic equations. A similar description could be adopted also in the case of mixing between an active neutrino and a sterile neutrino. However, being interested in the production of sterile neutrino DM that occurs mainly at high temperatures where the interactions of neutrinos in the plasma dominate over the vacuum oscillation, a simplified description by mean of the Boltzmann equations is allowed and justified. The Boltzmann equation that describes the evolution of the distribution function $f_s(p, T)$ of sterile neutrino DM produced through oscillation and collisions is a quasi-classical transport equation for the diagonal terms of the density matrix of active and sterile neutrinos. Such diagonal terms are the momentum space distributions of the active and sterile components [37]. The complete derivation of the Boltzmann equation from the quantum kinetic equations is beyond the scope of this work. Its discussion can be found in Section 5.2.1 of Ref. [36], or in Ref. [38].

The **Boltzmann equation** describing sterile neutrino production through DW mechanism is

$$\begin{aligned} \frac{\partial}{\partial t} f_s(p, t) - H p \frac{\partial}{\partial p} f_s(p, t) &\approx \left[\frac{\Gamma_\alpha(p, T)}{2} \langle P_m(\nu_\alpha \rightarrow \nu_s; p, t) \rangle \right] (f_\alpha(p, t) - f_s(p, t)) \approx \\ &\approx \frac{\Gamma_\alpha(p, T)}{4} \sin^2(2\theta_M) (f_\alpha(p, t) - f_s(p, t)) \end{aligned} \quad (2.7)$$

where $f_\alpha(p, t) = 1/(e^{p/T} + 1)$ is the Fermi-Dirac distribution function of active neutrinos ν_α that are reasonably assumed to be in equilibrium in the primordial plasma. $\Gamma_\alpha(p, T)$ is the active neutrino interaction rate with the particles in the plasma. In the SM, the total interaction rate takes the form $\Gamma_\alpha(p, T) = C_\alpha(T) G_F^2 T^4 p$ where $C_\alpha(T)$ depends on the number and type of relativistic species in the primordial plasma [37]. In our work, we use for $C_\alpha(T)$ the values given in Ref. [39]. $\langle P_m(\nu_\alpha \rightarrow \nu_s; p, t) \rangle$ is the oscillation probability of ν_α into ν_s , averaged over one oscillation period² and therefore the entire expression in square brackets in Eq. (2.7) is the probability for the neutrino state to collapse into ν_s in a collision. Such probability can also be called "damped conversion rate" because it encodes the matter effects on the neutrino oscillation and it is determined by the quantum damping rate $D(p) = \Gamma_\alpha(p)/2$ and by the effective mixing angle in matter, $\sin^2(2\theta_M)$.

The quantum damping rate, relative to the quantum Zeno effect, appears also in the denominator of Eq. (2.8). It tells us that the interactions of neutrinos with the plasma

²For sterile neutrino DM masses of $\mathcal{O}(\text{keV})$, the oscillation length (or time scale) $L_{\text{osc}} = 4\pi E/\Delta m^2$ is very small, thus a superposition of ν_α and ν_s is produced very quickly and it is sufficient to consider the averaged effect of oscillations. For small value of mixing angle, the neutrino state consists mostly of ν_α , with a small ($\sim 1/2 \sin^2(2\theta)$) admixture of ν_s and this is what justifies the last step in Eq. (2.7).

are fundamental for the production of sterile neutrino DM but they can also suppress the active-sterile conversions if the interaction length of neutrinos is much smaller than the oscillation length, namely if $\Gamma_\alpha(p)$ is very large. Indeed, no appreciable conversion is possible unless active neutrinos can propagate without interactions with the plasma enough to have a non-trivial probability to convert to sterile neutrinos [37]. The effective production of sterile neutrino DM at extremely high temperatures through DW mechanism is impeded precisely because of the strong temperature dependence of $\Gamma_\alpha(p)$. The expression for the mixing angle in matter is

$$\sin^2(2\theta_M) = \frac{\Delta^2(p) \sin^2(2\theta)}{\Delta^2(p) \sin^2(2\theta) + D^2(p) + [\Delta(p) \cos(2\theta) - V^D(p) - V^T(p)]^2} \quad (2.8)$$

where $\Delta(p) \equiv \frac{\delta m^2}{2p} = \frac{(m_s^2 - m_\alpha^2)}{2p} \simeq \frac{m_s^2}{2p}$. $V^D(T)$ and $V^T(p, T)$ together constitute the weak effective potential which represents the effects of neutrino forward scattering through neutral current and charged current on particles in the plasma carrying weak charge. The finite density potential [40]

$$V^D(T) = \pm \frac{2\sqrt{2}\zeta(3)}{\pi^2} G_F T^3 \frac{\eta}{4} \quad (2.9)$$

where "+" holds for $\alpha = e$ and "-" for $\alpha = \mu, \tau$, arises not from non-zero total densities alone but rather from asymmetries in weakly interacting particles, be they baryons or leptons. In a standard scenario such as the one that frames the DW mechanism, it is assumed that there is no significant asymmetry between leptons and antileptons in the very early Universe. Therefore, the only contribution to the finite density potential comes from the tiny baryon asymmetry $\eta = (n_b - n_{\bar{b}})/n_\gamma = (6.143 \pm 0.190) \times 10^{-10}$ [13] that we know exist.

The last term in the denominator of Eq. (2.8) is the finite temperature or thermal potential [40]

$$V^T(p, T) = -\frac{8\sqrt{2}G_F p_\nu}{3m_Z^2} (\langle E_{\nu_\alpha} \rangle n_{\nu_\alpha} + \langle E_{\bar{\nu}_\alpha} \rangle n_{\bar{\nu}_\alpha}) - \frac{8\sqrt{2}G_F p_\nu}{3m_W^2} (\langle E_\alpha \rangle n_\alpha + \langle E_{\bar{\alpha}} \rangle n_{\bar{\alpha}}). \quad (2.10)$$

Here, n_α ($n_{\bar{\alpha}}$) and $\langle E_\alpha \rangle$ ($\langle E_{\bar{\alpha}} \rangle$) are the number density and average energy of leptons (antileptons) of flavor α , and n_{ν_α} ($n_{\bar{\nu}_\alpha}$) and $\langle E_{\nu_\alpha} \rangle$ ($\langle E_{\bar{\nu}_\alpha} \rangle$) are the number density and average energy of the neutrinos (antineutrinos) of flavor α .

In the following, the dependence on $f_s(p, t)$ of the right hand side of the Boltzmann equation will be neglected. This is justified because we assume zero initial abundance of sterile neutrinos in the plasma (they are produced only later on exclusively through active neutrino conversion via oscillation and collisions), and even once ν_s are produced, due to the freeze-in nature of the process, their abundance is always small enough to make the back-conversion effect negligible.

In a cosmological context, the evolution of f_s can be tracked more conveniently in terms of the temperature T of the plasma, rather than in terms of time t . After the change of variable $t \rightarrow T$ and some manipulation reported in Appendix B, the Boltzmann equation looks like

$$\frac{\partial}{\partial T} f_s(p, T) + \left[\frac{1}{T} + \frac{1}{3} \frac{g'_{*s}(T)}{g_{*s}(T)} \right] p \frac{\partial}{\partial p} f_s(p, T) = -\frac{1}{H(T)} \left[\frac{1}{T} + \frac{1}{3} \frac{g'_{*s}(T)}{g_{*s}(T)} \right] h(p, T) f_\alpha(p, T), \quad (2.11)$$

where

$$h(p, T) = \frac{\Gamma_\alpha(p, T)}{4} \frac{\Delta^2(p) \sin^2(2\theta)}{\Delta^2(p) \sin^2(2\theta) + D^2(p) + [\Delta(p) \cos(2\theta) - V^D(T) - V^T(p, T)]^2}. \quad (2.12)$$

The solution of Eq. (2.11) can be found with the method of the characteristics as discussed in Appendix B and it is

$$f_{s,DW}(p, T_f) = \int_{T_i}^{T_f} -\frac{dT}{HT} \left(1 + \frac{T g'_{*s}(T)}{3 g_{*s}(T)} \right) h \left(\frac{T}{T_f} \left(\frac{g_{*s}(T)}{g_{*s}(T_f)} \right)^{1/3} p_f, T \right) \times \\ \times f_\alpha \left(\frac{T}{T_f} \left(\frac{g_{*s}(T)}{g_{*s}(T_f)} \right)^{1/3} p_f, T \right). \quad (2.13)$$

The **solution of the Boltzmann equation** derived here helps to shed light on an assumption regarding the distribution function of sterile neutrino DM produced through DW mechanism that is usually adopted in the literature but rarely justified. The usual assumption is that, see for example Refs. [35, 41], the DW mechanism produces sterile neutrino DM with a suppressed thermal spectrum. This assumption is not very accurate, as pointed out by the authors of Ref. [39], and it can be misleading especially in cases in which the high momentum part of the distribution is important, like in analyses concerning cosmological structure formation. From Eq. (2.13) it is clear that f_α depends on the temperature through the number of relativistic degrees of freedom $g_{*s}(T)$. The only case in which f_α can be pulled in front of the integral resembling a thermal distribution is when g_{*s} varies with temperature slowly enough to be possibly substituted by some average value $\langle g_{*s} \rangle$. However, this is not the case especially during the QDC phase transition happening around the peak of DW production [35]. Moreover, in order not to distort the thermal shape, even in case of $g_{*s}(T) = \langle g_{*s} \rangle$, also $h(p, T)$ would need to vary very slowly with the momentum p and this has been shown in Ref. [39] not to be true. Since the thermal shape approximation systematically underestimates the high momentum modes, which are in fact the most decisive ones to exclude the DW mechanism by cosmic structure formation, the final remark here is about the importance of using Eq. (2.13), and not its approximated form, when deriving such constraints.

Finally, an expression completely analogous to Eq. (2.13) describes the distribution function of sterile antineutrinos produced through oscillation and collisions thanks to their mixing with active electron antineutrinos. In a standard case, without CPT symmetry violation and without primordial asymmetry in the lepton sector, nothing distinguishes the abundance of sterile neutrino DM from the one of sterile antineutrino DM and the total abundance of DM is given by the sum of these two contributions.

2.1.2 Shi-Fuller Mechanism

Sterile neutrino DM that mixes with one (or more) active neutrino can be produced also through the Shi-Fuller mechanism [42] (SF mechanism, in the following), under the **assumption of a sizeable lepton asymmetry in the early Universe** (much larger than the baryon asymmetry). In this case, **the active neutrinos are subject to an extra Mikheyev–Smirnov–Wolfenstein (MSW) potential which can produce a resonance for certain values of momentum p and temperature T , enhancing the effective mixing angle in the plasma to $\sin^2(2\theta_M)$ while the value of mixing angle in vacuum remains small.**

The lepton asymmetry of a neutrino of flavor α is defined as

$$L_{\nu_\alpha} \equiv \frac{n_{\nu_\alpha} - n_{\bar{\nu}_\alpha}}{n_\gamma}, \quad (2.14)$$

where n_{ν_α} is the proper number density of neutrino species ν_α , and $n_\gamma = \frac{2\zeta(3)T^3}{\pi^2} \approx 0.243 T^3$ is the proper number density of photons at temperature T .

The **change in the Boltzmann equation** in the case of resonant production is **introduced by new terms in the finite density potential** that takes the general shape [40]

$$V^D(T) = \frac{2\sqrt{2}\zeta(3)}{\pi^2} G_F T^3 \left(\mathcal{L}^\alpha \pm \frac{\eta}{4} \right) \quad (2.15)$$

where

$$\mathcal{L}^\alpha = 2L_{\nu_\alpha} + \sum_{\beta \neq \alpha} L_{\nu_\beta}, \quad (2.16)$$

remembering that ν_α is the flavor that mixes with ν_s and the sum includes eventual contributions coming from possible asymmetries in the other flavors. In the following, for simplicity, we assume that the only existing asymmetry is in the flavor that mixes with the sterile neutrino and therefore the expression for the finite density potential simplifies to

$$V^D(T) = \frac{2\sqrt{2}\zeta(3)}{\pi^2} G_F T^3 \left(2L_{\nu_\alpha} \pm \frac{\eta}{4} \right). \quad (2.17)$$

While the contribution of the thermal potential $V^T(p)$ always goes in the direction of suppressing the effective mixing angle, the contribution of the finite density potential V^D depends on the sign of the asymmetry, that is whether there were more neutrinos or antineutrinos. This means that for a fixed sign of the asymmetry L_{ν_α} either the effective mixing angle between ν_s and ν_α or the one between $\bar{\nu}_s$ and $\bar{\nu}_\alpha$ will be enhanced, while the other one will be suppressed. In particular, if the asymmetry is large enough, for certain values of p and T , the resonance condition

$$\Delta(p) \cos(2\theta) - V^D(T) - V^T(p, T) = 0 \quad (2.18)$$

can be satisfied giving $\sin^2(2\theta_M) = 1$ that maximizes the active-sterile conversion and consequently the sterile (anti)neutrino production. Solving Eq. (2.18) it is possible to identify at which temperature a mode p enters the resonance, and this happens twice per each mode. Of course, the resonance depends on specific values of p and T but also on the absolute value of the asymmetry L_{ν_α} that must be large enough to make $V^D(T)$ of the same order of magnitude of $\Delta(p) \cos(2\theta)$ and $V^T(p, T)$. Plugging m_s of $\mathcal{O}(\text{keV})$ in the explicit expression of Eq. (2.18) one sees that the required lepton asymmetry is several order of magnitude larger than η .

These large values of lepton asymmetry are not straightforward to produce in baryogenesis/leptogenesis models. The reason is that, above the temperature of electroweak symmetry breaking, electroweak sphalerons keep baryon and lepton numbers in equilibrium. This implies that an eventual early lepton asymmetry is kept comparable in magnitude to the baryon asymmetry $\eta \sim 10^{-10}$ until then and a larger lepton asymmetry can be generated only at lower temperatures.

One framework in which this can happen is the ν MSM model [43] where a sizeable L_α [44] can be generated by the CP violating interactions of heavy sterile neutrinos that also generate the observed baryon asymmetry of the Universe [10, 11, 45]. However,

pushing the asymmetry produced at these low temperatures to the large values needed for resonant DM production requires some tuning [10, 11] unless some of the asymmetry produced before the heavy neutrinos come into equilibrium is protected from the washout due to an almost conserved quantum number [46] or because it can be stored in magnetic fields [47]. Another possibility to generate sizeable lepton asymmetry is by mean of Q-balls associated with the Affleck-Dine leptogenesis [48, 49]. Observational constraints on L_{ν_α} arise from CMB [50, 51] and BBN [52, 53]. The reported limits between different analyses are conflicting and in Chapter 4 we use values $L_{\nu_\alpha} \lesssim 0.3$ that, although much larger than the baryon asymmetry, seem rather conservative.

The shape of the Boltzmann equation describing the evolution of the distribution function of sterile neutrino DM in the context of the Shi-Fuller mechanism is almost identical to the one of the DW mechanism given in Eq. (2.11). The only difference comes from the new definition of the finite density potential $V^D(T)$ that includes the non-zero primordial lepton asymmetry in the SF mechanism. Since the change in $V^D(T)$ in presence of lepton asymmetry does not introduce new dependence on T or p in the Boltzmann equation, the analytic shape of the solution $f_{s,\text{SF}}(p, T_f)$ looks analogous to $f_{s,\text{DW}}(p, T_f)$ given in Eq. (2.13). What changes is the final abundance Ω_s and, therefore, the points in the parameter space of sterile neutrinos $(\sin^2(2\theta), m_s)$ that satisfy the condition $\Omega_s h^2 = \Omega_{\text{DM}} h^2 = 0.12$. The final abundance of resonantly produced sterile neutrino DM and their momentum distribution depend on different factors. As the Universe cools down, different modes p enter the resonance at different times. The duration of resonant production in that mode corresponds to the time for which $\sin^2(2\theta_M)$ for that mode remains of order unity; and the number of produced particles is determined by the value of the scattering rate $\sin^2(2\theta_M)\Gamma_\alpha(p, T)$ during that time. Beyond the dependence on time coming from $T(t)$ due to Hubble expansion, also the depletion of the lepton asymmetry L_{ν_α} due to the DM production is time-dependent and it influences the sterile neutrino DM production. In particular, the change in L_{ν_α} modifies the production while it is still going on and it ends the resonant production when the condition of Eq. (2.18) cannot be fulfilled any more. Making explicit the l.h.s. of Eq. (2.18) one can see that low momentum modes enter the resonance first, and this corresponds to a colder spectrum for sterile neutrino DM produced through SF mechanism compared to that produced through DW mechanism [54].

2.1.3 Extra Gauge Interactions

Although **sterile neutrino DM** is not directly charged under SM interactions, it **can participate in gauge interactions of an extension of the SM gauge group that allow its production in the early Universe**. In this case, if we do not fine-tune the parameters of such new interactions, **the thermalization of sterile neutrinos is almost unavoidable**. The only possibility to avoid equilibration is that the sterile neutrino freeze-out temperature [55]

$$T_{s,f} \sim g_*^{1/6} \left(\frac{M_{\text{new int.}}}{M_W} \right)^{4/3} \times 1 \text{ MeV}, \quad (2.19)$$

exceeds the maximal temperature of the thermal bath, that is the temperature of reheating of the Universe T_{RH} . If this is not the case, sterile neutrino DM can be considered a thermal relic: a particle that reaches thermal equilibrium and freezes out when it is still relativistic and later becomes non-relativistic when the temperature of the Universe decreases and becomes $T < m_s$. As it is for any thermal relic, the number density in

comoving volume is determined by the freeze-out temperature, and the contribution to the energy density budget of the Universe is proportional to the mass of the particle. The typical result for sterile neutrino DM with a mass of \mathcal{O} (keV) that undergoes thermalization is overproduction: $\Omega_s \gg \Omega_{\text{DM}}$, according to [54]

$$\frac{\Omega_s}{\Omega_{\text{DM}}} = \frac{1}{S} \left(\frac{10.75}{g_{*s}(T_f)} \right) \left(\frac{m_s}{\text{keV}} \right) \times 100, \quad (2.20)$$

where $g_{*s}(T_f)$ is the number of relativistic degrees of freedom at the freeze-out temperature of sterile neutrinos, and S is the entropy produced in non-equilibrium processes after sterile neutrino freeze-out. From Eq. (2.20), we see that there are three ways how overproduction can be avoided. The first possibility, although unlikely, is that $g_{*s}(T_f)$ would change by three orders of magnitude, meaning that at sterile neutrino freeze-out, the plasma was populated by a huge number of relatively light exotic species. The second possibility is that sterile neutrinos have some new interactions that remained efficient after they decoupled from the SM and allowed them to reduce their number densities by self-annihilation [56], or that sterile neutrino decay. However, we must remember that substantial sterile neutrino decay would exclude them from the list of good DM candidates. The third possibility is **entropy injection in the plasma after sterile neutrino decoupling**. This would correspond to a large value of S in Eq. (2.20). Entropy injection does not change the number of sterile neutrinos but changes the Universe's expansion history and effectively dilutes the abundance of sterile neutrinos. The entropy can be produced in decays of heavy particles relatively long-lived [34, 57] such as, for example, heavier sterile neutrinos. Two general considerations have to be implemented properly in concrete models: such dilution by mean of entropy production must not spoil BBN, and this translates into an upper bound on the lifetime of the decaying particle and implies a lower bound on its mass; for the dilution to be efficient, the decaying heavy particle has to freeze-out while relativistic, and this translates into a lower bound on the mass of the mediator leading to thermalization of the heavy particle [55].

The case of dilution by the decay of heavy sterile neutrinos embedded in a minimal left-right symmetric theory is presented in detail in Ref. [58], while a general discussion of this mechanism without reference to specific particle models is reported in Ref. [59].

In this scenario of production through extra gauge interactions and subsequent dilution by entropy injection, **the evolution of the distribution function and of the number density of sterile neutrino DM is described by the Boltzmann equation typical of a thermal relic**. To get the abundance today, we should then properly re-scale the value of the abundance calculated at the freeze-out of sterile neutrinos, taking into account the entropy injection and its effect on the scaling of the comoving volume through the Hubble parameter.

Two last noticeable points regarding sterile neutrinos produced through extra gauge interactions and subsequently diluted by entropy injection are related to constraints from structure formation and sterile neutrino decay. On the one hand, entropy dilution has the effect of cooling down the momentum distribution of sterile neutrino DM by a factor of $S^{-1/3}$, which leads to weaker limits from structure formation (Lyman- α) compared to the case of production via oscillation and collisions. On the other hand, extra gauge interactions could, in principle, lead to additional decay channels for sterile neutrinos. This aspect of model-building must be taken care of concerning the requirement of stability of a good DM candidate and the limits coming from X-ray observations.

2.1.4 Decay of Scalar Field

Finally, the fourth class of mechanisms for production of sterile neutrinos is the **production by decay of a heavy particle**. The **only requirement** is that **the parent particle is heavier than the sterile neutrino and interacts with it**. Thus, for example, in the type-I seesaw framework, ν_s could be produced by decay of pions, the Higgs boson, and W bosons. However, such processes are subdominant in comparison to the production through oscillation and collisions. Therefore, to have a production dominated by decay, new particles have to be introduced. Among the numerous possibilities, the simplest scenarios involve a scalar singlet ϕ that can couple to sterile neutrino through Yukawa interaction $y \phi \bar{\nu}_s \nu_s$ [60, 61]. The scalar field ϕ can be identified with the inflaton field, or with some other new heavy degree of freedom, a generic scalar singlet. The parent scalar can be assumed in thermal equilibrium [60–62] or out of equilibrium [63–66] when the production of sterile neutrino DM starts. In the second case, the non-equilibrium initial condition of the scalar leads to a colder sterile neutrino DM spectrum [67]. However, in this case, the details are quite model dependent because they derive from how the scalar ϕ couples to the primordial plasma. Therefore, in the following we consider only the most general case in which the scalar is in equilibrium, for example, due to its strong mixing with the neutral Higgs boson. Under this hypothesis, most of sterile neutrino DM is produced at $T \sim m_\phi$ when they are relativistic, while at later times the production is exponentially suppressed due to the Boltzmann suppression of the parent number density. Assuming that the inverse decay process $\bar{\nu}_s \nu_s \rightarrow \phi$ is negligible, the Boltzmann equation for the sterile neutrino distribution function reduces to [60]

$$\frac{\partial f_s(p, t)}{\partial t} - H p \frac{\partial f_s(p, t)}{\partial p} = \frac{2 m_\phi \Gamma}{p^2} \int_{p+\frac{m_\phi}{4p}}^{\infty} f_\phi(E) dE, \quad (2.21)$$

where H is the Hubble parameter, E is the energy of the parent particle ϕ , $f_\phi(E)$ is its distribution function, and $\Gamma = y^2 m_\phi / 16\pi$ is the partial width of the scalar for $\phi \rightarrow \bar{\nu}_s \nu_s$ decay. The latter equation can be solved semi-analytically if the number of relativistic degrees of freedom is considered constant, and one gets

$$f_s(p, T) \simeq \frac{10 \Gamma M_{Pl} p^2}{3 m_\phi^2 \sqrt{g_*} T^2} \int_1^{\infty} \frac{(z-1)^{3/2}}{\exp(\frac{p}{T}z) - 1} dz \quad (2.22)$$

leading to the number density

$$n_s(T) = \int \frac{d^3 p}{(2\pi)^3} f_s(p, T) = \frac{15 \Gamma M_{Pl} \zeta(5)}{16 \pi m_\phi^2} T^3. \quad (2.23)$$

Sterile neutrino DM produced through this mechanism contributes to the Universe density parameter today with [60]

$$\Omega_s \approx \frac{y^2}{S} \frac{3.9}{g_*(T_{prod})} \frac{M_{Pl} m_s}{m_\phi \text{ keV}} \quad (2.24)$$

where we see that the parameters that determine this contribution have to do with the features of the parent scalar and the coupling between the scalar and sterile neutrinos, and not with the active-sterile mixing.

As a final remark, using Eq. (2.22) to calculate the average momentum of sterile neutrinos right after their production, we find

$$\langle p \rangle = \frac{\pi^6}{378 \zeta(5)} T = 2.45 T \quad (2.25)$$

This value is smaller than $\langle p_T \rangle = 3.15 T$ which is the typical momentum for an equilibrium thermal distribution. This means that sterile neutrinos produced by decay of a scalar are colder than those produced thermally, and therefore, as it happens in the case of production through extra gauge interactions and subsequent entropy dilution, the constraints from structure formation are less strict for them.

2.2 Existing Bounds on Sterile Neutrino Dark Matter

The existence of sterile neutrino DM mixing with active neutrinos is subject to several tests and bounds from cosmology and observations of astrophysical objects.

Sterile neutrinos can be constrained using:

- considerations about the phase-space density of DM dense objects (Tremaine-Gunn bound [68, 69]);
- the impact of their free streaming on formation of structures in the early Universe (testable through Lyman- α forest [70–72], weak lensing [73, 74], 21-cm line [75, 76] and observing abundance and structures of cosmic voids [77, 78]);
- the impact of their free streaming on the formation of structures in the late Universe (testable through counts of dwarf galaxies satellites of the Milky Way [71, 79, 80], collapsed objects at high redshift (see Subsection 3.3.4 of Ref. [54]), and through the determination of the distribution of matter within individual DM dominated objects such as cores of galactic halos (see Subsection 3.3 of Ref. [81]);
- an indirect effect of their free streaming on other processes such as re-ionization [82];
- precise determination of the number of relativistic degrees of freedom at the time of CMB decoupling [83, 84];
- their direct impact on fundamental dynamics of celestial objects such as supernovae [85–90] and pulsars [91, 92];
- the requirement of their stability over timescale comparable with the age of the Universe [54, 93];
- indirect detection measurements of their decay products [94, 95].

In the following, the most relevant bounds are discussed more in detail.

2.2.1 Tremaine-Gunn Bound

The Tremaine-Gunn Bound [68] is a phase-space argument that applies to fermionic DM candidates such as sterile neutrinos. It is derived assuming that **the phase-space density of sterile neutrinos in a galaxy does not exceed the phase-space density of a degenerate Fermi gas.**

The strongest constraint excluding values of m_s smaller than $\mathcal{O}(100)$ eV comes from the dwarf spheroidal satellites of the Milky way (dSph) [54]. We only report a rough estimate since the exact numerical value depends on how to estimate the phase-space density of DM particles based on the observational data and the set of dSphs used. This "vanilla" bound can be strengthened by considering a particular phase-space distribution of DM particles that obeys the Liouville theorem in the process of evolution, according to the results reported in Ref. [69].

Since the Tremaine-Gunn bound is less strict than the one from Milky Way satellites, in the plots representing the results in Chapters 4 and 5, we will show only the latter.

2.2.2 Limit from Milky Way Satellites

The number of observed dwarf galaxies satellites of the Milky Way (MW) provides a powerful test for non-cold DM scenarios. **The colder the DM is, the more it tends to clump and give origin to structures on small scales.** We observe such structures today, and while it is possible that there are some unobserved or unobservable ones, it is impossible that there are fewer than those we observe. The number of dwarf galaxies satellites of the Milky Way decreases with decreasing mass of the DM particle [79]. Therefore, **assuming that the number of DM satellites must exceed or equal the number of observed satellites of the Milky Way, it is possible to derive lower limits on the DM particle mass.** This limit depends, in general, also on the mass of the Milky Way and on the DM production mechanism.

In order to derive the bound on m_s , N-body simulations of the growth of Milky Way-like galaxies in warm DM (WDM) cosmologies for a variety of WDM particle masses are needed, and the number of satellite halos in the simulated Milky Ways must be compared to the observed number of luminous satellites for the actual Milky Way. Since the derivation from scratch of this limit is beyond the scope of this work, we use results already existing in the literature, and we adapt them to our case of interest. Different authors have carried out estimates of the limit from Milky Way satellites for the cases of sterile neutrinos produced through standard Dodelson-Widrow mechanism (non-resonant), Shi-Fuller mechanism (resonant), Higgs decay mechanism and for thermal dark matter particles [71, 79, 80].

In this work, the Milky Way satellite counts bound is reported in the plots showing the results obtained in non-standard cosmological scenarios (Chapter 4). Since we are interested in a scenario considering low-temperature production of sterile neutrino DM for which structure formation limits have not been considered in the literature yet, we estimate the constraint from Milky Way satellite counts following a procedure outlined in Ref. [96]. This procedure consists of a re-scaling of the limit based on the features of the momentum distribution considered. First, taking into account Eq. (4.3) in Ref. [97] and the corresponding discussion on the impact of a temperature cutoff, we calculate the averaged sterile neutrino momentum over temperature, $\langle p/T \rangle$ for the production mechanism under exam. Then, we use Eq. (7) of [96] to re-scale the limit taken from Ref. [39] that was derived for sterile neutrino DM produced through the DW standard mechanism, assuming the Milky Way mass of $3 \times 10^{12} M_\odot / h$ [98]. This mass value can be regarded as an upper limit, given the multitude of previous measurements [99]. Although recent Gaia results seem to indicate a somewhat smaller Milky Way mass, such measurement currently has significant uncertainties [100]. The choice of a large Milky Way mass adopted here is conservative and allows to give the weakest possible value for the constraint, leaving open the best scenario for detection in terrestrial experiments. The general dependence of the limit from Milky Way satellite counts on the Milky Way mass can be inferred from [39]. The limit from Milky Way satellite counts calculated according to the procedure outlined above will be shown only in the plots in which the condition $\Omega_s h^2 = \Omega_{\text{DM}} h^2 = 0.12$. Indeed, in case $\Omega_s h^2 < 0.12$, other components are necessary to cover the entire DM abundance, and such additional components could be colder than sterile neutrinos. This changes the limits from structure formation even drastically depending on the fraction of DM they contribute.

2.2.3 Limit from Lyman- α Forest

Among all the constraints from structure formation that reduce the available parameter space of sterile neutrino DM, those obtained from Lyman- α forests [70] are typically

the strongest limits. As reported in Ref. [70], ν_s produced through oscillation and collisions in a non-resonant way [35] are the most affected with a lower limit on the mass that exceeds 20 keV. Somewhat milder constraints of $m_s \gtrsim 10$ keV arise in the case of resonant production [42] due to a colder spectrum [71]. However, as pointed out in Ref. [72], the gas dynamics of the inter-galactic medium can yield a striking effect on the absorption spectra and has, consequently, a potentially drastic impact on the sterile neutrino exclusion. Due to such considerations, Lyman- α bounds are often not shown in sterile neutrino literature [94, 101], and we follow this conduct in the coming chapters.

2.2.4 Requirement of Stability over Cosmological Timescale

Due to the mixing of ν_s with active neutrinos, sterile neutrinos can decay. In the following, we proceed according to the assumption made in Section 2.1 that sterile neutrinos mix with only one species of active neutrinos ν_α , with mixing angle θ . If $m_s < 2m_e$, the **dominant decay channel** is $\nu_s \rightarrow \nu_\alpha \nu_\beta \bar{\nu}_\beta$. The total decay width is [93]

$$\Gamma_{\nu_s \rightarrow 3\nu} = \frac{G_F^2 m_s^5}{96\pi^3} \theta^2 \approx \frac{1}{1.5 \times 10^{14} \text{sec}} \left(\frac{m_s}{10 \text{ keV}} \right)^5 \theta^2. \quad (2.26)$$

This dominant decay channel gives an **upper bound on the lifetime** of ν_s , τ_{ν_s} . Any DM candidate is required to be stable over a cosmological timescale in order to be still around in the Universe today playing the role of DM. Therefore, the estimated lifetime of ν_s of Eq. (2.26) must be compared with the age of the Universe t_U and by requiring $\tau_{\nu_s} > t_U = 4.4 \times 10^{17} \text{ sec}$ [102] it is possible to derive the upper bound on θ relative to different values of m_s [54]

$$\theta^2 < 3.3 \times 10^{-4} \left(\frac{10 \text{ keV}}{m_s} \right)^5. \quad (2.27)$$

This upper bound is represented by a gray dashed line delimiting a gray triangle in the top right corner of the parameter space in the figures summarizing the results of Chapters 4 and 5. Sterile neutrinos with mixing larger than this limit are excluded as DM candidates, although they could anyway exist and play some other role in particle physics and cosmology.

It has to be kept in mind that this bound is derived in the "vanilla" scenario in which sterile neutrinos interact with SM particles exclusively through their mixing with active neutrinos. In more exotic scenarios that allow further decay channels for sterile neutrinos, the limit would become more cumbersome.

2.2.5 X-ray Bound

The dominant decay channel discussed in the previous subsection is not the only one that can provide an upper limit on m_s and $\sin^2(2\theta)$. Indeed, sterile neutrinos that mix with active neutrinos can decay sub-dominantly also via **radiative decay** as $\nu_s \rightarrow \nu_\alpha \gamma$. The decay width is [93]

$$\Gamma_{\nu_s \rightarrow \nu_\alpha \gamma} = \frac{9\alpha G_F^2}{256 \cdot 4\pi^4} \sin^2(2\theta) m_s^5 = 1.38 \times 10^{-32} \left(\frac{\sin^2(2\theta)}{10^{-10}} \right) \left(\frac{m_s}{1 \text{ keV}} \right)^5 \text{ sec}^{-1}. \quad (2.28)$$

Although it is suppressed by a factor of $\sim \frac{1}{128}$ with respect to the dominant channel, the constraint that derives from this process is much more stringent than the one expressed by Eq. (2.27). This is due to the fact that, in the case of radiative decay, there is a

photon in the final state that is mono-energetic and carries away half of the energy of the decaying sterile neutrino. Assuming that decaying DM is approximately at rest, for a sterile neutrino mass of $\mathcal{O}(\text{keV})$, the energy of the emitted photon will be in the X-ray band. The presence of an easily detectable particle in the final state, opens an exciting possibility of astrophysical searches of sterile neutrino DM. In particular, it is possible to distinguish two types of X-ray signal produced by decay of sterile neutrino DM.

On one hand, decays of DM particles throughout the history of the Universe should produce a contribution to the **diffuse X-ray background** (XRB) [103–105] with

$$F_{\text{XRB}} \simeq \frac{\Gamma_{\nu_s \rightarrow \nu_\alpha \gamma} \rho_s^0}{2\pi H_0} \simeq 8 \times 10^{-11} \left(\frac{\theta^2}{10^{-11}} \right) \left(\frac{m_s}{7 \text{ keV}} \right)^5 \frac{\text{erg}}{\text{cm}^2 \cdot \text{s} \cdot \text{sr}} \quad (2.29)$$

where ρ_s^0 and H_0 are respectively the sterile neutrino DM density in the Universe and the Hubble constant today. Neutrinos decaying at different red-shifts produce a broad X-ray line with extended "red" tail in principle distinguishable from the broad-band continuum of observed X-ray background [106, 107] and the non-observation of the DM decay feature in the X-ray background sets a bound on $\sin^2(2\theta)$ and m_s of roughly [105]

$$\Omega_s \sin^2(2\theta) \lesssim 3 \times 10^{-5} \left(\frac{1 \text{ keV}}{m_s} \right)^5. \quad (2.30)$$

On the other hand, considering DM decaying more recently, pointing telescopes towards spots on the sky with large DM overdensities, we expect to see a **distinct nearly monochromatic line in the X-ray band** with $E_\gamma \approx \frac{1}{2}m_s$ and intensity proportional to $\sin^2(2\theta)$ [40]. The emission is not perfectly monoenergetic because of the Doppler broadening induced by the DM velocity dispersion in the astrophysical object considered. For example, in a galaxy cluster the typical velocity dispersion is of order $v \sim 1000$ km/sec and the subsequent relative line width is $\sqrt{(1+v)/(1-v)} - 1 \sim 0.3\%$ [108].

The vast variety of astrophysical objects or targets of different nature that can be considered for such observations (for example, dwarf spheroidal galaxies satellites of the Milky Way, the halo of the Milky Way, other galaxies (M31) and galaxy clusters, and peculiar 'dark blobs' like the Bullet cluster and A520) offers two main advantages [54]. First, choosing the observational targets one can avoid complicated astrophysical backgrounds; second, if a candidate line is seen, the observation can be compared with those of other objects with the same expected signal for a cross check.

In the past years, a number of X-ray telescopes looked for such decaying DM signal in the keV–MeV mass range: XMM-Newton, Chandra, Suzaku, Swift, INTEGRAL, HEAO-1, and Fermi/GBM. Their results were complemented by those of a rocket-borne X-ray microcalorimeter called NuStar. An overview of the outcomes up to 2021 can be found in Refs. [37, 109].

Such measurement campaigns gave null result (thus setting upper bounds on m_s and $\sin^2(2\theta)$) except from an **unidentified line at around 3.5 keV** in the X-ray spectra of galaxy clusters [110, 111], Andromeda galaxy [111] and the Milky Way [112], observed independently by two research groups in 2014. This discovery hinted to the exciting possibility that the line is the product of the decay of 7.1 keV sterile neutrino. While a DM explanation has been advocated also in recent publications [113], it is fair to stress the existence of alternative explanations that do not involve BSM physics. The charge-exchange mechanism [114] is the most notable example of that. Since no consensus has been reached yet about the interpretation of the mentioned 3.5 keV line, in a conservative approach we adopt the point of view that, at the moment, there is no direct confirmation

of the existence of keV sterile neutrino DM from data of astrophysical observations. The line representing the X-ray bound in the plots containing the results of Chapters 4 and 5, is the outcome of non-observation of monochromatic lines in the X-ray band and it comes from the combination of the lines reported in Fig. 4 of Ref. [115], Fig. 1 of Ref. [94], and Fig. 5 of Ref. [95]. Such limits will possibly become more stringent in the future with the advent of new X-ray telescopes such as XRISM [116], ATHENA [117], eXTP [118], and Lynx [119] that will be sensitive to smaller values of $\sin^2(2\theta)$, and based on the results of the eROSITA/SRG mission [120, 121].

The "vanilla" scenario in which sterile neutrino DM is connected to the SM only via the mixing with active neutrinos and, therefore, is produced exclusively through oscillations and collisions (Dodelson-Widrow mechanism, Shi-Fuller mechanism in the standard case or in case of CPT violation discussed in the following chapters) is threatened by the X-ray bound in its full glory. However, there are some considerations that have to be taken into account. They can lead to the relaxation partial or even complete of the X-ray bound discussed in the following Subsections 2.2.6, 2.2.7, and 2.2.8.

Although all the three possibilities for X-ray bound relaxation presented in the following subsections can in principle be successful, in Chapter 4 and 5 we will consider only the effect of the first to relaxation scenarios presented ("DM Cocktail" and relaxation by cancellation studied in Ref.[2]) and assume a one-to-one correspondence between DM decay and β -decay.

2.2.6 X-ray Bound Relaxation in "Dark Matter Cocktail" Scenarios

The observable used to set the X-ray bound is the flux of photons from ν_s decay received by the telescopes. This flux is proportional to the energy density of sterile neutrino DM ρ_s and to the decay width $\Gamma_{\nu_s \rightarrow \nu_\alpha \gamma}$. It is given by

$$\Phi = \frac{\Gamma_{\nu_s \rightarrow \nu_\alpha \gamma}}{4\pi m_s} \int dl d\Omega \rho_s(l, \Omega), \quad (2.31)$$

where l is the distance along the line of sight and Ω is the solid angle.

Due to the dependence of Φ on ρ_s , in the case of **multi-component DM**, the constraint would be naturally relaxed depending on the fraction of the total DM budget constituted by sterile neutrinos. Indeed, in this case, in addition to sterile neutrino DM, there are other species of DM particles, such as, for example, WIMPs, that would make the total DM abundance, $\Omega_{\text{DM}} h^2 = 0.12$ [24], consistent with observation and would not influence X-ray spectra. In the following, this scenario will go under the name of "DM cocktail" scenario.

From the prefactor of Eq. (2.31) and the expression for the sterile neutrino decay rate via exchange of a SM W_L boson [93] (relative to the left diagram in Fig. 2.2),

$$\Gamma_{\nu_s \rightarrow \nu_\alpha \gamma} = 1.38 \times 10^{-32} \left(\frac{\sin^2(2\theta)}{10^{-10}} \right) \left(\frac{m_s}{1 \text{ keV}} \right)^5 \text{ sec}^{-1}, \quad (2.32)$$

it is possible to see that at a given value of m_s , the constraint on $\sin^2(2\theta)$ is relaxed by a factor of $(\Omega_{\text{DM}} h^2 / \Omega_s h^2)$ [2], where $\Omega_s h^2$ is the abundance of sterile neutrinos in the multi-component DM scenario.

In the following chapters, two cases of DM cocktail in which sterile neutrinos constitute the 10% and the 1% of the DM budget will be studied and compared to the case in which $\Omega_s h^2 = \Omega_{\text{DM}} h^2 = 0.12$.

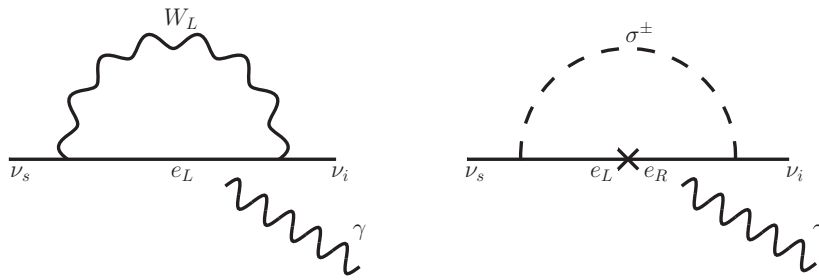


FIGURE 2.2: Feynman diagrams for the radiative decay $\nu_s \rightarrow \nu_\alpha \gamma$. In each diagram, the photon line can be attached to any of the internal charged particles. In the left panel, we show the "standard" case with the electroweak W_L boson, whereas in the right panel, a new scalar particle is exchanged, whose features and role are discussed in Subsection 2.2.7.

2.2.7 X-ray Bound Relaxation due to Cancellation by New Physics

As suggested by the expression of Eq. (2.31), another scenario in which the X-ray bound should be considered in a relaxed version, is the case of a **reduced decay width** $\Gamma_{\nu_s \rightarrow \nu_\alpha \gamma}$. The general expression $\Gamma \propto \int d\text{Phase} |\mathcal{M}|^2$ decreases if the transition amplitude \mathcal{M} gets contributions not only from the standard diagram on the left in Fig. 2.2 but also from one or more other diagrams representing further channels which destructively interfere with the former one. In this case, the re-scaling of the limit generally works as follows, according to the results of Ref. [2]. We denote the amplitude relative to the standard diagram on the left of Fig. 2.2 as \mathcal{M}_1 and the one relative to the diagram that interferes destructively with the first one as \mathcal{M}_2 . It is possible to parameterize the total amplitude in terms of \mathcal{M}_1 as $\mathcal{M} = \mathcal{M}_1 + \mathcal{M}_2 = \chi \mathcal{M}_1$, where $\chi < 1$. Then, the total rate for the process and, consequently, the flux decrease by a factor of χ^{-2} for a value of $\sin^2(2\theta)$ kept constant. For instance, $\chi^2 = 1/10$ leads to an order of magnitude reduction of the decay rate. Vice versa, the same X-ray flux observed by telescopes corresponds to larger values of the mixing angle, and for a given value of m_s , the limit on $\sin^2(2\theta)$ gets relaxed by a factor of χ^{-2} .

In the following, one example of how this can be realized within a minimal extension of the SM is presented³. We follow the "cookbook" from Ref. [123], where general formulas for 1-loop processes in which a fermion decays into a lighter fermion and a photon are provided. The amplitude for $\nu_s(p_1) \rightarrow \nu_i(p_2)\gamma(q)$, where i identifies an active neutrino in mass basis, is $\mathcal{M} = e\epsilon_\mu^* \zeta^\mu$, with ϵ polarization of the outgoing photon and [123]

$$\zeta^\mu = \bar{u}_{\nu_i} i\sigma^{\mu\nu} q_\nu (\sigma_L P_L + \sigma_R P_R) u_{\nu_s}. \quad (2.33)$$

Here, u denotes spinors and $P_{L(R)}$ is the left (right) projector. The results present in the literature [55] have been reproduced for the left diagram in Fig. 2.2 neglecting sub-eV active neutrino masses:

$$i\sigma_R = \frac{3}{64\pi^2} \frac{g^2}{m_{W_L}^2} m_s U_{ei}^* \sin\theta, \quad (2.34)$$

where g is the weak coupling constant, m_{W_L} is the mass of the W_L boson, and U_{ei} is an element in the first row of the leptonic mixing matrix.

³The relaxation of X-ray limits has also been investigated in a supersymmetric framework in Ref. [122]. The authors found mild effects due to diagrams involving heavy supersymmetric particles and additional mixing angle suppression.

In Ref. [2], it has been demonstrated that σ_R in Eq. (2.34) can be greatly reduced, by introducing a scalar doublet $\Sigma = (\sigma^0, \sigma^-) \sim (1, 2, -1)$. The relevant part of the Lagrangian involving this state and ν_s reads

$$\mathcal{L} \supset \lambda \bar{\nu}_s \Sigma^\dagger L_e + \lambda' \bar{e}_R \tilde{\Sigma}^\dagger L_e + h.c., \quad (2.35)$$

where L_e lepton doublet of the first generation, and for simplicity, we assume Σ interacts only with leptons of the first generation. The Feynman diagram given in the right panel of Fig. 2.2 where ν_s decays via exchange of a charged particle from the Σ doublet can be constructed with the two Yukawa interactions described by Eq. (2.35) and already studied in the context of sterile neutrinos and the 3.5 keV line in Ref. [124]. By following again Ref. [123], one can get

$$i\sigma_R = \frac{\lambda\lambda'}{16\pi^2 m_\Sigma^2} m_e \left[\text{Log} \left(\frac{m_e^2}{m_\Sigma^2} \right) + 1 \right] U_{ei}^*, \quad (2.36)$$

where m_e is the electron mass that appears in the amplitude due to the chirality flip drawn in the right diagram in Fig. 2.2 and necessary to preserve gauge invariance. By using Eqs. (2.34 and 2.36, the condition for the complete cancellation between the amplitudes of the two considered diagrams

$$\sin(\theta) = \left(\frac{-4\lambda\lambda'}{3g^2} \right) \frac{m_e m_{WL}^2}{m_s m_\Sigma^2} \left[\text{Log} \left(\frac{m_e^2}{m_\Sigma^2} \right) + 1 \right], \quad (2.37)$$

can be obtained. To get an idea of the order of magnitude of the parameters involved in the cancellation such that it gets interesting for future experimental searches, we can take $\sin^2(2\theta) \sim 10^{-4}$, in the ballpark of KATRIN/TRISTAN sensitivity, and $m_s \sim 1$ keV, and we see that the cancellation would work for $m_\Sigma \sim 1$ TeV and $\lambda\lambda' \sim 10^{-6}$.

Thermalization of ν_s with the SM bath must be avoided to prevent its abundance would overshoot the measured DM abundance by 1-2 orders of magnitude [55, 96]. By imposing this requirement, it is possible to estimate the size of the coupling λ . The first term in Eq. (2.35) facilitates (inverse) decays $\sigma^\pm \leftrightarrow e^\pm + \nu_s$. The requirement that the rate for this process is lower than the Hubble rate at $T \gtrsim m_\Sigma$ yields $\lambda \lesssim 10^{-7}$. Setting λ to such values does not allow sufficient relaxation of the ν_s decay rate since it would force the coupling λ' to very large, practically non-perturbative values. This suggests an alternative solution to avoid overproduction that relies on the fact that the Universe was reheated after inflation only up to a sub-TeV temperature. In this case, these processes would be absent due to the lack of energy necessary to produce σ^\pm . An interesting point is that sub-TeV reheating is consistent with our working hypothesis, central for the discussion in Chapter 4, that the production mechanism for sterile neutrinos stems from active to sterile neutrino oscillations at $T \lesssim 100$ MeV.

Two conclusive comments can be made. First, although in principle it would be possible to completely cancel the X-ray bound according to Eq. (2.37), in the following we consider only its partial relaxation to the extent that leaves accessible the sensitivity regions of experiments in the parameter space. This still requires a certain level of fine-tuning of the parameters involved, but remains a viable possibility. Second, it is important to remember that the Σ doublet introduced in this subsection is only one among the possible options for generating additional diagrams for $\nu_s \rightarrow \nu_i \gamma$ able to relax the X-ray bound. Several other scenarios that could be adopted in the context of keV-scale sterile neutrino DM are discussed in Ref. [124].

2.2.8 X-ray Bound Relaxation by Decoupling of β -Decay from X-ray Decay

Finally, for the sake of thoroughness, there is a third situation in which the X-ray bound does not constitute a problem anymore for the perspective of detection of sterile neutrino DM in terrestrial experiments. It is the case in which **DM decay and β -decay are decoupled**.

In Ref. [125], this has been demonstrated in a left-right symmetric framework where the β -decay could be mediated by the exchange of a heavy W_R boson. In this case, it is the large mass of W_R , M_{W_R} , which suppresses the β -decay, in contrast to the small mixing angle θ of the standard scenario. Also the decay of sterile neutrino DM can occur via small mixing θ or via right-handed currents, and it is suppressed respectively due to the smallness of the mixing and the large W_R mass. The suppression of the decay of ν_s via right-handed currents comes from the fact that only decays in active SM neutrinos would be kinematically possible, but active SM neutrinos are sterile with respect to right-handed currents. This guarantees the stability of the DM candidate over cosmological timescales. What is important for sterile neutrino DM experimental searches is that, while astrophysical observations constrain the mixing angle θ , β -decay can occur dominantly via W_R exchange, which is the leading contribution as long as $(m_{W_L}/M_{W_R})^4$ is larger than θ^2 . In this way, the parameter space in which experiments are expected to be sensitive to sterile neutrino DM is not excluded by the X-ray bound. Unfortunately, despite the appeal of this scenario, it is challenging to implement in its simplest realization due to the strength of limits on M_{W_R} coming from LHC. For the still allowed values of M_{W_R} , W_L - W_R mixing needs to be very small in order to suppress additional diagrams for DM decay. Other options for new interactions of keV sterile neutrinos in β -decay are less constrained [126] but have not been studied yet regarding DM decay. Nevertheless, the mentioned example in left-right symmetric models demonstrates that DM decay and β -decay may not necessarily be related, and therefore X-ray limits can be evaded.

Chapter 3

Experimental Searches for Sterile Neutrino Dark Matter

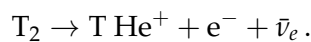
Analogously to the case of WIMP searches, also for sterile neutrino DM, it is possible to distinguish two classes of direct detection experiments [81].

To the first class belong experiments in which the DM particle is produced in a laboratory and detected by applying kinematic considerations. The latter is an important remark because it makes such experiments completely model-independent: the only assumption needed is that sterile neutrinos ν_s have non-zero mixing with ν_e and/or with $\bar{\nu}_e$. The experiments belonging to the second class use large-scale detectors to detect the DM that was produced in the early Universe and is now accumulated in the dark halo of our galaxy. A general discussion regarding such large-scale experiments can be found in Section 8.4 of Ref. [81] and references therein. In the following sections, the landscape of experiments belonging to the first class mentioned having among their goals the detection of sterile neutrino dark matter is detailed.

All these experiments can be further grouped based on the different processes and techniques on which they rely. For the sake of synthesis, only the most relevant exponent in each of these groups is described, while the others are just mentioned.

3.1 KATRIN/TRISTAN

One method that can be used to detect keV sterile neutrino DM is the **high-resolution spectroscopy of tritium β -decay**



The leading experiment in this context is KATRIN¹ [127] (or, more precisely, its upgrade TRISTAN² [128]), whose precursors are the Mainz [129] and the Troitsk [130] experiments.

The **primary goal of these tritium β -decay experiments** is to measure the effective electron antineutrino mass $m_{\bar{\nu}_e}^2 = \sum_{i=1}^3 |U_{ei}|^2 m_{\nu_i}^2$. This quantity can be extracted from the β -decay spectrum given as a superposition of the spectra of each neutrino mass eigenstate m_{ν_i} , weighted by the amplitude of its mixing with the electron flavor $|U_{ei}|$. The expected effect of a non-zero electron antineutrino mass is a distortion of the final part of the spectrum of electrons emitted by the tritium β -decay, very close to the endpoint, similar to the one represented in Fig. 3.1.

¹ KATRIN is the acronym for "KARlsruhe TRITium Neutrino experiment"

² TRISTAN is the acronym for "TRITium Beta Decay to Search for STerile Neutrinos"

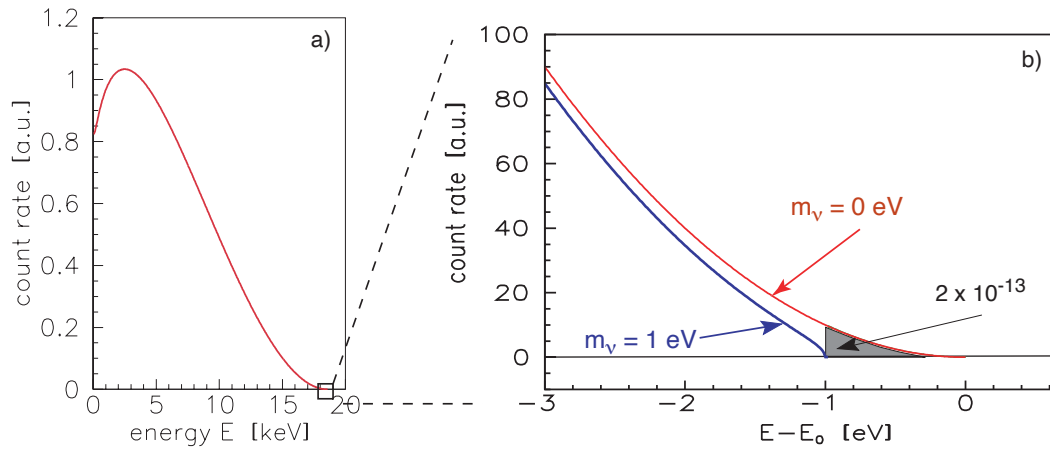


FIGURE 3.1: Energy spectrum of the electron emitted in tritium β -decay: (a) complete and (b) narrow region around endpoint E_0 . The distortion in the β spectrum is shown for neutrino masses of 1 eV with respect to the spectrum expected in the case of massless neutrinos. Figure taken from Ref. [127].

The massive experimental effort of the KATRIN collaboration recently led to the first upper limit on the effective electron antineutrino mass that falls below the eV level being $m_{\bar{\nu}_e} < 0.8 \text{ eV } c^{-2}$ at 90% C.L. [131], obtained combining the results of the first and the second neutrino-mass campaigns.

Some characteristics of tritium specified further below make KATRIN and similar experiments excellent candidates also for the search of sterile neutrino DM. In particular, the **advantages of using tritium** for this purpose are that:

- it has a short half-life of 12.3 yrs that allows for high signal rates even with low source densities (in KATRIN, the signal rate is then further enhanced by the use of a relatively large amount of tritium in the source);
- the Q-value of its β -decay, $E_0 = 18.575 \text{ keV}$, is large enough to provide access to search for sterile neutrinos in a mass range of astrophysical interest;
- the β -decay is very well known, and the simple nuclear structure of tritium makes it possible to rely on a precise theoretical description of the spectral shape.

In this context, the **signature of the presence of a sterile neutrino** that mixes with the active electron antineutrino is expected to be a kink in the spectrum at energy determined by $E_0 - m_s$, where E_0 is the Q-value of the tritium β -decay and m_s is the sterile neutrino mass. The depth of the kink instead is determined by the amplitude of the mixing between the active and the sterile neutrino, parameterized by the mixing angle θ and, more precisely, proportional to $\sin^2(2\theta)$. A simulation of the entire spectrum of tritium β -decay modified by the presence of a heavy sterile neutrino is represented in Fig. 3.2. The characteristic shape of the tritium β -decay spectrum in the presence of heavy sterile neutrinos emerges according to the following considerations. In the absence of sterile neutrinos, due to the small splittings between the three active neutrino mass eigenstates, it is not possible to resolve the three mass eigenvalues. However, if the electron antineutrino state gets a contribution also from a fourth heavier mass eigenstate ($\mathcal{O}(\text{keV})$) introduced by the existence of a sterile neutrino eigenstate that mixes with the

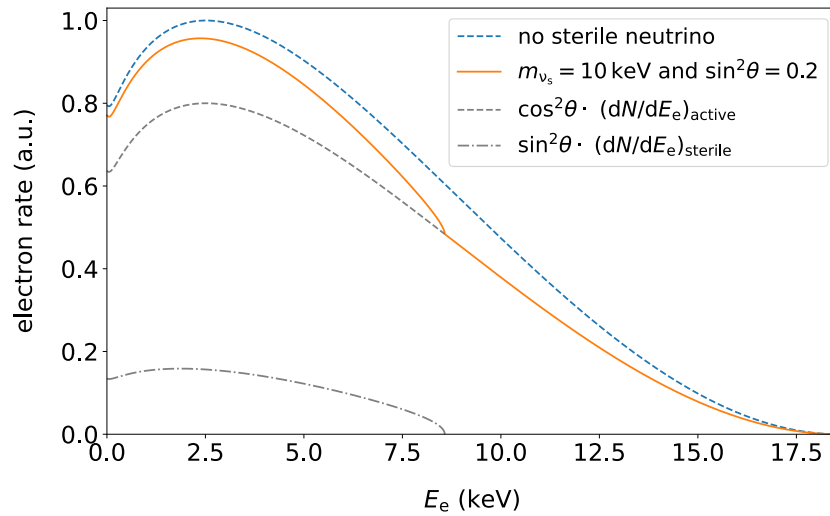


FIGURE 3.2: Signature of keV sterile neutrino in a differential tritium β -decay spectrum. The blue dashed line represents the spectrum in the absence of sterile neutrinos. The solid orange line shows the spectrum expected in case of existence of sterile neutrino with $m_s = 10$ keV and a very large mixing amplitude of $\sin^2(\theta) = 0.2$. The solid orange line results from the contribution of the active branch (gray dashed line) and the sterile branch (gray dot-dashed line). Figure taken from Ref. [132].

active ones, the different mass eigenstate form no longer one single effective mass term. In this situation, due to the large mass splitting, the superposition of the spectra relative to the light effective mass term $m_{\bar{\nu}_e}$ and the heavy mass eigenstate m_s is detectable, provided that the mixing θ between the active and sterile neutrinos is large enough. Indeed, the differential spectrum can be written as

$$\frac{d\Gamma}{dE} = \cos^2(\theta) \frac{d\Gamma}{dE}(m(\bar{\nu}_e)) + \sin^2(\theta) \frac{d\Gamma}{dE}(m_s). \quad (3.1)$$

As it is clear from Fig. 3.2, the kink in the spectrum results precisely from the superposition of the two different spectra.

In Fig. 3.3, the **experimental apparatus of KATRIN** is represented and, in the following, its **main components** are presented together with the working principle of the experiment.

In the beginning of the 70-meters long beamline, we see the **windowless gaseous tritium source** (WGTS) where molecular tritium is circled and purified in a closed loop system. The gas density profile is kept stationary, and a fraction of the T_2 molecules experiences β -decay during their flight within the source beam tube emitting the electrons whose spectrum is measured to extract effective neutrino mass and signal of sterile neutrino DM. One of the strengths of KATRIN is the high luminosity of its tritium source. Its activity reaches $\lambda_d \approx 10^{11}$ decays per second corresponding to a count rate in the detector of $\lambda_r \approx 1.5 \times 10^{10}$ counts per second. This leads to an estimated total statistics of $N_{\text{decays}} \approx 1.4 \times 10^{18}$ measured electrons after three years of measurement time. This feature is relevant for the neutrino mass measurement because only 10^{-13} β -decay electrons are produced with energy that falls within the last 1 eV of the spectrum and, therefore, to reach the optimal neutrino mass sensitivity an extremely high decay rate is needed.

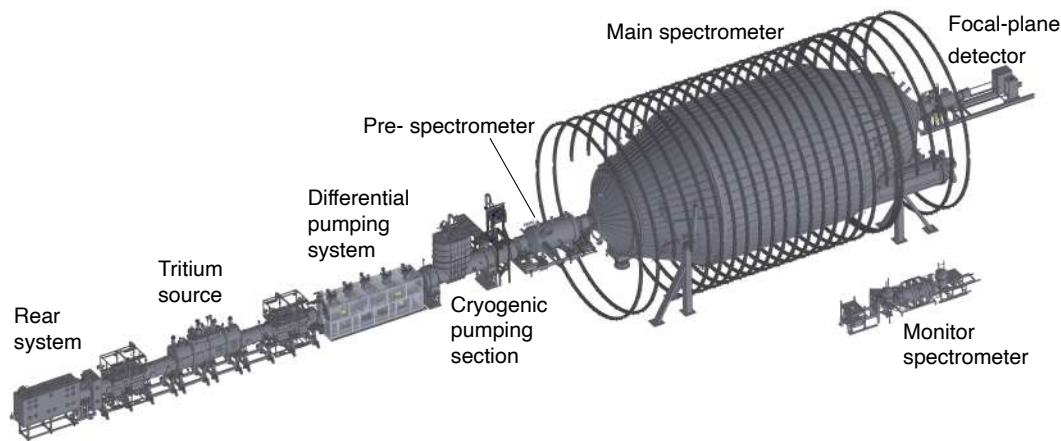


FIGURE 3.3: Engineering drawing of the KATRIN beamline, taken from Ref. [132].

The high statistic allowed by the ultra-luminous tritium source is also beneficial for the sterile neutrino DM searches if combined with the use of a new detector that can handle the great number of electrons needed to give shape to the entire spectrum [81]. The electrons emitted in the downstream direction are guided by superconducting magnets through two consecutive pumping stages, relying on different techniques, able together to reduce the flow of neutral tritium by 14 orders of magnitude from the source to the spectrometer.

This **retention system** does not involve the presence of any wall between the source and the spectrometer; this is why the source is qualified as windowless.

Further along the beamline, the electrons enter the tandem of **pre-spectrometer and main spectrometer**, where their energy is analyzed. In the most superficial view, the spectrometer is an electrostatic high-pass filter: the system is put on negative high voltage such that the electrons feel a repelling potential, and only those that have enough kinetic energy can overcome the potential barrier, they are re-accelerated, and they hit the detector at the end of the beamline. KATRIN's main spectrometer is designed according to the principle of magnetic adiabatic collimation with electrostatic filtering (MAC-E filter) in order to maximize the number of electrons analyzed, including those emitted under a large angle, up to 51 degrees. Electrons are emitted isotropically, and the emission with a non-zero angle implies that some energy (proportional to the emission angle) is stored in a transversal direction and contributes to cyclotron motion. This transversal motion does not help them to get over the potential barrier. The MAC-E filter transforms the cyclotron motion into longitudinal motion by means of a variable magnetic field between the entrance and the center of the spectrometer. This varying magnetic field aligns the momenta such that the full kinetic energy can be used and analyzed by the electrostatic field. The strengths of KATRIN's MAC-E filter are the high resolution (how sharply the energy is cut) of less than 1 eV and the large angle acceptance.

In the end, the integral shape of the energy spectrum is obtained by counting the electrons as a function of the voltage adopted for the spectrometer, i.e. the potential that sets the energy needed for the electron to pass the filter. The measured spectrum is then fitted with the model to infer the neutrino mass or to identify the signature of sterile neutrino DM. The **focal-plane detector** employed in KATRIN to reach the primary goal of measuring the antineutrino mass is a monolithic silicon p-i-n diode segmented into 148 equal-area pixels.

In addition to the main components whose names appear in Fig. 3.3 which are indispensable for the concrete realization of the measurement, the experimental setup encompasses many components that are needed for the measurement to be valuable. These are the **calibration and monitoring systems** that are located in different positions along the beamline. As for calibration, an electron gun located before the tritium source provides calibration electrons with controlled angle and energy and allows to measure the amount of gas in the source; a condensed $^{83\text{m}}\text{Kr}$ source is positioned in the cryogenic pumping section providing calibration electrons from a specific location and controlled starting potential; also the detector section is fitted with electron and photon sources for efficiency measurements and energy calibration. As for monitoring, the tritium purity of the gas injected into the source is measured by a laser-Raman spectroscopy system; a gold-plated rear wall is used to control the conditions of the source plasma better; silicon drift detectors monitor the source activity by detecting X-rays from β interactions in the rear wall, and other silicon detectors located in the cryogenic pumping section are employed to sample the β rate at the edge of the flux tube; finally, the retarding potential of the main spectrometer is monitored by a monitor spectrometer, parallel to the main one.

Beyond this concise overview, an extended technical description of the KATRIN apparatus can be found in Ref. [133].

One of the biggest challenges in using the original KATRIN experimental setup to search for keV-scale sterile neutrinos arises from the high count rates needed to measure the entire β -decay spectrum. It was shown in Refs. [134–136] that it is possible to perform a first, proof-of-principle low-statistics measurement using the present KATRIN apparatus with only minor modifications in the source and the electromagnetic design parameters. However, to use the full KATRIN source strength and obtain interesting results in this context, a **novel detector system** is required. Indeed, the 148-pixel silicon detector and the electronics and DAQ systems presently in use are not designed to deal with these electron rates [134]. The development of such new detector and read-out system is the main objective of the TRISTAN project. In order to reduce systematic uncertainties, a combination of an integral and a differential measurement mode is planned. The integral mode uses the KATRIN main spectrometer, which determines the high energy resolution of the measurement, and a detector that just counts the electrons. An extremely stable counting rate is required for this mode. In the differential mode, the spectrometer is continuously operated at low filter voltage, and the detector determines each electron's energy. Therefore, an excellent detector energy resolution and a precise understanding of the detector response even at high counting rates are required for measurement in this mode. Since the two measurement modes are affected by different systematic uncertainties, their combination allows for a powerful cross-check. Prototypes of the new detector have been constructed, and their performances in response to electrons from different sources are under test.

For what concerns the **timeline** of expected results from KATRIN/TRISTAN regarding sterile neutrino DM, as a proof of principle, KATRIN data taken in 2018 have already been used to search for keV-scale sterile neutrinos in a mass range of up to 1.6 keV, and the results have been published recently in Ref. [137].

As for the TRISTAN project, the first module has been tested; 9 modules will be installed in the KATRIN beamline in 2024, when the neutrino mass measurement is over, to explore deeper into the tritium spectrum. If it goes well, there is also the option to scale up to 21 modules.

As reported in Ref. [132], data coming from 1 year of KATRIN operation at full source

strength will reach a statistical sensitivity of the order of $\sin^2(2\theta) = 10^{-8}$. However, at this level, the control of systematic uncertainties is extremely challenging. Therefore, the **targeted design sensitivity** is $\sin^2(2\theta) = 10^{-6}$, which will exceed the sensitivity of previous laboratory-based searches and reach a region of cosmological interest. The latest estimated sensitivity of different phases of the KATRIN/TRISTAN experiment is reported in Fig. 3.4, taken from Ref. [132], together with the total measurement time for each phase. What is called "statistical limit" in Fig. 3.4 (that will appear in the

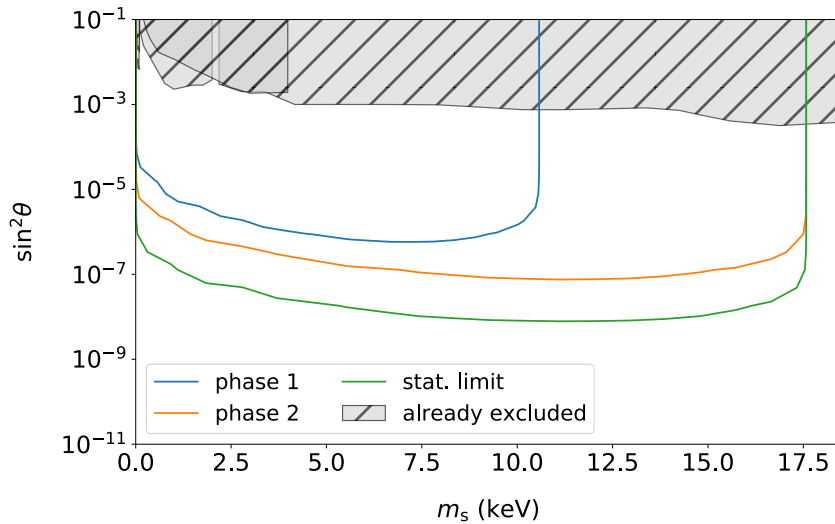


FIGURE 3.4: Sensitivity to keV-scale sterile neutrinos of the KATRIN experiment upgraded, including the TRISTAN detector in different scenarios. Phase 1 (in blue) denotes the first stage of TRISTAN operation with a reduced amount of TRISTAN modules (approx. 1000 pixels) and a lowered KATRIN source strength (0.3% of the nominal column density). The spectrum is scanned on an energy interval of (8 keV - 18 keV) with a total measurement time of $t_{\text{meas}} = 0.5$ yrs. Phase 2 (in orange) corresponds to the use of the TRISTAN detector with all 3500 pixels. The tritium spectrum is scanned on the full energy range at a reduced source activity of 2 % of the nominal column density for $t_{\text{meas}} = 1.0$ yrs. The statistical limit assumes 10^{18} electrons over the full energy range, corresponding to $t_{\text{meas}} = 1.0$ yrs at the full KATRIN source strength. The already excluded parameter space is based on Refs. [138–141]. Figure taken from Ref. [132].

following plots as "TRISTAN statistical limit") is the limit that could be reached from a purely statistical point of view assuming 10^{18} electrons over the full energy range, corresponding to a measurement time of one year at the full KATRIN source strength. Corrections that would alter this sensitivity can come both from theoretical uncertainties related to the tritium spectrum calculation and from experimental uncertainties related to the new detector energy resolution. The impact of the first ones, reduces the statistical sensitivity roughly by a factor of five [134]. The impact of experimental uncertainties, studied in Ref. [134] for the case of a differential measurement with a silicon-based detector, depends on the correlation between different systematic effects, with full (no) correlation being the best (worst) scenario for the sensitivity of the experiment, as shown in Fig. 11 in Ref. [134].

Other experiments exist, which are based on tritium β -decay and, differently from KATRIN/TRISTAN, deploy the measurement of the cyclotron radiation of the β electron, in the case of Project 8 [142, 143], or cryogenic techniques, in the case of Ptolemy [144,

145]. However, the sensitivity of such experiments to sterile neutrino dark matter is not expected to be relevant in the near-future experimental landscape, which is why they are just mentioned in this document.

3.2 ECHo

Beyond β -decay, another process that can be taken into account to look for signals of the existence of relatively heavy sterile neutrinos mixed with electron neutrinos is electron capture (EC) decay. The ECHo³ experiment [146] belongs to a class of experiments including also HOLMES⁴ and NuMECS⁵, which perform **high-resolution spectroscopy of holmium electron capture**



using low-temperature metallic magnetic calorimeters. From the formula of the process written above, we see that the daughter dysprosium is produced in an excited state. In the following, only the leading first-order excitations of dysprosium with one hole in the internal shell and one electron more in an external shell will be considered. Higher order excitations would include the presence of more than one hole in the atomic shells, and their structures would make the analysis of the spectrum more complicated, both for the determination of ν_e mass and for the identification of the signature of eventual sterile neutrinos. We can neglect such higher order excitations because they happen with a much lower probability [81].

As it is for the KATRIN experiment, the **primary goal of ECHo** is not the investigation of sterile neutrino DM but rather the determination of the electron neutrino mass that in a standard scenario can be written as

$$m_{\nu_e}^2 = \sum_{i=1}^3 |U_{ei}|^2 m_{\nu_i}^2. \quad (3.3)$$

The presence of a non-zero electron neutrino mass is expected to influence the spectrum of ${}^{163}\text{Ho}$ EC and distort it mainly close to the endpoint, as shown in Fig. 3.5 taken from Ref. [146]. For this primary purpose, ${}^{163}\text{Ho}$ is considered the best candidate among all nuclides undergoing EC processes because the extremely low energy available for the decay $Q_{\text{EC}} = 2.833 \pm 0.030_{\text{stat}} \pm 0.015_{\text{syst}}$ keV [147, 148] allows for a reasonable fraction of counts in the endpoint region of the spectrum.

Under the hypothesis that ν_e mixes with a sterile neutrino state ν_s that contributes predominantly to a fourth mass eigenstate ν_4 such that $\nu_4 \simeq \nu_s$ and $m_4 \simeq m_s$, we expect a sterile neutrino state to be emitted instead of ν_e in the ${}^{163}\text{Ho}$ EC with a probability determined by the active-sterile mixing, in particular $\propto \sin^2(2\theta)$. The emission of such sterile neutrino would distort the spectrum of ${}^{163}\text{Ho}$ EC generating a kink whose position in energy is determined by m_s as $Q_{\text{EC}} - m_s$ and whose magnitude depends on the mixing between ν_e and ν_s . This kind of **signature of heavy sterile neutrinos** can be deduced

³ ECHo is the acronym for "Electron Capture in ${}^{163}\text{Ho}$ "

⁴ HOLMES is the acronym for "Electron Capture Decay of ${}^{163}\text{Holmium}$ to Measure the Electron Neutrino Mass with sub-eV sensitivity"

⁵ NuMECS is the acronym for "Neutrino Mass via ${}^{163}\text{Ho}$ Electron Capture Spectroscopy"

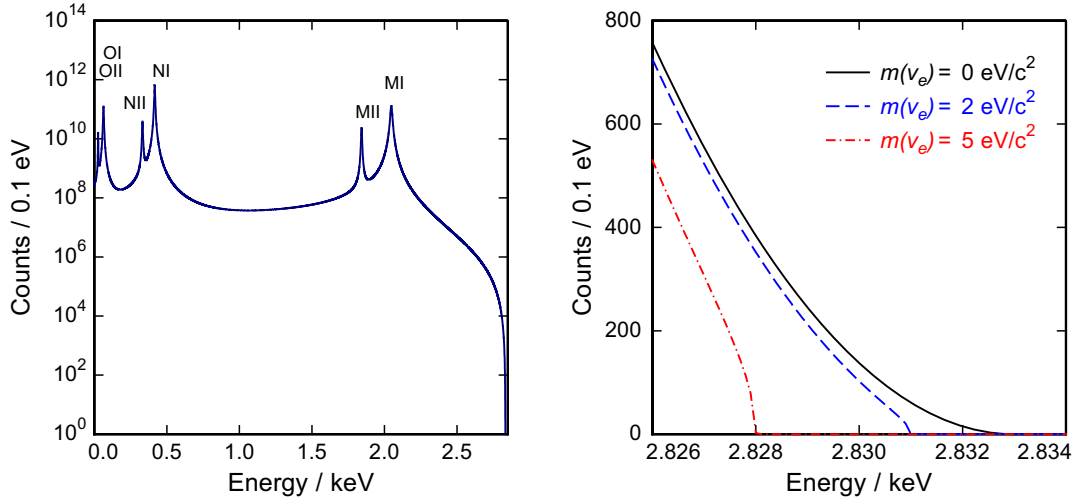


FIGURE 3.5: Left: Calculated ^{163}Ho EC spectrum for a total number of 10^{14} events using the $Q_{\text{EC}} = 2.833$ keV [147], considering only first order excitations for the daughter ^{163}Dy atom and assuming zero neutrino mass. Right: Calculated shape of the spectrum near the endpoint in the presence of neutrino masses of 0, 2, and 5 eV/ c^2 , respectively, showing the effect of a finite electron neutrino mass on a linear scale (right). Figure taken from Ref. [146].

considering the shape of the spectrum of ^{163}Ho EC [146]

$$\frac{dN}{dE} = A(Q_{\text{EC}} - E)^2 \sqrt{1 - \frac{m_{\nu_e}^2}{(Q_{\text{EC}} - E)^2}} \sum_{\text{H}} C_{\text{H}} n_{\text{H}} B_{\text{H}} \phi_{\text{H}}^2(0) \frac{\Gamma_{\text{H}}/2\pi}{(E - E_{\text{H}})^2 + \Gamma_{\text{H}}^2/4} \quad (3.4)$$

which encodes the resonances of intrinsic width Γ_{H} centered at energy E_{H} , where H is the level from which the electron is captured, with intensities given by the squared wavefunction of the captured electron calculated at the nucleus $\phi_{\text{H}}^2(0)$, corrected through B_{H} for exchange and overlap, and multiplied by the nuclear shape factors C_{H} and the fraction of occupancy of the H-atomic shell n_{H} . The phase space factor that modulates the resonances depends on the square of the electron neutrino mass $m_{\nu_e}^2$ and the energy available to the decay Q_{EC} , while A is a constant.

If we substitute in Eq. (3.4) the expression of the electron neutrino mass in the case in which it gets a non-standard contribution from the fourth neutrino mass eigenstate ν_4 that is much heavier than the active ones,

$$m_{\nu_e}^2 = \sum_{i=1}^3 |U_{ei}|^2 m_{\nu_i}^2 + |U_{e4}|^2 m_{\nu_4}^2, \quad (3.5)$$

and if we assume that the active neutrino masses are negligible with respect to m_4 , we get

$$\begin{aligned} \frac{dN}{dE} = A & \left((Q_{\text{EC}} - E)^2 (1 - |U_{e4}|^2) + (Q_{\text{EC}} - E)^2 |U_{e4}|^2 \sqrt{1 - \frac{m_4^2}{(Q_{\text{EC}} - E)^2}} \right) \\ & \times \sum_{\text{H}} C_{\text{H}} n_{\text{H}} B_{\text{H}} \phi_{\text{H}}^2(0) \frac{\Gamma_{\text{H}}/2\pi}{(E - E_{\text{H}})^2 + \Gamma_{\text{H}}^2/4} \end{aligned} \quad (3.6)$$

where the phase space between $Q_{\text{EC}} - m_4$ and Q_{EC} is reduced by the existence of a fourth neutrino mass eigenstate which is mostly sterile, and thus we can write $m_4 = m_s$. A representation of the signature that we expect to see in case of sterile neutrino with $m_s = 2$ keV and an exaggerated mixing $|U_{e4}|^2 = 0.5$ is given by the red line in Fig. 3.6 taken from Ref. [81]. We notice that the distortion of the spectrum originated by sterile

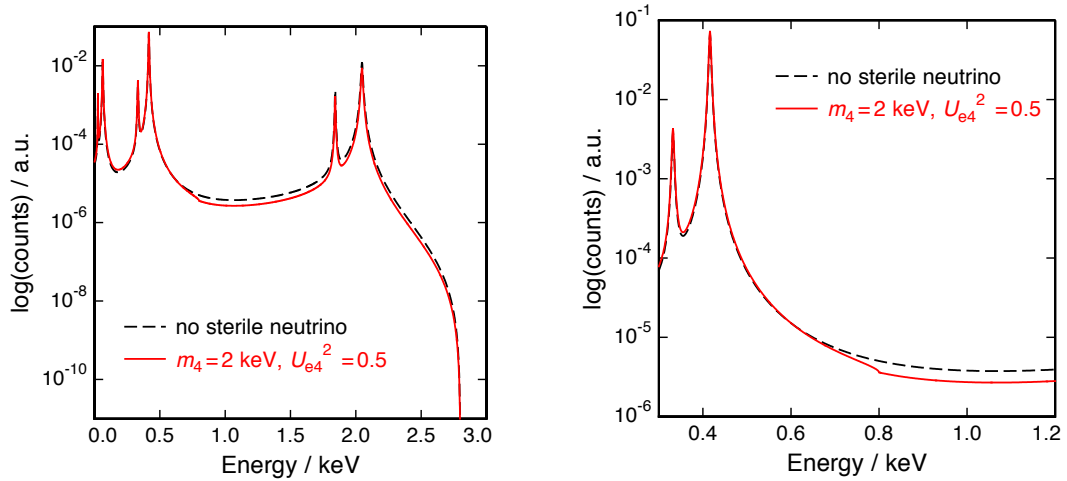


FIGURE 3.6: Expected spectrum of ^{163}Ho EC calorimetrically measured in the case of no sterile neutrino (black dashed line) and in the case of a heavy neutrino mass $m_s = 2$ keV with a mixing of $|U_{e4}|^2 = 0.5$. Entire spectrum, on the left, and magnification of the portion of spectrum presenting the kink, on the right. Figure taken from Ref. [81].

neutrinos is very small despite the large mixing angle. In order to identify it in the data, a very precise theoretical prediction for the shape of the ^{163}Ho EC spectrum is needed, together with an exceptional energy resolution of the measurements. It is not trivial to produce such a prediction, and the approach currently adopted for this purpose is the *ab initio* calculation. A more detailed discussion regarding the theoretical prediction for the spectrum of ^{163}Ho EC can be found in Refs. [149–151].

Obviously, the only sterile neutrinos that can be emitted in ^{163}Ho EC instead of ν_e are those with $m_s < Q_{\text{EC}}$. Therefore, the small Q-value of this reaction that makes ^{163}Ho the best nuclide to investigate the active neutrino mass represents a drawback in the perspective of searches for sterile neutrino signals constraining the accessible mass range to (0 - 2.8) keV. Finally, the knowledge of the Q-value of ^{163}Ho is of utmost importance not only for the investigation of the effective electron neutrino mass but also for the search for sterile neutrinos. Indeed, the position of the eventual kink representing the signature of sterile neutrinos is determined by the relation between Q_{EC} and m_s . Therefore, it is crucial to know precisely Q_{EC} to accurately determine the value of m_s from the data. In the past, there has been no agreement between values of Q_{EC} suggested by different sources: $Q_{\text{EC}} \simeq 2.8$ keV from analysis of calorimetrically measured spectra [152, 153] against $Q_{\text{EC}} = (2.55 \pm 0.016)$ keV published by the Atomic Mass Evaluation [154]. A further measurement performed with the technique of high precision Penning traps mass spectrometry strongly reduced the uncertainties giving $Q_{\text{EC}} = (2.833 \pm 0.030_{\text{stat}} \pm 0.015_{\text{syst}})$ keV [147]. An even more precise measurement (1 eV precision level) is expected to come from measurements of the masses of ^{163}Ho and ^{163}Dy with the newly developed PENTATRAP [155, 156] at the Max Planck Institute for Nuclear Physics in Heidelberg.

ECHo is an experiment located in the Kirchhoff Institute for Physics at Heidelberg University. Beyond the necessity of a good understanding of the spectral shape of the ^{163}Ho EC decay and a precise measurement of its Q-value, for successful measurement of the electron neutrino mass, there are further requirements that ECHo needs to fulfill and that oriented the choices regarding the **experimental apparatus**.

First of all, to keep at a minimal level the background in the ^{163}Ho EC spectrum deriving from contaminations in the ^{163}Ho source due to natural radioactivity and cosmic rays, a careful material screening of all the used components has been done, and an active muon veto with plastic scintillators surrounding the setup has been built and tested. Secondly, the ^{163}Ho source produced by thermal neutron activation of enriched ^{163}Er targets has been purified by chemical separation and implanted in the detectors. Moreover, the detectors need to have a good energy resolution to avoid smearing in the region of interest, and they need to have a pretty fast rise time τ_r to reduce the intrinsic background coming from unresolved pile-up events. To fulfill such requirements, metallic magnetic calorimeters (MMCs) have been chosen as detectors to be operated at temperatures below 50 mK. A detailed and precise description of the working principle of the MMCs can be found in Refs. [157, 158]. Finally, to limit the unresolved pile-up effect, a reduced activity per pixel must be combined with a large number of single detectors to be simultaneously measured and not lag behind in terms of sensitivity. The solution for this issue adopted in ECHo is a microwave SQUID⁶ multiplexing scheme to read out all the channels efficiently.

It is important to underline that the calorimetric measurement constitutes a **strength of the ECHo experiment** because intrinsic to the calorimetric measurement approach is the fact that all events occurring in the detectors give a measurable signal. Therefore, in this case, while the data needed to reach the primary goal of measuring the active neutrino mass are acquired, also the data of the entire spectrum needed for the investigation of sterile neutrinos come "for free", without the need to modify the setup.

As for the **sensitivity of the ECHo experiment** to sterile neutrino DM, two phases of ECHo are foreseen for which different sensitivities are expected [146].

ECHo-1k is a medium-scale experiment operating with the prototypes of MMC array with implanted ^{163}Ho . The sum of the activity of all the pixels in this phase was initially planned to be approximately 1 kBq, but in the end, it was reduced to 200 Bq due to problems of the single detectors in handling 10 Bq each [157]. This total activity is planned to be distributed over about 200 detectors to be read out in parallel. With a measuring time of about one year, a total statistics in the spectrum of about 10^{10} events is expected to be acquired, which would correspond to the sensitivity represented by the gray line in Fig. 3.7, taken from Ref. [146]. In this phase, the best sensitivity to detect a kink in the spectrum is expected for a heavy neutrino mass $1 \text{ keV} < m_s < 2 \text{ keV}$, which corresponds to the part of the spectrum between the M- and N-lines. In this energy range it will be possible to test the mixing element down to about $|U_{e4}|^2 = 4 \times 10^{-5}$ [146].

ECHo-1M will have a huge number of single pixels (10^5 detectors) that will need to be multiplexed, and it will have a source of the order of 1 MBq. With such an activity, it will be possible to acquire a ^{163}Ho EC spectrum shaped by 10^{14} events in one year of measuring time. The sensitivity will be improved subsequently reaching mixing elements down to $|U_{e4}|^2 \sim 4 \times 10^{-7}$ in the mass range $1 \text{ keV} < m_s < 2 \text{ keV}$, as shown by the blue line in Fig. 3.7.

For what concerns the **timeline of ECHo**, the data acquisition was completed in May

⁶Superconducting Quantum Interference Device

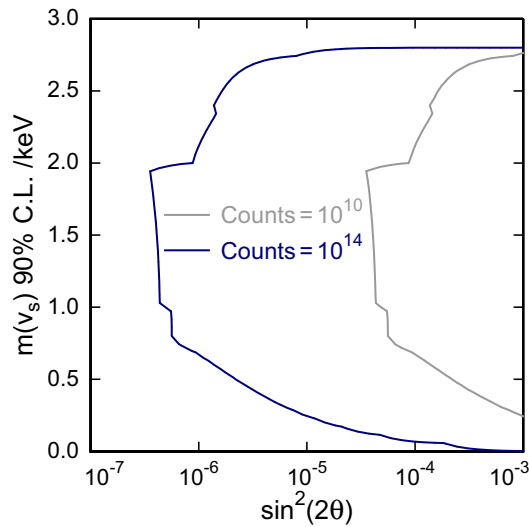


FIGURE 3.7: Expected sensitivity of ECHO to a kink in the calorimetrically measured spectrum of ^{163}Ho EC, in the case of a perfect knowledge of the expected shape of the spectrum. The gray line corresponds to the total statistics foreseen for the ECHO-1k experiment (10^{10} events), and the blue line corresponds to the best sensitivity achievable by ECHO-1M (10^{14} events). Figure taken from Ref. [146].

2020, and the data analysis is currently ongoing [158]. Currently, the production of detectors and electronics for the multiplexing readout system of ECHO-100k (an intermediate phase between ECHO-1k and ECHO-1M) is taking place. The start of ECHO-100k is expected by 2023, and three years of data taking will follow to collect sufficient statistics.

3.3 HUNTER

Another promising method for direct detection of keV sterile neutrinos in the laboratory is the complete energy-momentum reconstruction of individual electron capture events. One way to realize it is by measuring the momentum of all decay products from neutral atoms suspended in a Magneto-Optical Trap (MOT). In such experiments, keV-range sterile neutrinos would be identified as ‘missing mass’ and isolated as a separated population with respect to the active neutrinos that originate a larger peak at almost zero-missing mass.

This experimental principle was proposed originally in 1992 in Refs. [159, 160] in the context of the investigation of the active neutrino mass. Later, it was applied to K-capture in ^{37}Ar [161] and to β -decay of ^{38m}K [162] to set sterile neutrino coupling limits $\sim 10^{-2}$ in the mass range 370 - 640 keV and 0.7 - 3.5 MeV, respectively. The following years saw a fast growth of the interest of the community in sterile neutrinos that could constitute the dark matter content of the Universe. Such sterile neutrinos were expected to be lighter, $m_s \sim 5 - 10$ keV, and have much smaller mixing with the active ones, at the level of $\sim 10^{-6}$. This motivated Bezrukov and Shaposhnikov [163] to focus on the investigation of the possibility of a more precise reconstruction of tritium β -decay events, together with higher event rates, in order to reach these lower values. The task of detecting keV-scale sterile neutrinos using reconstruction techniques was recognized to be very challenging, and only recently the potential capability of this method has been studied in greater practical detail in Ref. [164].

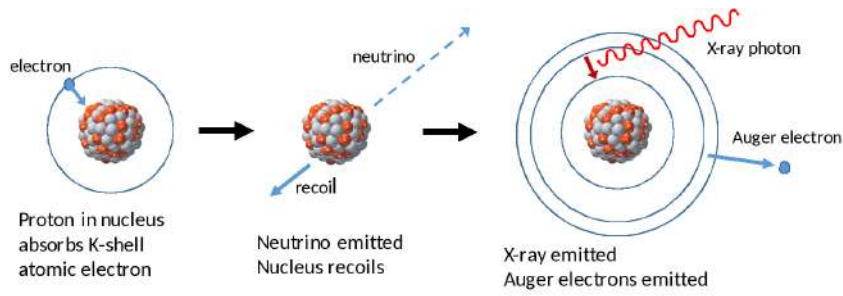
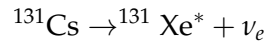


FIGURE 3.8: EC β -decay of ^{131}Cs , including the collateral emission of X-ray and Auger electron from rearrangement of the daughter nucleus.

Figure taken from Ref. [165]

The HUNTER⁷ experiment is based on this method, and it will operate the **complete energy-momentum reconstruction of ^{131}Cs K-capture**, measuring also an X-ray and several Auger electrons in addition to the atomic recoil.

In particular, the decay process



represented in Fig. 3.8 develops as follows:

1. ^{131}Cs captures an electron from the K shell and converts it into an excited ^{131}Xe atom with the emission of a neutrino. At this point, the atom that recoils and the neutrino have equal and opposite momenta;
2. the K-shell is filled from an outer shell, emitting an X-ray within < 1 ps. This causes a slight change in nuclear recoil momentum, depending on the X-ray momentum and the random isotropic emission angle;
3. one or more Auger electrons are emitted due to the further rearrangement of outer electronic shells. This alters the nuclear recoil direction by an amount that depends on the random (isotropic) direction of the vector sum of the Auger electrons, denoted by \vec{p}_a in the following.

The **working principle of this experiment** is based on the capability to measure the energies and momenta of all the particles involved in the process to extract for each event the value of the mass of the nearly mono-energetic neutrino emitted that is given by

$$m_\nu^2 = (Q_{\text{EC}} + E_a + E_\gamma + E_N)^2 - (\vec{p}_\gamma + \vec{p}_a + \vec{p}_N)^2,$$

where Q_{EC} is the Q-value of the decay, E_a and p_a are, respectively, the total energy and net momentum of one or more emitted Auger electron, E_γ and p_γ are those of the emitted X-ray, and E_N and p_N are energy and momentum of the nucleus.

Effective mass reconstruction is performed both by making use of position-sensitive detectors and by using an additional photon emitted by the decaying nuclide as time trigger for the time-of-flight determination of the recoil. For this purpose, the emission direction of the X-ray needs to be measured. Also the Auger electrons emitted in the rearrangement of atomic states need to be collected and measured. Indeed, although their kinetic energy is relatively low, they have sufficient momenta to contribute significantly

⁷ HUNTER is the acronym for "Heavy Unseen Neutrinos from Total Energy-momentum Reconstruction"

to the mass reconstruction.

A schematic representation of the expected **signature of the presence of sterile neutrino DM** is reported in Fig. 3.9 in the form of a cartoon representation and a simulated spectrum, both taken from Ref. [166].

In the absence of sterile neutrinos, each event would be consistent with an emitted

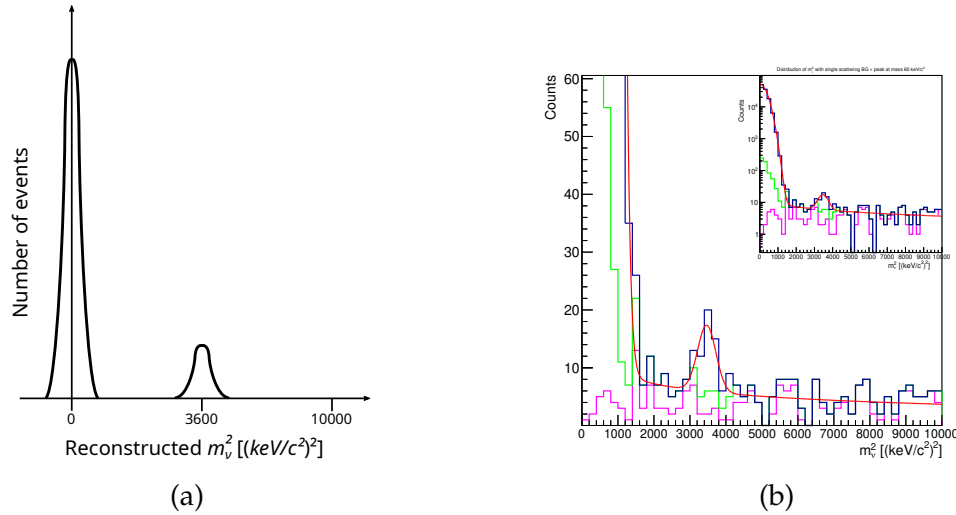


FIGURE 3.9: (a) Cartoon of the expected signature of sterile neutrino with $m_s^2 = 60 \text{ keV}^2$ in the HUNTER experiment. (b) Simulated spectrum of m_ν^2 where the red line fits the data reported in blue, including backgrounds (identified by green and magenta lines), the zero-mass peak on the left, and a hypothetical sterile neutrino mass peak. The sterile neutrino mass peak would correspond to $\sin^2(\theta) = 2 \times 10^{-4}$ and it is fitted by a Gaussian with mean of $m_s^2 = (60 \text{ keV}/c^2)^2$, based on 2.1×10^5 one-year events among which 40 sterile neutrino events would constitute a 5σ signal.

Figure taken from Ref. [166].

neutrino mass close to zero due to the smallness of the active neutrino masses, producing the big peak on the left of Fig. 3.9 (a) and (b). Actually, in principle, each neutrino mass eigenstate would originate a different peak. However, the differences in mass for active neutrinos are so tiny that the experiment cannot distinguish the three peaks. The existence of a sterile neutrino with m_s of $\mathcal{O}(\text{keV})$, which mixes with the electron neutrino produced in the decay, would result instead in a separated population of events with non-zero reconstructed missing mass (up to the Q-value $Q_{\text{EC}} = 352 \text{ keV}$, available energy of the reaction) that is represented by the smaller peak on the right. The position of this peak is determined by m_s^2 while its fractional area is determined by the active-sterile mixing and a phase space factor [160, 167].

There are at least two **advantages in EC-based searches with total energy-momentum reconstruction** with respect to β -decay searches operated, for example, by KATRIN/TRISTAN:

- the capture of all decay products is easier and possible also without an enormous apparatus that is instead needed in β -decay experiments to measure very energetic emitted electrons to the required accuracy;
- the signature of keV sterile neutrinos is expected to be clearer: as already mentioned and shown in Fig. 3.9, keV-neutrino events would manifest in a complete

kinematical reconstruction as a separated population, while in β -decay experiments they would produce a small kink in a large spectrum background.

The choice of caesium to perform this study has been made starting from the fact that there are 65 nuclides that decay by electron capture from K shell with half-lives in the range (~ 3 days - ~ 2 years). Among them, only 15 decay directly to the nuclear ground state of the preceding element, avoiding additional nuclear photons contributing to the kinematics. A further criterion for the choice is that the element can be successfully trapped in a MOT, and this reduces the list to 5 good candidates that are caesium, strontium, chromium, argon, and dysprosium. Among them, ^{131}Cs is the best.

The **advantages of using caesium** for this measurements are that:

- it has a short half-life of 9.6 days, which contributes to a high event rate, although it requires frequent replenishment of the source. Moreover, a short half-life is crucial for the possibility that the majority of the atoms decay within the trapping lifetime, originating signals and not background;
- it has a large Q-value, $Q_{\text{EC}} = 352$ keV, which allows to search in a region of the sterile neutrino DM parameter space that is complementary to those spanned by KATRIN/TRISTAN and ECHO;
- it is commercially available and affordable;
- it does not emit very penetrating radiation, and this feature makes it easy to manage from the safety point of view;
- it has one of the best prospects for achieving an MOT source containing as many as $10^8 - 10^{10}$ atoms, having been already successfully trapped in the past.

The latter point is crucial. Indeed, while the capability of separating reconstructed neutrinos with $m_s^2 \leq 100$ keV² (in the region of interest for dark matter searches) depends on the position resolution, the sensitivity to active-sterile mixing is independent of the measurement precision and depends on the number of events that can be processed. Therefore, the source atom population is among the most decisive factors that determine the region of the parameter space of sterile neutrino DM in which HUNTER will be sensitive in its different phases. The other experimental factors playing a role in determining the experimental sensitivity are the fraction of decays with accepted triggers, the solid angle capture efficiency of all decay products, and the detection efficiency for each type of particle [164].

The main components of the **experimental apparatus of HUNTER** are briefly presented in the following.

The core of Fig. 3.10, where the structure of the HUNTER setup is represented, is the Magneto-Optical Trap (MOT) which has the double function of cooling and confining target atoms via position- and velocity-dependent forces generated by the scattering of photons produced by laser beams. The working principle of this tool is explained in detail in Ref. [166]. The three pairs of oppositely directed laser beams and the magnetic field coils needed for the MOT to be operative in trapping the atoms cloud are also part of the apparatus, although they are not represented in Fig. 3.10. The same holds for the loading system that feeds the MOT from above using a push laser. The HUNTER measurement procedure is called MOTRIMS, and the use of the MOT is complemented by the use of Reaction Ion Momentum (RIM) spectrometers. These are axially-symmetric devices that use a set of planar annular electrodes surrounding the atom trap to apply a

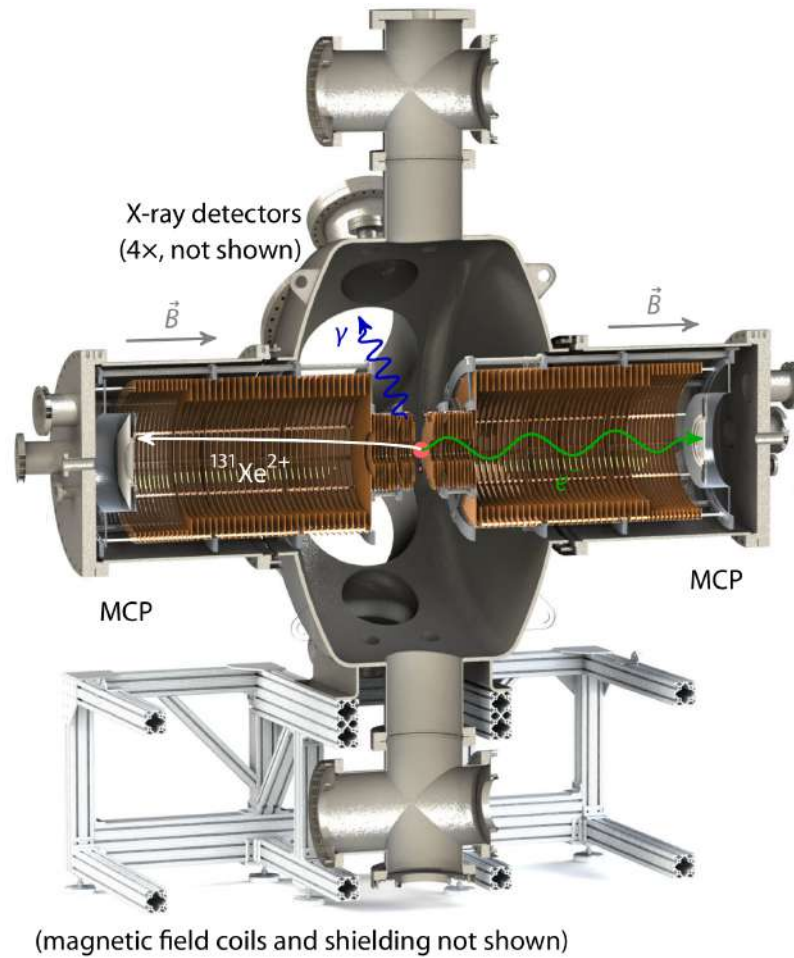


FIGURE 3.10: Cutaway elevation view of HUNTER apparatus, taken from Ref. [165].

very uniform electric field of a few V/cm to the trap region. This field is used to accelerate the ions and Auger electrons respectively to the left and to the right in Fig. 3.10 where Micro-Channel Plates (MCPs), which are position-sensitive detectors, measure the transverse momentum of the daughter atom and the Auger electrons using their radial impact position. Four position-sensitive scintillator panels arrayed azimuthally around the MOT (and not shown in Fig. 3.10) measure the momentum of atomic X-rays and provide the start signal for the measurements of the time-of-flight from source to MCP detectors of the recoil ion and the Auger electrons needed to determine their longitudinal momenta. These X-ray detectors are organized together with the ion trap so that the MOT electrodes let unobstructed lines of sight from the MOT cloud to the detectors. Finally, the last component of the HUNTER apparatus not shown in Fig. 3.10 is the magnetic shield in place to reduce ambient magnetic fields to $\lesssim 3$ milliGauss, in order to achieve the required uniform axial magnetic field for electron collection. Further technical details on the features of the components of the experimental setup and their performances, as well as on the error estimate, can be found in Refs. [164–166].

HUNTER **sensitivity to sterile neutrinos** is represented in Fig. 3.11.

The parameters originating the projection of sensitivity for Phase 1 are reported in the first column of Table 2 of Ref. [165]. Their values are based on simulations which include

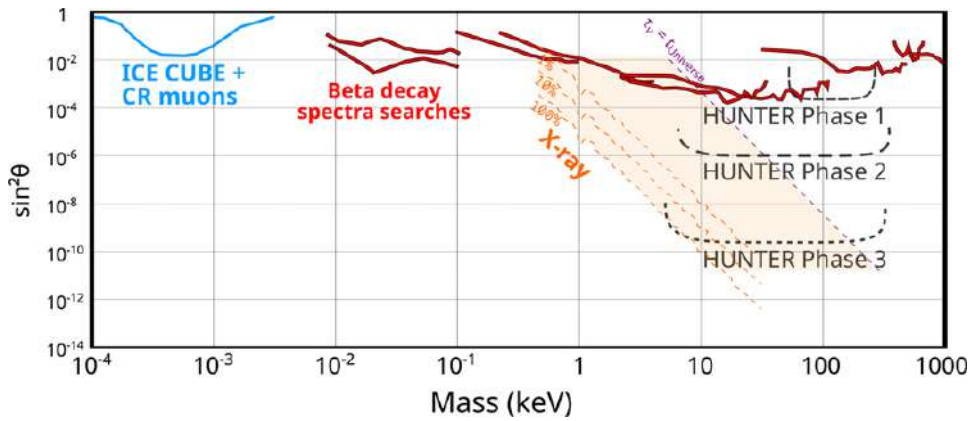


FIGURE 3.11: Thick lines represent limits on sterile neutrino coupling strength versus mass over a wide mass range: (red) beta decay searches; (blue) from IceCube. Dashed lines (orange) show astrophysical limits coming from the non-observation of X-rays expected from sterile neutrino decay in DM-dominated objects, assuming 100%, 10%, 1% of DM is constituted by sterile neutrinos of a single mass. Black dashed curves show projected HUNTER phase 1 and possible future upgrades, which would reach the sensitivity of the current astrophysical limits. Figure taken from Ref. [165].

the actual decay kinematics, charged-particle-collection efficiencies from simulations, the X-ray detector solid angle and resolutions, the manufacturer’s tabulated particle detection efficiencies for the MCPs, event reconstruction, and analysis cuts. The sensitivity expected for Phase 2 has been estimated considering an upgraded apparatus with 40 times the trap population, three times the X-ray collecting solid angle, and modest increases in electron detection efficiency thanks to the use of 150 mm MCPs, which are becoming commercially available. This results in an overall event rate increase of about 200 relative to Phase 1. Finally, to reach the expected sensitivity for Phase 3, the trapped atom population will have to be increased to 3×10^{11} ; the X-ray detection area will have to be increased to cover 60% of 4π requiring the development of accelerating electrodes transparent to X-rays; the X-ray selection efficiency would be increased eightfold by accepting events produced by K capture with M refilling and L captures. Moreover, Phase 3 would also include improved spectrometer resolution deriving from adding more MCP area, which could also allow efficient detection of events with up to three Auger electrons bringing the number of reconstructed events to almost 10^{11} per year of live time [165].

For what concerns the **timeline** of the HUNTER experiment, Phase 1 is funded and under construction and has the potential to reach sterile neutrino mixing angles down to $\sin^2(\theta) \sim 10^{-4}$ using data from 1 year of live-time (expected $\sim 1.5 \times 10^5$ events collected). The calibration of the experiment is expected for December 2022 with the subsequent start of data taking.

The sensitivity of Phase 2 and Phase 3 summarized in Table 2 of Ref. [165], is at the moment only illustrative of possible upgrades meant to increase the efficiency and reach smaller values of sterile neutrino masses. The practical realization of such upgrades is subordinate to the achievements of Phase 1.

3.4 BeEST

Another experiment exploiting the **complete energy-momentum reconstruction of individual K-captures** to look for signals of sterile neutrinos is the BeEST⁸ experiment. Its basic principle is the same as the one of the HUNTER experiment. However, the choice of a different nuclide, ⁷Be in this case, imposes the use of a different experimental setup (involving superconducting tunnel junction instead of MOTRIMS) and leads to a different expected signal and sensitivity region in the sterile neutrino parameter space (spanning primarily at the 100–1000 keV mass range).

The process on which the BeEST experiment is based is the K-capture decay of ⁷Be represented in Fig. 3.12, which has a Q-value of around 860 keV. In the 90% of cases, this process produces ⁷Li in its ground state, with no emitted X-ray, but the vacancy left by the K-capture filled with the release of a single Auger electron of known kinetic energy $E_{e,A} = 45$ eV [168].

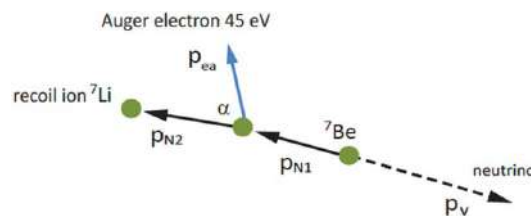


FIGURE 3.12: Representation of the K-capture decay of ⁷Be into ⁷Li, at the basis of the BeEST experiment. Figure taken from Ref. [164].

There are many **advantages of the choice of beryllium** from the point of view of the experimental setup and data analysis [164] that derive from the features of the selected process:

- ⁷Be has a very simple atomic structure;
- since there is no X-ray to be detected, there is no need for a special X-ray detector;
- the single Auger electron emitted with fixed 45 eV energy provides a time-of-flight trigger and can be collected with a large solid angle using an electric field;
- the detection of the Auger electron by Micro-Channel Plate (MCP) occurs with a time resolution of 0.3 ns and a position resolution of 40 μm ;
- the large Q-value of the reaction allows the search of sterile neutrinos with masses in a wider range, complementary to the range investigated by KATRIN/TRISTAN, ECHO, and, to a certain extent, HUNTER;
- the high Q-value and low atomic mass of the parent particle result for the daughter particle in a recoil velocity 40 times higher, and kinetic energy 100 times higher than in the case of K-capture of caesium, making the source temperature correspondingly less critical.

The efficiency of detection and data collection can be greatly enhanced (even up to 2 or 3 orders of magnitude [164]) for beryllium with respect to other nuclides, including

⁸ BeEST is the acronym for "Beryllium Electron capture in Superconducting Tunnel junctions"

caesium, thanks to the fact that for beryllium, the decay by electron capture is overall less complex. This is a crucial point for the experiment that can reach low coupling levels only by processing a sufficient number of events per year. To have an idea, to reach the coupling level $\lesssim 10^{-10}$ may require the processing of $\sim 10^{12}$ decays per year [164] and gaining 2 or 3 orders of magnitude in efficiency can make a big difference.

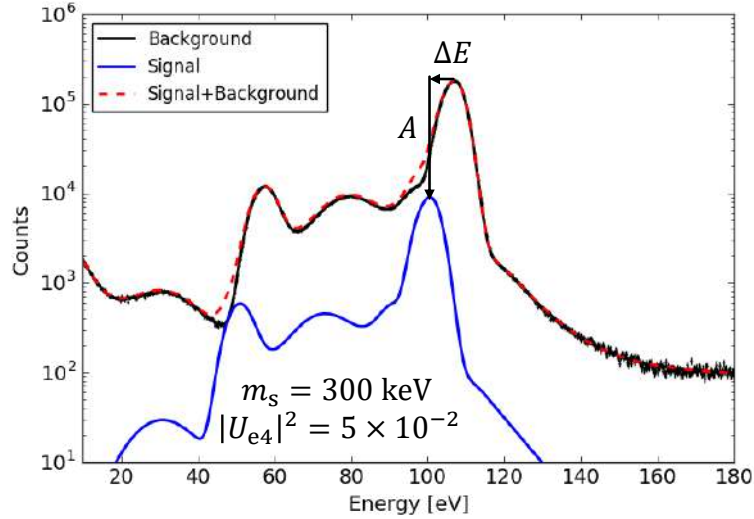


FIGURE 3.13: Simulated spectrum of the recoil of ${}^7\text{Li}$ produced in ${}^7\text{Be}$ EC. The thick black line represents the background to the search for sterile neutrinos, namely the spectrum in the case in which only electron neutrinos are emitted. The blue thick line represents the signal of the presence of a sterile neutrino with mass $m_s = 300$ keV and mixing $|U_{e4}|^2 = 0.05$. This signal has to be added on top of the standard spectrum to give the observed spectrum in the presence of sterile neutrinos, marked by the red dashed line. Figure taken from Ref. [169].

The observable measured in the BeEST experiment is the spectrum of the recoil of ${}^7\text{Li}$ emitted in the EC decay of ${}^7\text{Be}$ together with the emission of an electron neutrino. Two distinct atomic capture processes (with electron captured from K or L shell) and two nuclear states of the daughter particle (ground state of ${}^7\text{Li}$ and excited state of ${}^7\text{Li}$ at 478 keV) are possible. This results in four possible channels and a spectrum with four peaks. The expected **signature of sterile neutrino** emission instead of the standard emission of an electron neutrino is a copy of the standard spectrum overlaid on top of the SM signal, shifted towards lower energies (with ΔE depending on the value of m_s) and with smaller amplitude (A depending on the active sterile mixing that can be expressed in terms of $|U_{e4}|^2$).

In the presence of sterile neutrino, the spectrum of ${}^7\text{Li}$ recoil would be described by the function

$$f(E) = [1 - A(U_{e4})] f_0(E) + A(U_{e4}) f_0(E - \Delta E) \quad (3.7)$$

where the first term describes the active neutrino contribution plus other backgrounds, the second term describes the sterile neutrino contribution, and $f_0(E)$ is the EC spectral shape with active neutrinos in the final state.

An example of this kind of signature is shown in Fig. 3.13 where we see the standard spectrum in black while the red line shapes the spectrum generated in case of the existence of a sterile neutrino with $m_s = 300$ keV and $|U_{e4}|^2 = 0.05$.

Although beryllium presents many advantages in the perspective of detecting sterile neutrinos, it also has a non-negligible problem when it comes to trapping it. Indeed, contrary to caesium, no one ever managed to successfully trap beryllium in an MOT. This circumstance required developing a different **experimental strategy** to apply the principle of complete energy-momentum reconstruction and carry out a precision measurement of the spectrum of ${}^7\text{Li}$ nuclear recoil at an energy of about 50 eV with a resolution of < 1 eV. The solution was found in implanting ions of ${}^7\text{Be}$ into sensitive superconducting tunnel junction (STJ) quantum sensors [170]. Fig. 3.14 represents the design of a STJ used for the measurements (upper panel) and a cartoon explaining its functioning (lower panel).

The STJ is a cryogenic charge-sensitive detector; it does not measure a thermal signal but

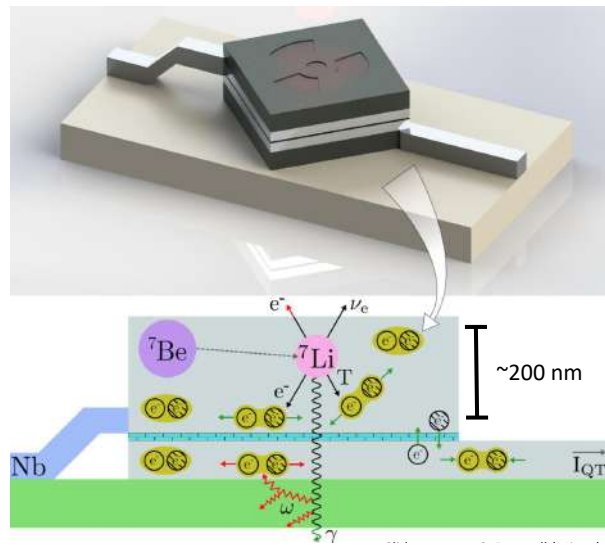


FIGURE 3.14: Schematic representation of the superconducting tunnel junction (STJ) sensor (upper panel) and cartoon explaining the functioning of the STJ (lower panel). Figure taken from Ref. [171].

a charge signal. It is a type of Josephson junction that consists of two superconducting electrodes separated by a thin tunnel barrier. The outer absorbent layer has the ${}^7\text{Be}$ embedded inside. When ${}^7\text{Be}$ decays into ${}^7\text{Li}$, the energy released breaks the Cooper pairs of the superconducting ground state inside the absorbent layer, and we have excess charge carriers. These quasiparticles can tunnel across a very thin (few nanometers thick) tunnel barrier (in aqua green in the cartoon in the lower panel of Fig. 3.14), and, on the other side, a tunneling current is read out. This tunneling current is proportional to the amount of energy deposited in the sensor. The superconducting energy gap Δ is of order meV, and this gives high energy resolution (\sim eV) and enables to distinguish the signals of the different ${}^7\text{Be}$ decay channels, including a potential signal from an admixture of heavy sterile neutrinos. The recombination time of excess charges is of $\mathcal{O}(10)$ μs . Therefore, STJs can be operated at high rates (up to 10^4 counts/s/pixel [172]) and capture a high statistics data set in realistic run times [173].

The background sources for the BeEST experiment are discussed carefully in Ref. [170].

Looking at the projected **sensitivity of BeEST** represented in Fig. 3.15 compared to the projected sensitivity of KATRIN/TRISTAN, we see that sterile neutrinos that are optimal candidates for discovery at BeEST are quite heavier than those target of KATRIN/TRISTAN.

Such heavier sterile neutrinos can be considered cold DM candidates, and we focused in

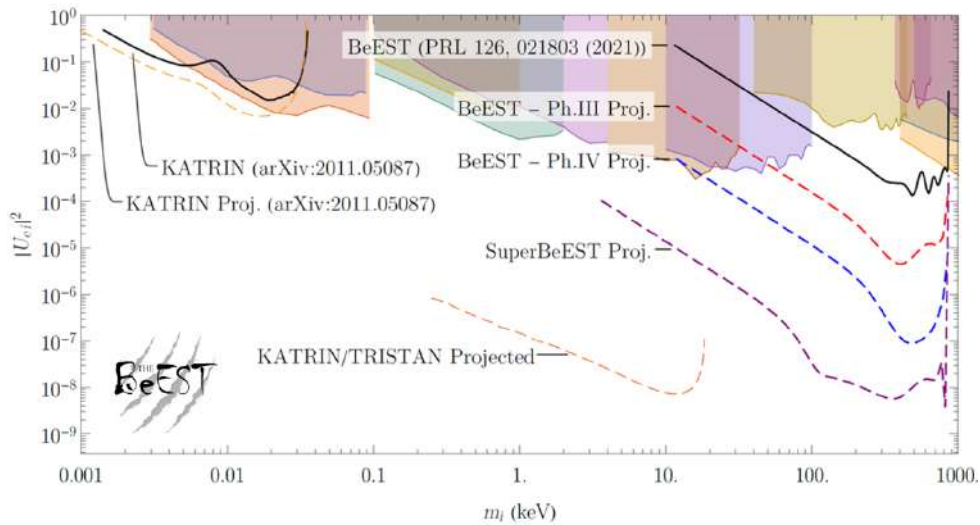


FIGURE 3.15: Current and projected sensitivity of the BeEST experiment compared to the regions already excluded by other measurements and compared to the projected sensitivity KATRIN/TRISTAN. This plot has been taken from Ref. [174].

our study on lighter sterile neutrinos that can be considered warm DM candidates and whose mass lies below 100 keV. Therefore, in the following chapters, the lines enclosing the expected sensitivity of the BeEST experiment are not shown in the plots representing the parameter space of sterile neutrinos. A further reason for this choice is that the region of expected sensitivity of the BeEST experiment in its first phases is excluded by the requirement of stability of sterile neutrinos hypothesized to constitute DM.

However, it is important to underline that, since the energy-momentum reconstruction of β -decay provides a model-independent probe of any new physics in the neutrino sector that couples to the neutrino mass, in the next years, the BeEST experiment will play a crucial role also in the search of new physics different from sterile neutrinos. One example of that is a probe of Majoron's effects.

For what concerns the **timeline of the BeEST experiment**, Phase I, meant to provide a proof of concept, has been completed in 2020, demonstrating the feasibility of high-resolution nuclear recoil detection with STJs [170]. In 2021, Phase II focused on precision calibration and provided the first limits published in Ref. [173] and reported in Fig. 3.16. Such limits are based on only 28 days of counting at a very low activity (10 counts per second per pixel instead of the 10^4 counts per second per pixel possible), using a single tantalum-based pixel. Even in these conditions, they outdo by almost an order of magnitude the other limits from laboratory searches in the mass range (100 keV, 860 keV). The following steps will be oriented to push further down in values of m_s and try to reach the 10 keV region. In this region, the sensitivity is limited by the resolution broadening of the sensor due to chemical shifts that result from embedding the beryllium into a solid matrix. In this respect, studies are going on with the goal of modeling those energy shifts to get a handle on this broadening.

The BeEST experiment is now in its Phase III, which involves theoretical modeling of the resolution broadening both from an atomic and a material standpoint and a scaling from one pixel to 36 pixels. After Phase III, Phase IV is forecast to operate until 2025 with 128-pixel arrays of aluminium-based STJs, which have a higher resolution and will count at a much higher rate. In its Phase IV, within the next three years, the BeEST experiment

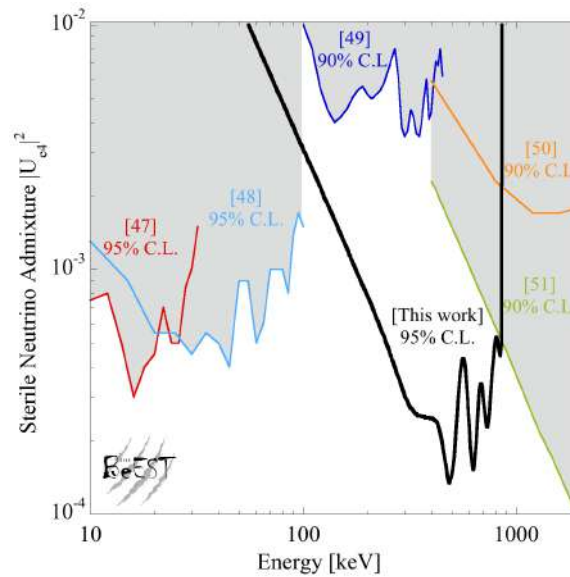


FIGURE 3.16: First limits from the BeEST experiment published in Ref. [173]. They are represented in the typical parameter space of sterile neutrino DM, where the energy corresponds to the mass parameter m_s , while the sterile neutrino admixture is associated with the mixing angle $\sin^2(2\theta)$.

is expected to reach sensitivity to couplings as small as 10^{-7} in the few-hundreds keV mass range. Following Phase IV, a further improvement in sensitivity is planned using large arrays (10^4 pixels) of STJs with new materials whose development is ongoing with the goal to probe couplings down to $|U_{e4}|^2 \leq 10^{-9}$ [174]. The final limits from the BeEST experiment will result from a 128-pixel aluminium-based STJ array counting at 10^3 counts/sec/pixel for 100 days [172].

3.5 Challenges of the "Vanilla" Dodelson-Widrow Scenario in the Perspective of Sterile Neutrino DM Detection

The "vanilla" Dodelson-Widrow mechanism is undoubtedly very fascinating because of its simplicity. Indeed, the only requirement for it to be active is that sterile neutrinos mix with one or more species of active neutrinos. This thing is automatic, for example, in the framework of the type-I seesaw mechanism. However, when it comes to the possibility of detecting in terrestrial experiments sterile neutrino DM produced in this way, this mechanism faces at least two major challenges: the problem of overproduction and the X-ray bound.

Such limitations are evident if we consider the typical parameter space of sterile neutrino DM where, in the simplest scenario, the only two relevant parameters are the active-sterile mixing expressed in terms of $\sin^2(2\theta)$ and the sterile neutrino mass m_s . This parameter space is represented in Fig. 3.17 where we see on the right the dashed lines marking the sensitivity regions of KATRIN/TRISTAN (gray), ECHo (blue), and HUNTER (beige).

The purple line disfavors the region on its right based on non-observation of any monochromatic line in the X-ray band that would be expected to come from sterile

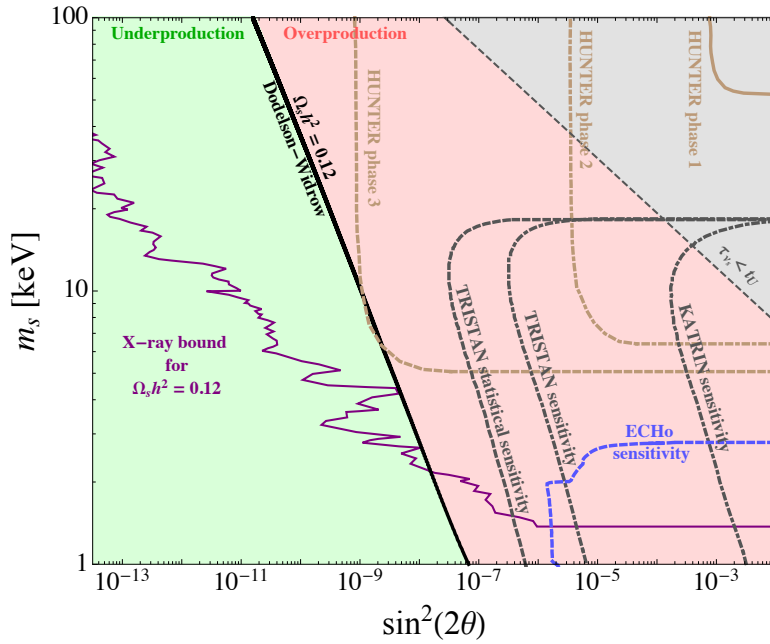


FIGURE 3.17: Typical parameter space of sterile neutrino DM. Dashed lines circumscribe the sensitivity regions of KATRIN/TRISTAN (gray), ECHO (blue), and HUNTER (beige). Black thick line represents values of $\sin^2(2\theta)$ and m_s for which the condition $\Omega_s h^2 = \Omega_{\text{DM}} h^2 = 0.12$ is satisfied if sterile neutrinos are produced through DW mechanism. The purple line represents the limit from X-ray observations, and it is given by a combination of lines reported in Refs. [94, 95, 115].

neutrino DM decay at the radiative level. This constraint can be relaxed in a number of ways as discussed in Subsections 2.2.6, 2.2.7 and 2.2.8 based on Refs. [2] and [125]. Such relaxation of the X-ray bound is crucial for the detection perspective in terrestrial experiments because, in some cases, it can make accessible again the region in which experiments will be sensitive to sterile neutrino DM.

The black thick line corresponds to the couples of values of $\sin^2(2\theta)$ and m_s that give $\Omega_s h^2 = \Omega_{\text{DM}} h^2 = 0.12$ in the case that sterile neutrino DM is produced exclusively through oscillation and collisions via DW mechanism. The challenge here is that there is only minimal overlap between this black line and the sensitivity region of HUNTER, while the black line lies quite far from both the sensitivity regions of KATRIN/TRISTAN and ECHO. For the latter experiments to have any chance to detect sterile neutrino DM, much larger mixing angles are required that in the DW framework would result in overproduction of sterile neutrinos: for larger mixing angles, the energy density of sterile neutrino DM would exceed the observed energy density of DM in the Universe. Chapters 4 and 5 are devoted to presenting the work done to investigate how this limitation is lightened in the case of sterile neutrino DM produced through oscillations and collisions but in non-standard scenarios. In particular, we will see how large mixing angles do not constitute a problem in non-standard cosmological scenarios in which the start of the production of sterile neutrino dark matter is delayed until the Universe reaches a relatively low critical temperature (Chapter 4) and in the case in which active neutrinos are subject to further non-standard interactions among each other (Chapter 5). Indeed, in both cases, the black line corresponding to the condition $\Omega_s h^2 = \Omega_{\text{DM}} h^2 = 0.12$ gets shifted towards the right side of the parameter space.

Chapter 4

Sterile Neutrino Dark Matter in Non-Standard Cosmological Scenarios

In this chapter, we consider the freeze-in production of sterile neutrino dark matter through oscillations and collisions in three different variants of the production mechanism. We examine the "vanilla" Dodelson-Widrow [35] non-resonant production, the standard Shi-Fuller [42] resonant production, and the modified Shi-Fuller production in which the occurrence of CPT violation in the sterile neutrino sector combined with the primordial lepton asymmetry suppresses the production of sterile neutrino dark matter. We study how these three scenarios and their detection perspectives are modified in case of non-standard cosmological histories preceding Big Bang Nucleosynthesis. The code used to solve the Boltzmann equations numerically, calculate the sterile neutrino dark matter abundance, and produce all the plots representing our results of this chapter and published in Ref. [2], was written from scratch in the Mathematica package specifically for this purpose and is now publicly available at the link <https://github.com/cristinabenso92/sterile-neutrino-in-non-standard-cosmology>.

4.1 Details of the Particle Model

In this chapter, assuming as standard starting point the modified SM in which all three active neutrinos have non-zero mass, we extend it to **include a sterile neutrino ν_s that is a Dirac particle** and can play the role of DM. To do that **we add a fourth neutrino mass eigenstate $\nu_4 = \sin \theta \nu_a + \cos \theta \nu_s$** which is a superposition of the active flavor eigenstates ν_a and sterile eigenstate ν_s .

To keep the formalism simple and focus on the phenomenology, we consider the mixing of the sterile neutrino species with only one active neutrino flavor, chosen to be the electron flavor. The choice of the first generation of leptons for mixing with the sterile neutrino is motivated by the features of the upcoming experiments in the landscape of sterile neutrino searches introduced in Chapter 3. All of them will operate with β -decay and electron capture; therefore, they will be sensitive to the mixing of sterile neutrinos with ν_e and not with ν_μ or ν_τ . Finally, unless this is prohibited by some exceptional condition, as it is in the case of CPT violation discussed in Subsection 4.4.3, sterile antineutrinos are assumed to be dark matter as well, and they are assumed to mix with active antineutrinos $\bar{\nu}_e$ with the same strength with which sterile neutrinos mix with ν_e .

4.2 Non-Standard Cosmological Scenarios and Critical Temperature T_c

The standard history of the Universe that is usually assumed begins with the Big Bang followed by a period of exponential expansion called inflation and driven by the inflaton field. During this period, the spacetime is stretched, the curvature of the Universe is reduced, and the abundances of any species produced in the Big Bang are tremendously diluted. At the end of inflation, the inflaton is assumed to decay into lighter degrees of freedom which are the particles described by the standard model, and in this way the Universe is populated again and its temperature is enhanced due to the injection of this new radiation up to what is called reheating temperature T_{RH} . The value of the reheating temperature depends on the considered model of inflation and reheating and it is defined as [175]

$$T_{\text{RH}} \simeq 0.2 \left(\frac{200}{g_*} \right)^{1/4} \sqrt{\Gamma_\phi M_{\text{Pl}}},$$

where g_* is the number of relativistic degrees of freedom, Γ_ϕ is the decay rate of the inflaton and M_{Pl} is the Planck mass. Despite the variability induced by the arbitrary choice of the model for inflation, T_{RH} is typically assumed to fall in the range $(10^8 - 10^{10})$ GeV. After reheating, the Universe consists in a dense and hot plasma constituted by the SM particles that interact among each other and cool down due to the expansion of the spacetime that goes on at a much lower rate compared to the one during inflation. Since at very high temperatures the particles in the plasma are relativistic because their energy is dominated by their momentum rather than by their mass, we say that in this period the Universe is radiation-dominated. Due to the different dependence of the energy density of radiation, matter and cosmological constant on the scale factor of the Universe, these three components contribute differently in different periods of the evolution of the Universe. Therefore, the phase of radiation domination is followed by a phase of matter domination and finally by a phase of domination of the cosmological constant. The subsequent milestones of standard cosmology after reheating are the electroweak phase transition (EWPT), occurring at $T_{\text{EW}} \sim 150$ GeV in which the SM particles get mass through the Higgs mechanism, the QCD phase transition, occurring at $T_{\text{QCD}} \sim 150$ MeV, the Big Bang Nucleosynthesis (BBN) starting at $T_{\text{BBN}} \sim 1$ MeV, and the CMB decoupling at the time of recombination $T_{\text{rec}} \sim 0.3$ eV.

Although the standard cosmological framework described above is the one that is typically assumed, this choice is not really justified by observations for temperatures higher than T_{BBN} . Given that the detection technology for primordial gravitational waves is still under development, to date **the abundances of light elements produced during BBN are the earliest probe available regarding the early Universe**. This means that **the assumptions on the value of the reheating temperature rely on purely theoretical conjectures**. The only experimental constraint on the reheating temperature is a lower bound requiring $T_{\text{RH}} > 4$ MeV in the most general case [176], based on combined data of light elements abundance measurements, CMB, and large scale structures.

Another arbitrary but usual decision regarding the cosmological history before BBN is to neglect the possibility of other events involving a hidden sector that can be related to the active one by sterile neutrinos acting as a portal. Such events would possibly not conflict with any other observation regarding the active sector, due to the features of the hidden sector, and therefore their occurrence is not excluded by data.

An important point to remember here is that **the mechanism through which active**

neutrinos gain mass is still shrouded in mystery as well as the eventual dynamical evolution of these parameters along the history of the Universe.

For example, it is well possible that sterile neutrinos get mass as a consequence of a **phase transition** in the already mentioned hidden sector. This phase transition would not have anything to do with the electroweak one and could have happened at a temperature below T_{EW} . Considering the Lagrangian of a hidden scalar ϕ that breaks the symmetry in the hidden sector [97]

$$\mathcal{L} = \frac{f}{2} \phi \bar{\nu}_s^c \nu_s + \text{h.c.} \quad (4.1)$$

where f is its coupling to ν_s , in the very early Universe sterile neutrinos could have had $m_{s,\text{early}} = 0$ as long as the symmetric phase lasts, and after the symmetry breaking they could have got $m_s = f\langle\phi\rangle \sim \text{keV}$, where $\langle\phi\rangle$ is the VEV of ϕ .

Another possibility is that the sterile neutrino mass in the very early Universe is given by $m_{s,\text{early}} = m_s + M_{s,i}$ where $m_s \sim \text{keV}$ is its today's value of the sterile neutrino mass and $M_{s,i} = g\Phi_i \gg m_s$. The second contribution to $m_{s,\text{early}}$ could arise from a kind of **misalignment mechanism** thanks to the coupling of ν_s to a massive scalar Φ whose dynamics is described by the Lagrangian [97]

$$\mathcal{L} = \frac{1}{2}(\partial\Phi)^2 - \frac{1}{2}m_\Phi^2\Phi^2 + \frac{g}{2}\Phi\bar{\nu}_s^c\nu_s + \text{h.c.} \quad (4.2)$$

where g is the coupling between Φ and ν_s and m_Φ is the mass of Φ . Φ_i is the initial value of the scalar field Φ that can in principle be very large and is kept constant by the Hubble friction in the hot Universe. When the Hubble rate drops below the scalar field mass, Φ starts to oscillate with decreasing amplitude and, as a consequence, also the scalar contribution to the sterile neutrino mass drops and becomes negligible leaving only the bare mass $m_s \sim \text{keV}$.

Each of the three non-standard cosmological scenarios introduced above could be associated to a new energy scale in the early Universe, that is the scale at which the non-standard events happen, that we will call **critical temperature** T_c in the following. Such critical temperature can be taken as the temperature that **marks the start of the production of sterile neutrinos that is instead suppressed at temperature $T > T_c$ due to the specific features of each non-standard cosmological scenario.**

Indeed, in the case in which T_c is associated to a low T_{RH} , the Universe was never hot enough to produce sterile neutrinos at temperatures higher than T_c .

In the case in which T_c is related to the scale of a dynamical change of the sterile neutrino mass, it is possible to see that the production is suppressed by looking at the definition of the mixing angle in matter in the following parameterization [97]

$$\sin^2 2\theta_M = \frac{m_D^2}{m_D^2 + [c\Gamma_a E/m_{s,\text{early}} + m_{s,\text{early}}/2]^2}$$

where m_D is the Dirac mass that comes from the EW symmetry breaking, $c \approx 63$, and $\Gamma_a \approx 1.27 G_F^2 T^4 E$ is the active neutrino interaction rate in the plasma. In both cases in which $m_{s,\text{early}} = 0$ (phase transition) or $m_{s,\text{early}}$ very large (misalignment mechanism), $\sin^2 2\theta_M$ is suppressed and the production of sterile neutrinos is inhibited, since it is proportional to $\sin^2 2\theta_M$.

In the standard Dodelson-Widrow mechanism, the production of sterile neutrinos has a peak $T_{\text{peak}} \simeq 133(\frac{m_s}{\text{keV}})^{1/3} \text{ MeV}$ [35]. If the temperature T_c at which the production starts

in the mentioned non-standard cosmological scenarios is lower than T_{peak} , larger values of the active-sterile mixing angle in vacuum θ are required to compensate the delay in the production and produce enough sterile neutrinos. This Chapter 4 is devoted to the description of the modification of sterile neutrino production in this specific case and through different production mechanisms.

4.3 "Dark Matter Cocktail" with Sterile Neutrinos produced through Dodelson-Widrow Mechanism

In order to describe what we call "ordinary matter" the entire standard model of particle physics is needed, which includes a number of stable and unstable fermionic matter fields, gauge bosons and the Higgs boson, organised in a non-trivial way. Therefore, it is reasonable to admit that a similar situation could occur also in a dark sector partially isolated or completely secluded from the standard model sector. In this scenario, the stable particles of this dark sector could play the role of dark matter and a various "cocktail" of dark matter candidates could be at work in our Universe producing the observational large scale evidences that puzzle us.

In this section, we take the "dark matter cocktail" as working hypothesis. In the following, we explore how the parameter space of sterile neutrinos does change if we assume them to constitute only the 10% or the 1% of the entire DM content of the Universe and to have been produced through the standard Dodelson-Widrow mechanism starting at different values of critical temperature T_c .

As already discussed in Section 2.1 of Chapter 2, the Boltzmann equation describing the evolution of $f_s(p, T)$ in the Dodelson-Widrow scenario can be written as

$$\begin{aligned} \frac{\partial}{\partial T} f_s(p, T) + \left[\frac{1}{T} + \frac{1}{3} \frac{g'_{*s}(T)}{g_{*s}(T)} \right] p \frac{\partial}{\partial p} f_s(p, T) = - \frac{1}{H(T)} \left[\frac{1}{T} + \frac{1}{3} \frac{g'_{*s}(T)}{g_{*s}(T)} \right] \times f_s(p, T) \times \\ \times \frac{\Gamma_\alpha(p, T)}{4} \frac{\Delta^2(p) \sin^2(2\theta)}{\Delta^2(p) \sin^2(2\theta) + D^2(p) + [\Delta(p) \cos(2\theta) - V^D(T) - V^T(p, T)]^2} \end{aligned} \quad (4.3)$$

Its solution derived in Appendix B following [39] is

$$\begin{aligned} f_s(p_f, T_f) = - \int_{T_i}^{T_f} \sqrt{\frac{90}{8 \pi^3 g_{*s}(T)}} \frac{M_{Pl}}{T^3} \left(1 + \frac{T}{3} \frac{g'_{*s}(T)}{g_{*s}(T)} \right) \frac{1}{\exp\left(\frac{p_f}{T}\right) + 1} \times \\ \times \frac{\Gamma_e(p_r, T)}{4} \frac{\Delta^2(p_r) \sin^2(2\theta)}{\Delta^2(p_r) \sin^2(2\theta) + \frac{\Gamma_e(p_r, T)^2}{4} + [\Delta(p_r) \cos(2\theta) - V^D(T) - V^T(p_r, T)]^2} \end{aligned} \quad (4.4)$$

where for the sake of brevity $p_r = \frac{T}{T_f} \left(\frac{g_{*s}(T)}{g_{*s}(T_f)} \right)^{1/3} p_f$ is the redshifted momentum, $V^D(T)$ is the finite density potential in absence of lepton asymmetry, and $V^T(p_r, T)$ is the thermal potential.

The impact on the final sterile neutrino abundance of the introduction of the critical temperature occurs through the modification of the parameter named T_i in Eq. (4.4) that is the temperature at which the production of sterile neutrinos starts.

In the standard cosmological scenario, a convenient choice for the value of T_i is 10 GeV. Indeed, for $T > 10$ GeV the production of sterile neutrinos is naturally damped by the dependence on the temperature of the denominator of $\sin^2(2\theta)$ reported in Eq. (2.8), and to set $T_i > 10$ GeV would imply just more numerical power used to get the same result for the parameter $\Omega_s h^2$.

In non-standard cosmological scenarios, $T_i = T_c$ and it can be as low as 4 MeV [97, 176].

Based on such considerations, we wrote from scratch a code in the Mathematica package that is now publicly available¹ and we used it to solve the Boltzmann equation under the hypothesis of different values of the critical temperature. The results are presented in the following.

For what concerns the peculiarity of the "DM cocktail" scenario, since today's abundance of sterile neutrinos is $\Omega_s h^2 \propto f_s(p, T) \propto \sin^2(2\theta)$, smaller abundance of sterile neutrino corresponds to smaller values of the mixing angle θ needed to produce it.

As already disclosed in Subsection 2.2.6 of Chapter 2, the requirement that only a fraction of $\Omega_{\text{DM}} h^2$ is constituted by sterile neutrinos modifies also the X-ray bound. In this conditions, this limit gets considerably relaxed towards the right side of the parameter space and leaves free and accessible again larger values of the active-sterile mixing angle in vacuum.

Another noticeable point about the "DM cocktail" scenario is that on the one hand it is in general less constrained also from the point of view of structure formation and other observational limits because the rest of dark matter could take shapes useful to lighten the requirements for sterile neutrinos. On the other hand, the reduced abundance of every dark matter candidate contributing to the total budget makes things more difficult in the perspective of direct detection reducing the chances to reveal them.

Figure 4.1 represents quantitatively the above considerations together with the sensitivity regions of the experiments mentioned in Chapter 3. The lines marking the sensitivity regions of KATRIN have been taken from Ref. [128]. "KATRIN sensitivity" results from an integral measurement with much reduced (by a factor 10^6) source strength and 7 days of data taking, corresponding to 6×10^{11} electrons. "TRISTAN sensitivity" denotes the sensitivity resulting from a differential measurement using the novel detector with 3 years of data taking, corresponding to 10^{16} electrons with a reduced source strength by a factor 100. "TRISTAN statistical sensitivity" corresponds to the sensitivity reachable with 3 years of data taking deploying the full strength of the source. The sensitivity of the ECHo experiment reported in Figure 4.1 corresponds to the anticipated final stage of the experiment when it will be possible to acquire around 10^{14} events in the ^{163}Ho spectrum in a single year [177]. The strongest sensitivity is achieved for $m_s \simeq 1 - 2$ keV and $\sin^2(2\theta) \simeq 10^{-6}$. Finally, the sensitivity lines of the HUNTER experiment refer to its Phase 1, currently under construction, and two possible future upgrades with increased event rate (by a factor of 200 with respect to phase 1 for Phase 2, and to almost 10^{11} per year of live time for Phase 3) [165].

The gray triangle in the upper right corner of each plot in Fig. 4.1 marks a region of the parameter space that is ruled out by the requirement that keV sterile neutrinos are stable over time scales comparable with the age of the Universe, to be able to play the role of DM today. The derivation of the line limiting this region can be found in Subsection 2.2.4 in Chapter 2.

¹<https://github.com/cristinabenso92/sterile-neutrino-in-non-standard-cosmology>

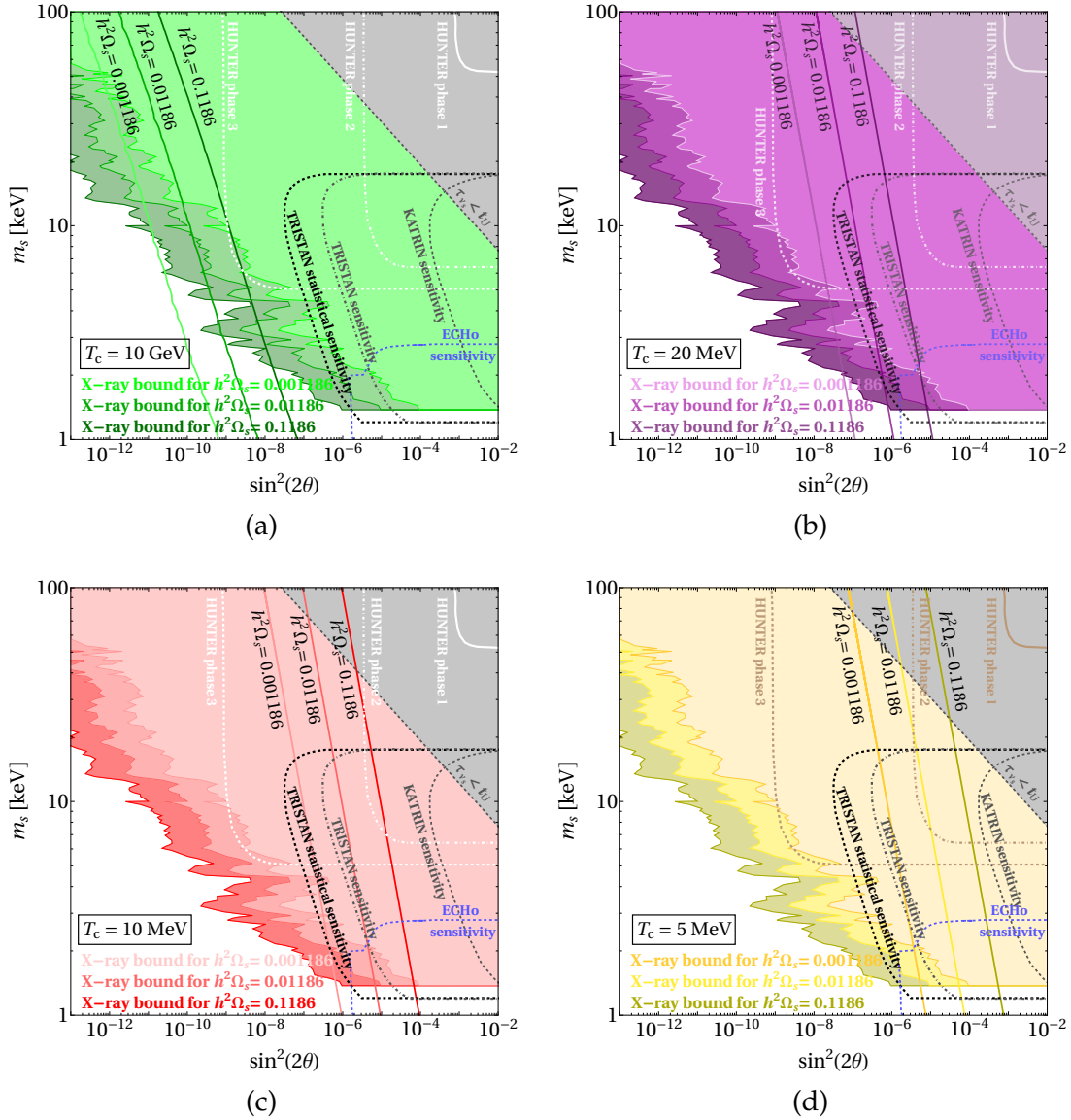


FIGURE 4.1: The colored regions in all panels show the X-ray constraints [94, 95, 115] for the indicated contributions of sterile neutrinos to the total DM density distinguished in each panel by different shades of the same color. The straight lines show the parameter space where the indicated amount of DM is produced via the Dodelson-Widrow mechanism below a critical temperature that is different in each panel and written in the black box. We also show Hunter, [165], KATRIN/TRISTAN [128], and ECHO [177] sensitivity for testing keV-scale sterile neutrinos as well as the constraint on sterile neutrino lifetime (gray-shaded region), arising from its main decay channel into three active neutrinos. By comparing X-ray constraints and respective lines for the DM production, and by focusing on the regions where the experiments will be sensitive, one can infer that for $\Omega_s h^2 = 0.12$ and $\Omega_s h^2 = 0.012$ only very marginal parameter space is testable for $T_c \lesssim 20$ MeV. On the other hand, if sterile neutrinos represent 1% of DM, KATRIN/TRISTAN is sensitive to $m_s \simeq 2$ -3 keV, region in which X-ray bounds are typically evaded; in such case T_c should not exceed $T_c \simeq 10$ MeV in order to have the scenario testable in KATRIN/TRISTAN and ECHO, while it should be $10 \text{ GeV} > T_c > 20$ MeV for HUNTER phase 3.

The four panels of Fig. 4.1 reproduce the typical parameter space of sterile neutrino DM in four different cosmological scenarios, namely four values of the critical temperature $T_c = 10 \text{ GeV}, 20 \text{ MeV}, 10 \text{ MeV}$ and 5 MeV (from top left to bottom right). The first case clearly corresponds to the "vanilla" Dodelson-Widrow scenario, while in the remaining ones DM production is delayed to lower temperatures. Different colors correspond to different values of T_c , while different shades of the same color correspond to different fractions of the total Ω_{DM} constituted by sterile neutrinos. In each panel, we observe how the straight lines representing the abundance of sterile neutrinos place more and more towards smaller values of the mixing angle as we impose the conditions $\Omega_s h^2 = 100\% \Omega_{\text{DM}} h^2, 10\% \Omega_{\text{DM}} h^2$, and $1\% \Omega_{\text{DM}} h^2$. For the same decrement in the required abundance of sterile neutrino DM we observe a shift of the X-ray bound that gets relaxed in the opposite direction, towards larger values of the mixing angle. For $T_c = 10 \text{ GeV}$ (panel (a)), $\Omega_s h^2 = 0.12$ is in clear tension with the X-ray bound in a vast portion of parameter space. The situation improves upon assuming that sterile neutrinos represent only a subdominant component of DM. Still, the compatibility between DM production and the absence of X-ray limits occurs only in the parameter space that is far away from KATRIN/TRISTAN sensitivity. This changes as expected if we lower T_c towards MeV-scale values. In particular, the effect of the critical temperature is evident in all remaining cases shown in panels (b), (c), and (d). The interesting region, in which KATRIN/TRISTAN and ECHO will be sensitive, is intersected by $\Omega_s h^2 = 0.12$ curves; however, these regions are chiefly disfavored by X-ray limits that are still too strong in case that sterile neutrinos account for all the DM in the Universe. The $\Omega_s h^2 = 0.1 \times 0.12$ lines also intersect KATRIN/TRISTAN sensitivity curves but the X-ray bound still poses a problem, even upon relaxation. The viable range of masses for $\Omega_s h^2 = 0.01 \times 0.12$ is $m_s = 2 - 3 \text{ keV}$, but in this scenario KATRIN/TRISTAN and ECHO will be sensitive only for $T_c \lesssim 10 \text{ MeV}$. On the other hand, a small region of the parameter space will be accessible by searches with HUNTER phase 3 in case of $\Omega_s h^2 = 0.01 \times 0.12$ and $10 \text{ GeV} > T_c > 20 \text{ MeV}$. In general, we conclude that HUNTER, KATRIN/TRISTAN and ECHO have all limited probability to discover sterile neutrino DM in our "DM cocktail" scenario provided T_c is low enough and sterile neutrinos contribute only marginally to DM. As a final remark, we compared these results with those presented in Fig. 3 of Ref. [97] where the authors made similar claims. In particular, they also find that the consistency with X-ray limits can be achieved in the cocktail scenario. Moreover, they identified that, for $\Omega_s h^2 = 0.12$, the aforementioned $m_s \lesssim \mathcal{O}(1) \text{ keV}$ range is viable. As stressed above, however, this is not particularly interesting for terrestrial experiments since the sensitivity in this mass range strongly declines. Moreover, the curves representing DM production were also compared to recent ones in the literature [178, 179] where other non-standard cosmological scenarios have been explored, and found in agreement.

4.4 Reduction of the Decay Rate due to Additional Decay Channel

This section is devoted to the study of the **effect of non-standard cosmological scenarios on different production mechanism for sterile neutrino DM under the condition that $\Omega_s h^2 = \Omega_{\text{DM}} h^2 = 0.12$** . The **X-ray bound** is assumed to get relaxed due to the presence of new physics that decreases the decay rate of sterile neutrinos by disruptive interference with the standard decay channel, as explained in Subsection 2.2.7 of Chapter 2. The production mechanisms that are analysed are the **Dodelson-Widrow mechanism**, a **standard version of the Shi-Fuller mechanism in which the production of sterile neutrinos is resonantly enhanced**, and a **special version of the**

Shi-Fuller mechanism in which the production is suppressed due to violation of CPT by sterile neutrinos.

4.4.1 Dodelson-Widrow Mechanism

As already mentioned, the Dodelson-Widrow mechanism relies only on the hypothesis that there is mixing between ν_s and an active neutrino that in our case is ν_e (and that there is mixing also between $\bar{\nu}_s$ and $\bar{\nu}_e$). In this case, the Boltzmann equation and its solution, the distribution function $f_s(p, T)$, are those already reported in Eqs. (4.3) and (4.4). To solve numerically the Boltzmann equation and calculate $\Omega_s h^2$ from its solution, we used the code mentioned in the introduction of this Chapter 4. Each result obtained, corresponding to a colored straight line plotted in Fig. 4.2, comes from the integration over the temperature parameter ranging from $T_i = T_c$, upper integration extreme with different value for every line, and $T = 1$ MeV, lower integration extreme common to all lines. The lower extreme of integration is determined by the temperature of decoupling of active neutrinos from the primordial plasma, usually assumed to be $\sim 1 - 2$ MeV. Indeed, since the collision of active neutrinos with other particles in the plasma is crucial for the collapse of the neutrino wave function and the increment of the population of sterile neutrinos, once active neutrinos decouple from the plasma and do not interact anymore, the production ends. The upper integration extreme coincides with what we defined to be the critical temperature in Section 4.2. For this parameter we chose a bunch of discrete values, just to give an idea of the impact it has on the production of sterile neutrinos.

As already shown in Fig. 4.1, also from Fig. 4.2 it is evident that due to the effect of the critical temperature, some lines fall in the ballpark of the experiments sensitivities. This occurs for $T_c \lesssim 100$ MeV. A partial relaxation of the X-ray bound is anyway still necessary in order to make such parameter space viable. In Subsection 2.2.7 of Chapter 2 a particular realization of the cancellation of the X-ray bound is discussed. In that specific concrete scenario, another diagram for the radiative decay of the sterile neutrino into an active neutrino and a photon interferes destructively with the standard diagram and the limit gets relaxed towards allowing larger values of the mixing angle. In Fig. 4.2, several levels of relaxation of the X-ray bound happening in this way are reported in different shades of purple. In order to have a sufficient reduction of the X-ray bound such that the statistical sensitivity region of TRISTAN becomes viable, the sterile neutrino decay rate should be 3 - 4 orders of magnitude weaker. This is expected as KATRIN/TRISTAN sensitivity can reach $\sin^2(2\theta) \sim 10^{-7}$, while present X-ray limits are in the ballpark of 10^{-11} for $m_s \simeq 10$ keV. Instead, for phase 3 of the HUNTER experiment to be in the conditions of detecting a signal of sterile neutrino DM, a relaxation of 2 orders of magnitude in the X-ray bound would be enough. Since here we assume that the entire abundance of DM is constituted by sterile neutrinos, structure formation limits apply and to this end we show bounds from Milky Way satellite counts, discussed in Subsection 2.2.2, which disfavor detection at KATRIN/TRISTAN and ECHO for $m_s \lesssim 8$ keV, leaving however still a significant portion of the parameter space open.

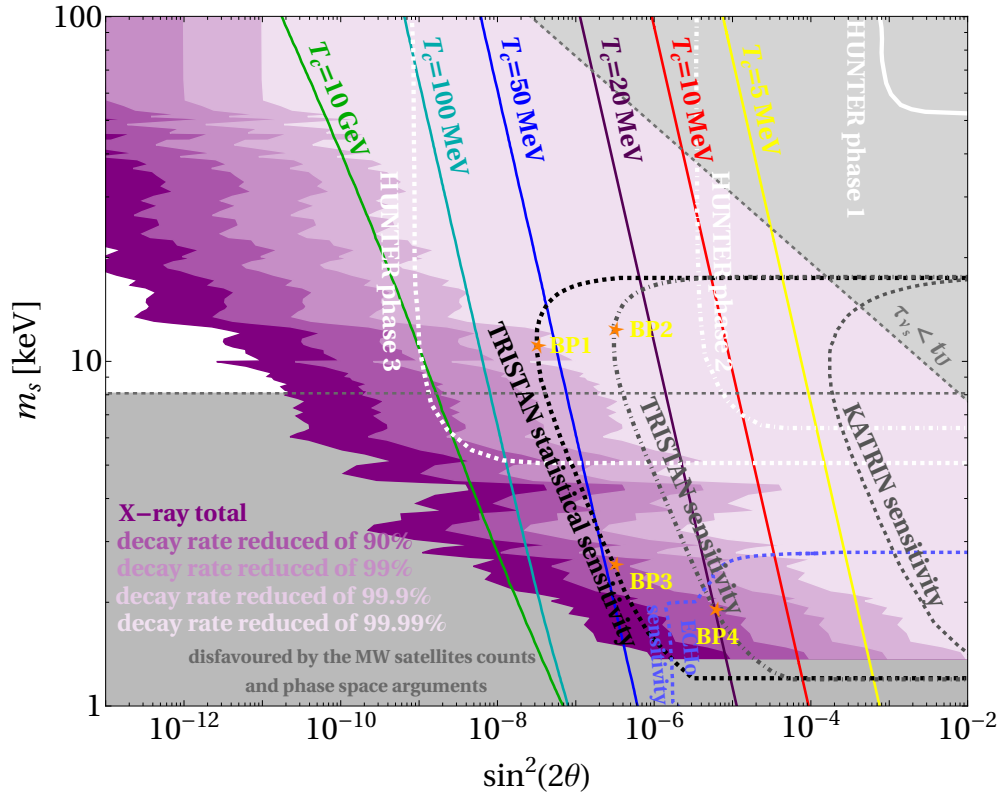


FIGURE 4.2: The regions shaded in purple represent various X-ray limits, depending on the level of relaxation. The decay rate needs to be reduced by 3 – 4 orders of magnitude in order to have TRISTAN statistical sensitivity region free from X-ray limits. Instead, to make accessible the sensitivity region of phase 3 of the HUNTER experiment, a relaxation of the X-ray bound of 2 orders of magnitude is enough. The colored lines indicate the parameter space in which sterile neutrinos constitute the total DM abundance for the indicated values of T_c . We show the sensitivities of KATRIN at different stages of the experiment (black and gray lines), the one of ECHO (blue lines) and those of the different phases of HUNTER (white lines) (see Section 4.3 for extended discussion of these lines) as well as the limit from structure formation (bottom gray region). Stars indicate four benchmark points, which lie in the future sensitivity region of KATRIN/TRISTAN, for which we further explore connection between DM abundance and T_c in Fig. 4.3.

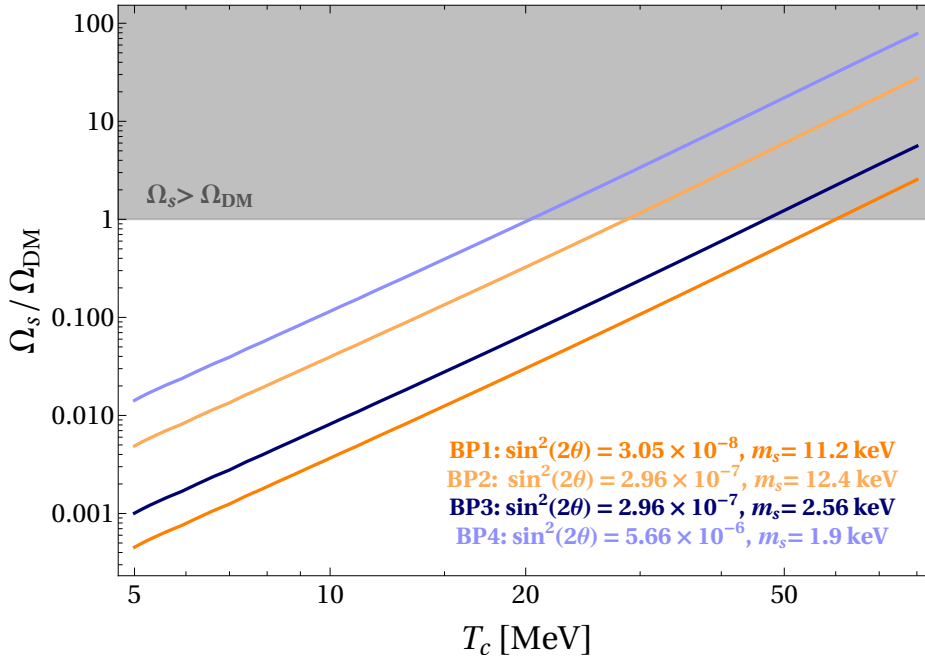


FIGURE 4.3: The figure represents, for four chosen benchmark points, the dependence of the abundance of sterile neutrino DM (normalized to the observed amount of DM) on T_c . BP1 and BP3 lie on the TRISTAN full statistical sensitivity curve, while BP2 and BP4 indicate the potential of TRISTAN to search for sterile neutrinos in a shorter period of data taking (see also Fig. 4.2). In the considered low T_c regime, the produced sterile neutrino DM abundance linearly depends on T_c on our logarithmic scale. For the chosen benchmark points, T_c values for which the correct amount of DM is produced lie between $T_c = 20$ MeV and $T_c = 60$ MeV.

In Fig. 4.2 four benchmark points are marked, two of which lie at the border of TRISTAN sensitivity and the remaining two are on the line corresponding to the full statistical sensitivity of TRISTAN. For these points we illustrate in Fig. 4.3 the dependence of DM production on T_c . The figure clearly shows that by increasing T_c more DM gets produced, if $T_c \lesssim 100$ MeV, that is circa the temperature of the peak in the production in the standard Dodelson-Widrow scenario. Once T_c exceeds $T \simeq 100$ MeV, one is effectively in the "vanilla" Dodelson-Widrow regime and in this case the produced DM abundance is independent of T_c .

4.4.2 Standard Shi-Fuller Mechanism

The Shi-Fuller mechanism can be considered as a variant of the Dodelson-Widrow mechanism relying on the assumption that an asymmetry in the leptonic sector was present in the early Universe, as discussed more thoroughly in Subsection 2.1.2 of Chapter 2. Such lepton asymmetry can be defined as $L = (n_\nu - n_{\bar{\nu}}) / n_\gamma$, where n_ν , $n_{\bar{\nu}}$, and n_γ are the number densities of neutrinos, antineutrinos and photons respectively. For simplicity, we assumed the asymmetry to be present only in the flavor of neutrinos that mix with sterile neutrinos, that is in the electron neutrinos. $L \neq 0$ gives rise to an additional term that contributes to the finite density potential $V^D(T)$ in the denominator

of $\sin^2(2\theta_M)$. This additional term is called lepton asymmetry potential

$$V_L(T) = \frac{4\sqrt{2}\zeta(3)}{\pi^2} G_F T^3 L.$$

The Boltzmann equation of the standard DW mechanism and its solution are modified by the presence of this term and in the framework of the Shi-Fuller mechanism they take the shape

$$\begin{aligned} \frac{\partial}{\partial T} f_s(p, T) + \left[\frac{1}{T} + \frac{1}{3} \frac{g'_{*s}(T)}{g_{*s}(T)} \right] p \frac{\partial}{\partial p} f_s(p, T) = -\frac{1}{H(T)} \left[\frac{1}{T} + \frac{1}{3} \frac{g'_{*s}(T)}{g_{*s}(T)} \right] \times f_s(p, T) \times \\ \times \frac{\Gamma_\alpha(p, T)}{4} \frac{\Delta^2(p) \sin^2(2\theta)}{\Delta^2(p) \sin^2(2\theta) + D^2(p) + [\Delta(p) \cos(2\theta) - V_L^D(T) - V^T(p, T)]^2} \end{aligned} \quad (4.5)$$

and

$$\begin{aligned} f_s(p_f, T_f) = - \int_{T_i}^{T_f} \sqrt{\frac{90}{8\pi^3 g_{*s}(T)}} \frac{M_{Pl}}{T^3} \left(1 + \frac{T}{3} \frac{g'_{*s}(T)}{g_{*s}(T)} \right) \frac{1}{\exp\left(\frac{p_r}{T}\right) + 1} \times \\ \times \frac{\Gamma_e(p_r, T)}{4} \frac{\Delta^2(p_r) \sin^2(2\theta)}{\Delta^2(p_r) \sin^2(2\theta) + \frac{\Gamma_e(p_r, T)^2}{4} + [\Delta(p_r) \cos(2\theta) - V_L^D(T) - V^T(p_r, T)]^2} \end{aligned} \quad (4.6)$$

where $p_r = \frac{T}{T_f} \left(\frac{g_{*s}(T)}{g_{*s}(T_f)} \right)^{1/3} p_f$ is the redshifted momentum, and the finite density potential is now

$$V_L^D(T) = \pm \frac{2\sqrt{2}\zeta(3)}{\pi^2} G_F T^3 \frac{\eta_B}{4} + \frac{4\sqrt{2}\zeta(3)}{\pi^2} G_F T^3 L. \quad (4.7)$$

The lepton asymmetry introduces a resonance in $\sin^2(2\theta_M)$ for certain values of p and T . Depending on the sign of the asymmetry, the production of sterile neutrinos gets enhanced and the production of sterile antineutrinos suppressed, or vice versa due to resonant MSW transitions. However, since we assume both sterile neutrinos and antineutrinos to mix with ν_e and $\bar{\nu}_e$ and constitute dark matter, the net effect is an enhanced production of sterile neutrino DM for the same values of mixing angle in vacuum. As a result, in general, in order to produce DM in the amount that matches observations, smaller mixing angles in comparison to those in "vanilla" Dodelson-Widrow mechanism are sufficient. In a standard cosmological scenario, this dynamics would push successful regions in the parameter space even further from the domain of experimental sensitivity. However, the introduction of a critical temperature that indicates a delay in sterile neutrino production can reconcile the standard Shi-Fuller scenario with the possibility of detection in terrestrial experiments. To identify which ranges of values of T_c and L make sterile neutrino dark matter produced through Shi-Fuller mechanism testable in terrestrial experiments, we need to solve the Boltzmann equation. The presence of resonance in the denominator of $\sin^2(2\theta_M)$, makes the Boltzmann equation very difficult to treat and solve with Mathematica. To get the results plotted in Figure 4.4 we use `sterile - dm` [180] that is currently the only available tool that can treat the evolution of asymmetries properly. We have modified its source code in such a way that the production occurs only below a chosen T_c . The code has only interaction rates for muon

neutrinos implemented and we are dominantly interested in the electron flavor, but the error that this introduces is rather small. This was verified by comparing results for low T_c in the absence of asymmetries obtained by (i) running `sterile - dm` code and (ii) solving Eq. (4.3) and calculating $\Omega_s h^2$ numerically, for which we found very small differences in the output in terms of $\Omega_s h^2$.

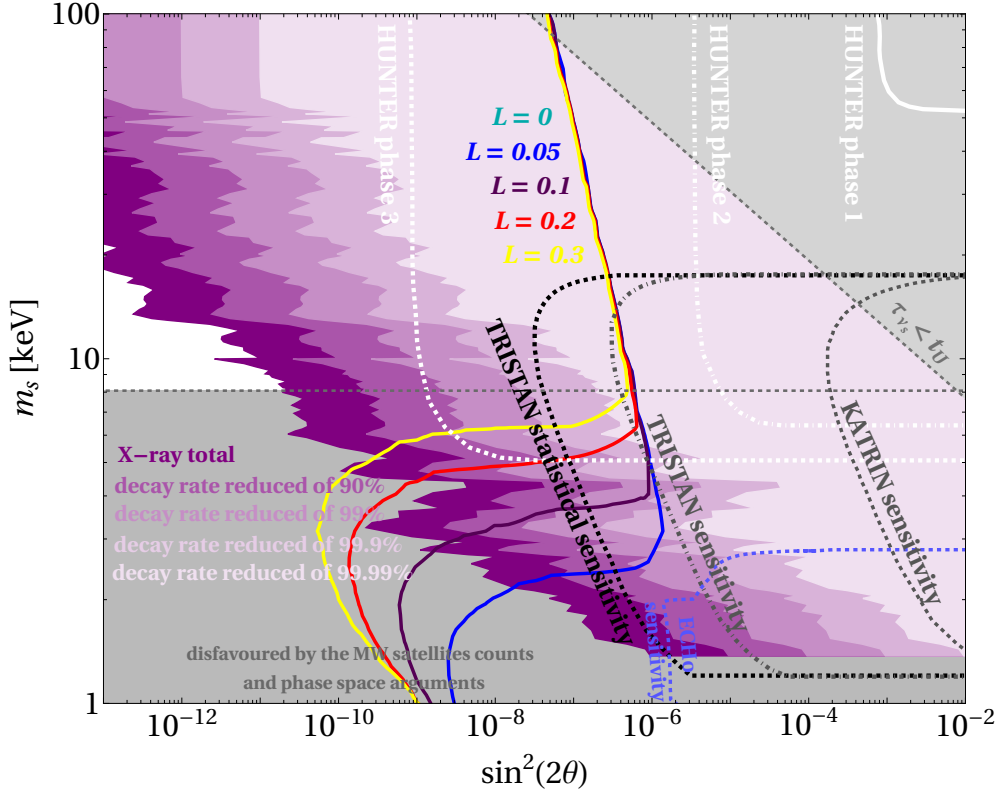


FIGURE 4.4: The colored curves indicate the parameter space with $\Omega_s h^2 = 0.12$ for $T_c = 30$ MeV and several values of L ranging between 0.05 and 0.3. These curves match the corresponding Dodelson-Widrow line at larger values of m_s while resonant effects stemming from lepton asymmetries are prominent for $m_s \lesssim 10$ keV. Part of the region in which the curves deviate from the Dodelson-Widrow line is testable at KATRIN/TRISTAN and HUNTER, however in some tension with structure formation limits. We also show relaxed X-ray limits as discussed in Subsection 4.4.1 and presented in Fig. 4.2.

Fig. 4.4 shows the results obtained in this framework for a representative case of $T_c = 30$ MeV. The initial asymmetry values for which we did the calculation are $L = 0.05, 0.1, 0.2$ and 0.3 . It is noteworthy that the final values of the asymmetry, as a consequence of the resonant transition, can in some regions of the parameter space be at least a factor of a few times smaller in comparison to its initial values. Although the chosen values are particularly large in comparison to the measured baryon asymmetry of the Universe, they are not excluded. In particular, observational constraints on L arise from CMB [50, 51] and BBN [52, 53]. In this context, the reported limits between different analyses are conflicting and we use values $L \lesssim 0.3$ that seem rather conservative. The curves in Fig.4.4 are determined by the requirement $\Omega_s h^2 = \Omega_{\text{DM}} h^2 = 0.12$ for the indicated values of

the lepton asymmetry. For larger values of m_s all curves with $L \neq 0$ match the Dodelson-Widrow ($L = 0$) line for $T_c = 30$ MeV. This is because at large m_s the impact of V_L^D is not competitive with the other terms in the potential. For values of $m_s \lesssim 10$ keV, V_L^D becomes much more relevant and we observe that the regions corresponding to $\Omega_s h^2 = 0.12$ are shifted to smaller values of $\sin^2(2\theta)$ due to resonances that enhance the production. The regions with strongest resonant effects are not observable testable in experiments. However, KATRIN/TRISTAN and HUNTER are still sensitive in the region where lines corresponding to $L \neq 0$ start departing from the Dodelson-Widrow line. If one of these two experiments makes a discovery in such parameter space, a complementary cosmological determination of T_c will be required, to break the degeneracy between Dodelson-Widrow scenario with higher T_c and Shi-Fuller scenario where $L \neq 0$ modifies the production. As a final comment, there seem to be tension with satellite count limits in this region and the tension is milder for larger values of L .

4.4.3 Shi-Fuller Mechanism in the Presence of CPT Violation

Another scenario that might manifest in terrestrial experiments is the one in which sterile neutrino dark matter violate CPT symmetry and only ν_s (or $\bar{\nu}_s$) mixes with ν_e (or $\bar{\nu}_e$), while the mixing of the $\bar{\nu}_s$ (or ν_s) is zero. As already mentioned for the standard Shi-Fuller mechanism, the presence of a primordial asymmetry in the lepton sector suppresses the production of one of the two species, either neutrinos or antineutrinos, and enhances the production of the other, due to MSW effect. If both ν_s and $\bar{\nu}_s$ mix with active neutrinos and antineutrinos and if DM is constituted by both ν_s and $\bar{\nu}_s$, as it is in the standard Shi-Fuller case, the final DM abundance results overall enhanced. However, if only ν_s ($\bar{\nu}_s$) mixes with ν_e ($\bar{\nu}_e$), only the sterile (anti)neutrino that has non-zero mixing will constitute DM. For example, if the following three conditions are satisfied at a time:

- the mixing of sterile antineutrino is zero,
- the lepton asymmetry is such that the effective mixing of the sterile neutrino is suppressed and results smaller than the vacuum one,
- DM is constituted by ν_s ,

the final abundance of DM will be suppressed by mean of CPT violation with respect to the standard Dodelson-Widrow case.

In this case, the Boltzmann equation and the distribution function of sterile neutrino DM take the same shape as in the standard Shi-Fuller case (Eq. (4.5) and (4.6)) but the final DM abundance is calculated only taking into account one between $f_s(p, T)$ and $f_{\bar{s}}(p, T)$, the one that is suppressed. To calculate the values of the final abundance of DM in this scenario we resorted again to the `sterile-dm` code with a modification of the source code. To take into account only sterile neutrinos with the sign of the potential such that they do not undergo resonant conversion, but rather feature suppression in the production, we suppress the usual lepton asymmetry and define a new one. We choose appropriately the sign of the asymmetry for both species to make sure that both sterile neutrinos and antineutrinos receive suppression in the production stemming from the asymmetry term and there are no resonant effects. In the code it is not possible to fully decouple either of the species. However, since in this realization both species are treated on equal footing, it is sufficient to simply divide the final DM abundance by a factor of two in order to obtain the DM abundance of sterile neutrinos. The newly defined lepton asymmetry remains constant throughout the evolution of the abundance, since transitions between sterile and active neutrinos are suppressed and thus do not lead to

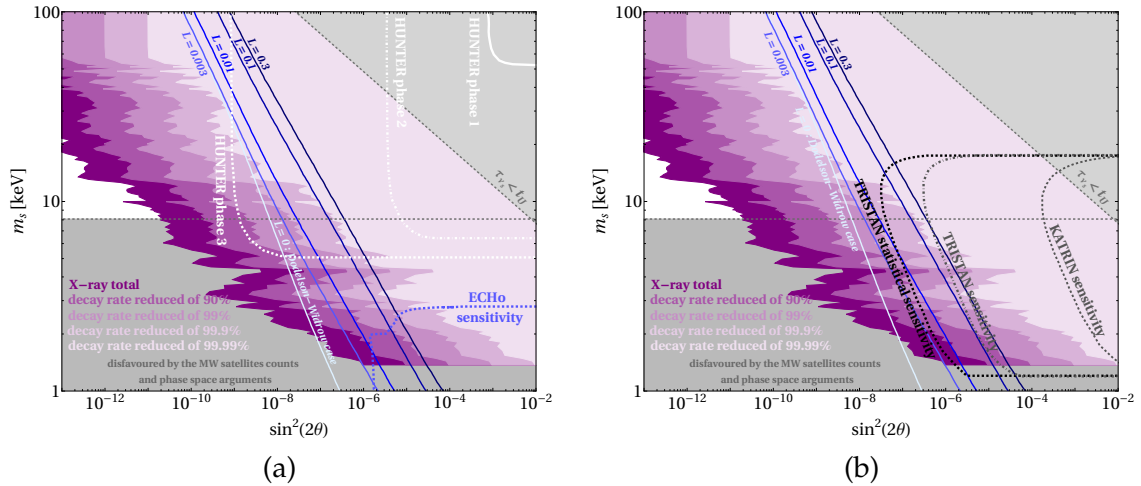


FIGURE 4.5: All the straight lines correspond to production of sterile neutrino or antineutrino DM starting at high temperatures ($T = 10$ GeV), with no introduction of a lower critical temperature, and they satisfy the condition $\Omega_s h^2 = \Omega_{\text{DM}} h^2 = 0.12$. Different shades of blue correspond to different values of the lepton asymmetry $L = 0.3, 0.1, 0.01$, and 0.003 , to be compared with the Dodelson-Widrow case represented by the light-blue line. Different shades of purple represent the relaxation of the X-ray bound discussed in Subsection 2.2.7 in Chapter 3. (a) Non-zero mixing between sterile and active neutrinos. The sensitivity regions of HUNTER and ECHO reveal that for any chosen value of the asymmetry $L \gtrsim 0.003$, these experiments should be able to see a signal of sterile neutrino DM produced under these conditions. (b) Non-zero mixing between sterile and active antineutrinos. The discovery with TRISTAN is feasible only with $L \gtrsim 0.1$ while the final KATRIN/TRISTAN stage will be able to test on order of magnitude smaller asymmetries.

significant changes of the initial value.

In Fig. 4.5, it is possible to see that the visible effect of this suppression due to the combined action of lepton asymmetry and CPT violation is that the line in the parameter space satisfying the condition $\Omega_s h^2 = \Omega_{\text{DM}} h^2 = 0.12$ is shifted towards larger values of the vacuum mixing angle where terrestrial experiments are expected to become sensitive. All straight lines correspond to production of sterile neutrino or antineutrino DM. Different shades of blue correspond to different values of the lepton asymmetry $L = 0.3, 0.1, 0.01$, and 0.003 , to be compared with the Dodelson-Widrow case represented by the light blue line. Different shades of purple represent the relaxation of the X-ray bound discussed in Subsection 2.2.7 in Chapter 2.

In Fig. 4.5 (a), we see the situation for sterile neutrino mixing $\neq 0$. If we consider the sensitivity regions of HUNTER and ECHO, we see that for any chosen value of the asymmetry $L \gtrsim 0.003$, these experiments should be able to see a signal of sterile neutrino DM produced under these conditions, if also the values of $\sin^2(2\theta)$ and m_s match.

Fig. 4.5 (b) shows the analogous case with non-zero mixing of sterile antineutrinos and lepton asymmetry with opposite sign. The discovery with TRISTAN is feasible only with $L \gtrsim 0.1$ while the final KATRIN/TRISTAN stage will be able to test on order of magnitude smaller asymmetries.

All these results are achieved with the production that starts at very high temperatures,

without the need of introducing a critical temperature. Consequently, in this case, the extent of the displacement of the lines depends on the magnitude of the lepton asymmetry and not on a different temperature for the start of the production.

Regarding the justification of this exotic scenario invoking CPT violation, it is noteworthy that differences of mixing angles or masses are not very strongly constrained [181] even for neutrinos and antineutrinos in the active sector. Moreover, it is not the first time that CPT violation is considered talking about sterile neutrinos: in [182] it was hypothesized in the context of eV-scale sterile neutrinos.

Chapter 5

Sterile Neutrino Dark Matter in the Presence of Neutrino Non-Standard Interactions

We call neutrino non-standard interactions possible interactions, beyond those established in the SM, that involve only neutrinos (in the case of non-standard self-interactions, NSSI) or neutrinos and other fermions (NSI). They can be seen as a parameterization of new physics in the neutrino sector that can serve as connection across different branches of physics such as particle physics, astrophysics, and cosmology. At the moment, there is no experimental evidence that such non-standard interactions exist, but the constraints on some of them are still extremely weak and a large fraction of their parameter space remains to date unexplored territory.

In this chapter, we look at the effects that non-standard self-interactions among active neutrinos (NSSI) have on the production of sterile neutrino DM in the early Universe that occurs through Dodelson-Widrow (DW) mechanism. We approach this study in a model-independent way by means of an effective field theory that does not depend on the details of the UV complete model. This framework is convenient in order to see how the perspectives of detection of such DM candidate in near future experiments change under the influence of neutrino NSSI.

The results presented in this chapter and published in Ref. [3] have been obtained using a code written in the Mathematica package, and later made publicly available at the link: <https://github.com/cristinabenso92/Sterile-neutrino-production-via-Dodelson-Widrow-with-NSSI>.

5.1 Neutrino Non-Standard Interactions

5.1.1 Motivation for NSI

The fact that neutrinos are not massless, contrary to what is assumed in the SM picture, constitutes the first experimental probe of the existence of new physics beyond the SM. **Most of the models which include mechanisms of neutrino mass generation (such as seesaw schemes), imply extra interactions called non-standard interactions (NSI)** [183]. Such NSI are usually included in the particle model via the following dimension-6

effective operators describing neutral (NC) and charged (CC) currents

$$\mathcal{L}_{\text{NC}} = -2\sqrt{2}G_F \sum_{f,P,\alpha,\beta} \epsilon_{\alpha\beta}^{f,P} (\bar{\nu}_\alpha \gamma^\mu P_L \nu_\beta) (\bar{f} \gamma_\mu P f), \quad (5.1)$$

$$\mathcal{L}_{\text{CC}} = -2\sqrt{2}G_F \sum_{f,P,\alpha,\beta} \epsilon_{\alpha\beta}^{f,P} (\bar{\nu}_\alpha \gamma^\mu P_L \ell_\beta) (\bar{f} \gamma_\mu P f'), \quad (5.2)$$

where G_F is the Fermi constant, ϵ are the NSI couplings that express the size of the new interaction relative to the weak scale, the sum is over matter fermions (typically $f, f' = e, u, d$), and $P = P_L, P_R$ are the chirality projection operators. The effective field theory (EFT) treatment is justified by the fact that, in this general case, the NSI involve neutrino and other SM fermions whose interactions at low energies are well known. Deviations from the standard scenario can be expected to come only from physics at high energies, e.g., from interactions mediated by new heavy particles whose description can be profitably expressed in terms of effective operators in analogy to the Fermi theory for weak interactions. One of the advantages of the EFT treatment is that it allows us to be agnostic about the specific features of the UV completion of the SM that generate the effective operators of the extended theory. Therefore it can be used to investigate the effects of unknown heavy particles in a model-independent way. On the other hand, complete models that embed NSI include various seesaw models, R-parity-violating supersymmetric models, left-right symmetric models, GUTs, and extra dimensions. More details about such UV complete models can be found in Ref. [184] and references therein.

Looking at Eq. (5.1) and (5.2), it is clear that, in principle, NSI could induce neutrino flavor conversions even in the absence of neutrino mass, if no further assumptions are made about the leptonic indices. Due to this fact, before the discovery of neutrino oscillations, NSI were hypothesized to explain neutrino flavor transitions responsible for the solar anomaly (deficit of the solar neutrino flux relative to standard solar model predictions) [185], and the atmospheric anomaly (deviation of the ratio of muon neutrino flux to the electron neutrino flux from 2 for atmospheric neutrinos that cross the Earth before reaching the detector) [4]. Now that the oscillation paradigm involving neutrino masses is solidly established, we know that NSI can only provide sub-leading effects to neutrino oscillations. Nevertheless, NSI could be active in the phenomenon of neutrino oscillations in all three phases of neutrino production (CC NSI), detection (CC NSI), and propagation (NC NSI). Their presence can also introduce a degeneracy that would affect the determination of the parameters characterizing the 3-neutrino scheme [186]. **Therefore, the primary motivation to study NSI is that, if they exist, we need to know their effects also in order to be able to disentangle such effects from standard physics, avoiding further problems from arising in the development of our knowledge of the standard scenario.**

Moreover, since NSI parametrizes new interactions between neutrinos and other SM matter fields that take part in scattering processes, NSI provide also a **valuable framework to connect constraints on new physics derived from scattering experiments and oscillation experiments.**

5.1.2 Motivation for NSSI

Contrary to neutrino interactions with other fermions, neutrino self-interactions have never been measured. Also, the decay width of Z-boson into invisible products $\Gamma_{Z \rightarrow \text{inv}}$

measured at LEP [187] is only an indirect measurement and does not exclude the presence of additional mediators of new interactions involving only neutrinos [188]. Therefore, the possibility that active neutrinos can interact with each other through non-standard self-interactions (NSSI) even much stronger than the standard weak interaction is, to date, very poorly constrained. Such NSSI are extremely interesting to be studied from a theoretical point of view because of the variety of new phenomena that can be originated in their presence. Motivations to study NSSI include the fact that they can be involved in mechanisms for neutrino mass generation [189–191], they can be connected to DM abundance [3, 192–194], and they are included in models that provide explanation to unsolved puzzles such as the Hubble tension [195–198], and the muon $g - 2$ anomaly [199–201]. Moreover, we can expect neutrino self-interactions to be more relevant in very dense environments such as the primordial plasma, forge of DM, and supernovae. Thus, it is of great importance to investigate the possible effects of NSSI in these special conditions so that our current and future knowledge about these extreme environments can be used, in turn, to constrain such exotic interactions.

As shown below in Fig. 5.1, taken from Ref. [188], according to the state of the art of experimental searches, NSSI can be mediated by new particles with a wide range of masses and couplings. Contrary to NSI, for which light mediators are already experi-

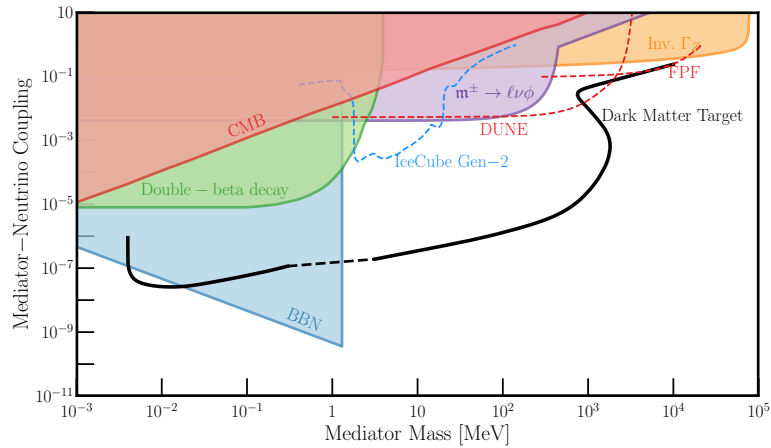


FIGURE 5.1: The parameter space of mediators of NSSI is represented in terms of their mass (on the horizontal axis) and their coupling to neutrinos (on the vertical axis). The coupling to neutrinos is assumed to be flavor universal, and the relative importance of laboratory, astrophysical, and cosmological observations depends on its flavor structure. Cosmological constraints from BBN and CMB and laboratory bounds from searches for $0\nu\beta\beta$ decay, rare meson, τ and Z decays are represented by thick lines limiting colored portions of the plot. Limits from collider searches for new neutrino scattering (DUNE, FPF) and from the observed spectrum of high-energy neutrinos at IceCube are represented by dashed lines. The solid black line identifies a theoretically motivated target in the mediator mass-coupling parameter space relative to the impact of NSSI on the production of dark matter via a freeze-in mechanism ([188]). Figure taken from Ref. [188].

mentally excluded, NSSI can also be mediated by light new particles, provided that their coupling to neutrinos is sufficiently small. In this case, the consideration of a precise, complete model is required, and the study of NSSI can only be model-dependent. On the contrary, limiting our interest to heavy mediators, we can represent these interactions in

the Lagrangian in the shape of additional dimension-6 effective operators, analogous to those describing NSI in Eq. (5.2) and Eq. (5.1)

$$\mathcal{L}_{\text{NSSI}} = -\frac{G_F}{\sqrt{2}} \sum_j \sum_{\alpha, \beta, \gamma, \delta} \epsilon_j^{\alpha\beta\gamma\delta} (\bar{\nu}_\alpha \mathcal{O}_j \nu_\beta) (\bar{\nu}_\gamma \bar{\mathcal{O}}_j \nu_\delta). \quad (5.3)$$

Here, G_F is the Fermi constant, $\alpha, \beta, \gamma, \delta$ are neutrino flavor indices, the sum over j includes all kinds of possible interactions described by the operators $\mathcal{O}_j = \{\mathbb{I}, \gamma^\mu, i\gamma^5, \gamma^\mu \gamma^5, \sigma^{\mu\nu}\}$, and the couplings ϵ_j parameterize the strength of each type of NSSI with respect to the weak interaction. To date, the parameter space of such heavy mediators is significantly less constrained than the one of light mediators, and in the rest of this chapter, we adopt the effective description of NSSI, and we take advantage of this freedom.

5.1.3 Details of the Model Including NSSI

We consider the SM matter content extended by adding one Majorana sterile neutrino ν_s with a mass of $\mathcal{O}(\text{keV})$ that can play the role of DM. Although we do not deepen the point regarding the generation of neutrino masses in this context, our Majorana sterile neutrino DM could, in principle, take part in the type-I seesaw, and it is **defined through its contribution to a fourth neutrino mass eigenstate** $\nu_4 = \cos(\theta)\nu_s + \sin(\theta)\nu_\alpha$. For simplicity, we assume that ν_s mixes only with one active neutrino species ν_α and that such mixing is the only connection between sterile neutrinos and SM particles. We choose the mixing to be between ν_s and ν_e (or $\bar{\nu}_e$ for sterile antineutrinos). As already mentioned in previous chapters, this choice derives from the fact that running and upcoming terrestrial experiments aiming at detecting sterile neutrino DM will be sensitive in particular to the mixing with ν_e and $\bar{\nu}_e$, and not to the mixing with neutrinos of other generations, making our scenario the first possible experimentally testable.

In addition to the extension of the SM content by the introduction of sterile neutrinos, **we hypothesize that active neutrinos are subject to non-standard self-interactions**. In previous works, different authors have studied neutrino non-standard self-interactions focusing on a single type of interaction at a time, most frequently scalar or vector. The purpose of this chapter is instead to provide a general description of

- the effects that active neutrino NSSI of any type (be it scalar, pseudoscalar, vector, axial-vector, or tensor) would have on the production of Majorana sterile neutrino DM in the early Universe,
- the subsequent implications of the existence of active neutrino NSSI for sterile neutrino detection in terrestrial experiments.

Here, we only study the case of flavor-conserving NSSI involving electron neutrinos and antineutrinos, leaving the flavor-changing case for future studies. Such NSSI are mediated by new particles that should be added to the model content. However, as mentioned in this chapter's introduction, **we are interested in giving an effective description of these interactions and their effects**. Therefore, we assume the mediators to be much heavier than the energy scale at which the processes relevant for sterile neutrino DM production typically occur, and we introduce them in the Lagrangian through Fermi-like interaction terms like

$$\mathcal{L}_{\text{NSSI}} = -\frac{G_F}{\sqrt{2}} \sum_j \epsilon_j^{eeee} (\bar{\nu}_e \mathcal{O}_j \nu_e) (\bar{\nu}_e \bar{\mathcal{O}}_j \nu_e), \quad (5.4)$$

where $\mathcal{O}_j = \{\mathbb{I}, \gamma^\mu, i\gamma^5, \gamma^\mu\gamma^5, \sigma^{\mu\nu}\}$. Concretely, we remember that the peak of production in the DW scenario happens to be at $T_{\text{peak}} \simeq 133(\frac{m_s}{\text{keV}})^{1/3}$ MeV [35], therefore, we consider mediators generically identified as ϕ with masses m_ϕ in the range (10 - 100) GeV. Given the effective approach adopted, the new degrees of freedom associated with mediators of NSSI do not appear in the final Lagrangian reported in Eq. (5.4) and we do not worry further about their specific features. At the end of Subsection 5.2.1, an *a posteriori* argument in favor of the validity of the effective treatment adopted in this specific case is given and discussed.

Since the physics relevant for this study takes place at temperatures at which the electroweak symmetry is already broken, we consider neutrinos to be decoupled from charged leptons. We consider only neutrinophilic interactions, and we do not force the associated operators to satisfy the condition of gauge invariance¹. In a comprehensive and rigorous approach, this point, as well as the point of including flavor-changing NSSI, would be more critical. However, the purpose of this work is not to cover all the possibilities meticulously but rather to serve as a pilot study of a simple concrete case, to reveal the magnitude of effects of NSSI on sterile neutrino DM production and detection perspective and help evaluate the worthiness of further, more extended investigations.

As a final remark on the framework of this study, although in principle we are interested in a general description that can be applied in case of any type of interaction, the choice of Majorana neutrinos automatically reduces the spectrum of NSSI that give a non-zero contribution. Indeed, applying the definition of the Majorana field to each term of Eq. (5.4) we see that the contribution of vector and tensor interactions cancels automatically. Therefore, from now on, the only types of interaction that will be considered are scalar, pseudoscalar and axial-vector interactions corresponding respectively to $\mathcal{O}_j = \{\mathbb{I}, i\gamma^5, \gamma^\mu\gamma^5\}$.

The effective form of the Lagrangian that we use in the rest of this chapter can be derived from the Lagrangian of UV, a complete theory by integrating out the heavy degrees of freedom that, in our case, are the mediators of neutrino NSSI. Here we focus on the terms describing the coupling of active neutrinos to new heavy mediators that mediate their self-interactions. Below the scale of EW symmetry breaking, NSSI can usually be described by a schematic Yukawa-like interaction $\nu\nu\phi$ where ϕ is a scalar or vector mediator particle. Although the specific shape of this additional term varies according to the kind of interaction, for simplicity, in the following, we report as an example only the case of NSSI mediated by a complex scalar ϕ , since for the other types of interactions the derivation of the effective Lagrangian is analogous.

The full Lagrangian of this new mediator is

$$\mathcal{L}_\phi = \partial_\mu\phi^\dagger\partial^\mu\phi - m^2\phi^\dagger\phi + \lambda_\phi\bar{\nu}\mathcal{O}\nu\phi + \lambda_\phi^*\phi^\dagger\bar{\nu}\bar{\mathcal{O}}\nu, \quad (5.5)$$

where $\bar{\mathcal{O}} = \gamma^0\mathcal{O}^\dagger\gamma^0$, and \mathcal{O} is one among the bilinear covariants that survive for Majorana neutrinos $\{\mathbb{I}, i\gamma^5, \gamma^\mu\gamma^5\}$. Assuming $m_\phi \gg T \sim$ typical energy of the interaction, and being interested in the phenomenology of this theory at low energies, we are allowed to integrate out the heavy new degree of freedom ϕ .

¹The involvement of charged leptons in the gauge invariant perspective would possibly considerably reduce the range of values allowed for NSSI couplings since non-standard interactions of charged leptons are extremely well constrained by lepton flavor violation (LFV) and universality violation. Nevertheless, there are several ways to evade the strong correlation between LFV and non-standard interactions that are discussed in detail in Ref. [202].

Proceeding as reported in detail in Appendix C, deriving the equations of motion for ϕ and ϕ^\dagger from the Euler-Lagrange equations, extracting from there their expressions and substituting them in Eq. (5.5), we obtain

$$\mathcal{L}_{\text{NSSI}} = \lambda_\phi^2 \frac{(\bar{\nu}\mathcal{O}\nu)(\bar{\nu}\bar{\mathcal{O}}\nu)}{(\square + m_\phi^2)}. \quad (5.6)$$

At the zeroth order in momentum, from Eq. (5.6) we would get the familiar term analogous to those of the Fermi theory for weak interactions depending only on the mass of the mediator, matching Eq. (5.4) for $G_\phi = G_F \epsilon_j^{eeee} = \frac{\sqrt{2}\lambda_\phi^2}{m_\phi^2}$. However, as explained further in the following and in Appendix E, the dependence on the momentum p in our case is not negligible if we want to appreciate the effect of NSSI through the change they induce in the thermal potential. Therefore, we have to keep one more term in the effective expansion, and the final form of the effective Lagrangian used in the following is

$$\mathcal{L}_{\text{NSSI}} = \frac{G_F \epsilon}{\sqrt{2}} (\bar{\nu}\mathcal{O}\nu)(\bar{\nu}\bar{\mathcal{O}}\nu) - \frac{G_F \epsilon}{\sqrt{2}} (\bar{\nu}\mathcal{O}\nu) \frac{\square}{m_\phi^2} (\bar{\nu}\bar{\mathcal{O}}\nu), \quad (5.7)$$

where $\mathcal{O} = \{\mathbb{1}, i\gamma^5, \gamma^\mu\gamma^5\}$ for scalar, pseudoscalar, and axial-vector NSSI, respectively.

5.1.4 Specific Constraints on NSSI

Since NSSI involve only neutrinos, many of the experiments that can be used to constrain NSI are not helpful in the hunt for NSSI since they are based on the detection of electrically charged or color-charged particles. Among them, there are oscillation experiments, scattering experiments, and experiments at accelerators that are sensitive only to interactions of neutrinos with other fermions.

In principle, supernovae are environments in which neutrino self-interactions could play an essential role due to the high density by which supernovae are characterized. Secret interactions among neutrinos have been studied in Refs. [203–207]. However, on the one hand, a self-consistent *ab initio* treatment of the supernova process would be needed to derive robust constraints, and this treatment is not possible at the moment. On the other hand, the masses of mediators of NSSI that could be constrained are anyway $m_\phi < 1$ GeV. Therefore, constraints from supernovae are not relevant for the case we are interested in.

Also the constraints set (or expected to be set in the future) by IceCube, both considering the scattering of high energy astrophysical neutrinos con the C ν B [208–211] and using those using the information from time and direction coincidence with an identifiable neutrino source [212], concern lighter NSSI mediators than those considered in our study.

Other observations that can be used to constrain NSSI are those of CMB [213, 214] and of BBN [215]. However, the limits from CMB are very loose ($G_\phi \lesssim 2.5 \times 10^7 G_F$ [213]), and those from BBN constrain only relatively light mediators.

From the point of view of particle physics experiments, bounds on active neutrino NSSI could come from meson decays. However, also in this case, the limits concern only relatively light mediators [216]. The same holds for possible constraints coming from double beta decay [217].

The only relevant limits for the case presented in this work come from Z-boson decay at one loop level [218–220]. Using only vector NSSI among Dirac neutrinos, the authors of Refs. [218, 219] showed that the constraints on NSSI couplings can be as strong as $|\epsilon| \lesssim 2$. However, there is a possibility of cancellation of NSSI couplings among different

neutrino flavors, which can loosen the bound to $|\epsilon| \lesssim 250$. While these bounds cannot be directly applied to scalar, pseudoscalar, or axial-vector NSSI among Majorana neutrinos, one can translate these bounds using Fierz rearrangement. We do not explicitly calculate the bounds, but based on these considerations, we restrict our NSSI couplings to be $|\epsilon_{S,P,A}| \lesssim 100$.

5.2 Impact of NSSI on Sterile Neutrino Dark Matter

5.2.1 Non-Standard Boltzmann Equation, Solution and Evolution of the Distribution Function

In the "vanilla" DW mechanism, introduced in Subsection 2.1.1 of Chapter 2, assuming mixing between ν_s and ν_e , the Boltzmann equation for sterile neutrino DM is solved by the distribution function

$$f_s(p_f, T_f) = - \int_{T_i}^{T_f} \sqrt{\frac{90}{8 \pi^3 g_{*s}(T)}} \frac{M_{Pl}}{T^3} \left(1 + \frac{T g'_{*s}(T)}{3 g_{*s}(T)} \right) \frac{1}{\exp\left(\frac{p_r}{T}\right) + 1} \times \\ \times \frac{\Gamma_e(p_r, T)}{4} \frac{\Delta^2(p_r) \sin^2(2\theta)}{\Delta^2(p_r) \sin^2(2\theta) + \frac{\Gamma_e(p_r, T)^2}{4} + [\Delta(p_r) \cos(2\theta) - V^D(T) - V^T(p_r, T)]^2} \quad (5.8)$$

where for the sake of brevity $p_r = \frac{T}{T_f} \left(\frac{g_{*s}(T)}{g_{*s}(T_f)} \right)^{1/3} p_f$ is the redshifted momentum,

$$V^D(T) = \frac{2\sqrt{2}\zeta(3)}{\pi^2} G_F T^3 \frac{\eta_B}{4} \quad (5.9)$$

is the finite density potential in the absence of lepton asymmetry, and

$$V^T(p_r, T) = V_{SM}^T(p_r, T) = \\ = - \frac{8\sqrt{2}G_F p_r}{3m_Z^2} (\langle E_{\nu_\alpha} \rangle n_{\nu_\alpha} + \langle E_{\bar{\nu}_\alpha} \rangle n_{\bar{\nu}_\alpha}) - \frac{8\sqrt{2}G_F p_r}{3m_W^2} (\langle E_\alpha \rangle n_\alpha + \langle E_{\bar{\alpha}} \rangle n_{\bar{\alpha}}) \simeq \\ \simeq -3.72 G_F p_r T^4 \left(\frac{2}{m_W^2} + \frac{1}{m_Z^2} \right) \quad (5.10)$$

is the thermal potential where the expressions and values for number density and average energy of electrons, positrons, neutrinos, and antineutrinos have been substituted.

Being interested in the modifications induced by the presence of NSSI in the production of sterile neutrino DM occurring through DW mechanism, we have to remember that **interactions of neutrinos with each other enter** in two terms of Eq. (5.8): **in the interaction rate $\Gamma_e(p_r, T)$ and in the thermal potential $V^T(p_r, T)$** . Then, to include the effect of NSSI, we have calculated the additional contribution to $\Gamma_e(p_r, T)$ and $V^T(p_r, T)$ in presence of more interactions among neutrinos described by Eq. (5.7).

The detailed calculation of $\Gamma_{e,NSSI}(p, T)$ is reported in Appendix D and it has been carried out following Refs. [193, 221–223] and using the FeynCalc tool [224–226] to calculate the amplitudes of the processes.

The results of the calculation of $\Gamma_{e,\text{NSSI}}(p, T)$ for different types of interactions are reported in Table 5.1.

NSSI	Interaction rate
Scalar	$\Gamma_{e,S}(p, T) = \frac{7\pi}{180}\epsilon_S^2 G_F^2 p T^4$
Pseudoscalar	$\Gamma_{e,P}(p, T) = \frac{7\pi}{180}\epsilon_P^2 G_F^2 p T^4$
Axial-vector	$\Gamma_{e,A}(p, T) = \frac{7\pi}{135}\epsilon_A^2 G_F^2 p T^4$

TABLE 5.1: Interaction rates for electron neutrinos subject to scalar pseudoscalar, and axial-vector additional NSSI.

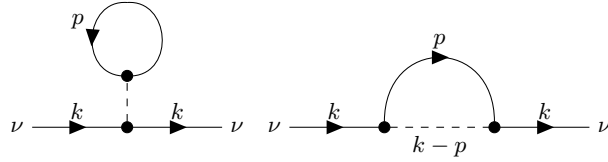


FIGURE 5.2: Tadpole (left) and sunset (right) self-energy diagrams relevant for the thermal potential.

The contribution to the potential arises from the self-energy diagrams depicted in Fig. 5.2. The tadpole diagram gives a contribution proportional to the lepton asymmetry, and it can be ignored in the framework of the DW mechanism, where such primordial asymmetry in the lepton sector is assumed to be zero. If one integrates out the mediator in the sunset diagram (right panel of Fig. 5.2), there is no way to introduce a momentum dependence in the self-energy since the dependence comes from the momentum of the mediator. As a result, the EFT needs to be expanded to higher orders to compute the potential. This is why we need to use the Lagrangian reported in Eq. (5.7). The detailed calculation of $V_{\text{NSSI}}^T(p, T)$, carried out following Ref. [227], is reported in Appendix E. The results of the calculation for different types of interactions are reported in Table 5.2.

NSSI	Thermal potential
Scalar	$V_S^T(p, T) = -\frac{7\sqrt{2}\pi^2}{45m_\phi^2}\epsilon_S G_F p T^4$
Pseudoscalar	$V_P^T(p, T) = -\frac{7\sqrt{2}\pi^2}{45m_\phi^2}\epsilon_S G_F p T^4$
Axial-vector	$V_A^T(p, T) = -\frac{14\sqrt{2}\pi^2}{45m_\phi^2}\epsilon_S G_F p T^4$

TABLE 5.2: Thermal potential terms for electron neutrinos subject to scalar pseudoscalar, and axial-vector additional NSSI.

From Tables 5.1 and 5.2 it is clear that scalar and pseudoscalar NSSI are indistinguishable from an EFT perspective based on their effects on the DW production. Therefore, if experiments see a signal of sterile neutrino DM in the region of the parameter space made

available by the presence of scalar or pseudoscalar NSSI, further direct searches focused on the mediator of the NSSI will be needed to break this degeneracy. From Tables 5.1 and 5.2 it is also evident that, as expected, all interactions exhibit the same dependence on temperature T and momentum p and only a small numerical factor distinguishes the axial-vector NSSI from the scalar and pseudoscalar ones (beyond the couplings that could be of course very different from each other). Moreover, notice that based on the assumption to consider only flavor-diagonal NSSI, given that all interactions give contributions with the same sign, we expect for each kind of interaction effects that go in the same direction and give analogous results. Based on such considerations, since the pseudoscalar interaction has been rarely considered in the literature, in the following, we show only the results obtained for pseudoscalar NSSI (and axial-vector NSSI for what concerns the sterile neutrino parameter space).

The production of sterile neutrino DM through the DW mechanism modified by the presence of pseudoscalar NSSI is well described by the Boltzmann equation

$$\begin{aligned} \frac{\partial}{\partial T} f_s(p, T) + \left[\frac{1}{T} + \frac{1}{3} \frac{g'_{*s}(T)}{g_{*s}(T)} \right] p \frac{\partial}{\partial p} f_s(p, T) = - \frac{1}{H(T)} \left[\frac{1}{T} + \frac{1}{3} \frac{g'_{*s}(T)}{g_{*s}(T)} \right] \frac{1}{\exp\left(\frac{p}{T}\right) + 1} \times \\ \times \frac{\Gamma_{e,\text{TOT}}(p, T)}{4} \frac{\Delta^2(p) \sin^2(2\theta)}{\Delta^2(p) \sin^2(2\theta) + \frac{\Gamma_{e,\text{TOT}}(p, T)^2}{4} + [\Delta(p_r) \cos(2\theta) - V^D(T) - V_{\text{TOT}}^T(p, T)]^2} \end{aligned} \quad (5.11)$$

where

$$\Gamma_{e,\text{TOT}}(p, T) = \Gamma_{e,\text{SM}} + \Gamma_{e,P} = C_e(T) G_F^2 p T^4 + \frac{7\pi}{180} \epsilon_p^2 G_F^2 p T^4 \quad (5.12)$$

with values of $C_e(T)$ reported in Ref. [39], and

$$V_{\text{TOT}}^T(p, T) = V_{\text{SM}}^T + V_P^T = -3.72 G_F p T^4 \left(\frac{2}{m_W^2} + \frac{1}{m_Z^2} \right) - \frac{14\sqrt{2}\pi^2}{45 m_\phi^2} \epsilon_S G_F p T^4. \quad (5.13)$$

To solve the Boltzmann equation and carry out the results published in [3] and presented in the following, we used the code mentioned in the introduction of this chapter, that we wrote in the *Mathematica* package and later made public.

The first observable where the effects of NSSI are evident is the **momentum distribution** $r^2 f_s(r)$, with $r = p/T$, as shown in Fig. 5.3. Comparing the two black lines (solid for "vanilla" DW mechanism and dashed for DW mechanism in the presence of pseudoscalar NSSI) representing the distribution functions that satisfy the condition $\Omega_s h^2 = \Omega_{\text{DM}} h^2 = 0.12$, we notice that the action of NSSI slightly distorts the shape of $f_s(r)$ with respect to the one obtained in the canonical DW scenario. The colored bands are instead the result of the juxtaposition of lines representing other distribution functions obtained for different values of the NSSI coupling ϵ_p , but overproducing or underproducing sterile neutrino DM. The result shown in Fig. 5.3 has been obtained choosing $m_\phi = 10$ GeV. Although not shown here, we also verified that the distortion in the distribution function induced by pseudoscalar NSSI gets milder and milder for the same choice of values of $\sin^2(2\theta)$, m_s and ϵ_p but for larger and larger values of the mediator mass m_ϕ .

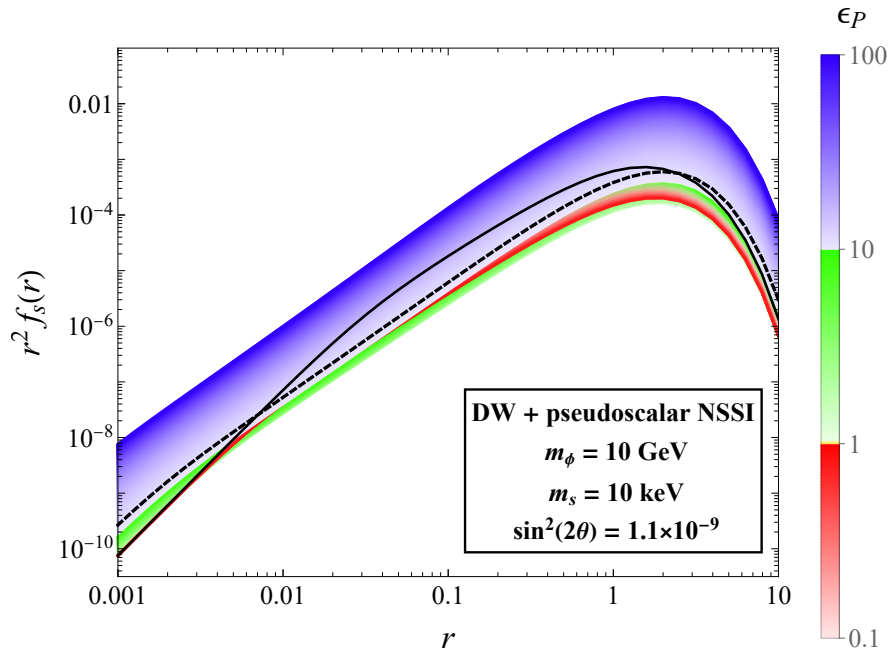


FIGURE 5.3: Sterile neutrino momentum distribution $r^2 f(r)$ where $r = p/T$ in the case of Dodelson-Widrow production in the "vanilla" scenario and in the presence of pseudoscalar NSSI. The values of the sterile neutrino parameters are chosen as $m_s = 10$ keV, $\sin^2(2\theta) = 1.1 \times 10^{-9}$ (BP2 in Fig. 5.5). The result is obtained for a relatively light mediator of pseudoscalar NSSI with $m_\phi = 10$ GeV. The black solid line represents the distribution function that gives $\Omega_s h^2 = \Omega_{\text{DM}} h^2 = 0.12$ in the "vanilla" DW scenario, with no NSSI involved. The black dashed line corresponds to the distribution function that satisfies the same condition that fixes the solid black line but in the case in which the production of sterile neutrino DM is modified by the presence of pseudoscalar NSSI. In different shades of red, green, and blue, we observe the result corresponding to different values of ϵ_P for which $\Omega_s h^2 \neq \Omega_{\text{DM}} h^2$.

Secondly, the presence of additional pseudoscalar NSSI influences the **evolution of the production** of sterile neutrino DM.

This can be seen in Fig. 5.4. Here, we show the evolution of the production rate of sterile neutrinos with $m_s = 10$ keV and $\sin^2(2\theta) = 1.1 \times 10^{-9}$ produced while the Universe cools down from 1 GeV to 1 MeV. In the "vanilla" Dodelson-Widrow scenario (black thick line), the peak of the production occurs between $T \sim 200$ MeV and $T \sim 300$ MeV in agreement with the prediction given in Ref. [35] for $T_{\text{peak}} \simeq 133 (m_s/\text{keV})^{\frac{1}{3}}$ MeV. The presence of pseudoscalar NSSI with a light ($m_\phi = 10$ GeV) mediator modifies the mechanism and shifts the peak of the production towards lower temperatures. As shown by the progression of the colors in the plot, the larger the strength of NSSI, the lower the temperature of the peak. In particular, the abundance of sterile neutrinos sufficient to constitute the entire content of DM in the Universe corresponds to the value of ϵ_p represented by the black dashed line whose peak is at $T \sim 100$ MeV. This temperature is much lower than the value of the NSSI mediator, and thus our choice of treating the impact of NSSI in an effective framework with truncation at the second order in the expansion in p is justified.

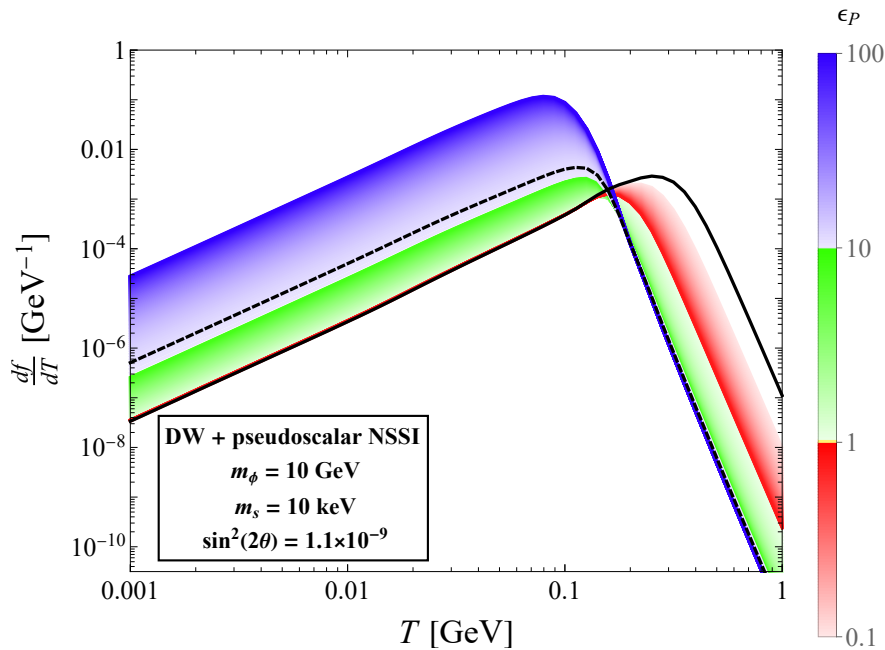


FIGURE 5.4: Evolution with temperature of the production rate of sterile neutrino DM with $m_s = 10$ keV and $\sin^2(2\theta) = 1.1 \times 10^{-9}$ (BP2 in Fig. 5.5). The thick black line corresponds to the "vanilla" Dodelson-Widrow production case without NSSI. The black dashed line corresponds to the production assisted by pseudoscalar NSSI with ϵ_p such that $\Omega_s h^2 = \Omega_{\text{DM}} h^2 = 0.12$. Different shades of red, green, and blue correspond to the increasing strength of NSSI involved in the sterile neutrino production. All the lines are obtained under the hypothesis that the NSSI mediator has mass $m_\phi = 10$ GeV.

5.2.2 Impact of NSSI on Sterile Neutrino Dark Matter Production and Detection

In this subsection, we consider again the **typical parameter space of sterile neutrino DM** ($\sin^2(2\theta), m_s$) and discuss **what changes in terms of these two parameters for production in the early Universe and detection in today's experiments, with the introduction of non-standard self-interactions among active neutrinos.**

Figs. 5.5 and 5.6 summarize the impact of, respectively, pseudoscalar and axial-vector NSSI on the production of sterile neutrinos in the early Universe, visible in their abundance today. The case of scalar NSSI is not shown because the impact of such interaction on the thermal potential and the interaction rate of active neutrinos is indistinguishable from the one of pseudoscalar NSSI. Subsequently, also the final abundance of sterile neutrino DM is affected in an identical way, and it is not worth showing it here. The differences between scalar and pseudoscalar interactions emerge only at the level of UV complete models, but the investigation of such models goes beyond the purpose of this work.

In the left panels of both figures, we see that the region of the parameter space that satisfies the condition $\Omega_s h^2 = \Omega_{\text{DM}} h^2 = 0.12$ is broadened by the presence of NSSI: depending on the strengths $\epsilon_{P,A}$ of the NSSI, we obtain a colored band instead of the black line that represents the "vanilla" Dodelson-Widrow case. Furthermore, depending on the mass of the NSSI mediator, the effect of NSSI shifts the DW line towards smaller or larger mixing angles differently. In particular, for the lightest mediator considered ($m_\phi = 10$ GeV), NSSI with small $\epsilon_{P,A}$ suppress the sterile neutrino production leading to larger values of the mixing angle needed to reach $\Omega_s h^2 = \Omega_{\text{DM}} h^2$. On the other hand, for $\epsilon_{P,A} > 2$, the effect of NSSI goes in the opposite direction, enhancing the production of sterile neutrinos and shifting the DW line towards smaller values of the mixing angle. This happens because as ϵ switches on, there is a new contribution to the interaction rate Γ_e and the potential V^T , which is proportional to ϵ^2 and ϵ , respectively. Initially, there is a suppression of the active-sterile conversion due to the damping term $D(p) = \Gamma_e/2$ in the denominator of Eq. (5.11), that leads to larger mixing angles being needed to produce the observed relic density of DM. However, as ϵ increases, the rate at which active neutrinos are produced in the early Universe through the new interaction also increases. This results in the production of the observed relic for smaller mixing angles. The suppressing power of NSSI decreases in the presence of heavier mediators, and for $m_\phi = 100$ GeV the values of allowed $\sin^2(2\theta)_{\text{NSSI}}$ are mostly less than $\sin^2(2\theta)_{\text{DW}}$. The expected sensitivities of upcoming experiments are also reported on the plots where the sensitivity regions are enclosed by blue lines for ECHO [146], black and gray lines for TRISTAN [128], and beige lines for HUNTER [165]. We do not report in the plots any line to represent the lines of the BeEST experiment [170] because in the first phases of the experiment, the sensitivity is too limited to be significant for our study, and it is strongly reduced by the constraint deriving from the requirement for the DM candidate to be stable on timescales comparable with the age of the Universe (the gray region in the top right corner of the plots). While TRISTAN's and ECHO's sensitivities are way too far from the region interested by the effects of NSSI, Phase 3 of the HUNTER experiment will probe masses and mixing angles for which the entire abundance of DM could be constituted by sterile neutrinos for $\epsilon_{P,A} \lesssim 10$. In the case of light NSSI mediator ($m_\phi = 10$ GeV), the interesting region of the parameter space probed by HUNTER will be larger, but some values of m_s , $\sin^2(2\theta)$, and $\epsilon_{P,A}$ will be probed also in case of heavier mediators ($m_\phi = 50, 100$ GeV).

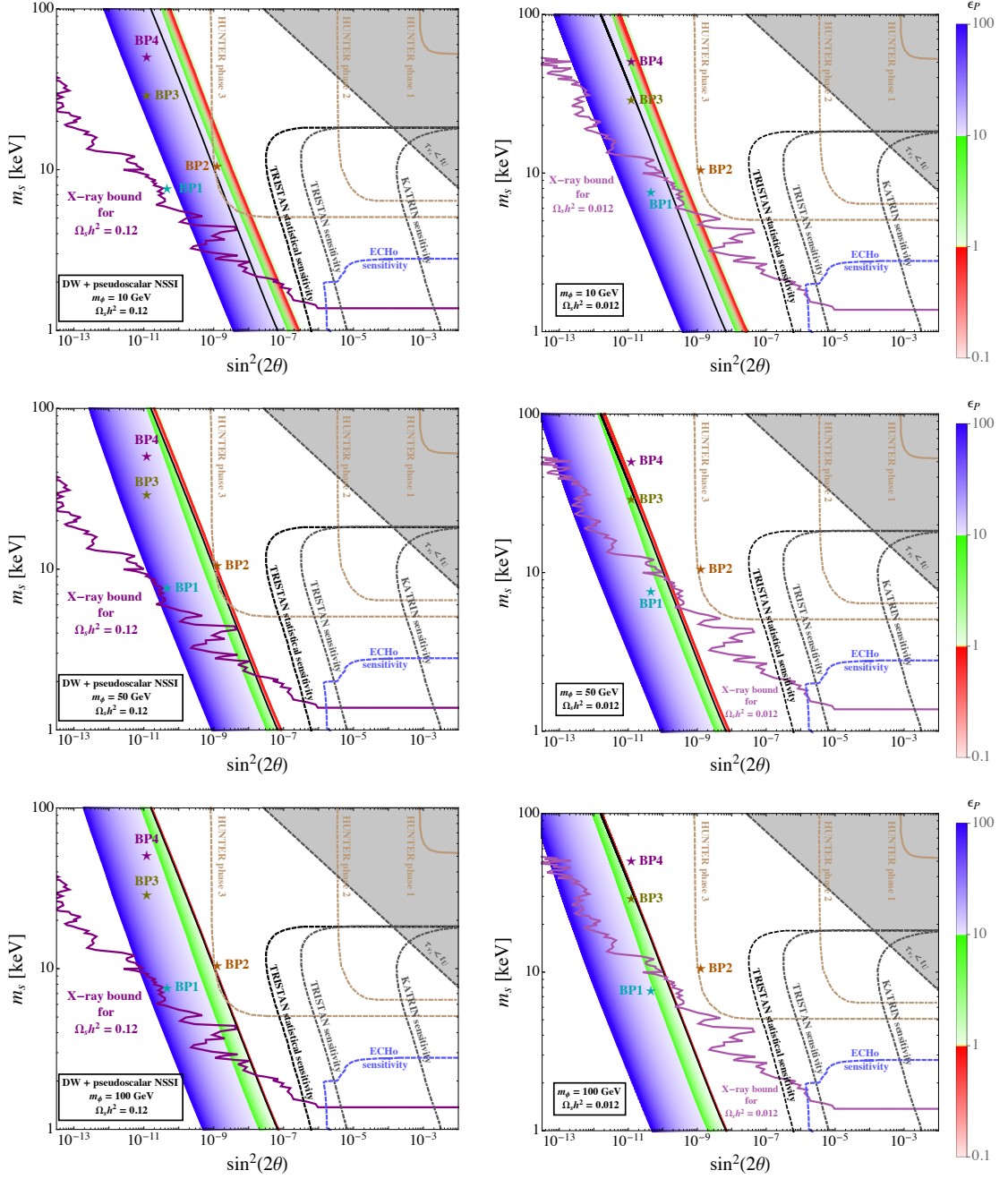


FIGURE 5.5: Pseudoscalar mediator case. The oblique straight lines are constituted by the points corresponding to the values of m_s and $\sin^2(2\theta)$ for which the conditions $\Omega_s h^2 = \Omega_{\text{DM}} h^2 = 0.12$ (left panel) and $\Omega_s h^2 = 0.1 \times \Omega_{\text{DM}} h^2 = 0.012$ (right panel) are satisfied, for different strengths of NSSI parameterized by ϵ_p . The black line corresponds to the case of "vanilla" Dodelson-Widrow production, i.e., $\epsilon_p = 0$, while different shades of red, green, and blue correspond to increasing values of ϵ_p in the range $[0.1, 100]$. The regions in which upcoming experiments will be sensitive are enclosed by beige (HUNTER), black and gray (TRISTAN), and blue (ECHO) lines. The purple line represents the current constraint from X-ray observations. Three values of mediator mass were chosen, $m_\phi = 10, 50, 100$ GeV for the upper, middle and lower panel. Four benchmark points BP1-4 are also given; see main text. The scalar mediator case looks identical, as expected.

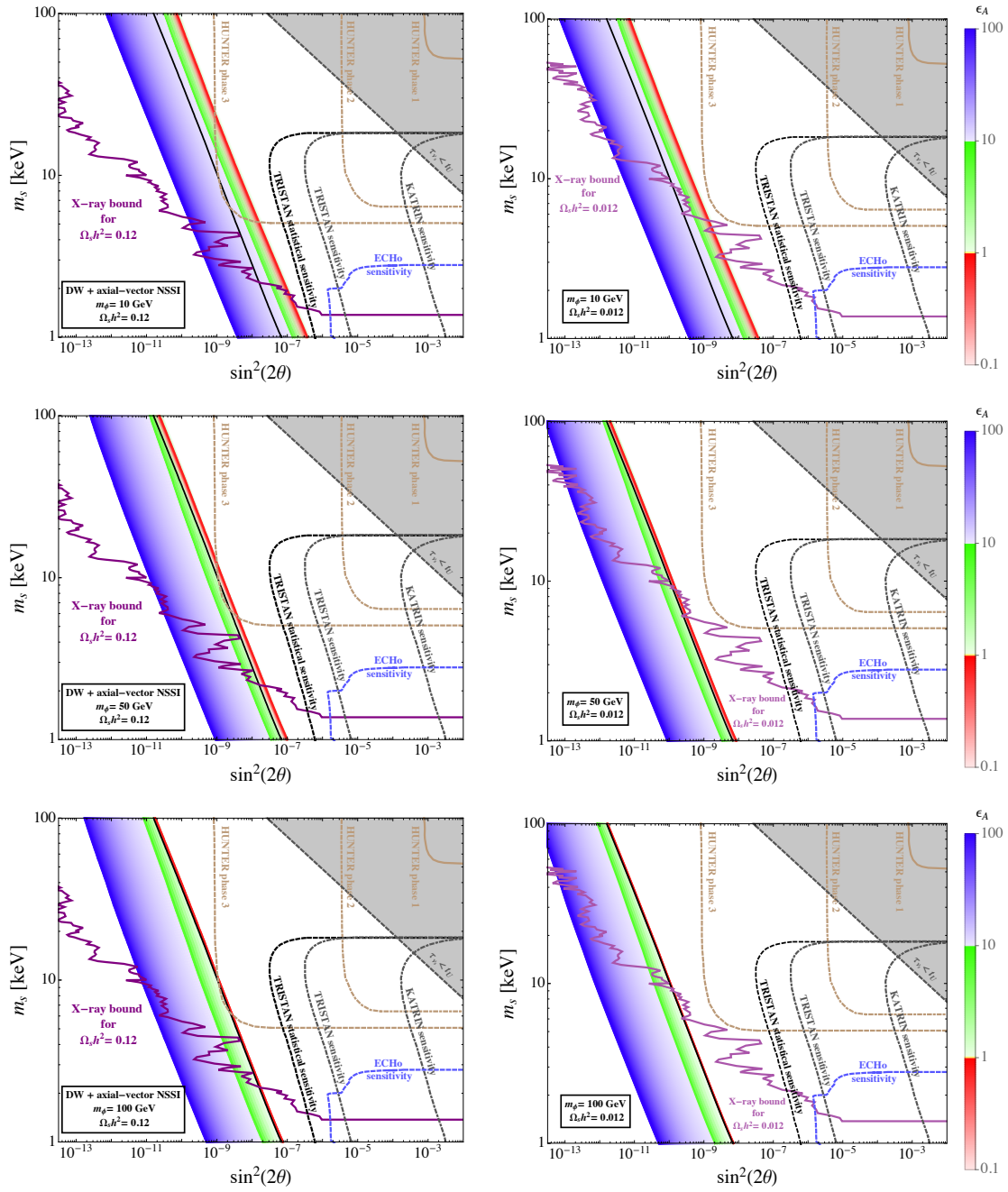


FIGURE 5.6: Axial-vector mediator case. The oblique straight lines are constituted by the points corresponding to the values of m_s and $\sin^2(2\theta)$ for which the conditions $\Omega_s h^2 = \Omega_{\text{DM}} h^2 = 0.12$ (left panel) and $\Omega_s h^2 = 0.1 \times \Omega_{\text{DM}} h^2 = 0.012$ (right panel) are satisfied, for different strengths of NSSI parameterized by ϵ_A . The black line corresponds to the case of "vanilla" Dodelson-Widrow production, i.e., $\epsilon_A = 0$, while different shades of red, green, and blue correspond to increasing values of ϵ_A in the range $[0.1, 100]$. The regions in which upcoming experiments will be sensitive are enclosed by beige (HUNTER), black and gray (TRISTAN), and blue (ECHO) lines. The purple line represents the current constraint from X-ray observations. Three values of mediator mass were chosen, $m_\phi = 10, 50, 100$ GeV for the upper, middle and lower panel.

The right panels of Figs. 5.5 and 5.6 summarize the results obtained for the case of "DM cocktail": we assume that only a fraction of dark matter (10% in the plots we show) is constituted by sterile neutrinos, while we remain agnostic about the composition of the rest of the DM abundance. In this case, the band relative to the production assisted by NSSI is shifted towards smaller values of the mixing angle. The sensitivity region of upcoming experiments is unvaried by this assumption since it depends only on the value of the mixing angle in the vacuum and not on the abundance of sterile neutrinos. This implies that the parameter space region in which the condition $\Omega_s h^2 = 0.1 \times \Omega_{\text{DM}} h^2 = 0.012$ is verified will not be testable even by HUNTER. On the other hand, as already discussed in Subsection 2.2.6, the constraint from X-ray observations is visibly relaxed in this scenario thanks to its dependence on the sterile neutrino abundance. Therefore, in this case, even larger ranges of values of m_s and $\sin^2(2\theta)$ are allowed from this point of view. A further advantage of the "DM cocktail" scenario is that the remaining fraction of DM might have completely different features from those of sterile neutrinos, and the mixture of the two or more candidates could fit much easier also all the constraints coming from other observables, such as, for example, from structure formation.

In Fig. 5.5, we added four benchmark points equal for the scenario in which $\Omega_s h^2 = 0.1 \times \Omega_{\text{DM}} h^2 = 0.012$ and the "DM cocktail" scenario:

- BP1 corresponds to the observed X-ray monochromatic line at 3.55 keV [110, 111], only in the case of $\Omega_s = \Omega_{\text{DM}}$ (since such signal depends on the abundance of DM constituted by sterile neutrinos);
- BP2 corresponds to the smallest mixing angle that will be probed by HUNTER and, at the same time, fulfills the condition $\Omega_s = \Omega_{\text{DM}}$ in the presence of NSSI with all three mediator mass values considered here;
- BP3 is characterized by the large m_s value not constrained by any phase space argument and, at the same time, by fulfilling both the conditions $\Omega_s = \Omega_{\text{DM}}$ and $\Omega_s = 0.1 \times \Omega_{\text{DM}}$ in different NSSI scenarios;
- BP4 is characterized by a mass that makes it an almost "cold" DM candidate in the standard DW scenario.

Such benchmark points are also relevant for the discussion regarding the impact of NSSI on structure formation in the next Section 5.3.

5.3 Indirect Impact of NSSI on Structure Formation

An excellent approximate estimate ² of the impact of WDM candidates on structure formation can be obtained in terms of their free-streaming horizon or length λ_{FS} . This quantity, which can be interpreted as the mean distance the DM particles would travel if they were not gravitationally bound [34], identifies the scale below which warm and cold DM particles behave differently concerning the formation of structures. By definition, cold DM (CDM) particles are non-relativistic when they are produced, and their abundance is fixed. On the contrary, the definition of warm DM (WDM) particles says that they are relativistic at their production, and they become non-relativistic only in a second moment when the temperature of the Universe falls below the value of their mass

²The most rigorous approach would dictate to determine the velocity profile of the DM candidate and do the full simulation of the resulting structures in the Universe using that profile [63]. However, this approach requires a very heavy numerical effort.

due to the Hubble expansion. Sterile neutrinos with a mass of $\mathcal{O}(\text{keV})$ are considered WDM candidates because they are produced relativistic predominantly at temperatures around 100 MeV, and they become non-relativistic during the radiation domination era. While they are still relativistic, they stream out of the smallest overdensities, and the result is a suppressed matter power spectrum of sterile neutrino DM on scales below λ_{FS} as compared to the power spectrum expected in a CDM cosmology with the same cosmological parameters.

There are three main approaches to probe this suppression in the matter power spectrum:

- by measuring the matter power spectrum directly at relevant scales, using Lyman- α forest, weak lensing, or 21 cm line;
- by counting the number of collapsed structures in the Local Group as a function of their masses and redshift, directly focusing on dwarf galaxies satellites of the Milky Way, or indirectly probing the reionization history;
- by determining the distribution of matter within individual DM-dominated objects such as cores in galactic haloes.

Unfortunately, all these methods are subject to large statistical and systematic uncertainties [228].

The **free-streaming horizon** is defined as [228]

$$\lambda_{\text{FS}} = \int_{t_{\text{in}}}^{t_0} \frac{\langle v(t) \rangle}{a(t)} dt, \quad (5.14)$$

where t_{in} is the time at which DM is produced, t_0 indicates today, $\langle v(t) \rangle$ is the typical velocity of DM particles and $a(t)$ is the scale factor. For sterile neutrinos with a mass of $\mathcal{O}(\text{keV})$, it can be approximated as [40]

$$\lambda_{\text{FS}} \simeq 1.2 \text{ Mpc} \left(\frac{\text{keV}}{m_s} \right) \frac{\langle p/T \rangle}{3.15}, \quad (5.15)$$

where $\langle p/T \rangle$ is the averaged momentum over the temperature of sterile neutrinos, and it is compared to the value of $\langle p/T \rangle$ calculated for active neutrinos whose distribution function is a thermal Fermi distribution. The value of the free-streaming length **depends on the features of the production through $f_s(p, T)$ used to obtain the typical value of the rescaled momentum $p/T = r$** as [40]

$$\langle r \rangle = \frac{\int d^3 \vec{p} \left(\frac{p}{T} \right) f_s(p, T)}{\int d^3 \vec{p} f_s(p, T)} = \frac{\int_{r=0}^{\infty} r^3 dr f_s(r)}{\int_{r=0}^{\infty} r^2 dr f_s(r)} \quad (5.16)$$

where $f_s(r)$ is the solution of the Boltzmann equation reported in Eq. (5.11), just in terms of the rescaled momentum r .

We expect sterile neutrino DM produced through oscillation and collisions to be WDM, and we wanted to verify that this is true also for sterile neutrinos produced through the DW mechanism modified by the presence of neutrino NSSI. For a DM candidate to be considered "warm", and thus compatible with the structures that we observe in today's Universe, the free-streaming horizon must be $0.01 \text{ Mpc} \lesssim \lambda_{\text{FS}} \lesssim 0.1 \text{ Mpc}$ [63]. The white region represents this condition in Fig. 5.7, where we plot λ_{FS} as a function of different strengths of pseudoscalar NSSI.

Different colors of the lines representing λ_{FS} correspond to the different values of the sterile neutrino parameters $(\sin^2(\theta), m_s)$ identified by the chosen benchmark points in Fig. 5.5. Different line types are associated with different mass values of the mediators

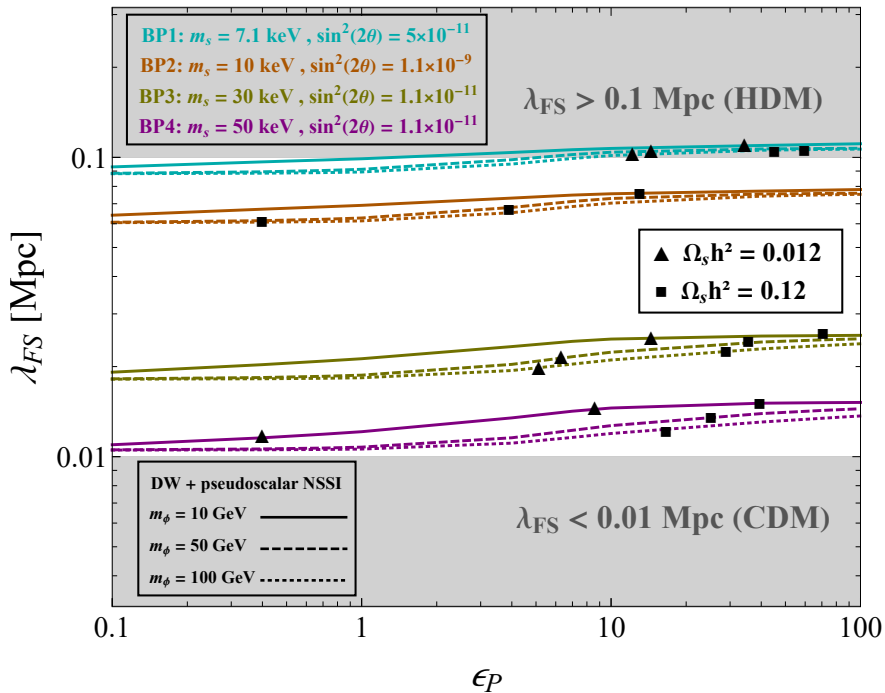


FIGURE 5.7: Variation of the free-streaming length of sterile neutrino DM determined by the increasing strength of NSSI for different values of $\sin^2(2\theta)$ and m_s . Each color refers to a benchmark point given in Figs. 5.5 and 5.6. Each line type corresponds to a different value of the NSSI mediator mass. Black squares pinpoint to values of ϵ_P for which the condition $\Omega_s h^2 = \Omega_{\text{DM}} h^2 = 0.12$ is satisfied. Black triangles identify values of ϵ_P such that only the 10% of the DM abundance is constituted by sterile neutrinos in the "DM cocktail" scenario.

of pseudoscalar NSSI. We pinpoint the values of ϵ_P , $\sin^2(\theta)$ and m_s that give $\Omega_s h^2 = \Omega_{\text{DM}} h^2 = 0.12$ by black squares and those that give $\Omega_s h^2 = 0.1 \times \Omega_{\text{DM}} h^2 = 0.012$ by black triangles.

Two cases are worthy of attention. First, if we consider BP1 that identifies the famous observed X-ray line at 3.55 keV [110, 111], we see that large NSSI would be needed to produce an abundance of such sterile neutrinos large enough to constitute a non-negligible percentage of the Universe's DM content. However, such large NSSI would put sterile neutrinos with such features in conflict with constraints coming from structure formation: they would have been produced with too high velocities modifying large structures that we observe today. Second, also BP2 is particularly interesting. It represents a case in which the NSSI effect is crucial to allow sterile neutrinos to be produced in the correct abundance, and at the same time, it does not lead to tensions with structure formation. Moreover, being at the border of the sensitivity region expected for Phase 3 of the HUNTER experiment, the values of the parameters relative to this point will be available for experimental test.

In general, the lines corresponding to the chosen benchmark points span the entire region where sterile neutrinos can be considered warm DM candidates, and we notice that their trend does not change much, varying the strength of NSSI. We see that even for substantial values of ϵ_P , almost all the lines remain in the white region of the parameter space where they start at $\epsilon_P = 0$. This tells us that no effect of NSSI in the allowed

range of values of ϵ is strong enough to drastically modify the impact of sterile neutrino dark matter on structure formation from the "cold" regime to the "hot" one, or vice versa. Although in principle the free-streaming horizon depends on the production mechanism, from Fig. 5.7 it seems that, in our case, the major difference in locating the lines in the parameter space is made by the value of the sterile neutrino mass rather than by the NSSI among active neutrinos. Based on such considerations, we conclude that the influence of NSSI on the free-streaming length is limited, and the impact is small even for large values of ϵ_P . This allows us to say that the existence of NSSI acting with strengths ϵ_P within the current limits would not put sterile neutrinos in tension with structure formation constraints unless they are very light.

5.4 Outlook

The results obtained for the introduction of non-standard self-interaction involving Majorana neutrinos show that such extra interactions impact the production of sterile neutrino DM in the early Universe and the discovery potential of terrestrial experiments that hunt such DM candidates. Given the promising results of this pilot study, it would be interesting to see what would happen with non-standard interactions involving other particles.

NSSI involving Dirac neutrinos have been studied in the context of UV complete theories in Refs. [192, 193]. In these works, only two types of mediators have been considered: scalar and vector. A possible follow-up of the work presented in this dissertation would be to develop the EFT formalism analogous to the one adopted in Chapter 5 but involving Dirac neutrinos. This would allow to study the impact of NSSI among Dirac neutrinos in a model-independent way and to investigate the contribution of other types of interactions (vector and tensor) that are zero for Majorana neutrinos.

Moreover, both scenarios involving Majorana and Dirac neutrinos could be studied relaxing the assumption of flavor conservation in the NSSI. This would allow to have a phase in the couplings ϵ and possibly negative couplings, resulting in a different interplay of the two modified terms in the denominator of the effective mixing angle, Γ_e and V^T .

Other promising directions to extend this kind of study are represented by considering non-standard interactions involving other species.

In the case of interactions with charged leptons, these could be straightforwardly tested with traditional ν scattering and oscillation experiments [188].

A different perspective would prospect if we consider non-standard interactions involving active and sterile neutrinos, as proposed in Ref. [229] in a UV complete theory framework. In the latter scenario, one has to keep in mind that including non-standard interactions between active and sterile neutrinos in the production of sterile neutrinos in the early Universe could lead to difficulties from the point of view of the numerical solution of the Boltzmann equations. Indeed, in this case, the distribution function of sterile neutrinos that in principle also appears on the r.h.s. of the Boltzmann equation and is usually neglected would not be negligible anymore and would considerably complicate the numerical solution of the equation.

Finally, it could be interesting to investigate also the effect on sterile neutrino production and evolution of NSSI involving exclusively sterile neutrinos, taking inspiration from what was done in Ref. [230].

Chapter 6

Summary and Conclusion

The question of the existence and nature of dark matter, as one of the most abundant components of our Universe, has thrilled and puzzled by now many generations of physicists. Sterile neutrinos with a mass of $\mathcal{O}(\text{keV})$ emerged as very good candidates to play the role of DM, as discussed in the first two chapters of this thesis. Indeed, sterile neutrinos can be considered the most natural extension of the SM and be easily embedded in models able to explain not only the DM problem but also the active neutrino masses and the baryonic asymmetry. They are almost completely decoupled from the SM, can be stable over cosmological timescales, and can be produced in the early Universe in abundance correct to match the abundance of DM in several minimal new physics scenarios, introduced in Chapter 2, and for wide ranges of values of their characteristic parameters. Moreover, despite the plethora of astrophysical and cosmological observables that can be used to constrain them indirectly, large regions of their parameter space are not yet ruled out, leaving them as a viable solution to the DM puzzle.

Last but not least, a promising experimental program aimed at their direct detection, outlined in Chapter 3, is at its dawn. A number of experiments based on diversified techniques will soon be able to probe large regions of the accessible parameter space relevant for sterile neutrinos that qualify to play the role of DM. All these features and circumstances make them a fascinating subject to be studied from the theoretical and phenomenological point of view and to be investigated experimentally.

In the original research works on which this thesis is based, we studied the production of this fascinating DM candidate in the early Universe in two non-standard scenarios (involving non-standard cosmological history and non-standard interactions among active neutrinos) with a particular interest in the phenomenology of these models. We aimed to discover what changes, in these non-standard scenarios, in the phenomenology of sterile neutrino DM that is relevant for their detection in upcoming terrestrial experiments, such as KATRIN/TRISTAN, ECHo, and HUNTER.

In this perspective, we first discussed the constraint on sterile neutrino DM coming from X-ray observations that, to date, is the one that disfavors the most the region of the parameter space that is most interesting for sterile neutrino experimental searches. In Chapter 2 of this thesis, we showed that there are at least three cases in which the X-ray limit should be considered in a looser strength than what is usually assumed. In particular, we demonstrated for the first time in this work that this constraint could be considered model-dependent and that it can be relaxed and even disappear completely in a scenario in which minimal new physics is included, which reduces the sterile neutrino decay width by disruptive interference.

Although the concrete realization proposed as an example in Chapter 2 requires a bit of tuning of the parameters to realize the complete cancellation of the X-ray bound, it is

noteworthy that the one taken as an example is not the only possible solution and that similar result can be obtained in different frameworks involving different new degrees of freedom. On the other hand, the results obtained concerning the relaxation of the X-ray limit are of utmost importance from the point of view of running and upcoming experiments because they make accessible again their sensitivity region that would be otherwise completely ruled out.

In Chapter 4 of this thesis, we presented the study of the production of sterile neutrino DM in the context of non-standard cosmological scenarios. We considered the production of Dirac sterile neutrinos through oscillation and collisions via the Dodelson-Widrow mechanism, Shi-Fuller standard mechanism, and Shi-Fuller mechanism modified by the occurrence of CPT violation in the sterile sector. As for the non-standard cosmological pictures, we focused on scenarios involving a low reheating temperature or a new energy scale associated with the dynamical change of the sterile neutrino mass value m_s . We introduced a new parameter called critical temperature T_c associated with these new energy scales. The consequence of being in such non-standard cosmologies is that the production of sterile neutrino DM is suppressed in the very early Universe and can start only at temperatures lower than T_c . If $T_c < T_{\text{peak}}$, temperature at which the production mechanism is most efficient, the delay in the production results in an overall suppression of the abundance that has to be compensated by larger values of the active-sterile mixing with respect to the standard case, to satisfy the condition $\Omega_s h^2 = \Omega_{\text{DM}} h^2 = 0.12$. We demonstrated that in non-standard cosmological scenarios perfectly suitable to describe the very early Universe according to the currently available data, the typical parameters of sterile neutrino DM, i.e. its mixing angle with an active species parameterized by $\sin^2(2\theta)$ and its mass m_s , have to take values that fall in the region of the parameter space in which terrestrial experiments are expected to be sensitive in the near future. This conclusion is valid for all the three production mechanisms considered based on active-sterile conversion via oscillation and collisions.

This implies that, provided that the X-ray limit is relaxed according to what is described in Chapter 2, the results of this study constitute a strong motivation for KATRIN/TRISTAN, ECHo, and HUNTER experiments to proceed with their schedule and push to reach the best performances possible.

In Chapter 5 of this thesis, the non-standard ingredient added to the "vanilla" Dodelson-Widrow production mechanism is non-standard self-interactions (NSSI) among active neutrinos. These new neutrino-philic interactions can, in principle, be of any type (scalar, pseudoscalar, vector, axial-vector, and tensor), although only scalar, pseudoscalar, and axial-vector interactions give non-zero contribution for Majorana neutrino of a single species involved. They are at the moment very loosely constrained by data, and, on the other hand, they are naturally expected to be part of numerous models aiming at active neutrino mass generation. Working under the assumption of sterile neutrino DM having a Majorana nature and mixing with the active electron species, we looked at how flavor-conserving NSSI involving active electron neutrinos would impact sterile neutrino production that occurs through the simplest mechanism based on oscillation and collisions. We found out that NSSI modify the active neutrino interaction rate Γ_e and the thermal potential V^T terms in the effective mixing angle expression. We decided to treat the problem in the most general way possible, and we opted for an effective field theory perspective to include the NSSI in the particle model. Therefore, we developed the effective formalism needed to calculate the additional contributions to interaction rate and thermal potential due to the NSSI presence. This formalism is a

tool that will be useful for further developments of this study that might involve non-standard interactions of neutrinos with charged leptons or Dirac neutrinos. Including in the production mechanism the contributions coming from NSSI, we demonstrated that the latter have the effect of widening the accessible region of the parameter space of sterile neutrino DM, changing the line characteristic of the "vanilla" Dodelson-Widrow mechanism into a broad range of values of $\sin^2(2\theta)$ and m_s that satisfy the condition $\Omega_s h^2 = \Omega_{\text{DM}} h^2 = 0.12$.

The most remarkable result of Chapter 5, together with the EFT machinery that could be used in other contexts, is the discovery that the presence of NSSI enhances the possibility that the HUNTER experiment could detect sterile neutrino DM in its most advanced stage, again under the assumption of a considerable relaxation of the X-ray bound according to what discussed in Chapter 2. Moreover, in Chapter 5 we showed that NSSI among active neutrinos do not change much the impact of sterile neutrino DM on large-scale structures.

To summarize, the relevance of this theoretical and phenomenological work is twofold. From the theoretical point of view, it increased the knowledge about possible scenarios describing the early Universe and the behavior and phenomenology of sterile neutrino DM in this fascinating period. On the other hand, equal or even greater significance can be claimed concerning experiments investigating sterile neutrino DM. Indeed, the results presented in Chapters 4 and 5 provide further solid motivation to search for signatures of such DM candidates in regions of the parameter space inaccessible in the standard scenarios but extremely interesting in relation with the expected sensitivity of the near future experiments.

Regarding the outlook of the work presented in this thesis, two points are worthy of mention.

First of all, as previously discussed, the work presented in Chapter 5 should be considered a kind of pilot study of the possible impact of NSI on sterile neutrino DM production and detection perspective. Based on the positive findings we obtained, the conclusion is that it would be interesting to extend the same effective approach to study the impact of other neutrino non-standard interactions involving different particles, for example, charged leptons or sterile neutrinos, or to carry out an effective study of NSSI involving Dirac neutrinos for which vector and tensor interactions would give non-zero contribution too. In particular, although more stringently constrained, NSI between active neutrinos and charged leptons would present a phenomenology more favorable to experimental tests thanks to the involvement of charged particles in the process. Moreover, another assumption that can be relaxed is the flavor-conserving nature of the considered NSSI, and it is possible to study the effect of NSSI involving neutrinos of different generations, with potential surprises coming from the phase that can change the sign of the NSSI contribution to the thermal potential. These developments are left to future work.

Secondly, at the end of this thesis's writing process, I found new constraints on sterile neutrino DM from combined data of gravitational lensing, Milky Way satellites, and Lyman- α forest have been derived and made public in the arXiv preprint [231]. They seem to disfavor the production through oscillation and collisions for a wide range of mass values, including the mass values more promising in the perspective of the work presented in this thesis. However, as discussed in Section 5.3 in Chapter 5, constraints coming from observation of structures heavily rely on the momentum distribution of the DM candidate that in turn depends on the production mechanism. The constraints reported in Ref. [231] have not been derived yet for the two non-standard production

mechanisms presented in this thesis. Therefore, another possible and valuable development of the work presented in Chapters 4 and 5 will be to derive the magnitude of the constraints discussed in Ref. [231], in the specific scenarios involving non-standard cosmological histories and NSSI, in order to carefully verify how heavily the results of this thesis are affected by these new constraints.

Appendix A

Neutrino Oscillation

Neutrino oscillation is a quantum mechanical phenomenon produced in the three-flavor picture thanks to the mismatch between neutrino flavor eigenstates $|\nu_\alpha\rangle$, with $\alpha = e, \mu, \tau$, and mass eigenstates $|\nu_k\rangle$, with $k = 1, 2, 3$. Flavor eigenstates $\{|\nu_\alpha\rangle\}$ can be described as a superposition of mass eigenstates $\{|\nu_k\rangle\}$

$$|\nu_\alpha\rangle = \sum_k U_{\alpha k}^* |\nu_k\rangle \quad (\text{A.1})$$

and vice versa, and the two orthonormal bases of eigenstates are related by a unitary transformation described by the so-called PMNS matrix U satisfying

$$U^\dagger U = 1 \quad \sum_k U_{\alpha k} U_{\beta k}^* = \delta_{\alpha\beta} \quad \sum_\alpha U_{\alpha k} U_{\alpha j}^* = \delta_{kj}. \quad (\text{A.2})$$

The PMNS matrix can be parameterized by three mixing angles θ_{ij} with $i, j = 1, 2, 3$ and a CP-violating phase δ_{CP} in the case of Dirac neutrinos¹. Its parameterization can be factorized in three rotations, each of which depends on a different mixing angle as follows

$$\begin{aligned} U_{\text{PMNS}} &= \begin{pmatrix} 1 & 0 & 0 \\ 0 & c_{23} & s_{23} \\ 0 & -s_{23} & c_{23} \end{pmatrix} \begin{pmatrix} c_{13} & 0 & s_{13}e^{-i\delta_{\text{CP}}} \\ 0 & 1 & 0 \\ -s_{13}e^{i\delta_{\text{CP}}} & 0 & c_{13} \end{pmatrix} \begin{pmatrix} c_{12} & s_{12} & 0 \\ -s_{12} & c_{12} & 0 \\ 0 & 0 & 1 \end{pmatrix} \\ &= \begin{pmatrix} c_{12}c_{13} & s_{12}c_{13} & s_{13}e^{-i\delta_{\text{CP}}} \\ -s_{12}c_{23} - c_{12}s_{13}s_{23}e^{i\delta_{\text{CP}}} & c_{12}c_{23} - s_{12}s_{13}s_{23}e^{i\delta_{\text{CP}}} & c_{13}s_{23} \\ s_{12}s_{23} - c_{12}s_{13}c_{23}e^{i\delta_{\text{CP}}} & -c_{12}s_{23} - s_{12}s_{13}c_{23}e^{i\delta_{\text{CP}}} & c_{13}c_{23} \end{pmatrix} \quad (\text{A.3}) \end{aligned}$$

with $s_{ij} = \sin(\theta_{ij})$ and $c_{ij} = \cos(\theta_{ij})$.

A.1 In the Vacuum

Neutrinos are produced in weak interaction processes in flavor eigenstates $|\nu_\alpha\rangle$. However, their propagation is governed by the free Hamiltonian \mathcal{H} with eigenvalues $E_k = \sqrt{m_k^2 + \vec{p}_k^2}$ and eigenstates $|\nu_k\rangle$. So, those that evolve in space during propagation are the mass eigenstates, and their propagation is described by the Schrödinger equation

$$i \frac{d}{dt} |\nu_k(t)\rangle = \mathcal{H} |\nu_k(t)\rangle \quad (\text{A.4})$$

¹In the case of Majorana neutrinos two more phases have to be included in the parameterization.

whose solution is the plane wave

$$|v_k(t)\rangle = e^{-iE_k t} |v_k\rangle. \quad (\text{A.5})$$

The flavor eigenstate that will be detected after a propagation lasting a time t (with production at $t = 0$), is then

$$|v_\alpha(t)\rangle = \sum_k U_{\alpha k}^* e^{-iE_k t} |v_k\rangle \quad (\text{A.6})$$

such that

$$|v_\alpha(t=0)\rangle = |v_\alpha\rangle. \quad (\text{A.7})$$

However, $|v_\alpha(t)\rangle$ is possibly different from $|v_\alpha\rangle$: it can be a different superposition of mass eigenstates with respect to the initial one. This is the case if the mass eigenvalues are non-degenerate. Indeed, if $m_k \neq m_j$, this difference generates a difference in phase changing the coefficients with which every mass state contributes to the final flavor state. Using the relation

$$|v_k\rangle = \sum_\beta U_{\beta k} |v_\beta\rangle \quad (\text{A.8})$$

we obtain

$$|v_\alpha(t)\rangle = \sum_{\beta=e,\mu,\tau} \left(\sum_{k=1,2,3} U_{\alpha k}^* e^{-iE_k t} U_{\beta k} \right) |v_\beta\rangle. \quad (\text{A.9})$$

The transition amplitude is

$$A_{v_\alpha \rightarrow v_\beta}(t) \equiv \langle v_\beta | v_\alpha(t) \rangle = \sum_k U_{\alpha k}^* U_{\beta k} e^{-iE_k t} \quad (\text{A.10})$$

and the probability to detect a neutrino flavor state $|v_\beta\rangle$ at t , having produced at $t = 0$ a flavor state $|v_\alpha\rangle$ is

$$P_{v_\alpha \rightarrow v_\beta}(t) = \left| A_{v_\alpha \rightarrow v_\beta}(t) \right|^2 = \sum_{k,j} U_{\alpha k}^* U_{\beta k} U_{\alpha j} U_{\beta j}^* e^{-i(E_k - E_j)t}. \quad (\text{A.11})$$

The dispersion relation of ultra-relativistic neutrinos can be approximated as

$$E_k \simeq E + \frac{m_k^2}{2E}. \quad (\text{A.12})$$

Therefore, the energy difference can be written in terms of the squared mass difference

$$E_k - E_j \simeq \frac{m_k^2 - m_j^2}{2E} = \frac{\Delta m_{kj}^2}{2E} \quad (\text{A.13})$$

and the oscillation probability becomes

$$P_{v_\alpha \rightarrow v_\beta}(t) = \left| A_{v_\alpha \rightarrow v_\beta}(t) \right|^2 = \sum_{k,j} U_{\alpha k}^* U_{\beta k} U_{\alpha j} U_{\beta j}^* \exp \left(-i \frac{\Delta m_{kj}^2 t}{2E} \right). \quad (\text{A.14})$$

Since in oscillation experiments the time is not measured, while we know the distance of propagation from the source to the detector L , for convenience, the time t is usually expressed in terms of the distance L , remembering that ultra-relativistic particles travel almost at the speed of light, thus allowing the relation $L \simeq t$.

The final expression for the oscillation probability from a flavor eigenstate $|\nu_\alpha\rangle$ to another flavor eigenstate $|\nu_\beta\rangle$, in the three-flavor picture, is then

$$P_{\nu_\alpha \rightarrow \nu_\beta}(L, E) = \left| A_{\nu_\alpha \rightarrow \nu_\beta}(t) \right|^2 = \sum_{k,j} U_{\alpha k}^* U_{\beta k} U_{\alpha j} U_{\beta j}^* \exp\left(-i \frac{\Delta m_{kj}^2 L}{2E}\right). \quad (\text{A.15})$$

A.1.1 Two-Flavor Picture

There are situations in which the oscillation phenomenon is well described in the picture involving only two flavors because the oscillation in the third flavor is negligible. In such cases, the description is simplified: only one mixing angle is needed and no phase. The mixing matrix reduces to

$$\begin{pmatrix} \cos(\theta_a) & \sin(\theta_a) \\ -\sin(\theta_a) & \cos(\theta_a) \end{pmatrix} \quad (\text{A.16})$$

where $0 \leq \theta_a \leq \pi/2$ and there is only one squared mass difference $\Delta m^2 = \Delta m_{21}^2 = m_2^2 - m_1^2$.

The expression for the transition probability (oscillation with $\nu_\beta \neq \nu_\alpha$) in this simplified case is

$$P_{\nu_\alpha \rightarrow \nu_\beta}(L, E) = \sin^2(2\theta_a) \sin^2\left(\frac{\Delta m^2 L}{4E}\right). \quad (\text{A.17})$$

It is convenient to define the oscillation length

$$L_{\text{osc}} = \frac{4\pi E}{\Delta m^2} \quad (\text{A.18})$$

which is the distance at which the phase generated by Δm^2 becomes 2π . Moreover, it is good to keep in mind that the average probability takes the shape

$$\langle P_{\nu_\alpha \rightarrow \nu_\beta} \rangle = \frac{1}{2} \sin^2(2\theta_a) \quad (\text{A.19})$$

which depends only on the mixing angle and corresponds to what is called "incoherent transition probability" in Ref. [1]. This expression is significant in the context of the production of sterile neutrino DM through oscillation and collisions, which happens thanks to the decoherence introduced by frequent interactions of neutrinos with particles in the plasma.

A.2 In a Medium

Neutrinos that propagate in a medium can undergo coherent forward scattering. Although in this process they are not absorbed and they do not change flavor, they moderately "feel" the presence of the plasma in a way that can be parameterized through an effective potential that modifies their effective mass and mixing. This effective mixing angle is the one involved in the sterile neutrino production in the early Universe through the Dodelson-Widrow and the Shi-Fuller mechanisms. In particular, in the latter production mechanism the presence of a primordial lepton asymmetry intensifies this effect leading to the enhancement of the effective mixing angle to very large values, with subsequent enhanced active-sterile conversion, even for small values of the vacuum mixing angle.

The magnitude of the effective potential depends on the kind of interactions that neutrinos have with particles of the medium. In the following, we consider the example of a single active neutrino ν_α propagating through the primordial plasma and oscillating only into a sterile neutrino ν_s (two-flavor picture) with a mixing matrix called U .

Assuming only standard model interactions, for the active neutrino ν_α we expect a potential V_α proportional to the Fermi constant (for the weak interaction) and proportional to the sum of the densities of every species of particles present in the plasma with which the electron neutrino does interact. We do not specify further because especially the density of the various species varies along the history of the Universe.

To see how the transition amplitude evolves in these conditions we remember that the evolution of the neutrino states is governed by the total Hamiltonian $\mathcal{H}_{\text{tot}} = \mathcal{H}_0 + \mathcal{H}_I$ where the free Hamiltonian \mathcal{H}_0 acts on the mass eigenstates as $\mathcal{H}_0|v_k\rangle = E_k|v_k\rangle$ with $E_k^2 = m_k^2 + \vec{p}_k^2$, and the interaction Hamiltonian \mathcal{H}_I acts on the interaction eigenstates as $\mathcal{H}_I|v_\alpha\rangle = V_\alpha|v_\alpha\rangle$.

The evolution of $|v_\alpha\rangle$ is described by the Schrödinger equation

$$i \frac{d}{dt} |v_\alpha(t)\rangle = \mathcal{H}_{\text{tot}} |v_\alpha(t)\rangle \quad (\text{A.20})$$

Since $A_{\alpha\beta}(t) = A_{\nu_\alpha \rightarrow \nu_\beta}(t) = \langle v_\beta | v_\alpha(t) \rangle$,

$$\begin{aligned} i \frac{d}{dt} A_{\alpha\beta}(t) &= i \frac{d}{dt} \langle v_\beta | v_\alpha(t) \rangle \\ &= \langle v_\beta | \mathcal{H}_{\text{tot}} | v_\alpha(t) \rangle = \langle v_\beta | \mathcal{H}_0 | v_\alpha(t) \rangle + \langle v_\beta | \mathcal{H}_I | v_\alpha(t) \rangle \\ &= \sum_\eta \sum_k U_{\beta k} E_k U_{\eta k}^* \langle v_\eta | v_\alpha(t) \rangle + V_\beta \langle v_\beta | v_\alpha(t) \rangle. \end{aligned} \quad (\text{A.21})$$

Here, in the last step, for the first term we rotated interaction eigenstates into mass eigenstates and then again into interaction eigenstates in order to extract the energy eigenvalue E_k , and for the second term we used $\mathcal{H}_I|v_\beta\rangle = V_\beta|v_\beta\rangle$ and took the hermitian conjugate $\langle v_\beta | \mathcal{H}_I = \langle v_\beta | V_\beta$.

Finally, to have the same indices, we can use that

$$V_\beta \langle v_\beta | v_\alpha(t) \rangle = \sum_\eta \delta_{\eta\beta} V_\beta \langle v_\eta | v_\alpha(t) \rangle \quad (\text{A.22})$$

and we get

$$i \frac{d}{dt} A_{\alpha\beta}(t) = \sum_\eta \left[\sum_k U_{\beta k} E_k U_{\eta k}^* + \delta_{\eta\beta} V_\beta \right] A_{\alpha\eta}(t) = \text{I} + \text{II}. \quad (\text{A.23})$$

Introducing the approximation for ultra-relativistic neutrinos $E_k \simeq E + \frac{m_k^2}{2E}$ and using $m_k^2 = m_k^2 - m_i^2 + m_i^2 = \Delta m_{ki}^2 + m_i^2$, we get

$$\begin{aligned} \mathbb{I} &= \sum_{\eta} \left[\sum_k U_{\beta k} E U_{\eta k}^* \right] A_{\alpha\eta}(t) + \sum_{\eta} \left[\sum_k U_{\beta k} \frac{m_k^2}{2E} U_{\eta k}^* \right] A_{\alpha\eta}(t) \\ &= \left(E + \frac{m_i^2}{2E} \right) \sum_{\eta} \left[\sum_k U_{\beta k} U_{\eta k}^* \right] A_{\alpha\eta}(t) + \sum_{\eta} \left[\sum_k U_{\beta k} \frac{\Delta m_{ki}^2}{2E} U_{\eta k}^* \right] A_{\alpha\eta}(t) \\ &= \left(E + \frac{m_i^2}{2E} \right) A_{\alpha\beta}(t) + \sum_{\eta} \left[\sum_k U_{\beta k} \frac{\Delta m_{ki}^2}{2E} U_{\eta k}^* \right] A_{\alpha\eta}(t). \end{aligned} \quad (\text{A.24})$$

Therefore,

$$\begin{aligned} i \frac{d}{dt} A_{\alpha\beta}(t) &= \left(E + \frac{m_i^2}{2E} \right) A_{\alpha\beta}(t) + \sum_{\eta} \left[\sum_k U_{\beta k} \frac{\Delta m_{ki}^2}{2E} U_{\eta k}^* + \delta_{\beta\eta} V_{\beta} \right] A_{\alpha\eta}(t) \\ &= F(x) A_{\alpha\beta}(t) + G A_{\alpha\eta}(t) \end{aligned} \quad (\text{A.25})$$

where only the second term generates the relevant phase shift because $E + \frac{m_i^2}{2E}$ corresponds to the free Hamiltonian.

For ultra-relativistic neutrinos $t \simeq x$ and so we can write Eq. (A.25) in terms of the distance x instead of the time variable t and keep only the part relevant for flavor transition and we get

$$i \frac{d}{dx} A_{\alpha\beta}(t) = \sum_{\eta} \left[\sum_k U_{\beta k} \frac{\Delta m_{ki}^2}{2E} U_{\eta k}^* + \delta_{\beta\eta} V_{\beta} \right] A_{\alpha\eta}(t). \quad (\text{A.26})$$

We can make explicit the conditions that we are interested in, namely the oscillation in a two-flavor picture involving only one active neutrino and a sterile neutrino, and we can write Eq. (A.26) in matrix form

$$i \frac{d}{dx} \Psi_{\alpha} = \mathcal{H}_{\text{F}} \Psi_{\alpha} = (U \mathbb{M}^2 U^{\dagger} + \mathbb{V}) \Psi_{\alpha} \quad (\text{A.27})$$

where

$$\begin{aligned} \Psi_{\alpha} &= \begin{pmatrix} A_{\alpha\alpha} \\ A_{\alpha s} \end{pmatrix}, \quad U = \begin{pmatrix} \cos \theta & \sin \theta \\ -\sin \theta & \cos \theta \end{pmatrix}, \\ \mathbb{M}^2 &= \begin{pmatrix} 0 & 0 \\ 0 & \frac{\Delta m_{k4}^2}{2E} \end{pmatrix}, \quad \mathbb{V} = \begin{pmatrix} V_{\alpha} & 0 \\ 0 & 0 \end{pmatrix}. \end{aligned} \quad (\text{A.28})$$

Doing the products, we get

$$i \frac{d}{dx} \begin{pmatrix} A_{\alpha\alpha} \\ A_{\alpha s} \end{pmatrix} = \frac{1}{2} \begin{pmatrix} V_{\alpha} - \Delta(p) \cos(2\theta) & \Delta(p) \sin(2\theta) \\ \Delta(p) \sin(2\theta) & \Delta(p) \cos(2\theta) - V_{\alpha} \end{pmatrix} \begin{pmatrix} A_{\alpha\alpha} \\ A_{\alpha s} \end{pmatrix} \quad (\text{A.29})$$

where, for sterile neutrinos much heavier than the active ones, $\Delta(p) = \frac{\Delta m_{k4}^2}{2E} \simeq \frac{\Delta m_{ks}^2}{2E} \approx \frac{m_s^2}{2E}$. We can diagonalize the effective Hamiltonian that is written in the flavor basis

$$\mathcal{H}_{\text{F}} = \frac{1}{2} \begin{pmatrix} V_{\alpha} - \Delta(p) \cos(2\theta) & \Delta(p) \sin(2\theta) \\ \Delta(p) \sin(2\theta) & \Delta(p) \cos(2\theta) - V_{\alpha} \end{pmatrix} \quad (\text{A.30})$$

with an orthogonal transformation operated by

$$U_M = \begin{pmatrix} \cos \theta_M & \sin \theta_M \\ -\sin \theta_M & \cos \theta_M \end{pmatrix} \quad (\text{A.31})$$

that is the effective mixing matrix in matter with the mixing angle given by

$$\tan(2\theta_M) = \frac{\tan(2\theta)}{1 - \frac{V_\alpha}{\Delta(p)^2 \cos^2(2\theta)}}. \quad (\text{A.32})$$

The diagonalization gives us

$$\mathcal{H}_M = U_M^T \mathcal{H}_F U_M = \text{diag}(-\Delta_M, \Delta_M) \quad (\text{A.33})$$

where

$$\Delta_M = \sqrt{\Delta(p)^2 \sin^2(2\theta) + (\Delta(p)^2 \cos^2(2\theta) - V_\alpha)^2}. \quad (\text{A.34})$$

Eq. (A.29) can be written as

$$i \frac{d}{dx} \begin{pmatrix} A_{\alpha\alpha} \\ A_{\alpha s} \end{pmatrix} = \begin{pmatrix} -\Delta_M \cos(2\theta_M) & \Delta_M \sin(2\theta_M) \\ \Delta_M \sin(2\theta_M) & \Delta_M \cos(2\theta_M) \end{pmatrix} \quad (\text{A.35})$$

where

$$\cos(2\theta_M) = \frac{\Delta(p) \cos(2\theta) - V_\alpha}{\Delta_M}, \quad \sin(2\theta_M) = \frac{\Delta(p) \sin(2\theta)}{\Delta_M}. \quad (\text{A.36})$$

The active-sterile neutrino probability in the primordial plasma is then

$$P_{\nu_\alpha \rightarrow \nu_\beta}(t) = \sin^2(2\theta_M) \sin^2\left(\frac{\Delta_M t}{2}\right) \quad (\text{A.37})$$

and the time-averaged probability is

$$\langle P_{\nu_\alpha \rightarrow \nu_\beta}(t) \rangle = \frac{1}{2} \sin^2(2\theta_M) = \frac{1}{2} \frac{\Delta(p)^2 \sin^2(2\theta)}{\Delta(p)^2 \sin^2(2\theta) + (\Delta(p)^2 \cos^2(2\theta) - V_\alpha)^2} \quad (\text{A.38})$$

where θ is the active-sterile mixing angle in the vacuum.

From Eq. (A.32) we can see that the resonance condition is

$$V_\alpha = \Delta(p)^2 \cos^2(2\theta). \quad (\text{A.39})$$

At the resonance, the effective mixing angle is $\frac{\pi}{4}$, and if the resonance is wide enough, there is a complete transition between the two flavors. To achieve the resonance condition in the case of keV sterile neutrino DM, the contribution of a large lepton asymmetry is needed, which is one of the assumptions of the Shi-Fuller mechanism discussed in Subsection 2.1.2 of Chapter 2.

An analogous result can be obtained for different species of neutrinos that propagate and for different mediums, for example, considering the ordinary matter of earth instead of the primordial plasma, simply by calculating the correct effective potential contribution for the specific case.

Appendix B

Boltzmann Equation in the Dodelson-Widrow Scenario and its Solution

The Boltzmann equation, which describes the evolution of the distribution function of sterile neutrino DM $f_s(p, t)$ in case of non-resonant production through oscillation and collisions is

$$\begin{aligned} \frac{\partial}{\partial t} f_s(p, t) - H p \frac{\partial}{\partial p} f_s(p, t) &\approx \left[\frac{\Gamma_\alpha(p, T)}{2} \langle P_m(\nu_\alpha \rightarrow \nu_s; p, t) \rangle \right] (f_\alpha(p, t) - f_s(p, t)) \approx \\ &\approx \frac{\Gamma_\alpha(p, T)}{4} \sin^2(2\theta_M) (f_\alpha(p, t) - f_s(p, t)) \end{aligned} \quad (\text{B.1})$$

where $f_\alpha(p, t) = 1/(e^{p/T} + 1)$ is the Fermi-Dirac distribution function of active neutrinos ν_α that are reasonably assumed to be in equilibrium in the primordial plasma. $\Gamma_\alpha(p, T)$ is the active neutrino interaction rate with the particles in the plasma. In the SM, the total interaction rate takes the form $\Gamma_\alpha(p, T) = C_\alpha(T) G_F^2 T^4 p$ where $C_\alpha(T)$ depends on the number and type of relativistic species in the primordial plasma [37]. In our work we use for $C_\alpha(T)$ the values given in Ref. [39]. $\langle P_m(\nu_\alpha \rightarrow \nu_s; p, t) \rangle$ is the oscillation probability of ν_α into ν_s , averaged over one oscillation period. Therefore, the entire expression in square brackets is the probability for the neutrino state to collapse to ν_s in a collision. Such probability can also be called "damped conversion rate" because it encodes the matter effects on the neutrino oscillation, and it is determined by the quantum damping rate $D(p) = \Gamma_\alpha(p)/2$ and by the effective mixing angle in matter ($\sin^2(2\theta_M)$). The expression for the mixing angle in matter is

$$\sin^2(2\theta_M) = \frac{\Delta^2(p) \sin^2(2\theta)}{\Delta^2(p) \sin^2(2\theta) + D^2(p) + [\Delta(p) \cos(2\theta) - V^D - V^T(p)]^2} \quad (\text{B.2})$$

where $\Delta(p) \equiv \frac{\delta m^2}{2p} = \frac{(m_s^2 - m_\alpha^2)}{2p} \simeq \frac{m_s^2}{2p}$. In a standard scenario, there is no significant asymmetry between leptons and antileptons in the very early universe. Therefore, the finite density potential

$$V^D = \pm \frac{2\sqrt{2}\zeta(3)}{\pi^2} G_F T^3 \frac{\eta_B}{4} \quad (\text{B.3})$$

with "+" holds for $\alpha = e$ and "-" for $\alpha = \mu, \tau$, is determined only by the tiny baryon asymmetry $\eta_B = \frac{n_B}{n_\gamma} = (6.143 \pm 0.190) \times 10^{-10}$ [13] that we know exist. The last term in

the denominator of B.2 is the finite temperature or thermal potential

$$V^T(p) = -\frac{8\sqrt{2}G_F p_\nu}{3m_Z^2} (\langle E_{\nu_\alpha} \rangle n_{\nu_\alpha} + \langle E_{\bar{\nu}_\alpha} \rangle n_{\bar{\nu}_\alpha}) - \frac{8\sqrt{2}G_F p_\nu}{3m_W^2} (\langle E_\alpha \rangle n_\alpha + \langle E_{\bar{\alpha}} \rangle n_{\bar{\alpha}}). \quad (\text{B.4})$$

Here, n_α ($n_{\bar{\alpha}}$) and $\langle E_\alpha \rangle$ ($\langle E_{\bar{\alpha}} \rangle$) are the number density and average energy of leptons (anti-leptons) of flavor α , and n_{ν_α} ($n_{\bar{\nu}_\alpha}$) and $\langle E_{\nu_\alpha} \rangle$ ($\langle E_{\bar{\nu}_\alpha} \rangle$) are the number density and average energy of the neutrinos (antineutrinos) of flavor α .

In the following, the dependence on $f_s(p, t)$ of the right-hand side of the equation will be neglected. This is justified because we assume zero initial abundance of sterile neutrinos in the plasma (they are produced only later on exclusively through active neutrino conversion via oscillation and collisions), and even once ν_s are produced, due to the freeze-in nature of the process, their abundance is always small enough to make the back-conversion effect negligible.

It is more convenient to use the temperature of the plasma T instead of the time coordinate t to parameterize the evolution of f_s , and we change the variable $t \rightarrow T$. In order to lighten the following steps of the solution of the Boltzmann equation, we define

$$h(p, T) = \frac{\Gamma_\alpha(p, T)}{4} \frac{\Delta^2(p) \sin^2(2\theta)}{\Delta^2(p) \sin^2(2\theta) + D^2(p) + [\Delta(p) \cos(2\theta) - V^D - V^T(p)]^2}. \quad (\text{B.5})$$

So Eq.(B.1) becomes

$$\frac{dT}{dt} \frac{\partial}{\partial T} f_s(p, T) - H p \frac{\partial}{\partial p} f_s(p, T) = h(p, T) f_\alpha(p, T) \quad (\text{B.6})$$

and dividing both members by $\frac{dT}{dt}$ we get

$$\frac{\partial}{\partial T} f_s(p, T) - \frac{dt}{dT} H p \frac{\partial}{\partial p} f_s(p, T) = \frac{dt}{dT} h(p, T) f_\alpha(p, T). \quad (\text{B.7})$$

We define the redshift integral [39]

$$\kappa(T) = \frac{dt}{dT} H(T) = \frac{dt}{dT} \frac{da}{adt} = \frac{1}{a} \frac{da}{dT} \quad (\text{B.8})$$

where $a(T)$ is the scale factor and the Hubble rate is defined as $H(T) = \frac{\dot{a}}{a}$.

Using the entropy conservation $S = s(T)a^3(T) = \text{const}$ with $s(T) = \frac{2\pi^2}{45} g_{*s}(T) T^3$,

$$\begin{aligned} 0 &= \frac{dS}{dT} = \frac{d(s(T)a^3(T))}{dT} = \frac{ds}{dT} a^3 + 3s a^2 \frac{da}{dT} = \\ &= \frac{2\pi^2}{45} \left[\frac{dg_{*s}(T)}{dT} T^3 a^3 + 3g_{*s}(T) T^2 a^3 + 3g_{*s}(T) T^3 a^2 \frac{da}{dT} \right] \end{aligned} \quad (\text{B.9})$$

we can define

$$\begin{aligned} \kappa(T) &= \frac{1}{a} \frac{da}{dT} = -\frac{1}{3g_{*s}(T) T^3 a^3} \left[\frac{dg_{*s}(T)}{dT} T^3 a^3 + 3g_{*s}(T) T^2 a^3 \right] = \\ &= -\frac{1}{T} \left[1 + \frac{T g'_{*s}(T)}{3 g_{*s}(T)} \right], \end{aligned} \quad (\text{B.10})$$

and consequently

$$\frac{dt}{dT} = \frac{\kappa(T)}{H(T)} = -\frac{1}{T H(T)} \left[1 + \frac{T g'_{*s}(T)}{3 g_{*s}(T)} \right]. \quad (\text{B.11})$$

The resulting Boltzmann equation in terms of momentum and temperature

$$\frac{\partial}{\partial T} f_s(p, T) + \left[\frac{1}{T} + \frac{1}{3} \frac{g'_{*s}(T)}{g_{*s}(T)} \right] p \frac{\partial}{\partial p} f_s(p, T) = -\frac{1}{H(T)} \left[\frac{1}{T} + \frac{1}{3} \frac{g'_{*s}(T)}{g_{*s}(T)} \right] h(p, T) f_\alpha(p, T) \quad (\text{B.12})$$

is a linear 1st order partial differential equation (PDE) that can be written in the form

$$f_s(p, T)_T - \kappa(T) p f_s(p, T)_p = \left(\frac{dt}{dT} \right) h(p, T) f_\alpha(p, T) \quad (\text{B.13})$$

analogous to the typical PDE that can be solved with the method of the characteristic

$$a(p, T)u_T + b(p, T)u_p = C(p, T) \quad (\text{B.14})$$

where

$$\begin{aligned} a(p, T) &= 1 \\ b(p, T) &= -\kappa(T) p = -H(T) \left(\frac{dt}{dT} \right) p = \frac{1}{T} \left[1 + \frac{T g'_{*s}(T)}{3 g_{*s}(T)} \right] p \\ C(p, T) &= \left(\frac{dt}{dT} \right) h(p, T) f_\alpha(p, T). \end{aligned}$$

Eq.(B.14) satisfies

$$\frac{dT}{a(p, T)} = \frac{dp}{b(p, T)} = \frac{du}{C(p, T)} \quad (\text{B.15})$$

so Eq.(B.13) satisfies

$$\frac{dT}{1} = \frac{dp}{\left[\frac{1}{T} + \frac{1}{3} \frac{g'_{*s}(T)}{g_{*s}(T)} \right] p} = \frac{df_s}{\left(\frac{dt}{dT} \right) h(p, T) f_\alpha(p, T)}. \quad (\text{B.16})$$

We can use the first pair of ODEs in B.16 to get the characteristic curve for $p(T)$ integrating over a generic interval of temperatures

$$\begin{aligned}
\frac{dp}{p} &= \left[\frac{1}{T} + \frac{1}{3} \frac{g'_{*s}(T)}{g_{*s}(T)} \right] dT \\
\rightarrow \int_{p(T_1)}^{p(T_2)} \frac{dp}{p} &= \int_{T_1}^{T_2} \frac{dT}{T} + \int_{T_1}^{T_2} \frac{dT}{3} \frac{g'_{*s}(T)}{g_{*s}(T)} \\
\ln(p(T_2)) - \ln(p(T_1)) &= \ln(T_2) - \ln(T_1) + \frac{1}{3} (\ln(g_{*s}(T_2)) - \ln(g_{*s}(T_1))) \\
\ln \left(\frac{p(T_2)}{p(T_1)} \right) &= \ln \left(\frac{T_2}{T_1} \right) + \ln \left(\frac{g_{*s}(T_2)}{g_{*s}(T_1)} \right)^{1/3} = \ln \left(\frac{T_2}{T_1} \left(\frac{g_{*s}(T_2)}{g_{*s}(T_1)} \right)^{1/3} \right) \\
\rightarrow p(T_2) &= p(T_1) \left(\frac{T_2}{T_1} \left(\frac{g_{*s}(T_2)}{g_{*s}(T_1)} \right)^{1/3} \right) \tag{B.17}
\end{aligned}$$

that gives us the expression for the evolution of momentum with temperature, that is the redshifted momentum considering the context of the expansion of the universe and the decrement of the temperature:

$$p(T) = p(T_i) \left(\frac{T}{T_i} \left(\frac{g_{*s}(T)}{g_{*s}(T_i)} \right)^{1/3} \right). \tag{B.18}$$

We can use this result, substituting in the second pair of ODEs

$$\frac{dT}{1} = \frac{df_s}{\frac{dt}{dT} h(p, T) f_\alpha(p, T)} \tag{B.19}$$

to obtain the solution of the Boltzmann equation by integrating

$$\begin{aligned}
df_s &= \left(\frac{dt}{dT} \right) h(p(T), T) f_\alpha(p(T), T) dT \\
\rightarrow \int_{f_s(p, T_i)}^{f_s(p, T_f)} df_s &= \int_{T_i}^{T_f} \left(\frac{dt}{dT} \right) h(p(T), T) f_\alpha(p(T), T) dT \\
f_s(p, T_f) - f_s(p, T_i) &= \int_{T_i}^{T_f} \left(\frac{dt}{dT} \right) h \left(\frac{T}{T_i} \left(\frac{g_{*s}(T)}{g_{*s}(T_i)} \right)^{1/3} p(T_i), T \right) \times \\
&\quad \times f_\alpha \left(\frac{T}{T_i} \left(\frac{g_{*s}(T)}{g_{*s}(T_i)} \right)^{1/3} p(T_i), T \right) dT \tag{B.20}
\end{aligned}$$

and assuming zero initial abundance

$$\begin{aligned} \rightarrow f_s(p, T_f) &= \int_{T_i}^{T_f} \left(\frac{dt}{dT} \right) h \left(\frac{T}{T_i} \left(\frac{g_{*s}(T)}{g_{*s}(T_i)} \right)^{1/3} p(T_i), T \right) \times \\ &\quad \times f_\alpha \left(\frac{T}{T_i} \left(\frac{g_{*s}(T)}{g_{*s}(T_i)} \right)^{1/3} p(T_i), T \right) dT \end{aligned} \quad (\text{B.21})$$

that is the solution of the Boltzmann equation.

Being interested in the final distribution function we can also rewrite Eq. (B.20) in terms not of p_i but in terms of p_f using Eq.(B.18). Making explicit also the factor (dt/dT) , we get

$$\begin{aligned} f_s(p_f, T_f) &= \int_{T_i}^{T_f} -\frac{dT}{HT} \left(1 + \frac{T g'_{*s}(T)}{3 g_{*s}(T)} \right) h \left(\frac{T}{T_f} \left(\frac{g_{*s}(T)}{g_{*s}(T_f)} \right)^{1/3} p_f, T \right) \times \\ &\quad \times f_\alpha \left(\frac{T}{T_f} \left(\frac{g_{*s}(T)}{g_{*s}(T_f)} \right)^{1/3} p_f, T \right) \end{aligned} \quad (\text{B.22})$$

In the perspective of the numerical calculation, it is convenient to change variable and write the distribution function in terms of the rescaled momentum $r = p/T$, with $p_f = r \cdot T_f$

$$\begin{aligned} f_s(r) &= \int_{T_i}^{T_f} -\frac{dT}{HT} \left(1 + \frac{T g'_{*s}(T)}{3 g_{*s}(T)} \right) h \left(r \cdot T \left(\frac{g_{*s}(T)}{g_{*s}(T_f)} \right)^{1/3}, T \right) \times \\ &\quad \times f_\alpha \left(r \cdot T \left(\frac{g_{*s}(T)}{g_{*s}(T_f)} \right)^{1/3}, T \right). \end{aligned} \quad (\text{B.23})$$

Finally, the most explicit form of the solution of the Boltzmann equation which is then numerically implemented is found by substituting the expression of the Hubble rate in the radiation-dominated era

$$H(T) = \sqrt{\frac{8 \pi^3 g_{*s}(T)}{90} \frac{T^2}{M_{Pl}}} \quad (\text{B.24})$$

and the Fermi-Dirac distribution function of active neutrinos in the primordial plasma

$$f_\alpha(p, T) = \frac{1}{\exp(p/T) + 1}. \quad (\text{B.25})$$

With this, we get

$$\begin{aligned} f_s(r) &= \int_{T_i}^{T_f} -\sqrt{\frac{90}{8 \pi^3 g_{*s}(T)} \frac{M_{Pl}}{T^3}} \left(1 + \frac{T g'_{*s}(T)}{3 g_{*s}(T)} \right) h \left(r \cdot T \left(\frac{g_{*s}(T)}{g_{*s}(T_f)} \right)^{1/3}, T \right) \times \\ &\quad \times \frac{1}{\exp \left(r \left(\frac{g_{*s}(T)}{g_{*s}(T_f)} \right)^{1/3} \right) + 1} dT. \end{aligned} \quad (\text{B.26})$$

Appendix C

Derivation of the Effective Lagrangian of Neutrino Non-Standard Self-Interactions

The effective form of the Lagrangian used to get the results presented in Chapter 5 can be derived from the Lagrangian of UV, a complete theory by integrating out the heavy degrees of freedom that, in our case, are the mediators of neutrino NSSI. We focus on the terms describing the coupling to active neutrinos to new heavy mediators that mediate their self-interactions. Below the scale of EW symmetry breaking, NSSI can usually be described by a schematic Yukawa-like interaction $\nu\nu\phi$ where ϕ is a scalar or vector mediator particle. Although the specific shape of this additional term varies according to the kind of mediator, for simplicity, in the following, we report as an example only the case of NSSI mediated by a complex scalar ϕ , since for the other types of interactions the derivation of the effective Lagrangian is analogous.

The full Lagrangian of this new mediator is

$$\mathcal{L}_\phi = \partial_\mu\phi^\dagger\partial^\mu\phi - m^2\phi^\dagger\phi + \lambda_\phi\bar{\nu}\mathcal{O}\nu\phi + \lambda_\phi^*\phi^\dagger\bar{\nu}\bar{\mathcal{O}}\nu, \quad (\text{C.1})$$

where $\bar{\mathcal{O}} = \gamma^0\mathcal{O}^\dagger\gamma^0$, and \mathcal{O} is one among the bilinear covariants that survive for Majorana neutrinos $\{\mathbb{1}, \gamma^\mu, i\gamma^5, \gamma^\mu\gamma^5, \sigma^{\mu\nu}\}$. Assuming $m_\phi \gg T$, and being interested in the phenomenology of this theory at low energies, we are allowed to integrate out the heavy new degree of freedom ϕ .

To do that, from the Euler-Lagrange equations for ϕ and ϕ^\dagger

$$\frac{\partial\mathcal{L}_\phi}{\partial\phi} - \partial_\mu\frac{\partial\mathcal{L}_\phi}{\partial(\partial_\mu\phi)} = 0 \quad \text{and} \quad \frac{\partial\mathcal{L}_\phi}{\partial\phi^\dagger} - \partial_\mu\frac{\partial\mathcal{L}_\phi}{\partial(\partial_\mu\phi^\dagger)} = 0 \quad (\text{C.2})$$

we first write down the equation of motion for ϕ and ϕ^\dagger

$$-m^2\phi^\dagger + \lambda_\phi\bar{\nu}\mathcal{O}\nu - \partial_\mu\partial^\mu\phi^\dagger = 0 \quad \Rightarrow \quad (\square + m^2)\phi^\dagger = \lambda_\phi\bar{\nu}\mathcal{O}\nu \quad (\text{C.3})$$

$$-m^2\phi + \lambda_\phi^*\bar{\nu}\bar{\mathcal{O}}\nu - \partial_\mu\partial^\mu\phi = 0 \quad \Rightarrow \quad (\square + m^2)\phi = \lambda_\phi^*\bar{\nu}\bar{\mathcal{O}}\nu. \quad (\text{C.4})$$

Then, solving for ϕ and ϕ^\dagger we get the expressions

$$\phi = \frac{\lambda_\phi^*\bar{\nu}\bar{\mathcal{O}}\nu}{(\square + m^2)} \quad \text{and} \quad \phi^\dagger = \frac{\lambda_\phi\bar{\nu}\mathcal{O}\nu}{(\square + m^2)} \quad (\text{C.5})$$

and substituting in Eq. (C.1) we get the effective Lagrangian

$$\mathcal{L}_{\text{NSSI}} = \lambda_\phi^2 \frac{(\bar{\nu}\mathcal{O}\nu)(\bar{\nu}\bar{\mathcal{O}}\nu)}{(\square + m_\phi^2)}. \quad (\text{C.6})$$

At the zeroth order in momentum, from Eq. (C.6) we would get the familiar term analogous to those of the Fermi theory for weak interactions depending only on the mass of the mediator, matching Eq. (5.4) for $G_\phi = G_F \epsilon_j^{eeee} = \frac{\sqrt{2}\lambda_\phi^2}{m_\phi^2}$. However, the dependence on the momentum p in our case is not negligible if we want to appreciate the effect of NSSI through the change they induce in the thermal potential. Therefore, we have to keep one more term in the effective expansion and the final form of the effective Lagrangian we use is

$$\mathcal{L}_{\text{NSSI}} = \frac{G_F \epsilon}{\sqrt{2}} (\bar{\nu}\mathcal{O}\nu)(\bar{\nu}\bar{\mathcal{O}}\nu) - \frac{G_F \epsilon}{\sqrt{2}} (\bar{\nu}\mathcal{O}\nu) \frac{\square}{m_\phi^2} (\bar{\nu}\bar{\mathcal{O}}\nu), \quad (\text{C.7})$$

where $\mathcal{O} = \mathbb{I}, i\gamma^5, \gamma^\mu\gamma^5$ for scalar, pseudoscalar, and axial-vector NSSI, respectively.

Appendix D

Calculation of the Interaction Rate for Neutrino Non-Standard Self-Interactions

The interaction rate Γ_{NSSI} , contribution to the total interaction rate of active neutrinos in the plasma that comes from the introduction of neutrino NSSI, corresponds to the thermal averaged reaction rate for a neutrino with fixed energy E_1 (where $E_1 = p_1$ for ultra-relativistic neutrinos). It is calculated by averaging the NSSI cross section over the phase space of the other neutrino (or anti-neutrino) it scatters with [193]

$$\Gamma_{\text{NSSI}}(p_1, T) = 2 \int \frac{d^3 \vec{p}_2}{(2\pi)^3} f_{\nu_e}(p_2, T) \sigma_{\text{NSSI}}(\vec{p}_1, \vec{p}_2) v_{\text{Møller}} \quad (\text{D.1})$$

where the prefactor 2 captures contributions from both helicity states of Majorana active neutrinos, $f_{\nu_e}(p_2, T) = 1/[\exp(p_2/T) + 1]$ is the Fermi-Dirac distribution of the active neutrino in the plasma, and $v_{\text{Møller}}$ is the Møller velocity that can be approximated by $(1 - \cos(\theta'))^1$ for ultra-relativistic neutrinos.

To calculate

$$\Gamma_{\text{NSSI}}(p_1, T) = 2 \int \frac{d^3 \vec{p}_2}{(2\pi)^3} \sigma_{\text{NSSI}}(\vec{p}_1, \vec{p}_2) (1 - \cos(\theta')) \frac{1}{\exp(p_2/T) + 1} \quad (\text{D.2})$$

we need to know the expression for the NSSI cross-section $\sigma_{\text{NSSI}}(\vec{p}_1, \vec{p}_2)$ that is calculated in the following.

D.1 Cross Section of NSSI

Notice that, while the second term of the Lagrangian

$$\mathcal{L}_{\text{NSSI}} = \frac{G_F \epsilon}{\sqrt{2}} (\bar{\nu} \mathcal{O} \nu) (\bar{\nu} \bar{\mathcal{O}} \nu) - \frac{G_F \epsilon}{\sqrt{2}} (\bar{\nu} \mathcal{O} \nu) \frac{\square}{m_\phi^2} (\bar{\nu} \bar{\mathcal{O}} \nu) \quad (\text{D.3})$$

is crucial for the calculation of the contribution of NSSI to the thermal potential, it is negligible in the calculation of the NSSI interaction rate. Indeed, it would contribute to the interaction rate with a term of $\mathcal{O}(m_\phi^{-8})$ significantly suppressed with respect to the contribution coming from the first term that is of $\mathcal{O}(m_\phi^{-4})$. In Eq. D.3 the flavor indices are not specified, but they are all "e" since we considered only flavor-conserving NSSI involving ν_e , that is the species that mixes with the sterile neutrino.

The only Feynman diagram representing the self-interactions of neutrinos at the effective

¹Here θ' is not the active-sterile mixing angle but the angle between \vec{p}_1 and \vec{p}_2

level is

and it encodes the three channels through which the interaction can happen in the UV

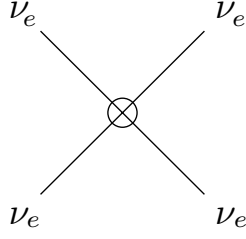


FIGURE D.1: Feynman diagram representing the effective electron neutrino non-standard self-interaction.

complete theory, represented in Fig. D.2

The matrix elements corresponding to these diagrams can be calculated following Refs.

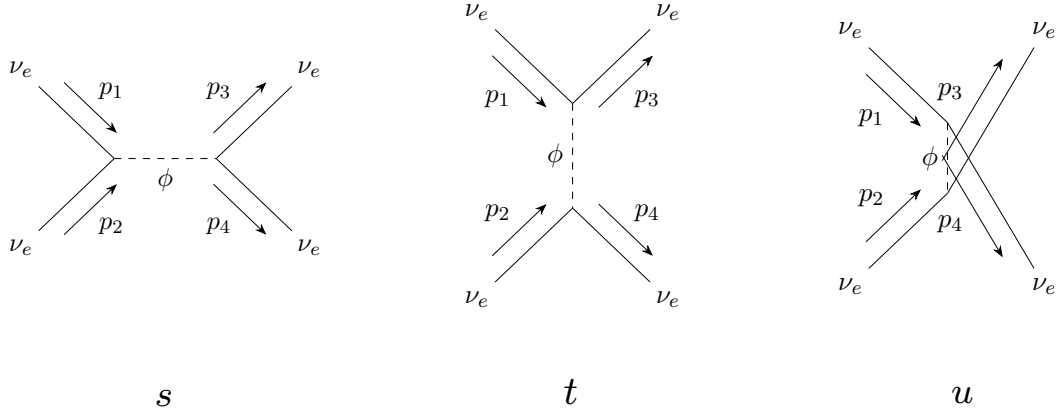


FIGURE D.2: Feynman diagrams representing the three channels (s, t, and u) through which neutrinos can interact among each other with NSSI in the UV complete picture of the theory.

[221, 222], where the Majorana nature of neutrinos is taken into account and encoded in the Feynman rules, and we find

$$\begin{aligned}
 -i\mathcal{M}_s &= -i\frac{G_F\epsilon_j}{\sqrt{2}} [(\bar{v}(p_1)\mathcal{O}_j u(p_2) - \bar{v}(p_2)\mathcal{O}_j u(p_1)) \times (\bar{u}(p_3)\mathcal{O}_j v(p_4) - \bar{u}(p_4)\mathcal{O}_j v(p_3))] \\
 &= -i\frac{G_F\epsilon_j}{\sqrt{2}} \left[(\bar{v}(p_1) [\mathcal{O}_j + \mathcal{C}\mathcal{O}_j^T\mathcal{C}^{-1}] u(p_2)) \times (\bar{u}(p_3) [\mathcal{O}_j + \mathcal{C}\mathcal{O}_j^T\mathcal{C}^{-1}] v(p_4)) \right]
 \end{aligned} \tag{D.4}$$

$$\begin{aligned}
 -i\mathcal{M}_t &= -i\frac{G_F\epsilon_j}{\sqrt{2}} [(\bar{v}(p_1)\mathcal{O}_j v(p_3) - \bar{u}(p_3)\mathcal{O}_j u(p_1)) \times (\bar{u}(p_4)\mathcal{O}_j u(p_2) - \bar{v}(p_2)\mathcal{O}_j v(p_4))] \\
 &= -i\frac{G_F\epsilon_j}{\sqrt{2}} \left[(\bar{v}(p_1) [\mathcal{O}_j + \mathcal{C}\mathcal{O}_j^T\mathcal{C}^{-1}] v(p_3)) \times (\bar{u}(p_4) [\mathcal{O}_j + \mathcal{C}\mathcal{O}_j^T\mathcal{C}^{-1}] u(p_2)) \right]
 \end{aligned} \tag{D.5}$$

$$\begin{aligned}
-i\mathcal{M}_u &= -i\frac{G_F\epsilon_j}{\sqrt{2}} [(\bar{v}(p_1)\mathcal{O}_jv(p_4) - \bar{u}(p_4)\mathcal{O}_ju(p_1)) \times (\bar{u}(p_3)\mathcal{O}_ju(p_2) - \bar{v}(p_2)\mathcal{O}_jv(p_3))] \\
&= -i\frac{G_F\epsilon_j}{\sqrt{2}} \left[(\bar{v}(p_1) [\mathcal{O}_j + \mathcal{C}\mathcal{O}_j^T\mathcal{C}^{-1}] v(p_4)) \times (\bar{u}(p_3) [\mathcal{O}_j + \mathcal{C}\mathcal{O}_j^T\mathcal{C}^{-1}] u(p_2)) \right]
\end{aligned} \tag{D.6}$$

where $\mathcal{O}_j = \mathbb{I}, i\gamma^5, \gamma^\mu, \gamma^\mu\gamma^5$ operators of the only NSSI which give non-zero contribution for Majorana neutrinos, \mathcal{C} is the charge conjugation matrix such that $\mathcal{C}\mathcal{O}_j^T\mathcal{C}^{-1} = \mathcal{O}_j$.

To calculate the cross-section, we need the amplitude squared averaged over initial spins and summed over final spins

$$|\overline{\mathcal{M}_{\text{tot}}}|^2 = \frac{1}{4} \sum \mathcal{M}_{\text{tot}}^\dagger \mathcal{M}_{\text{tot}} \tag{D.7}$$

that we calculated with the FeynCalc tool [224–226] for each type of interaction separately getting for:

Scalar NSSI

$$|\overline{\mathcal{M}_S}|^2 = 4(\epsilon_S)^2 G_F^2 (s^2 + 5t^2 + u^2); \tag{D.8}$$

Pseudoscalar NSSI

$$|\overline{\mathcal{M}_P}|^2 = 4(\epsilon_S)^2 G_F^2 (s^2 + 5t^2 + u^2); \tag{D.9}$$

Axial-vector NSSI

$$|\overline{\mathcal{M}_A}|^2 = 64(\epsilon_S)^2 G_F^2 (t^2), \tag{D.10}$$

where

$$\begin{aligned}
s &= (p_1 + p_2)^2 = 2 p_1 \cdot p_2 \\
t &= (p_1 - p_3)^2 = -2 p_1 \cdot p_3 \\
u &= (p_1 - p_4)^2 = -2 p_1 \cdot p_4
\end{aligned}$$

are the Mandelstam variables for massless particles.

We notice that every averaged amplitude squared is obtained in the form

$$|\overline{\mathcal{M}_j}|^2 = (\epsilon_j)^2 G_F^2 (K_{s,j} s^2 + K_{t,j} t^2 + K_{u,j} u^2). \tag{D.11}$$

with different coefficients in front of the Mandelstam variables squared for each type of interaction. This fact will be used to lighten the shape of the next steps of the calculation.

In natural units ($c = \hbar = 1$), the general formula for the differential cross section of a $2 \rightarrow j$ process is [232]

$$d\sigma = \mathcal{S} \frac{|\overline{\mathcal{M}}|^2}{4\sqrt{(p_1 \cdot p_2)^2 - m_1^2 m_2^2}} d\Pi_{\text{ps}} \tag{D.12}$$

where \mathcal{S} is a symmetry factor and

$$d\Pi_{\text{ps}} = \prod_j \frac{d^3\vec{p}_j}{(2\pi)^3} \frac{1}{2E_j} (2\pi)^4 \delta^4(p_1 + p_2 - p_a - p_b - \dots - p_j) \tag{D.13}$$

is the Lorentz-invariant phase space factor for j particles in the final state.

We are interested in scatterings of ultrarelativistic neutrinos of the form $nu_e(p_1) +$

$nu_e(p_2) \rightarrow nu_e(p_3) + nu_e(p_4)$, therefore in this case $\mathcal{S} = \frac{1}{2}$ and we neglect neutrino masses. The differential cross section is then

$$d\sigma = \frac{1}{4s} |\overline{\mathcal{M}}|^2 \frac{d^3\vec{p}_3}{2E_3 (2\pi)^3} \frac{d^3\vec{p}_4}{2E_4 (2\pi)^3} (2\pi)^4 \delta^4(p_1 + p_2 - p_3 - p_4). \quad (\text{D.14})$$

We work in the center of mass (COM) frame where $\vec{p}_2 = -\vec{p}_1$, and for elastic scattering between identical particles with $m_1 = m_2$, $|\vec{p}_{in}| = |\vec{p}_{fin}| = p$ and defining θ the angle between \vec{p}_2 and \vec{p}_3 ,

$$\begin{aligned} p_1 &= (E_1, \vec{p}_1) = (E, \vec{p}_i) \\ p_2 &= (E_2, \vec{p}_2) = (E, -\vec{p}_i) \\ p_3 &= (E_3, \vec{p}_3) = E_3(1, \sin\theta, 0, \cos\theta) \\ p_4 &= (E_4, \vec{p}_4) = E_4(1, -\sin\theta, 0, -\cos\theta) \end{aligned}$$

Therefore,

$$\begin{aligned} s &= (E_1 + E_2)^2 = 4E^2 \\ t &= -2p^2(1 - \cos\theta) \\ u &= -2p^2(1 + \cos\theta) \end{aligned} \quad (\text{D.15})$$

and we have

$$d\sigma = \frac{|\overline{\mathcal{M}}|^2}{4s(2\pi)^2} \frac{d^3\vec{p}_3}{2E_3} \frac{d^3\vec{p}_4}{2E_4} \delta(\sqrt{s} - E_3 - E_4) \delta^3(\vec{p}_3 + \vec{p}_4). \quad (\text{D.16})$$

To get the total cross section for the generic NSSI identified by the index j , we have to integrate over momenta

$$\sigma_{\nu\nu \rightarrow \nu\nu}^j = \frac{1}{4s(2\pi)^2} \int \frac{d^3\vec{p}_3}{2E_3} \frac{d^3\vec{p}_4}{2E_4} \delta(\sqrt{s} - E_3 - E_4) \delta^3(\vec{p}_3 + \vec{p}_4) (K_{s,j} s^2 + K_{t,j} t^2 + K_{u,j} u^2). \quad (\text{D.17})$$

To integrate over momenta, we can separate the parts that depend on each of the Mandelstam variables as

$$\sigma_{\nu\nu \rightarrow \nu\nu}^j = \sigma_{s,j} + \sigma_{t,j} + \sigma_{u,j} \quad (\text{D.18})$$

where

$$\sigma_{s,j} = \frac{1}{4s(2\pi)^2} \int \frac{d^3\vec{p}_3}{2E_3} \frac{d^3\vec{p}_4}{2E_4} \delta(\sqrt{s} - E_3 - E_4) \delta^3(\vec{p}_3 + \vec{p}_4) K_{s,j} s^2 \quad (\text{D.19})$$

$$\sigma_{t,j} = \frac{1}{4s(2\pi)^2} \int \frac{d^3\vec{p}_3}{2E_3} \frac{d^3\vec{p}_4}{2E_4} \delta(\sqrt{s} - E_3 - E_4) \delta^3(\vec{p}_3 + \vec{p}_4) K_{t,j} t^2 \quad (\text{D.20})$$

$$\sigma_{u,j} = \frac{1}{4s(2\pi)^2} \int \frac{d^3\vec{p}_3}{2E_3} \frac{d^3\vec{p}_4}{2E_4} \delta(\sqrt{s} - E_3 - E_4) \delta^3(\vec{p}_3 + \vec{p}_4) K_{u,j} u^2. \quad (\text{D.21})$$

In the following, we report the explicit calculation of $\sigma_{s,j}$ only, because $\sigma_{t,j}$ and $\sigma_{u,j}$ can be calculated analogously by using Eqs. D.15.

We use $\delta^3(\vec{p}_3 + \vec{p}_4)$ to get rid of the integral over \vec{p}_4 and remembering $|\vec{p}_3| = E_3 = E_4$

we are left with

$$\begin{aligned}
\sigma_{s,j} &= \frac{1}{64 \pi^2 s} \int_{-\infty}^{+\infty} d^3 \vec{p}_3 \frac{\delta(\sqrt{s} - 2p_3)}{p_3^2} K_{s,j} s^2 \\
&= \frac{1}{64 \pi^2 s} \int_0^{2\pi} d\phi \int_{-1}^1 d \cos \theta \int_0^\infty dp_3 p_3^2 \frac{1}{p_3} \delta(\sqrt{s} - 2p_3) K_{s,j} s^2 \\
&= \frac{2\pi}{64 \pi^2 s} K_{s,j} s^2 \int_{-1}^1 d \cos \theta \int_0^\infty dp_3 \delta(\sqrt{s} - 2p_3) \\
&= \frac{K_{s,j}}{32 \pi} s.
\end{aligned} \tag{D.22}$$

For the other two terms of the total cross-section, we get

$$\sigma_{t,j} = \frac{K_{t,j}}{3 \cdot 64 \pi} s \tag{D.23}$$

$$\sigma_{u,j} = \frac{K_{u,j}}{3 \cdot 64 \pi} s. \tag{D.24}$$

$$\tag{D.25}$$

Therefore the total cross section for the NSSI of type j is

$$\sigma_{\nu\nu \rightarrow \nu\nu}^j = \sigma_{s,j} + \sigma_{t,j} + \sigma_{u,j} = \frac{s}{64 \pi} \left(2K_{s,j} + \frac{K_{t,j}}{3} + \frac{K_{u,j}}{3} \right). \tag{D.26}$$

D.2 Interaction Rate of NSSI

Going back to Eq. (D.2) and remembering that θ' is the angle between the two momenta in the initial state \vec{p} and \vec{p}' , and therefore

$$s = 2 p_1 \cdot p_2 = 2(E_1 E_2 - p_1 \cdot p_2) = 2 |p_1| |p_2| (1 - \cos \theta'), \tag{D.27}$$

we have for a type j of NSSI

$$\begin{aligned}
\Gamma_j(p_1, T) &= 2 \int \frac{d^3 \vec{p}_2}{(2\pi)^3} \sigma_{\nu\nu \rightarrow \nu\nu}^j(\vec{p}_1, \vec{p}_2) (1 - \cos(\theta')) \frac{1}{\exp(p_2/T) + 1} \\
&= \frac{6K_{s,j} + K_{t,j} + K_{u,j}}{48\pi} \int \frac{d\Omega dp_2 p_2^2}{(2\pi)^3} \frac{1}{\exp(p_2/T) + 1} p_1 p_2 (1 - \cos(\theta')) \\
&= \frac{6K_{s,j} + K_{t,j} + K_{u,j}}{24(2\pi)^4} p_1 \int \frac{dp_2 p_2^3}{\exp(p_2/T) + 1} \int d\Omega (1 - \cos(\theta')).
\end{aligned} \tag{D.28}$$

$$\tag{D.29}$$

Integrating numerically, we get the general expression valid for any type of NSSI j

$$\Gamma_j(p, T) = (6K_{s,j} + K_{t,j} + K_{u,j}) \frac{p}{24(2\pi)^4} \cdot \frac{7\pi^4 T^4}{120} \cdot \frac{16\pi}{3} = (6K_{s,j} + K_{t,j} + K_{u,j}) \frac{7\pi}{8640} p T^4. \tag{D.30}$$

To get the final expressions for each type of interaction, we recall the coefficients calculated in Section D.1.

Scalar NSSI

$$\begin{aligned}
K_{s,S} &= 4\epsilon_S^2 G_F^2 & K_{t,S} &= 20\epsilon_S^2 G_F^2 & K_{u,S} &= 4\epsilon_S^2 G_F^2 \\
\implies \Gamma_S(p, T) &= \frac{7\pi\epsilon_S^2 G_F^2}{180} p T^4; & & & & (D.31)
\end{aligned}$$

Pseudoscalar NSSI

$$\begin{aligned}
K_{s,P} &= 4\epsilon_S^2 G_F^2 & K_{t,P} &= 20\epsilon_S^2 G_F^2 & K_{u,P} &= 4\epsilon_S^2 G_F^2 \\
\implies \Gamma_P(p, T) &= \frac{7\pi\epsilon_P^2 G_F^2}{180} p T^4; & & & & (D.32)
\end{aligned}$$

Axial-vector NSSI

$$\begin{aligned}
K_{s,A} &= 0 & K_{t,A} &= 64\epsilon_S^2 G_F^2 & K_{u,A} &= 0 \\
\implies \Gamma_A(p, T) &= \frac{7\pi\epsilon_A^2 G_F^2}{135} p T^4; & & & & (D.33)
\end{aligned}$$

Appendix E

Calculation of the Thermal Potential for Neutrinos with Non-Standard Self-Interactions

The dispersion relation of massless neutrinos propagating in a medium is different from the one of massless neutrinos in the vacuum ($\omega = \kappa$ where κ is the magnitude of the momentum vector). The modification can be represented in terms of an effective potential. The correction to the vacuum energy-momentum relation to leading order in g^2/m_ϕ^2 (where g^2 is the coupling of the interaction between neutrinos and particles in the medium and m_ϕ^2 is the mass of the mediator of such interaction) is proportional to the particle-antiparticle asymmetry in the medium. If the asymmetry is small or zero, corrections of $\mathcal{O}(g^2/m_\phi^4)$ arising from the momentum-dependent terms of the mediator propagators in the self-energy diagrams become important and can even be dominant. This justifies the consideration of higher order in the effective expansion in momentum that leads to the use of Eq. (5.7).

The calculation presented in this Appendix has been carried out following Ref. [227] in analogy to what was done there for the SM case.

E.1 Dispersion Relation of Neutrinos

The properties of a neutrino propagating through a medium are determined by the Dirac equation

$$(\not{k} - \Sigma_{\text{eff}})\psi = 0 \quad (\text{E.1})$$

in momentum space where $\not{k} = k_\mu \gamma^\mu$, k_μ is the neutrino momentum and Σ_{eff} is the neutrino self-energy, which embodies effects of the medium through which the neutrino propagates.

In vacuum, $\Sigma_{\text{eff}} = a\not{k}$, that is self-energy depends only on the neutrino four-momentum. Instead, if neutrinos are propagating in a medium which has velocity u_μ , the self-energy is

$$\Sigma_{\text{eff}} = a\not{k} + b\not{u} + c[\not{k}, \not{u}] \quad (\text{E.2})$$

where a , b , and c are functions of the scalar quantities k^2 , $u^2 = 1$ and $\omega = k \cdot u$, that is the energy of the neutrino in the rest frame of the medium. At one-loop level, $c = 0$ [233]. Therefore, we are left with

$$\Sigma_{\text{eff}} = a\not{k} + b\not{u} \quad (\text{E.3})$$

where a and b are functions of the invariant variables $\omega = k \cdot u$ and $\kappa = \sqrt{\omega^2 - k^2}$. Substituting the definition of self-energy we can rewrite the Dirac equation as

$$\begin{aligned} (k - a\not{k} + b\not{u})\psi &= 0 \\ ((1-a)\not{k} + b\not{u})\psi &= 0 \\ \not{V}\psi &= 0 \end{aligned} \quad (\text{E.4})$$

where $V_\mu = (1-a)k_\mu + bu_\mu$. The Dirac equation has non-trivial solutions only for ω and κ such that

$$V^2 = f(\omega)\bar{f}(\omega) = 0 \quad \implies \quad \text{for } f(\omega) = 0 \quad \text{or} \quad \bar{f}(\omega) = \bar{f}(-\bar{\omega}) = 0 \quad (\text{E.5})$$

where

$$\begin{aligned} f(\omega) &= (1-a)(\omega - \kappa) - b \\ \bar{f}(\omega) &= (1-a)(\omega + \kappa) - b \end{aligned}$$

and $\bar{\omega}$ is the antineutrino energy. The dispersion relation ω_κ that we are interested in is the solution to Eq. (E.5).

The self-energy can be separated into gauge-independent (subscript 0) and gauge-dependent (subscript ξ) parts. Analogously, we can write

$$f = f_0 + f_\xi = [(1-a_0)(\omega - \kappa) - b_0] + [-a_\xi(\omega - \kappa) - b_\xi], \quad (\text{E.6})$$

and in order for ω_κ to be gauge-independent (which must be), both f_0 and f_ξ have to vanish at $\omega = \omega_\kappa$. The requirement that the gauge-independent part f_0 vanishes at $\omega = \omega_\kappa$ implies

$$\omega_\kappa = \kappa + b_0 + a_0(\omega_\kappa - \kappa) \quad (\text{E.7})$$

where $a_0(\omega_\kappa - \kappa) \sim \mathcal{O}\left(\frac{g^4}{m_\phi^2}, \frac{g^2}{m_\phi^6}\right)$ [227]. To zeroth order, in vacuum, $\omega_\kappa = \kappa$. Therefore, we can write up to first order the dispersion relation for neutrinos as

$$\omega_\kappa = \kappa + b_0(\omega_\kappa - \kappa) + \text{h.o.} = \kappa + b_0(\kappa) + \text{h.o.} \quad (\text{E.8})$$

and analogously for antineutrinos

$$\bar{\omega}_\kappa = \kappa - b_0(-\kappa) + \text{h.o.} \quad (\text{E.9})$$

E.2 Effective Potential

The effective potential $V_\alpha = V^D + V^T$ (constituted in general by the finite density term and the finite temperature term) can be seen as the contribution to the self-energy of the particle due to the presence of the background:

$$\omega_\kappa = \kappa + V_\alpha. \quad (\text{E.10})$$

If we then compare the latter equation with Eqs. (E.8 and (E.9), we see that in the lowest order the effective potential coincides with b_0 , while in general it would receive contributions also from a_0 [227]. Therefore, to get the expression for the effective potential (which in the DW framework coincides with the thermal potential) we have to calculate the self-energy $\Sigma_{\text{eff}} = (a_0 + a_\xi)\not{k} + (b_0 + b_\xi)\not{u}$ and extract b_0 .

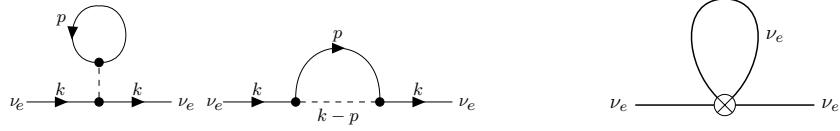


FIGURE E.1: Feynman diagrams of the contributions to neutrino self-energy from neutrino non-standard self-interactions, with the mediator resolved (left), and in the EFT perspective.

E.3 Self-Energy

The contribution of a generic type of neutrino NSSI j to the neutrino self-energy is

$$i\Sigma_{\text{eff}} = -\frac{G_F \epsilon_j}{\sqrt{2}} \int \frac{d^4 p}{(2\pi)^4} (\mathcal{O}_j + \mathcal{C} \mathcal{O}_j^T \mathcal{C}^{-1}) S_F(p) (\bar{\mathcal{O}}_j + \mathcal{C} \bar{\mathcal{O}}_j^T \mathcal{C}^{-1}) \left(1 + \frac{q_\mu q^\mu}{m_\phi^2} \right), \quad (\text{E.11})$$

where $q_\mu = k_\mu - p_\mu$ is the difference between the neutrino momentum k and the four-velocity of the medium u . The second term q^2/m_ϕ^2 in the final brackets comes from the second term in the Lagrangian Eq. (5.7) and leads to a temperature dependence in the potential. The terms involving the charge conjugation matrix \mathcal{C} come from the Feynman rules for Majorana neutrinos adopted following Ref. [222]. In the finite-temperature field theory formalism (FTFT) followed here according to Ref. [227], the fermion propagator $S_F(p)$ is given as

$$S_F(p) = (\not{p} + m_l) \left[\frac{1}{p^2 - m_l^2} + 2\pi i \delta(p^2 - m_l^2) \eta(p \cdot u) \right], \quad (\text{E.12})$$

where

$$\eta(p \cdot u) = \frac{\theta(p \cdot u)}{e^x + 1} + \frac{\theta(-p \cdot u)}{e^{-x} + 1}, \quad x = \frac{(p \cdot u - \mu)}{T} \quad (\text{E.13})$$

with $\theta(x)$ that is the unit step function and $n_\pm = (e^{\pm x} + 1)^{-1}$ that is the occupation number for the background fermions (n_+) and antifermions (n_-), in principle containing a chemical potential μ . In the fermion propagator, the first term only renormalizes the wave function and does not contribute to the dispersion relation in the lowest order [227]. Therefore, to simplify the calculations, we consider only the second term that is background-dependent

$$S_F^T(p) = 2\pi i \delta(p^2 - m_l^2) \eta(p \cdot u) (\not{p} + m_l), \quad (\text{E.14})$$

where the superscript T indicates the temperature dependence of the fermion propagator. Using $q_\mu q^\mu = (p - k)^2 \approx -2 p \cdot k$, the temperature dependent self-energy is,

$$i\Sigma_{\text{eff}}^{(T)} = -\frac{G_F \epsilon_j}{\sqrt{2}} \int \frac{d^4 p}{(2\pi)^4} (\mathcal{O}_j + \mathcal{C} \mathcal{O}_j^T \mathcal{C}^{-1}) S_F^T(p) (\bar{\mathcal{O}}_j + \mathcal{C} \bar{\mathcal{O}}_j^T \mathcal{C}^{-1}) \left(1 - \frac{2p \cdot k}{m_\phi^2} \right). \quad (\text{E.15})$$

E.3.1 Scalar NSSI

For scalar NSSI there is an additional minus sign due to the fact that the scalar propagator $\Delta_S = \frac{i}{q^2 - m_\phi^2}$ would have an extra minus sign compared to the vector propagator $\Delta_V =$

$-\frac{i g^{\mu\nu}}{q^2 - m_V^2}$.
We have

$$\mathcal{O}_S = \mathbb{I}, \quad \mathcal{C} \mathcal{O}_S^T \mathcal{C}^{-1} = \mathbb{I}, \quad \bar{\mathcal{O}}_S = \mathbb{I}, \quad \mathcal{C} \bar{\mathcal{O}}_S^T \mathcal{C}^{-1} = \mathbb{I}. \quad (\text{E.16})$$

Therefore, the contribution to the self-energy is

$$\begin{aligned} i\Sigma_{\text{eff},S}^{(T)} &= \frac{G_F \epsilon_S}{\sqrt{2}} \int \frac{d^4 p}{(2\pi)^4} (\mathcal{O}_S + \mathcal{C} \mathcal{O}_S^T \mathcal{C}^{-1}) S_F^T(p) (\bar{\mathcal{O}}_S + \mathcal{C} \bar{\mathcal{O}}_S^T \mathcal{C}^{-1}) \left(1 - \frac{2p \cdot k}{m_\phi^2}\right) \\ &= \frac{4 G_F \epsilon_S}{\sqrt{2}} \int \frac{d^4 p}{(2\pi)^4} S_F^T(p) \left(1 - \frac{2p \cdot k}{m_\phi^2}\right) \\ &= \frac{4 G_F \epsilon_S}{\sqrt{2}} \int \frac{d^4 p}{(2\pi)^4} (2\pi i \delta(p^2 - m_V^2) \eta(p \cdot u) \gamma^\mu p_\mu) \left(1 - \frac{2p \cdot k}{m_\phi^2}\right) \\ &= \frac{4 i G_F \epsilon_S}{\sqrt{2}} \int \frac{d^4 p}{(2\pi)^3} \delta(p^2 - m_V^2) \eta(p \cdot u) \gamma^\mu p_\mu \left(1 - \frac{2p \cdot k}{m_\phi^2}\right) \\ &= \frac{4 i G_F \epsilon_S}{\sqrt{2}} \gamma^\mu \left[I_\mu + \frac{2k^\nu}{m_\phi^2} I_{\mu\nu} \right] \end{aligned} \quad (\text{E.17})$$

where

$$I_\mu = \int \frac{d^4 p}{(2\pi)^3} \delta(p^2 - m_V^2) \eta(p \cdot u) p_\mu, \quad (\text{E.18})$$

$$I_{\mu\nu} = \int \frac{d^4 p}{(2\pi)^3} \delta(p^2 - m_V^2) \eta(p \cdot u) p_\mu p_\nu \quad (\text{E.19})$$

are two momentum-dependent integrals, calculated below.

$I_\mu = A u_\mu$ is manifestly covariant and has only u_μ dependence. We can calculate it by contracting it with u^μ .

$$I_\mu u^\mu = A u_\mu u^\mu = A = \int \frac{d^4 p}{(2\pi)^3} \delta(p^2 - m_V^2) \eta(p \cdot u) p_\mu u^\mu = J_1^{(v)} \quad (\text{E.20})$$

and so we have $I_\mu = J_1^{(v)} u_\mu$ where $J_n^{(f)}$ is defined as $J_n^{(f)} = \int \frac{d^4 p}{(2\pi)^3} \delta(p^2 - m_f^2) \eta(p \cdot u) (p \cdot u)^n$ and calculated below.

Similarly, $I_{\mu\nu}$ depends only on u and can be written as

$$I_{\mu\nu} = A g_{\mu\nu} + B u_\mu u_\nu. \quad (\text{E.21})$$

By contracting $I_{\mu\nu}$ with $u_\mu u_\nu$ and $g_{\mu\nu}$ we get the equations that define A and B .

$$g^{\mu\nu} I_{\mu\nu} = \int \frac{d^4 p}{(2\pi)^3} \delta(p^2 - m_V^2) \eta(p \cdot u) p_\mu g^{\mu\nu} p_\nu = m_V^2 J_0^{(v)} = 4A + B \quad (\text{E.22})$$

$$u^\mu u^\nu I_{\mu\nu} = \int \frac{d^4 p}{(2\pi)^3} \delta(p^2 - m_V^2) \eta(p \cdot u) p_\mu u^\mu u^\nu p_\nu = J_2^{(v)} = A + B. \quad (\text{E.23})$$

Solving for A and B , we get

$$A = \frac{1}{3} \left(m_\nu^2 J_0^{(\nu)} - J_2^{(\nu)} \right), \quad (\text{E.24})$$

$$B = \frac{1}{3} \left(4J_2^{(\nu)} - m_\nu^2 J_0^{(\nu)} \right). \quad (\text{E.25})$$

Substituting these expressions for I_μ and $I_{\mu\nu}$ into Eq. (E.17) we get

$$\begin{aligned} i\Sigma_{\text{eff},S}^{(T)} &= \frac{4i G_F \epsilon_S}{\sqrt{2}} \left[J_1^{(l)} \not{\mu} - \frac{2\gamma^\mu k^\nu}{3m_\phi^2} \left(m_l^2 J_0^{(l)} - J_2^{(l)} \right) g_{\mu\nu} - \frac{2\gamma^\mu k^\nu}{3m_\phi^2} \left(4J_2^{(l)} - m_l^2 J_0^{(l)} \right) u_\mu u_\nu \right] \\ &= \frac{4i G_F \epsilon_S}{\sqrt{2}} \left[J_1^{(l)} \not{\mu} - \frac{2}{3m_\phi^2} \left(m_l^2 J_0^{(l)} - J_2^{(l)} \right) \not{k} - \frac{2\omega}{3m_\phi^2} \left(4J_2^{(l)} - m_l^2 J_0^{(l)} \right) \not{\mu} \right] \end{aligned} \quad (\text{E.26})$$

Taking the neutrino mass $m_\nu \approx 0$, it simplifies to

$$i\Sigma_{\text{eff},S}^{(T)} = \frac{4i G_F \epsilon_S}{\sqrt{2}} \left[-\frac{2J_2^{(\nu)}}{3m_\phi^2} \not{k} + \left(J_1^{(\nu)} - \frac{8\omega}{3m_\phi^2} J_2^{(\nu)} \right) \not{\mu} \right] \quad (\text{E.27})$$

Comparing Eq. (E.27) and $\Sigma_{\text{eff}} = a_0 \not{k} + b_0 \not{\mu}$ one finds

$$b_0 = \frac{4 G_F \epsilon_S}{\sqrt{2}} \left(J_1^{(\nu)} - \frac{8\omega}{3m_\phi^2} J_2^{(\nu)} \right). \quad (\text{E.28})$$

From the calculation of $J_n^{(\nu)}$ provided in Subsection E.3.2, the result is

$$b_0 = \frac{4 G_F}{\sqrt{2}} \epsilon_S \left[\frac{1}{2} (n_\nu - n_{\bar{\nu}}) - \frac{8\omega}{3m_\phi^2} \cdot \frac{1}{2} (n_\nu \langle E_\nu \rangle + n_{\bar{\nu}} \langle E_{\bar{\nu}} \rangle) \right]. \quad (\text{E.29})$$

The first term becomes zero if we assume a lepton-symmetric universe. In this case the contribution of scalar NSSI to the thermal potential at the lowest order in ω , that is the neutrino momentum, is

$$V_S = -\frac{7\sqrt{2}\pi^2 G_F \epsilon_S}{45 m_\phi^2} \cdot \omega T^4. \quad (\text{E.30})$$

E.3.2 Evaluation of J_n^f

$$J_n^{(f)} = \int \frac{d^4 p}{(2\pi)^3} \delta(p^2 - m_f^2) \eta(p \cdot u) (p \cdot u)^n \quad (\text{E.31})$$

where

$$\begin{aligned} \delta(p^2 - m_f^2) &= \delta((p - m_f)(p + m_f)) \\ &= \delta(p_0^2 - \vec{p}^2 - m_f^2) \\ &= \delta(p_0^2 - \omega_p^2) \\ &= \delta((p_0 - \omega_p)(p_0 + \omega_p)) \\ &= \frac{1}{2\omega_p} [\delta(p_0 - \omega_p) + \delta(p_0 + \omega_p)] \end{aligned} \quad (\text{E.32})$$

with $\omega_p = \sqrt{p^2 + m_f^2} = E_p$ and

$$\eta(p \cdot u) = \frac{\theta(p \cdot u)}{e^{\frac{(p \cdot u - \mu)}{T}} + 1} + \frac{\theta(-p \cdot u)}{e^{-\frac{(p \cdot u - \mu)}{T}} + 1}. \quad (\text{E.33})$$

In the rest frame of the medium, $u_\mu = (1, 0, 0, 0)$,

$$\eta(p \cdot u) = \frac{\theta(p_0)}{e^{\frac{(p_0 - \mu)}{T}} + 1} + \frac{\theta(-p_0)}{e^{-\frac{(p_0 - \mu)}{T}} + 1} = \theta(p_0) f_f(p_0) + \theta(-p_0) f_{\bar{f}}(-p_0) \quad (\text{E.34})$$

where,

$$f_f(E) = \frac{1}{e^{\beta(E - \mu)} + 1} \quad \text{and} \quad f_{\bar{f}}(E) = \frac{1}{e^{\beta(E + \mu)} + 1} \quad (\text{E.35})$$

are the particle and antiparticle momentum distributions. The number densities are given by

$$n_{f, \bar{f}} = g_{f, \bar{f}} \int \frac{d^3 \vec{p}}{(2\pi)^3} f_{f, \bar{f}} \quad (\text{E.36})$$

and the thermal average of \mathcal{E}^n is

$$\langle \mathcal{E}_{f, \bar{f}}^n \rangle \equiv \frac{g_{f, \bar{f}}}{n_{f, \bar{f}}} \int \frac{d^3 \vec{p}}{(2\pi)^3} \mathcal{E}^n f_{f, \bar{f}}. \quad (\text{E.37})$$

Now, making explicit all these terms we get

$$\begin{aligned} J_n^{(f)} &= \int \frac{d^4 p}{(2\pi)^3} \delta(p^2 - m_f^2) \eta(p \cdot u) (p \cdot u)^n \\ &= \int \frac{d^3 \vec{p} dp_0}{(2\pi)^3} \frac{1}{2\omega_p} [\delta(p_0 - \omega_p) + \delta(p_0 + \omega_p)] [\theta(p_0) f_f(p_0) + \theta(-p_0) f_{\bar{f}}(-p_0)] (p_0)^n \\ &= \int \frac{d^3 \vec{p}}{(2\pi)^3} \left[\frac{\omega_p^n}{2\omega_p} f_f(\omega_p) + \frac{(-\omega_p)^n}{2\omega_p} f_{\bar{f}}(\omega_p) \right] \\ &= \frac{1}{2} \int \frac{d^3 \vec{p}}{(2\pi)^3} [E_f^{n-1} f_f(E_p) + (-1)^n E_{\bar{f}}^{n-1} f_{\bar{f}}(E_p)] \\ &= \frac{1}{2} \left[\frac{n_f}{g_f} \langle E_f^{n-1} \rangle + (-1)^n \frac{n_{\bar{f}}}{g_{\bar{f}}} \langle E_{\bar{f}}^{n-1} \rangle \right] \end{aligned} \quad (\text{E.38})$$

For neutrinos $g_\nu = g_{\bar{\nu}} = 1$ and we get

$$J_0^{(\nu)} = \frac{1}{2} \left[n_\nu \left\langle \frac{1}{E_\nu} \right\rangle + n_{\bar{\nu}} \left\langle \frac{1}{E_{\bar{\nu}}} \right\rangle \right] \quad (\text{E.39})$$

$$J_1^{(\nu)} = \frac{1}{2} \left[\frac{n_\nu}{g_\nu} - \frac{n_{\bar{\nu}}}{g_{\bar{\nu}}} \right] = \frac{1}{2} (n_\nu - n_{\bar{\nu}}) \quad (\text{E.40})$$

$$J_2^{(\nu)} = \frac{1}{2} [n_\nu \langle E_\nu \rangle + n_{\bar{\nu}} \langle E_{\bar{\nu}} \rangle] = \frac{7\pi^2 T^4}{240} \quad (\text{E.41})$$

E.3.3 Pseudoscalar NSSI

Also for pseudoscalar NSSI there is an additional minus sign with respect to the vector or axial-vector formula.

We have

$$\mathcal{O}_P = i\gamma^5, \quad \mathcal{C}\mathcal{O}_P^T\mathcal{C}^{-1} = i\gamma^5, \quad \bar{\mathcal{O}}_P = i\gamma^5, \quad \mathcal{C}\bar{\mathcal{O}}_P^T\mathcal{C}^{-1} = i\gamma^5. \quad (\text{E.42})$$

Therefore, the contribution to the self-energy is

$$\begin{aligned} i\Sigma_{\text{eff},P}^{(T)} &= \frac{G_F\epsilon_P}{\sqrt{2}} \int \frac{d^4p}{(2\pi)^4} (\mathcal{O}_P + \mathcal{C}\mathcal{O}_P^T\mathcal{C}^{-1}) S_F^T(p) (\bar{\mathcal{O}}_P + \mathcal{C}\bar{\mathcal{O}}_P^T\mathcal{C}^{-1}) \left(1 - \frac{2p \cdot k}{m_\phi^2}\right) \\ &= \frac{G_F\epsilon_P}{\sqrt{2}} \int \frac{d^4p}{(2\pi)^4} (i\gamma^5) S_F^T(p) (i\gamma^5) \left(1 - \frac{2p \cdot k}{m_\phi^2}\right) \\ &= \frac{G_F\epsilon_P}{\sqrt{2}} \int \frac{d^4p}{(2\pi)^4} S_F^T(p) \left(1 - \frac{2p \cdot k}{m_\phi^2}\right). \end{aligned} \quad (\text{E.43})$$

Manipulating as in the scalar case we obtain

$$i\Sigma_{\text{eff},P}^{(T)} = \frac{4iG_F\epsilon_P}{\sqrt{2}} \left[-\frac{2J_2^{(v)}}{3m_\phi^2} \not{k} + \left(J_1^{(v)} - \frac{8\omega}{3m_\phi^2} J_2^{(v)} \right) \not{\mu} \right]. \quad (\text{E.44})$$

Comparing with $\Sigma_{\text{eff}} = a_0\not{k} + b_0\not{\mu}$ one finds

$$b_0 = \frac{4G_F\epsilon_P}{\sqrt{2}} \left(J_1^{(v)} - \frac{8\omega}{3m_\phi^2} J_2^{(v)} \right). \quad (\text{E.45})$$

From the calculation of $J_n^{(v)}$ provided in Subsection E.3.2, the result is

$$b_0 = \frac{4G_F}{\sqrt{2}} \epsilon_P \left[\frac{1}{2} (n_\nu - n_{\bar{\nu}}) - \frac{8\omega}{3m_\phi^2} \cdot \frac{1}{2} (n_\nu \langle E_\nu \rangle + n_{\bar{\nu}} \langle E_{\bar{\nu}} \rangle) \right]. \quad (\text{E.46})$$

Assuming a lepton-symmetric universe the first term is zero. In this case, the contribution of pseudoscalar NSSI to the thermal potential at the lowest order in ω , that is the neutrino momentum, is

$$V_P = -\frac{7\sqrt{2}\pi^2 G_F \epsilon_P}{45 m_\phi^2} \cdot \omega T^4. \quad (\text{E.47})$$

E.3.4 Axial-vector NSSI

For axial-vector NSSI we have

$$\mathcal{O}_A = \gamma_\mu \gamma^5, \quad \mathcal{C}\mathcal{O}_A^T\mathcal{C}^{-1} = \gamma_\mu \gamma^5, \quad \bar{\mathcal{O}}_A = \gamma^\mu \gamma^5, \quad \mathcal{C}\bar{\mathcal{O}}_A^T\mathcal{C}^{-1} = \gamma^\mu \gamma^5. \quad (\text{E.48})$$

Therefore, the contribution to the self-energy is

$$\begin{aligned}
i\Sigma_{\text{eff,A}}^{(T)} &= -\frac{G_F \epsilon_A}{\sqrt{2}} \int \frac{d^4 p}{(2\pi)^4} (\mathcal{O}_A + \mathcal{C} \mathcal{O}_P^T \mathcal{C}^{-1}) S_F^T(p) (\bar{\mathcal{O}}_A + \mathcal{C} \bar{\mathcal{O}}_A^T \mathcal{C}^{-1}) \left(1 - \frac{2p \cdot k}{m_\phi^2}\right) \\
&= -\frac{4 G_F \epsilon_A}{\sqrt{2}} \int \frac{d^4 p}{(2\pi)^4} \gamma_\mu \gamma^5 S_F^T(p) \gamma^\mu \gamma^5 \left(1 - \frac{2p \cdot k}{m_\phi^2}\right) \\
&= -\frac{4 G_F \epsilon_A}{\sqrt{2}} \int \frac{d^4 p}{(2\pi)^4} \gamma_\mu S_F^T(p) \gamma^\mu \left(1 - \frac{2p \cdot k}{m_\phi^2}\right). \tag{E.49}
\end{aligned}$$

We evaluate

$$\gamma_\mu S_F^T(p) \gamma^\mu = 2\pi i \delta(p^2 - m_l^2) \eta(p \cdot u) \gamma_\mu \not{p} \gamma^\mu \tag{E.50}$$

where

$$\gamma_\mu \not{p} \gamma^\mu = \gamma_\mu \gamma^\nu p_\nu \gamma^\mu = \gamma_\mu p_\nu (2g^{\mu\nu} - \gamma^\mu \gamma^\nu) = 2\not{p} - 4\not{p} = -2\not{p} \tag{E.51}$$

so

$$\gamma_\mu S_F^T(p) \gamma^\mu = 2\pi i \delta(p^2 - m_l^2) \eta(p \cdot u) (-2\not{p}) = -2S_F^T(p) \tag{E.52}$$

and

$$i\Sigma_{\text{eff,A}}^{(T)} = \frac{8i G_F \epsilon_A}{\sqrt{2}} \left[-\frac{2J_2^{(\nu)}}{3m_\phi^2} \not{k} + \left(J_1^{(\nu)} - \frac{8\omega}{3m_\phi^2} J_2^{(\nu)} \right) \not{\mu} \right] \tag{E.53}$$

Comparing with $\Sigma_{\text{eff}} = a_0 \not{k} + b_0 \not{\mu}$ and using the expression for $J_n^{(\nu)}$ one finds

$$\begin{aligned}
b_0 &= \frac{8 G_F \epsilon_A}{\sqrt{2}} \left(J_1^{(\nu)} - \frac{8\omega}{3m_\phi^2} J_2^{(\nu)} \right) \\
&= \frac{8 G_F}{\sqrt{2}} \epsilon_A \left[\frac{1}{2} (n_\nu - n_{\bar{\nu}}) - \frac{8\omega}{3m_\phi^2} \cdot \frac{1}{2} (n_\nu \langle E_\nu \rangle + n_{\bar{\nu}} \langle E_{\bar{\nu}} \rangle) \right]. \tag{E.54}
\end{aligned}$$

Ignoring the first term that is zero in a symmetric universe, the contribution of axial-vector NSSI to the thermal potential at the lowest order in ω , that is the neutrino momentum, is

$$V_A = -\frac{14\sqrt{2} G_F \epsilon_P}{45 m_\phi^2} \cdot \omega T^4. \tag{E.55}$$

Acknowledgements

*tutto fu bene,
anche il mio male,
tutto
per me
Tu fosti e sei*

(Ada Negri)
– Atto d'Amore –

Looking back at the years of my doctoral studies, now that I am in the last stretch of the race to the finish line, many faces appear in my mind for which I am full of gratitude: to each of you, I owe a little of who I am today as a physicist and as a woman.

First of all, I would like to thank my supervisors, Werner Rodejohann and Manfred Lindner, for giving me the possibility to become a Ph.D. student at MPIK. By accepting me as a Ph.D. student, they offered me an opportunity that soon turned out to be greater and richer than I expected when I sent in my application for the position. I am grateful to be part of an extremely lively, stimulating, and at the same time, familiar research environment. Thanks for the great freedom to decide what to work on and which scientific interests to invest my time and energy in. Also, I would like to thank them for the possibility to travel a lot (taking into account the two and a half years of the pandemic) to visit schools and conferences where I was challenged to account for my work, and I had the chance to meet intelligent people and have valuable discussions for the development of my scientific interests.

A special thanks to Werner Rodejohann, leader of the MANITOP group, for always being available when I knocked on his door and for the discussions about the directions to steer the projects and the more concrete details of the work. Thanks for the possibility to follow my scientific interests even though they took me down a more winding and lonely road than others: this process was precious to my growth and laid the foundations for a more solid and richer way of working. Finally, thanks for the advent calendar that, like the other MANITOP people, I found on my desk the first year as soon as I arrived and then every year thereafter: a sign of attention as unexpected as it is appreciated.

A special thanks to Manfred Lindner for the encouragement to discover where my potential as a physicist lies and find new ways to put it to use without losing sight of the big picture. Thanks also for insisting on the importance of "not being shy" and asking the questions I had. Finally, thank you for always asking me to account for the requests I was making or the directions I wanted to take. Not a single word of these dialogues was wasted.

I would also like to thank Jörg Jäckel, who has been my internal supervisor at the University of Heidelberg, for his availability and time devoted every semester to discussing my progress in my Ph.D. studies and the prospects for the future, always with an extremely

positive approach.

Among all my colleagues, my first gratitude goes to Vedran, who welcomed me when I arrived at MPIK and has been my first mentor and collaborator. I am grateful for his patience, for valuing every small step and achievement, and for encouraging me to get involved fully in the department's life, starting from the Journal Club.

Thanks to Lukas, Tereza, and Tobias for simply sharing a bit of their lives with me during their years in Heidelberg.

Thanks to Karla and Ulises for their spontaneous and free affection.

Thanks to Andi, Manibrata, and Sudip for their friendship and support, for having answered many of my questions regarding physics, for the dinners together, and for their encouragement to persevere in my intention to travel to the US for conferences this summer.

Thanks to Janina for her positive and careful company during the NDM22 conference in Asheville and for the help in the preparation of the trip.

Thanks to Evgeny and Alexei for the fruitful discussions regarding neutrinos.

Thanks to all my former and current colleagues and fellow Ph.D. students, Thomas, Simone, Valentin, Susan, Ting, Philipp, Jonas, Andreas, Sophie, Sven, Tim, Nele, Frederik, Andrei, Johannes, Salva, and Josef, for every lunch that has often been a real breath of fresh air in the days of work.

A special thanks to my office mates, Tom, Christian, Ingolf, and Carlos, for the nice time spent together in the office in any circumstances; thanks for the jokes that lightened the atmosphere on the most stressful days; thanks for having always been there for me, to help me with a problem in physics, a technical or administrative issue, or just to have a chat. Thanks for being the best doctors helping me to fight against my impostor syndrome.

Thanks to my former and current collaborators, Manibrata, Aaroodd, Kai, Kohei, Kyohei, Thomas, Carlos, Oliver, Jakob, Tim, Christian, and Frederik, from which I learned a lot, and I got valuable feedback and advice.

Thanks to Britta and Anja for their always renewed kindness in my regard and for taking care of several big and small details concerning the daily life at the institute that made my life easier and nicer.

Thanks to my flatmates Martin, Sabri, Ruoyu, Lara, Simon, Paula, Patrick, Sophia, Farah, and Lillo for their company and friendship, fresh and simple.

In particular, a special thanks to Martin, in which I immediately found a very good friend who is always happy to discuss anything that is relevant for life and for true happiness.

A special thanks to Sabri for the profound peace that her presence brings in any situation and for reminding me multiple times by her example of what it means to love unconditionally.

A special thanks to Ruoyu for reminding me by his example of what it means to have a heart that is alive and willing to invest time and energies in looking for the answers to the big questions of life.

Thanks to my friends from the community of the catholic Movement of CL, David, Maria, Giuseppe, Massi and Carol, Hubert and Sylvia, Nunzia and Stefan, Cristina and Albert, Lorenzo and Anna, Paolo and Juliana, Mercedes and Marcelo, Carlo and Anna, Veronika and Laerte, Johanna and Manuel, to Sister Elisabeth, to Michelle and to Federica, and to many others, for reminding me by their lives and their love of the presence and love of the One who is the joy of my life.

I am also very grateful to Giuliana, Massimo, and Ecce, who gave my life a happy and significant shake in recent months.

Finally, I want to thank my parents, Marco and Silvia, and my siblings, Ping and Francesca, Mari, and Frenk, because, even though we are far apart, they are a solid point to which I can always return, sure to be embraced.

Dulcis in fundo, I am very grateful to Matteo, in this adventure, a much greater partner than I ever dared to hope and far beyond what I could deserve. Thank you for your inextinguishable and inspiring curiosity and passion. Thank you for having a tirelessly positive and loving gaze on me and always valuing me, even when I did not see myself in a positive light. Thank you for always being there for me, with your lively and sincere heart, generous in offering your help and listening. Thank you for being my guide in learning to love freedom, mine, and that of others.

Bibliography

- [1] Carlo Giunti and Chung W. Kim. *Fundamentals of Neutrino Physics and Astrophysics*. 2007. ISBN: 978-0-19-850871-7.
- [2] Cristina Benso et al. “Prospects for Finding Sterile Neutrino Dark Matter at KATRIN”. In: *Phys. Rev. D* 100.11 (2019), p. 115035. DOI: [10.1103/PhysRevD.100.115035](https://doi.org/10.1103/PhysRevD.100.115035). arXiv: [1911.00328](https://arxiv.org/abs/1911.00328) [hep-ph].
- [3] Cristina Benso et al. “Sterile neutrino dark matter production in presence of nonstandard neutrino self-interactions: An EFT approach”. In: *Phys. Rev. D* 105.5 (2022), p. 055016. DOI: [10.1103/PhysRevD.105.055016](https://doi.org/10.1103/PhysRevD.105.055016). arXiv: [2112.00758](https://arxiv.org/abs/2112.00758) [hep-ph].
- [4] Y. Fukuda et al. “Evidence for oscillation of atmospheric neutrinos”. In: *Phys. Rev. Lett.* 81 (1998), pp. 1562–1567. DOI: [10.1103/PhysRevLett.81.1562](https://doi.org/10.1103/PhysRevLett.81.1562). arXiv: [hep-ex/9807003](https://arxiv.org/abs/hep-ex/9807003).
- [5] Q. R. Ahmad et al. “Direct evidence for neutrino flavor transformation from neutral current interactions in the Sudbury Neutrino Observatory”. In: *Phys. Rev. Lett.* 89 (2002), p. 011301. DOI: [10.1103/PhysRevLett.89.011301](https://doi.org/10.1103/PhysRevLett.89.011301). arXiv: [nuc1-ex/0204008](https://arxiv.org/abs/nuc1-ex/0204008).
- [6] A. Zee. “A Theory of Lepton Number Violation, Neutrino Majorana Mass, and Oscillation”. In: *Phys. Lett. B* 93 (1980). [Erratum: *Phys.Lett.B* 95, 461 (1980)], p. 389. DOI: [10.1016/0370-2693\(80\)90349-4](https://doi.org/10.1016/0370-2693(80)90349-4).
- [7] A. Zee. “Quantum Numbers of Majorana Neutrino Masses”. In: *Nucl. Phys. B* 264 (1986), pp. 99–110. DOI: [10.1016/0550-3213\(86\)90475-X](https://doi.org/10.1016/0550-3213(86)90475-X).
- [8] K. S. Babu. “Model of ‘Calculable’ Majorana Neutrino Masses”. In: *Phys. Lett. B* 203 (1988), pp. 132–136. DOI: [10.1016/0370-2693\(88\)91584-5](https://doi.org/10.1016/0370-2693(88)91584-5).
- [9] Steven Weinberg. “Baryon and Lepton Nonconserving Processes”. In: *Phys. Rev. Lett.* 43 (1979), pp. 1566–1570. DOI: [10.1103/PhysRevLett.43.1566](https://doi.org/10.1103/PhysRevLett.43.1566).
- [10] Laurent Canetti, Marco Drewes, and Mikhail Shaposhnikov. “Sterile Neutrinos as the Origin of Dark and Baryonic Matter”. In: *Phys. Rev. Lett.* 110.6 (2013), p. 061801. DOI: [10.1103/PhysRevLett.110.061801](https://doi.org/10.1103/PhysRevLett.110.061801). arXiv: [1204.3902](https://arxiv.org/abs/1204.3902) [hep-ph].
- [11] Laurent Canetti et al. “Dark Matter, Baryogenesis and Neutrino Oscillations from Right Handed Neutrinos”. In: *Phys. Rev. D* 87 (2013), p. 093006. DOI: [10.1103/PhysRevD.87.093006](https://doi.org/10.1103/PhysRevD.87.093006). arXiv: [1208.4607](https://arxiv.org/abs/1208.4607) [hep-ph].
- [12] André de Gouvêa. “Neutrino Mass Models”. In: *Ann. Rev. Nucl. Part. Sci.* 66 (2016), pp. 197–217. DOI: [10.1146/annurev-nucl-102115-044600](https://doi.org/10.1146/annurev-nucl-102115-044600).
- [13] P. A. Zyla et al. “Review of Particle Physics”. In: *PTEP* 2020.8 (2020), p. 083C01. DOI: [10.1093/ptep/ptaa104](https://doi.org/10.1093/ptep/ptaa104).
- [14] A. D. Sakharov. “Violation of CP Invariance, C asymmetry, and baryon asymmetry of the universe”. In: *Pisma Zh. Eksp. Teor. Fiz.* 5 (1967), pp. 32–35. DOI: [10.1070/PU1991v034n05ABEH002497](https://doi.org/10.1070/PU1991v034n05ABEH002497).

- [15] Antonio Riotto. “Theories of baryogenesis”. In: *ICTP Summer School in High-Energy Physics and Cosmology*. July 1998, pp. 326–436. arXiv: [hep-ph/9807454](#).
- [16] Ian Affleck and Michael Dine. “A New Mechanism for Baryogenesis”. In: *Nucl. Phys. B* 249 (1985), pp. 361–380. DOI: [10.1016/0550-3213\(85\)90021-5](#).
- [17] Mark Trodden. “Electroweak baryogenesis”. In: *Rev. Mod. Phys.* 71 (1999), pp. 1463–1500. DOI: [10.1103/RevModPhys.71.1463](#). arXiv: [hep-ph/9803479](#).
- [18] Andrew G. Cohen, D. B. Kaplan, and A. E. Nelson. “Progress in electroweak baryogenesis”. In: *Ann. Rev. Nucl. Part. Sci.* 43 (1993), pp. 27–70. DOI: [10.1146/annurev.ns.43.120193.000331](#). arXiv: [hep-ph/9302210](#).
- [19] A. D. Dolgov. “NonGUT baryogenesis”. In: *Phys. Rept.* 222 (1992), pp. 309–386. DOI: [10.1016/0370-1573\(92\)90107-B](#).
- [20] Gilly Elor et al. “New Ideas in Baryogenesis: A Snowmass White Paper”. In: *2022 Snowmass Summer Study*. Mar. 2022. arXiv: [2203.05010 \[hep-ph\]](#).
- [21] M. Fukugita and T. Yanagida. “Baryogenesis Without Grand Unification”. In: *Phys. Lett. B* 174 (1986), pp. 45–47. DOI: [10.1016/0370-2693\(86\)91126-3](#).
- [22] Steve Blanchet and Pasquale Di Bari. “The minimal scenario of leptogenesis”. In: *New J. Phys.* 14 (2012), p. 125012. DOI: [10.1088/1367-2630/14/12/125012](#). arXiv: [1211.0512 \[hep-ph\]](#).
- [23] Evgeny K. Akhmedov, V. A. Rubakov, and A. Yu. Smirnov. “Baryogenesis via neutrino oscillations”. In: *Phys. Rev. Lett.* 81 (1998), pp. 1359–1362. DOI: [10.1103/PhysRevLett.81.1359](#). arXiv: [hep-ph/9803255](#).
- [24] N. Aghanim et al. “Planck 2018 results. VI. Cosmological parameters”. In: *Astron. Astrophys.* 641 (2020). [Erratum: *Astron. Astrophys.* 652, C4 (2021)], A6. DOI: [10.1051/0004-6361/201833910](#). arXiv: [1807.06209 \[astro-ph.CO\]](#).
- [25] F. Zwicky. “Die Rotverschiebung von extragalaktischen Nebeln”. In: *Helv. Phys. Acta* 6 (1933), pp. 110–127. DOI: [10.1007/s10714-008-0707-4](#).
- [26] J. N. Bahcall and C. L. Sarazin. “Parameters and predictions for the X-ray emitting gas of Coma, Perseus, and Virgo”. In: *ApJ* 213 (1977), pp. L99–L103. DOI: [10.1086/182418](#).
- [27] W. G. Mathews. “The enormous mass of the elliptical galaxy M87: a model for the extended X-ray source”. In: *ApJ* 219 (1978), pp. 413–423. DOI: [10.1086/155794](#).
- [28] Xiang-Ping Wu et al. “A comparison of different cluster mass estimates: consistency or discrepancy?” In: *Mon. Not. Roy. Astron. Soc.* 301 (1998), p. 861. DOI: [10.1046/j.1365-8711.1998.02055.x](#). arXiv: [astro-ph/9808179](#).
- [29] Vera C. Rubin and W. Kent Ford Jr. “Rotation of the Andromeda Nebula from a Spectroscopic Survey of Emission Regions”. In: *Astrophys. J.* 159 (1970), pp. 379–403. DOI: [10.1086/150317](#).
- [30] K. G. Begeman, A. H. Broeils, and R. H. Sanders. “Extended rotation curves of spiral galaxies: Dark haloes and modified dynamics”. In: *Mon. Not. Roy. Astron. Soc.* 249 (1991), p. 523. DOI: [10.1093/mnras/249.3.523](#).
- [31] M. Kowalski et al. “Improved Cosmological Constraints from New, Old and Combined Supernova Datasets”. In: *Astrophys. J.* 686 (2008), pp. 749–778. DOI: [10.1086/589937](#). arXiv: [0804.4142 \[astro-ph\]](#).
- [32] Marco Taoso, Gianfranco Bertone, and Antonio Masiero. “Dark Matter Candidates: A Ten-Point Test”. In: *JCAP* 03 (2008), p. 022. DOI: [10.1088/1475-7516/2008/03/022](#). arXiv: [0711.4996 \[astro-ph\]](#).

- [33] Lawrence J. Hall et al. “Freeze-In Production of FIMP Dark Matter”. In: *JHEP* 03 (2010), p. 080. DOI: [10.1007/JHEP03\(2010\)080](https://doi.org/10.1007/JHEP03(2010)080). arXiv: [0911.1120](https://arxiv.org/abs/0911.1120) [hep-ph].
- [34] Edward W. Kolb and Michael S. Turner. *The Early Universe*. Vol. 69. 1990. ISBN: 978-0-201-62674-2. DOI: [10.1201/9780429492860](https://doi.org/10.1201/9780429492860).
- [35] Scott Dodelson and Lawrence M. Widrow. “Sterile-neutrinos as dark matter”. In: *Phys. Rev. Lett.* 72 (1994), pp. 17–20. DOI: [10.1103/PhysRevLett.72.17](https://doi.org/10.1103/PhysRevLett.72.17). arXiv: [hep-ph/9303287](https://arxiv.org/abs/hep-ph/9303287).
- [36] Basudeb Dasgupta and Joachim Kopp. “Sterile Neutrinos”. In: *Phys. Rept.* 928 (2021), pp. 1–63. DOI: [10.1016/j.physrep.2021.06.002](https://doi.org/10.1016/j.physrep.2021.06.002). arXiv: [2106.05913](https://arxiv.org/abs/2106.05913) [hep-ph].
- [37] Kevork N. Abazajian. “Sterile neutrinos in cosmology”. In: *Phys. Rept.* 711-712 (2017), pp. 1–28. DOI: [10.1016/j.physrep.2017.10.003](https://doi.org/10.1016/j.physrep.2017.10.003). arXiv: [1705.01837](https://arxiv.org/abs/1705.01837) [hep-ph].
- [38] Lucas Johns. “Derivation of the sterile neutrino Boltzmann equation from quantum kinetics”. In: *Phys. Rev. D* 100.8 (2019), p. 083536. DOI: [10.1103/PhysRevD.100.083536](https://doi.org/10.1103/PhysRevD.100.083536). arXiv: [1908.04244](https://arxiv.org/abs/1908.04244) [hep-ph].
- [39] Alexander Merle, Aurel Schneider, and Maximilian Totzauer. “Dodelson-Widrow Production of Sterile Neutrino Dark Matter with Non-Trivial Initial Abundance”. In: *JCAP* 04 (2016), p. 003. DOI: [10.1088/1475-7516/2016/04/003](https://doi.org/10.1088/1475-7516/2016/04/003). arXiv: [1512.05369](https://arxiv.org/abs/1512.05369) [hep-ph].
- [40] Kevork Abazajian, George M. Fuller, and Wallace H. Tucker. “Direct detection of warm dark matter in the X-ray”. In: *Astrophys. J.* 562 (2001), pp. 593–604. DOI: [10.1086/323867](https://doi.org/10.1086/323867). arXiv: [astro-ph/0106002](https://arxiv.org/abs/astro-ph/0106002).
- [41] Stephane Colombi, Scott Dodelson, and Lawrence M. Widrow. “Large scale structure tests of warm dark matter”. In: *Astrophys. J.* 458 (1996), p. 1. DOI: [10.1086/176788](https://doi.org/10.1086/176788). arXiv: [astro-ph/9505029](https://arxiv.org/abs/astro-ph/9505029).
- [42] Xiang-Dong Shi and George M. Fuller. “A New dark matter candidate: Non-thermal sterile neutrinos”. In: *Phys. Rev. Lett.* 82 (1999), pp. 2832–2835. DOI: [10.1103/PhysRevLett.82.2832](https://doi.org/10.1103/PhysRevLett.82.2832). arXiv: [astro-ph/9810076](https://arxiv.org/abs/astro-ph/9810076).
- [43] Takehiko Asaka, Steve Blanchet, and Mikhail Shaposhnikov. “The nuMSM, dark matter and neutrino masses”. In: *Phys. Lett. B* 631 (2005), pp. 151–156. DOI: [10.1016/j.physletb.2005.09.070](https://doi.org/10.1016/j.physletb.2005.09.070). arXiv: [hep-ph/0503065](https://arxiv.org/abs/hep-ph/0503065).
- [44] M. Laine and M. Shaposhnikov. “Sterile neutrino dark matter as a consequence of nuMSM-induced lepton asymmetry”. In: *JCAP* 06 (2008), p. 031. DOI: [10.1088/1475-7516/2008/06/031](https://doi.org/10.1088/1475-7516/2008/06/031). arXiv: [0804.4543](https://arxiv.org/abs/0804.4543) [hep-ph].
- [45] Mikhail Shaposhnikov. “The nuMSM, leptonic asymmetries, and properties of singlet fermions”. In: *JHEP* 08 (2008), p. 008. DOI: [10.1088/1126-6708/2008/08/008](https://doi.org/10.1088/1126-6708/2008/08/008). arXiv: [0804.4542](https://arxiv.org/abs/0804.4542) [hep-ph].
- [46] Shintaro Eijima and Mikhail Shaposhnikov. “Fermion number violating effects in low scale leptogenesis”. In: *Phys. Lett. B* 771 (2017), pp. 288–296. DOI: [10.1016/j.physletb.2017.05.068](https://doi.org/10.1016/j.physletb.2017.05.068). arXiv: [1703.06085](https://arxiv.org/abs/1703.06085) [hep-ph].
- [47] Alexey Boyarsky, Jurg Frohlich, and Oleg Ruchayskiy. “Self-consistent evolution of magnetic fields and chiral asymmetry in the early Universe”. In: *Phys. Rev. Lett.* 108 (2012), p. 031301. DOI: [10.1103/PhysRevLett.108.031301](https://doi.org/10.1103/PhysRevLett.108.031301). arXiv: [1109.3350](https://arxiv.org/abs/1109.3350) [astro-ph.CO].
- [48] Masahiro Kawasaki and Kai Murai. “Lepton Asymmetric Universe”. In: (Mar. 2022). arXiv: [2203.09713](https://arxiv.org/abs/2203.09713) [hep-ph].

- [49] Graciela B. Gelmini et al. “Big Bang Nucleosynthesis constraints on sterile neutrino and lepton asymmetry of the Universe”. In: *JCAP* 09 (2020), p. 051. DOI: [10.1088/1475-7516/2020/09/051](https://doi.org/10.1088/1475-7516/2020/09/051). arXiv: [2005.06721](https://arxiv.org/abs/2005.06721) [hep-ph].
- [50] Isabel M. Oldengott and Dominik J. Schwarz. “Improved constraints on lepton asymmetry from the cosmic microwave background”. In: *EPL* 119.2 (2017), p. 29001. DOI: [10.1209/0295-5075/119/29001](https://doi.org/10.1209/0295-5075/119/29001). arXiv: [1706.01705](https://arxiv.org/abs/1706.01705) [astro-ph.CO].
- [51] Dominik J. Schwarz and Stuke Maik. “Does the CMB prefer a leptonic Universe?” In: *New J. Phys.* 15 (2013), p. 033021. DOI: [10.1088/1367-2630/15/3/033021](https://doi.org/10.1088/1367-2630/15/3/033021). arXiv: [1211.6721](https://arxiv.org/abs/1211.6721) [astro-ph.CO].
- [52] Emanuele Castorina et al. “Cosmological lepton asymmetry with a nonzero mixing angle θ_{13} ”. In: *Phys. Rev. D* 86 (2012), p. 023517. DOI: [10.1103/PhysRevD.86.023517](https://doi.org/10.1103/PhysRevD.86.023517). arXiv: [1204.2510](https://arxiv.org/abs/1204.2510) [astro-ph.CO].
- [53] Gianpiero Mangano et al. “Updated BBN bounds on the cosmological lepton asymmetry for non-zero θ_{13} ”. In: *Phys. Lett. B* 708 (2012), pp. 1–5. DOI: [10.1016/j.physletb.2012.01.015](https://doi.org/10.1016/j.physletb.2012.01.015). arXiv: [1110.4335](https://arxiv.org/abs/1110.4335) [hep-ph].
- [54] A. Boyarsky et al. “Sterile neutrino Dark Matter”. In: *Prog. Part. Nucl. Phys.* 104 (2019), pp. 1–45. DOI: [10.1016/j.pnpnp.2018.07.004](https://doi.org/10.1016/j.pnpnp.2018.07.004). arXiv: [1807.07938](https://arxiv.org/abs/1807.07938) [hep-ph].
- [55] F. Bezrukov, H. Hettmansperger, and M. Lindner. “keV sterile neutrino Dark Matter in gauge extensions of the Standard Model”. In: *Phys. Rev. D* 81 (2010), p. 085032. DOI: [10.1103/PhysRevD.81.085032](https://doi.org/10.1103/PhysRevD.81.085032). arXiv: [0912.4415](https://arxiv.org/abs/0912.4415) [hep-ph].
- [56] Johannes Herms, Alejandro Ibarra, and Takashi Toma. “A new mechanism of sterile neutrino dark matter production”. In: *JCAP* 06 (2018), p. 036. DOI: [10.1088/1475-7516/2018/06/036](https://doi.org/10.1088/1475-7516/2018/06/036). arXiv: [1802.02973](https://arxiv.org/abs/1802.02973) [hep-ph].
- [57] Robert J. Scherrer and Michael S. Turner. “Decaying Particles Do Not Heat Up the Universe”. In: *Phys. Rev. D* 31 (1985), p. 681. DOI: [10.1103/PhysRevD.31.681](https://doi.org/10.1103/PhysRevD.31.681).
- [58] Miha Nemevsek, Goran Senjanovic, and Yue Zhang. “Warm Dark Matter in Low Scale Left-Right Theory”. In: *JCAP* 07 (2012), p. 006. DOI: [10.1088/1475-7516/2012/07/006](https://doi.org/10.1088/1475-7516/2012/07/006). arXiv: [1205.0844](https://arxiv.org/abs/1205.0844) [hep-ph].
- [59] Amol V. Patwardhan et al. “Diluted equilibrium sterile neutrino dark matter”. In: *Phys. Rev. D* 92.10 (2015), p. 103509. DOI: [10.1103/PhysRevD.92.103509](https://doi.org/10.1103/PhysRevD.92.103509). arXiv: [1507.01977](https://arxiv.org/abs/1507.01977) [astro-ph.CO].
- [60] Mikhail Shaposhnikov and Igor Tkachev. “The nuMSM, inflation, and dark matter”. In: *Phys. Lett. B* 639 (2006), pp. 414–417. DOI: [10.1016/j.physletb.2006.06.063](https://doi.org/10.1016/j.physletb.2006.06.063). arXiv: [hep-ph/0604236](https://arxiv.org/abs/hep-ph/0604236).
- [61] Kalliopi Petraki and Alexander Kusenko. “Dark-matter sterile neutrinos in models with a gauge singlet in the Higgs sector”. In: *Phys. Rev. D* 77 (2008), p. 065014. DOI: [10.1103/PhysRevD.77.065014](https://doi.org/10.1103/PhysRevD.77.065014). arXiv: [0711.4646](https://arxiv.org/abs/0711.4646) [hep-ph].
- [62] Alexander Kusenko. “Sterile neutrinos, dark matter, and the pulsar velocities in models with a Higgs singlet”. In: *Phys. Rev. Lett.* 97 (2006), p. 241301. DOI: [10.1103/PhysRevLett.97.241301](https://doi.org/10.1103/PhysRevLett.97.241301). arXiv: [hep-ph/0609081](https://arxiv.org/abs/hep-ph/0609081).
- [63] Alexander Merle, Viviana Niro, and Daniel Schmidt. “New Production Mechanism for keV Sterile Neutrino Dark Matter by Decays of Frozen-In Scalars”. In: *JCAP* 03 (2014), p. 028. DOI: [10.1088/1475-7516/2014/03/028](https://doi.org/10.1088/1475-7516/2014/03/028). arXiv: [1306.3996](https://arxiv.org/abs/1306.3996) [hep-ph].

- [64] Adisorn Adulpravitchai and Michael A. Schmidt. “A Fresh Look at keV Sterile Neutrino Dark Matter from Frozen-In Scalars”. In: *JHEP* 01 (2015), p. 006. DOI: [10.1007/JHEP01\(2015\)006](https://doi.org/10.1007/JHEP01(2015)006). arXiv: [1409.4330](https://arxiv.org/abs/1409.4330) [hep-ph].
- [65] Alexander Merle and Maximilian Totzauer. “keV Sterile Neutrino Dark Matter from Singlet Scalar Decays: Basic Concepts and Subtle Features”. In: *JCAP* 06 (2015), p. 011. DOI: [10.1088/1475-7516/2015/06/011](https://doi.org/10.1088/1475-7516/2015/06/011). arXiv: [1502.01011](https://arxiv.org/abs/1502.01011) [hep-ph].
- [66] Johannes König, Alexander Merle, and Maximilian Totzauer. “keV Sterile Neutrino Dark Matter from Singlet Scalar Decays: The Most General Case”. In: *JCAP* 11 (2016), p. 038. DOI: [10.1088/1475-7516/2016/11/038](https://doi.org/10.1088/1475-7516/2016/11/038). arXiv: [1609.01289](https://arxiv.org/abs/1609.01289) [hep-ph].
- [67] Alexander Merle and Aurel Schneider. “Production of Sterile Neutrino Dark Matter and the 3.5 keV line”. In: *Phys. Lett. B* 749 (2015), pp. 283–288. DOI: [10.1016/j.physletb.2015.07.080](https://doi.org/10.1016/j.physletb.2015.07.080). arXiv: [1409.6311](https://arxiv.org/abs/1409.6311) [hep-ph].
- [68] S. Tremaine and J. E. Gunn. “Dynamical Role of Light Neutral Leptons in Cosmology”. In: *Phys. Rev. Lett.* 42 (1979). Ed. by M. A. Srednicki, pp. 407–410. DOI: [10.1103/PhysRevLett.42.407](https://doi.org/10.1103/PhysRevLett.42.407).
- [69] Alexey Boyarsky, Oleg Ruchayskiy, and Dmytro Iakubovskyi. “A Lower bound on the mass of Dark Matter particles”. In: *JCAP* 03 (2009), p. 005. DOI: [10.1088/1475-7516/2009/03/005](https://doi.org/10.1088/1475-7516/2009/03/005). arXiv: [0808.3902](https://arxiv.org/abs/0808.3902) [hep-ph].
- [70] Christophe Yèche et al. “Constraints on neutrino masses from Lyman-alpha forest power spectrum with BOSS and XQ-100”. In: *JCAP* 06 (2017), p. 047. DOI: [10.1088/1475-7516/2017/06/047](https://doi.org/10.1088/1475-7516/2017/06/047). arXiv: [1702.03314](https://arxiv.org/abs/1702.03314) [astro-ph.CO].
- [71] Aurel Schneider. “Astrophysical constraints on resonantly produced sterile neutrino dark matter”. In: *JCAP* 04 (2016), p. 059. DOI: [10.1088/1475-7516/2016/04/059](https://doi.org/10.1088/1475-7516/2016/04/059). arXiv: [1601.07553](https://arxiv.org/abs/1601.07553) [astro-ph.CO].
- [72] Girish Kulkarni et al. “Characterizing the Pressure Smoothing Scale of the Intergalactic Medium”. In: *Astrophys. J.* 812 (2015), p. 30. DOI: [10.1088/0004-637X/812/1/30](https://doi.org/10.1088/0004-637X/812/1/30). arXiv: [1504.00366](https://arxiv.org/abs/1504.00366) [astro-ph.CO].
- [73] Robert E. Smith and Katarina Markovic. “Testing the Warm Dark Matter paradigm with large-scale structures”. In: *Phys. Rev. D* 84 (2011), p. 063507. DOI: [10.1103/PhysRevD.84.063507](https://doi.org/10.1103/PhysRevD.84.063507). arXiv: [1103.2134](https://arxiv.org/abs/1103.2134) [astro-ph.CO].
- [74] Katarina Markovič and Matteo Viel. “Lyman- α Forest and Cosmic Weak Lensing in a Warm Dark Matter Universe”. In: *Publ. Astron. Soc. Austral.* 31 (2014), e006. DOI: [10.1017/pasa.2013.43](https://doi.org/10.1017/pasa.2013.43). arXiv: [1311.5223](https://arxiv.org/abs/1311.5223) [astro-ph.CO].
- [75] Aurel Schneider. “Constraining noncold dark matter models with the global 21-cm signal”. In: *Phys. Rev. D* 98.6 (2018), p. 063021. DOI: [10.1103/PhysRevD.98.063021](https://doi.org/10.1103/PhysRevD.98.063021). arXiv: [1805.00021](https://arxiv.org/abs/1805.00021) [astro-ph.CO].
- [76] Alexey Boyarsky et al. “21-cm observations and warm dark matter models”. In: *Phys. Rev. D* 100.12 (2019), p. 123005. DOI: [10.1103/PhysRevD.100.123005](https://doi.org/10.1103/PhysRevD.100.123005). arXiv: [1904.03097](https://arxiv.org/abs/1904.03097) [astro-ph.CO].
- [77] Darren S. Reed et al. “The same with less: The cosmic web of warm versus cold dark matter dwarf galaxies”. In: *Mon. Not. Roy. Astron. Soc.* 451.4 (2015), pp. 4413–4423. DOI: [10.1093/mnras/stv1233](https://doi.org/10.1093/mnras/stv1233). arXiv: [1410.1541](https://arxiv.org/abs/1410.1541) [astro-ph.CO].
- [78] Lin F. Yang et al. “Warmth Elevating the Depths: Shallower Voids with Warm Dark Matter”. In: *Mon. Not. Roy. Astron. Soc.* 451.4 (2015), pp. 3606–3614. DOI: [10.1093/mnras/stv1087](https://doi.org/10.1093/mnras/stv1087). arXiv: [1411.5029](https://arxiv.org/abs/1411.5029) [astro-ph.CO].

- [79] Emil Polisensky and Massimo Ricotti. “Constraints on the Dark Matter Particle Mass from the Number of Milky Way Satellites”. In: *Phys. Rev. D* 83 (2011), p. 043506. DOI: [10.1103/PhysRevD.83.043506](https://doi.org/10.1103/PhysRevD.83.043506). arXiv: [1004.1459](https://arxiv.org/abs/1004.1459) [astro-ph.CO].
- [80] Rachel Kennedy et al. “Constraining the warm dark matter particle mass with Milky Way satellites”. In: *Mon. Not. Roy. Astron. Soc.* 442.3 (2014), pp. 2487–2495. DOI: [10.1093/mnras/stu719](https://doi.org/10.1093/mnras/stu719). arXiv: [1310.7739](https://arxiv.org/abs/1310.7739) [astro-ph.CO].
- [81] M. Drewes et al. “A White Paper on keV Sterile Neutrino Dark Matter”. In: *JCAP* 01 (2017), p. 025. DOI: [10.1088/1475-7516/2017/01/025](https://doi.org/10.1088/1475-7516/2017/01/025). arXiv: [1602.04816](https://arxiv.org/abs/1602.04816) [hep-ph].
- [82] Christian Schultz et al. “The High- z Universe Confronts Warm Dark Matter: Galaxy Counts, Reionization and the Nature of Dark Matter”. In: *Mon. Not. Roy. Astron. Soc.* 442.2 (2014), pp. 1597–1609. DOI: [10.1093/mnras/stu976](https://doi.org/10.1093/mnras/stu976). arXiv: [1401.3769](https://arxiv.org/abs/1401.3769) [astro-ph.CO].
- [83] P. Hernandez, M. Kekic, and J. Lopez-Pavon. “ N_{eff} in low-scale seesaw models versus the lightest neutrino mass”. In: *Phys. Rev. D* 90.6 (2014), p. 065033. DOI: [10.1103/PhysRevD.90.065033](https://doi.org/10.1103/PhysRevD.90.065033). arXiv: [1406.2961](https://arxiv.org/abs/1406.2961) [hep-ph].
- [84] Aaron C. Vincent et al. “Revisiting cosmological bounds on sterile neutrinos”. In: *JCAP* 04 (2015), p. 006. DOI: [10.1088/1475-7516/2015/04/006](https://doi.org/10.1088/1475-7516/2015/04/006). arXiv: [1408.1956](https://arxiv.org/abs/1408.1956) [astro-ph.CO].
- [85] X. Shi and G. Sigl. “A Type II supernovae constraint on electron-neutrino - sterile-neutrino mixing”. In: *Phys. Lett. B* 323 (1994). [Erratum: *Phys.Lett.B* 324, 516–516 (1994)], pp. 360–366. DOI: [10.1016/0370-2693\(94\)91232-7](https://doi.org/10.1016/0370-2693(94)91232-7). arXiv: [hep-ph/9312247](https://arxiv.org/abs/hep-ph/9312247).
- [86] Georg G. Raffelt and Shun Zhou. “Supernova bound on keV-mass sterile neutrinos reexamined”. In: *Phys. Rev. D* 83 (2011), p. 093014. DOI: [10.1103/PhysRevD.83.093014](https://doi.org/10.1103/PhysRevD.83.093014). arXiv: [1102.5124](https://arxiv.org/abs/1102.5124) [hep-ph].
- [87] Carlos A. Argüelles, Vedran Brdar, and Joachim Kopp. “Production of keV Sterile Neutrinos in Supernovae: New Constraints and Gamma Ray Observables”. In: *Phys. Rev. D* 99.4 (2019), p. 043012. DOI: [10.1103/PhysRevD.99.043012](https://doi.org/10.1103/PhysRevD.99.043012). arXiv: [1605.00654](https://arxiv.org/abs/1605.00654) [hep-ph].
- [88] Anna M. Suliga, Irene Tamborra, and Meng-Ru Wu. “Tau lepton asymmetry by sterile neutrino emission – Moving beyond one-zone supernova models”. In: *JCAP* 12 (2019), p. 019. DOI: [10.1088/1475-7516/2019/12/019](https://doi.org/10.1088/1475-7516/2019/12/019). arXiv: [1908.11382](https://arxiv.org/abs/1908.11382) [astro-ph.HE].
- [89] Jun Hidaka and George M. Fuller. “Dark matter sterile neutrinos in stellar collapse: Alteration of energy/lepton number transport and a mechanism for supernova explosion enhancement”. In: *Phys. Rev. D* 74 (2006), p. 125015. DOI: [10.1103/PhysRevD.74.125015](https://doi.org/10.1103/PhysRevD.74.125015). arXiv: [astro-ph/0609425](https://arxiv.org/abs/astro-ph/0609425).
- [90] Jun Hidaka and George M. Fuller. “Sterile Neutrino-Enhanced Supernova Explosions”. In: *Phys. Rev. D* 76 (2007), p. 083516. DOI: [10.1103/PhysRevD.76.083516](https://doi.org/10.1103/PhysRevD.76.083516). arXiv: [0706.3886](https://arxiv.org/abs/0706.3886) [astro-ph].
- [91] Alexander Kusenko and Gino Segre. “Pulsar kicks from neutrino oscillations”. In: *Phys. Rev. D* 59 (1999), p. 061302. DOI: [10.1103/PhysRevD.59.061302](https://doi.org/10.1103/PhysRevD.59.061302). arXiv: [astro-ph/9811144](https://arxiv.org/abs/astro-ph/9811144).
- [92] George M. Fuller et al. “Pulsar kicks from a dark-matter sterile neutrino”. In: *Phys. Rev. D* 68 (2003), p. 103002. DOI: [10.1103/PhysRevD.68.103002](https://doi.org/10.1103/PhysRevD.68.103002). arXiv: [astro-ph/0307267](https://arxiv.org/abs/astro-ph/0307267).

- [93] Palash B. Pal and Lincoln Wolfenstein. “Radiative Decays of Massive Neutrinos”. In: *Phys. Rev. D* 25 (1982), p. 766. DOI: [10.1103/PhysRevD.25.766](https://doi.org/10.1103/PhysRevD.25.766).
- [94] Kerstin Perez et al. “Almost closing the ν MSM sterile neutrino dark matter window with NuSTAR”. In: *Phys. Rev. D* 95.12 (2017), p. 123002. DOI: [10.1103/PhysRevD.95.123002](https://doi.org/10.1103/PhysRevD.95.123002). arXiv: [1609.00667](https://arxiv.org/abs/1609.00667) [astro-ph.HE].
- [95] Kenny C. Y. Ng et al. “New Constraints on Sterile Neutrino Dark Matter from NuSTAR M31 Observations”. In: *Phys. Rev. D* 99 (2019), p. 083005. DOI: [10.1103/PhysRevD.99.083005](https://doi.org/10.1103/PhysRevD.99.083005). arXiv: [1901.01262](https://arxiv.org/abs/1901.01262) [astro-ph.HE].
- [96] Julian Heeck and Daniele Teresi. “Cold keV dark matter from decays and scatterings”. In: *Phys. Rev. D* 96.3 (2017), p. 035018. DOI: [10.1103/PhysRevD.96.035018](https://doi.org/10.1103/PhysRevD.96.035018). arXiv: [1706.09909](https://arxiv.org/abs/1706.09909) [hep-ph].
- [97] F. Bezrukov, A. Chudaykin, and D. Gorbunov. “Hiding an elephant: heavy sterile neutrino with large mixing angle does not contradict cosmology”. In: *JCAP* 06 (2017), p. 051. DOI: [10.1088/1475-7516/2017/06/051](https://doi.org/10.1088/1475-7516/2017/06/051). arXiv: [1705.02184](https://arxiv.org/abs/1705.02184) [hep-ph].
- [98] Qi Guo et al. “How do galaxies populate dark matter haloes?” In: *Monthly Notices of the Royal Astronomical Society* (Mar. 2010). DOI: [10.1111/j.1365-2966.2010.16341.x](https://doi.org/10.1111/j.1365-2966.2010.16341.x). URL: <https://doi.org/10.1111%5C%2Fj.1365-2966.2010.16341.x>.
- [99] Wenting Wang et al. “Estimating the dark matter halo mass of our Milky Way using dynamical tracers”. In: *Mon. Not. Roy. Astron. Soc.* 453.1 (2015), pp. 377–400. DOI: [10.1093/mnras/stv1647](https://doi.org/10.1093/mnras/stv1647). arXiv: [1502.03477](https://arxiv.org/abs/1502.03477) [astro-ph.GA].
- [100] Laura L. Watkins et al. “Evidence for an Intermediate-mass Milky Way from Gaia DR2 Halo Globular Cluster Motions”. In: *The Astrophysical Journal* 873.2 (2019), p. 118. DOI: [10.3847/1538-4357/ab089f](https://doi.org/10.3847/1538-4357/ab089f). URL: <https://doi.org/10.3847%5C%2F1538-4357%5C%2Fab089f>.
- [101] John F. Cherry and Shunsaku Horiuchi. “Closing in on Resonantly Produced Sterile Neutrino Dark Matter”. In: *Phys. Rev. D* 95.8 (2017), p. 083015. DOI: [10.1103/PhysRevD.95.083015](https://doi.org/10.1103/PhysRevD.95.083015). arXiv: [1701.07874](https://arxiv.org/abs/1701.07874) [hep-ph].
- [102] P. A. R. Ade et al. “Planck 2015 results. XIII. Cosmological parameters”. In: *Astron. Astrophys.* 594 (2016), A13. DOI: [10.1051/0004-6361/201525830](https://doi.org/10.1051/0004-6361/201525830). arXiv: [1502.01589](https://arxiv.org/abs/1502.01589) [astro-ph.CO].
- [103] A. D. Dolgov and S. H. Hansen. “Massive sterile neutrinos as warm dark matter”. In: *Astropart. Phys.* 16 (2002), pp. 339–344. DOI: [10.1016/S0927-6505\(01\)00115-3](https://doi.org/10.1016/S0927-6505(01)00115-3). arXiv: [hep-ph/0009083](https://arxiv.org/abs/hep-ph/0009083).
- [104] Michela Mapelli and A. Ferrara. “Background radiation from sterile neutrino decay and reionization”. In: *Mon. Not. Roy. Astron. Soc.* 364 (2005), pp. 2–12. DOI: [10.1111/j.1365-2966.2005.09507.x](https://doi.org/10.1111/j.1365-2966.2005.09507.x). arXiv: [astro-ph/0508413](https://arxiv.org/abs/astro-ph/0508413).
- [105] Alexey Boyarsky et al. “Constraints on sterile neutrino as a dark matter candidate from the diffuse x-ray background”. In: *Mon. Not. Roy. Astron. Soc.* 370 (2006), pp. 213–218. DOI: [10.1111/j.1365-2966.2006.10458.x](https://doi.org/10.1111/j.1365-2966.2006.10458.x). arXiv: [astro-ph/0512509](https://arxiv.org/abs/astro-ph/0512509).
- [106] D. E. Gruber et al. “The spectrum of diffuse cosmic hard x-rays measured with heao-1”. In: *Astrophys. J.* 520 (1999), p. 124. DOI: [10.1086/307450](https://doi.org/10.1086/307450). arXiv: [astro-ph/9903492](https://arxiv.org/abs/astro-ph/9903492).
- [107] E. Churazov et al. “INTEGRAL observations of the cosmic X-ray background in the 5-100 keV range via occultation by the Earth”. In: *Astron. Astrophys.* 467 (2007), p. 529. DOI: [10.1051/0004-6361:20066230](https://doi.org/10.1051/0004-6361:20066230). arXiv: [astro-ph/0608250](https://arxiv.org/abs/astro-ph/0608250).

- [108] Joachim Kopp. “Sterile neutrinos as dark matter candidates”. In: *SciPost Phys. Lect. Notes* 36 (2022), p. 1. DOI: [10.21468/SciPostPhysLectNotes.36](https://doi.org/10.21468/SciPostPhysLectNotes.36). arXiv: [2109.00767](https://arxiv.org/abs/2109.00767) [hep-ph].
- [109] Kevork N. Abazajian. “Neutrinos in Astrophysics and Cosmology: Theoretical Advanced Study Institute (TASI) 2020 Lectures”. In: *PoS TASI2020* (2021), p. 001. DOI: [10.22323/1.388.0001](https://doi.org/10.22323/1.388.0001). arXiv: [2102.10183](https://arxiv.org/abs/2102.10183) [hep-ph].
- [110] Esra Bulbul et al. “Detection of An Unidentified Emission Line in the Stacked X-ray spectrum of Galaxy Clusters”. In: *Astrophys. J.* 789 (2014), p. 13. DOI: [10.1088/0004-637X/789/1/13](https://doi.org/10.1088/0004-637X/789/1/13). arXiv: [1402.2301](https://arxiv.org/abs/1402.2301) [astro-ph.CO].
- [111] Alexey Boyarsky et al. “Unidentified Line in X-Ray Spectra of the Andromeda Galaxy and Perseus Galaxy Cluster”. In: *Phys. Rev. Lett.* 113 (2014), p. 251301. DOI: [10.1103/PhysRevLett.113.251301](https://doi.org/10.1103/PhysRevLett.113.251301). arXiv: [1402.4119](https://arxiv.org/abs/1402.4119) [astro-ph.CO].
- [112] Alexey Boyarsky et al. “Checking the Dark Matter Origin of a 3.53 keV Line with the Milky Way Center”. In: *Phys. Rev. Lett.* 115 (2015), p. 161301. DOI: [10.1103/PhysRevLett.115.161301](https://doi.org/10.1103/PhysRevLett.115.161301). arXiv: [1408.2503](https://arxiv.org/abs/1408.2503) [astro-ph.CO].
- [113] Nico Cappelluti et al. “Searching for the 3.5 keV Line in the Deep Fields with Chandra: the 10 Ms observations”. In: *Astrophys. J.* 854.2 (2018), p. 179. DOI: [10.3847/1538-4357/aaaa68](https://doi.org/10.3847/1538-4357/aaaa68). arXiv: [1701.07932](https://arxiv.org/abs/1701.07932) [astro-ph.CO].
- [114] Chintan Shah et al. “Laboratory measurements compellingly support charge-exchange mechanism for the ‘dark matter’ ~ 3.5 keV X-ray line”. In: *Astrophys. J.* 833.1 (2016), p. 52. DOI: [10.3847/1538-4357/833/1/52](https://doi.org/10.3847/1538-4357/833/1/52). arXiv: [1608.04751](https://arxiv.org/abs/1608.04751) [astro-ph.HE].
- [115] Shunsaku Horiuchi et al. “Sterile neutrino dark matter bounds from galaxies of the Local Group”. In: *Phys. Rev. D* 89.2 (2014), p. 025017. DOI: [10.1103/PhysRevD.89.025017](https://doi.org/10.1103/PhysRevD.89.025017). arXiv: [1311.0282](https://arxiv.org/abs/1311.0282) [astro-ph.CO].
- [116] “Science with the X-ray Imaging and Spectroscopy Mission (XRISM)”. In: (Mar. 2020). arXiv: [2003.04962](https://arxiv.org/abs/2003.04962) [astro-ph.HE].
- [117] Kirpal Nandra et al. “The Hot and Energetic Universe: A White Paper presenting the science theme motivating the Athena+ mission”. In: (June 2013). arXiv: [1306.2307](https://arxiv.org/abs/1306.2307) [astro-ph.HE].
- [118] Denys Malyshev et al. “*eXTP* perspectives for the ν MSM sterile neutrino dark matter model”. In: *Phys. Rev. D* 101.12 (2020), p. 123009. DOI: [10.1103/PhysRevD.101.123009](https://doi.org/10.1103/PhysRevD.101.123009). arXiv: [2001.07014](https://arxiv.org/abs/2001.07014) [astro-ph.HE].
- [119] “The Lynx Mission Concept Study Interim Report”. In: (Sept. 2018). arXiv: [1809.09642](https://arxiv.org/abs/1809.09642) [astro-ph.IM].
- [120] Fabio Zandanel, Christoph Weniger, and Shin’ichiro Ando. “The role of the eROSITA all-sky survey in searches for sterile neutrino dark matter”. In: *JCAP* 09 (2015), p. 060. DOI: [10.1088/1475-7516/2015/09/060](https://doi.org/10.1088/1475-7516/2015/09/060). arXiv: [1505.07829](https://arxiv.org/abs/1505.07829) [astro-ph.CO].
- [121] V. V. Barinov et al. “Towards testing sterile neutrino dark matter with the *Spectrum – Roentgen – Gamma* mission”. In: *Phys. Rev. D* 103.6 (2021), p. 063512. DOI: [10.1103/PhysRevD.103.063512](https://doi.org/10.1103/PhysRevD.103.063512). arXiv: [2007.07969](https://arxiv.org/abs/2007.07969) [astro-ph.CO].
- [122] T. Faber et al. “Revisiting neutrino and sneutrino dark matter in natural SUSY scenarios”. In: *Phys. Rev. D* 101.5 (2020), p. 055029. DOI: [10.1103/PhysRevD.101.055029](https://doi.org/10.1103/PhysRevD.101.055029). arXiv: [1909.11686](https://arxiv.org/abs/1909.11686) [hep-ph].
- [123] L. Lavoura. “General formulae for $f(1) \rightarrow f(2) \gamma$ ”. In: *Eur. Phys. J. C* 29 (2003), pp. 191–195. DOI: [10.1140/epjc/s2003-01212-7](https://doi.org/10.1140/epjc/s2003-01212-7). arXiv: [hep-ph/0302221](https://arxiv.org/abs/hep-ph/0302221).

- [124] Giorgio Arcadi, Laura Covi, and Federico Dradi. “3.55 keV line in Minimal Decaying Dark Matter scenarios”. In: *JCAP* 07 (2015), p. 023. DOI: [10.1088/1475-7516/2015/07/023](https://doi.org/10.1088/1475-7516/2015/07/023). arXiv: [1412.6351](https://arxiv.org/abs/1412.6351) [[hep-ph](#)].
- [125] James Barry, Julian Heeck, and Werner Rodejohann. “Sterile neutrinos and right-handed currents in KATRIN”. In: *JHEP* 07 (2014), p. 081. DOI: [10.1007/JHEP07\(2014\)081](https://doi.org/10.1007/JHEP07(2014)081). arXiv: [1404.5955](https://arxiv.org/abs/1404.5955) [[hep-ph](#)].
- [126] Patrick Otto Ludl and Werner Rodejohann. “Direct Neutrino Mass Experiments and Exotic Charged Current Interactions”. In: *JHEP* 06 (2016), p. 040. DOI: [10.1007/JHEP06\(2016\)040](https://doi.org/10.1007/JHEP06(2016)040). arXiv: [1603.08690](https://arxiv.org/abs/1603.08690) [[hep-ph](#)].
- [127] A. Osipowicz et al. “KATRIN: A Next generation tritium beta decay experiment with sub-eV sensitivity for the electron neutrino mass. Letter of intent”. In: (Sept. 2001). arXiv: [hep-ex/0109033](https://arxiv.org/abs/hep-ex/0109033).
- [128] Susanne Mertens et al. “A novel detector system for KATRIN to search for keV-scale sterile neutrinos”. In: *J. Phys. G* 46.6 (2019), p. 065203. DOI: [10.1088/1361-6471/ab12fe](https://doi.org/10.1088/1361-6471/ab12fe). arXiv: [1810.06711](https://arxiv.org/abs/1810.06711) [[physics.ins-det](#)].
- [129] Ch. Kraus et al. “Final results from phase II of the Mainz neutrino mass search in tritium beta decay”. In: *Eur. Phys. J. C* 40 (2005), pp. 447–468. DOI: [10.1140/epjc/s2005-02139-7](https://doi.org/10.1140/epjc/s2005-02139-7). arXiv: [hep-ex/0412056](https://arxiv.org/abs/hep-ex/0412056).
- [130] V. N. Aseev et al. “An upper limit on electron antineutrino mass from Troitsk experiment”. In: *Phys. Rev. D* 84 (2011), p. 112003. DOI: [10.1103/PhysRevD.84.112003](https://doi.org/10.1103/PhysRevD.84.112003). arXiv: [1108.5034](https://arxiv.org/abs/1108.5034) [[hep-ex](#)].
- [131] M. Aker et al. “Direct neutrino-mass measurement with sub-electronvolt sensitivity”. In: *Nature Phys.* 18.2 (2022), pp. 160–166. DOI: [10.1038/s41567-021-01463-1](https://doi.org/10.1038/s41567-021-01463-1). arXiv: [2105.08533](https://arxiv.org/abs/2105.08533) [[hep-ex](#)].
- [132] M. Aker et al. “KATRIN: Status and Prospects for the Neutrino Mass and Beyond”. In: (Mar. 2022). arXiv: [2203.08059](https://arxiv.org/abs/2203.08059) [[nucl-ex](#)].
- [133] M. et al. Aker. “The design, construction, and commissioning of the KATRIN experiment”. In: *JINST* 16.08 (2021), T08015. DOI: [10.1088/1748-0221/16/08/T08015](https://doi.org/10.1088/1748-0221/16/08/T08015). arXiv: [2103.04755](https://arxiv.org/abs/2103.04755) [[physics.ins-det](#)].
- [134] S. Mertens et al. “Sensitivity of Next-Generation Tritium Beta-Decay Experiments for keV-Scale Sterile Neutrinos”. In: *JCAP* 02 (2015), p. 020. DOI: [10.1088/1475-7516/2015/02/020](https://doi.org/10.1088/1475-7516/2015/02/020). arXiv: [1409.0920](https://arxiv.org/abs/1409.0920) [[physics.ins-det](#)].
- [135] Marc Korzeczek. “Sterile neutrino search with KATRIN - modeling and design-criteria of a novel detector system”. PhD thesis. Karlsruher Institut für Technologie (KIT), 2020. DOI: [10.5445/IR/1000120634](https://doi.org/10.5445/IR/1000120634).
- [136] Anton Huber. “Analysis of first KATRIN data and searches for keV-scale sterile neutrinos”. PhD thesis. Karlsruher Institut für Technologie (KIT), 2020. DOI: [10.5445/IR/1000128344](https://doi.org/10.5445/IR/1000128344).
- [137] M. Aker et al. “Search for keV-scale Sterile Neutrinos with first KATRIN Data”. In: (July 2022). arXiv: [2207.06337](https://arxiv.org/abs/2207.06337) [[nucl-ex](#)].
- [138] Christine Kraus et al. “Limit on sterile neutrino contribution from the Mainz Neutrino Mass Experiment”. In: *Eur. Phys. J. C* 73.2 (2013), p. 2323. DOI: [10.1140/epjc/s10052-013-2323-z](https://doi.org/10.1140/epjc/s10052-013-2323-z). arXiv: [1210.4194](https://arxiv.org/abs/1210.4194) [[hep-ex](#)].
- [139] K. H. Hiddemann, H. Daniel, and O. Schwentker. “Limits on neutrino masses from the tritium beta spectrum”. In: *J. Phys. G* 21 (1995), pp. 639–650. DOI: [10.1088/0954-3899/21/5/008](https://doi.org/10.1088/0954-3899/21/5/008).

- [140] E. Holzschuh et al. “Search for heavy neutrinos in the beta spectrum of Ni-63”. In: *Phys. Lett. B* 451 (1999), pp. 247–255. DOI: [10.1016/S0370-2693\(99\)00200-2](https://doi.org/10.1016/S0370-2693(99)00200-2).
- [141] J. N. Abdurashitov et al. “First measurements in search for keV-sterile neutrino in tritium beta-decay by Troitsk nu-mass experiment”. In: *Pisma Zh. Eksp. Teor. Fiz.* 105.12 (2017), pp. 723–724. DOI: [10.1134/S0021364017120013](https://doi.org/10.1134/S0021364017120013). arXiv: [1703.10779](https://arxiv.org/abs/1703.10779) [hep-ex].
- [142] Benjamin Monreal and Joseph A. Formaggio. “Relativistic Cyclotron Radiation Detection of Tritium Decay Electrons as a New Technique for Measuring the Neutrino Mass”. In: *Phys. Rev. D* 80 (2009), p. 051301. DOI: [10.1103/PhysRevD.80.051301](https://doi.org/10.1103/PhysRevD.80.051301). arXiv: [0904.2860](https://arxiv.org/abs/0904.2860) [nucl-ex].
- [143] D. M. Asner et al. “Single electron detection and spectroscopy via relativistic cyclotron radiation”. In: *Phys. Rev. Lett.* 114.16 (2015), p. 162501. DOI: [10.1103/PhysRevLett.114.162501](https://doi.org/10.1103/PhysRevLett.114.162501). arXiv: [1408.5362](https://arxiv.org/abs/1408.5362) [physics.ins-det].
- [144] S. Betts et al. “Development of a Relic Neutrino Detection Experiment at PTOLEMY: Princeton Tritium Observatory for Light, Early-Universe, Massive-Neutrino Yield”. In: *Community Summer Study 2013: Snowmass on the Mississippi*. July 2013. arXiv: [1307.4738](https://arxiv.org/abs/1307.4738) [astro-ph.IM].
- [145] M. G. Betti et al. “Neutrino physics with the PTOLEMY project: active neutrino properties and the light sterile case”. In: *JCAP* 07 (2019), p. 047. DOI: [10.1088/1475-7516/2019/07/047](https://doi.org/10.1088/1475-7516/2019/07/047). arXiv: [1902.05508](https://arxiv.org/abs/1902.05508) [astro-ph.CO].
- [146] L. Gastaldo et al. “The electron capture in ^{163}Ho experiment – ECHO”. In: *Eur. Phys. J. ST* 226.8 (2017), pp. 1623–1694. DOI: [10.1140/epjst/e2017-70071-y](https://doi.org/10.1140/epjst/e2017-70071-y).
- [147] S. Eliseev et al. “Direct Measurement of the Mass Difference of ^{163}Ho and ^{163}Dy Solves the Q-Value Puzzle for the Neutrino Mass Determination”. In: *Phys. Rev. Lett.* 115.6 (2015), p. 062501. DOI: [10.1103/PhysRevLett.115.062501](https://doi.org/10.1103/PhysRevLett.115.062501). arXiv: [1604.04210](https://arxiv.org/abs/1604.04210) [physics.ins-det].
- [148] Joachim Kopp and Alexander Merle. “Ultra-low Q values for neutrino mass measurements”. In: *Phys. Rev. C* 81 (2010), p. 045501. DOI: [10.1103/PhysRevC.81.045501](https://doi.org/10.1103/PhysRevC.81.045501). arXiv: [0911.3329](https://arxiv.org/abs/0911.3329) [hep-ph].
- [149] M. Braß et al. “Ab initio calculation of the calorimetric electron capture spectrum of $^{163}\text{Holmium}$: Intra-atomic decay into bound-states”. In: *Phys. Rev. C* 97.5 (2018), p. 054620. DOI: [10.1103/PhysRevC.97.054620](https://doi.org/10.1103/PhysRevC.97.054620). arXiv: [1711.10309](https://arxiv.org/abs/1711.10309) [physics.atom-ph].
- [150] M. Braß and M. W. Haverkort. “Abinitio calculation of the electron capture spectrum of ^{163}Ho : Auger–Meitner decay into continuum states”. In: *New J. Phys.* 22.9 (2020), p. 093018. DOI: [10.1088/1367-2630/abac72](https://doi.org/10.1088/1367-2630/abac72). arXiv: [2002.05989](https://arxiv.org/abs/2002.05989) [nucl-th].
- [151] Martin Braß. “Ab initio calculations of the electron capture spectrum in ^{163}Ho .” PhD thesis. U. Heidelberg (main), 2021. DOI: [10.11588/heidok.00029305](https://doi.org/10.11588/heidok.00029305).
- [152] P. C. -O. Ranitzsch et al. “First Calorimetric Measurement of OI-line in the Electron Capture Spectrum of ^{163}Ho ”. In: (Aug. 2014). arXiv: [1409.0071](https://arxiv.org/abs/1409.0071) [physics.ins-det].
- [153] F. Gatti et al. “Calorimetric measurement of the ^{163}Ho spectrum by means of a cryogenic detector”. In: *Physics Letters B* 398.3 (1997), pp. 415–419. DOI: [10.1016/S0370-2693\(97\)00239-6](https://doi.org/10.1016/S0370-2693(97)00239-6).
- [154] M. Wang et al. “The Ame2012 atomic mass evaluation”. In: *Chinese Physics C* 36.12 (2012), pp. 1603–2014. DOI: [10.1088/1674-1137/36/12/003](https://doi.org/10.1088/1674-1137/36/12/003).

- [155] J. Repp et al. “PENTATRAP: A Novel cryogenic multi-Penning trap experiment for high-precision mass measurements on highly charged ions”. In: (Oct. 2011). DOI: [10.1007/s00340-011-4823-6](https://doi.org/10.1007/s00340-011-4823-6). arXiv: [1110.2919](https://arxiv.org/abs/1110.2919) [physics.atom-ph].
- [156] C. Roux et al. “The trap design of PENTATRAP”. In: (Oct. 2011). DOI: [10.1007/s00340-011-4825-4](https://doi.org/10.1007/s00340-011-4825-4). arXiv: [1110.2920](https://arxiv.org/abs/1110.2920) [physics.atom-ph].
- [157] Clemens Velte. “Measurement of a high energy resolution and high statistics ^{163}Ho electron capture spectrum for the ECHO experiment”. PhD thesis. Heidelberg University, 2020. DOI: [10.11588/heidok.00027340](https://doi.org/10.11588/heidok.00027340).
- [158] Federica Mantegazzini. “Development and characterisation of high-resolution metallic magnetic calorimeter arrays for the ECHO neutrino mass experiment”. PhD thesis. Heidelberg University, 2022. DOI: [10.11588/heidok.00030250](https://doi.org/10.11588/heidok.00030250).
- [159] Steve Cook et al. “A Proposal to isolate the origin of the 17-keV kink in the Beta spectrum”. In: *Phys. Rev. D* 46 (1992), pp. 6–8. DOI: [10.1103/PhysRevD.46.R6](https://doi.org/10.1103/PhysRevD.46.R6).
- [160] Guido Finocchiaro and Robert E. Shrock. “An Experiment to search for a massive admixed neutrino in nuclear beta decay by complete kinematic reconstruction of the final state”. In: *Phys. Rev. D* 46 (1992), R888–R891. DOI: [10.1103/PhysRevD.46.R888](https://doi.org/10.1103/PhysRevD.46.R888).
- [161] M. M. Hindi et al. “Search for the admixture of heavy neutrinos in the recoil spectra of Ar-37 decay”. In: *Phys. Rev. C* 58 (1998), pp. 2512–2525. DOI: [10.1103/PhysRevC.58.2512](https://doi.org/10.1103/PhysRevC.58.2512).
- [162] M. Trinczek et al. “Novel Search for Heavy ν Mixing from the β^+ Decay of ^{32}Mg Confined in an Atom Trap”. In: *Phys. Rev. Lett.* 90 (2003), p. 012501. DOI: [10.1103/PhysRevLett.90.012501](https://doi.org/10.1103/PhysRevLett.90.012501).
- [163] F. L. Bezrukov. “nuMSM and its experimental tests”. In: *J. Phys. Conf. Ser.* 110 (2008). Ed. by Roger Barlow, p. 082002. DOI: [10.1088/1742-6596/110/8/082002](https://doi.org/10.1088/1742-6596/110/8/082002). arXiv: [0710.2501](https://arxiv.org/abs/0710.2501) [hep-ph].
- [164] Peter F Smith. “Proposed experiments to detect keV range sterile neutrinos using energy-momentum reconstruction of beta decay or K-capture events”. In: *New J. Phys.* 21.5 (2019), p. 053022. DOI: [10.1088/1367-2630/ab1502](https://doi.org/10.1088/1367-2630/ab1502). arXiv: [1607.06876](https://arxiv.org/abs/1607.06876) [physics.ins-det].
- [165] C. J. Martoff et al. “HUNTER: precision massive-neutrino search based on a laser cooled atomic source”. In: *Quantum Sci. Technol.* 6.2 (2021), p. 024008. DOI: [10.1088/2058-9565/abdb9b](https://doi.org/10.1088/2058-9565/abdb9b).
- [166] Francesco Granato. “Design of the electron spectrometer for the HUNTER experiment and timescale of electron thermalization in liquid Argon for directional detection of WIMP dark matter”. PhD thesis. Temple U., 2021.
- [167] R. E. Shrock. “New Tests For, and Bounds On, Neutrino Masses and Lepton Mixing”. In: *Phys. Lett. B* 96 (1980), pp. 159–164. DOI: [10.1016/0370-2693\(80\)90235-X](https://doi.org/10.1016/0370-2693(80)90235-X).
- [168] J. G. V. Taylor and Janet S. Merritt. “Branching ratio in the decay of Be^7 ”. In: *Canadian Journal of Physics* 40.7 (1962), pp. 926–929. DOI: [10.1139/p62-098](https://doi.org/10.1139/p62-098).
- [169] Geon-Bo Kim. “The First Result on the BeEST keV-scale Sterile Neutrino Search”. APS April Meeting 2021. 2021. URL: https://beest.mines.edu/wp-content/uploads/sites/345/2021/04/Kim_APS2021Apr_v2.pdf.
- [170] S. Fretwell et al. “Direct Measurement of the ^7Be L/K Capture Ratio in Ta-Based Superconducting Tunnel Junctions”. In: *Phys. Rev. Lett.* 125.3 (2020), p. 032701. DOI: [10.1103/PhysRevLett.125.032701](https://doi.org/10.1103/PhysRevLett.125.032701). arXiv: [2003.04921](https://arxiv.org/abs/2003.04921) [nucl-ex].

- [171] Kyle Leach. “The BeEST Experiment: A Search for keV-Scale Neutrinos in the EC Decay of ${}^7\text{Be}$ with Superconducting Quantum Sensors”. 2020 Meeting of the APS Division of Nuclear Physics. 2020. URL: https://beest.mines.edu/wp-content/uploads/sites/345/2020/11/20201030_DNP2020_BeEST.pdf.
- [172] K. G. Leach and S. Friedrich. “The BeEST Experiment: Searching for Beyond Standard Model Neutrinos using ${}^7\text{Be}$ Decay in STJs”. In: *19th International Workshop on Low Temperature Detectors*. Dec. 2021. arXiv: 2112.02029 [nucl-ex].
- [173] S. Friedrich et al. “Limits on the Existence of sub-MeV Sterile Neutrinos from the Decay of ${}^7\text{Be}$ in Superconducting Quantum Sensors”. In: *Phys. Rev. Lett.* 126.2 (2021), p. 021803. DOI: 10.1103/PhysRevLett.126.021803. arXiv: 2010.09603 [nucl-ex].
- [174] M. A. Acero et al. “White Paper on Light Sterile Neutrino Searches and Related Phenomenology”. In: (Mar. 2022). arXiv: 2203.07323 [hep-ex].
- [175] V. Mukhanov. *Physical Foundations of Cosmology*. Oxford: Cambridge University Press, 2005. ISBN: 978-0-521-56398-7. DOI: 10.1017/CB09780511790553.
- [176] Steen Hannestad. “What is the lowest possible reheating temperature?” In: *Phys. Rev. D* 70 (2004), p. 043506. DOI: 10.1103/PhysRevD.70.043506. arXiv: astro-ph/0403291.
- [177] K. Blaum et al. “The Electron Capture ${}^{163}\text{Ho}$ Experiment ECHO”. In: *The Future of Neutrino Mass Measurements: Terrestrial, Astrophysical, and Cosmological Measurements in the Next Decade*. June 2013. arXiv: 1306.2655 [physics.ins-det].
- [178] Graciela B. Gelmini, Philip Lu, and Volodymyr Takhistov. “Cosmological Dependence of Non-resonantly Produced Sterile Neutrinos”. In: *JCAP* 12 (2019), p. 047. DOI: 10.1088/1475-7516/2019/12/047. arXiv: 1909.13328 [hep-ph].
- [179] Graciela B. Gelmini, Philip Lu, and Volodymyr Takhistov. “Visible Sterile Neutrinos as the Earliest Relic Probes of Cosmology”. In: *Phys. Lett. B* 800 (2020), p. 135113. DOI: 10.1016/j.physletb.2019.135113. arXiv: 1909.04168 [hep-ph].
- [180] Tejaswi Venumadhav et al. “Sterile neutrino dark matter: Weak interactions in the strong coupling epoch”. In: *Phys. Rev. D* 94.4 (2016), p. 043515. DOI: 10.1103/PhysRevD.94.043515. arXiv: 1507.06655 [astro-ph.CO].
- [181] Gabriela Barenboim, Christoph Andreas Ternes, and Mariam Tórtola. “Neutrinos, DUNE and the world best bound on CPT invariance”. In: *Phys. Lett. B* 780 (2018), pp. 631–637. DOI: 10.1016/j.physletb.2018.03.060. arXiv: 1712.01714 [hep-ph].
- [182] V. Barger, D. Marfatia, and K. Whisnant. “LSND anomaly from CPT violation in four neutrino models”. In: *Phys. Lett. B* 576 (2003), pp. 303–308. DOI: 10.1016/j.physletb.2003.10.004. arXiv: hep-ph/0308299.
- [183] Francisco Javier Escrihuela Ferrándiz. “Phenomenology of non-standard neutrino interactions”. PhD thesis. U. Valencia (main), 2016.
- [184] Tommy Ohlsson. “Status of non-standard neutrino interactions”. In: *Rept. Prog. Phys.* 76 (2013), p. 044201. DOI: 10.1088/0034-4885/76/4/044201. arXiv: 1209.2710 [hep-ph].
- [185] Raymond Davis Jr., Don S. Harmer, and Kenneth C. Hoffman. “Search for neutrinos from the sun”. In: *Phys. Rev. Lett.* 20 (1968), pp. 1205–1209. DOI: 10.1103/PhysRevLett.20.1205.

- [186] Y. Farzan and M. Tortola. “Neutrino oscillations and Non-Standard Interactions”. In: *Front. in Phys.* 6 (2018), p. 10. DOI: [10.3389/fphy.2018.00010](https://doi.org/10.3389/fphy.2018.00010). arXiv: [1710.09360](https://arxiv.org/abs/1710.09360) [hep-ph].
- [187] S. Schael et al. “Precision electroweak measurements on the Z resonance”. In: *Phys. Rept.* 427 (2006), pp. 257–454. DOI: [10.1016/j.physrep.2005.12.006](https://doi.org/10.1016/j.physrep.2005.12.006). arXiv: [hep-ex/0509008](https://arxiv.org/abs/hep-ex/0509008).
- [188] Jeffrey M. Berryman et al. “Neutrino Self-Interactions: A White Paper”. In: *2022 Snowmass Summer Study*. Mar. 2022. arXiv: [2203.01955](https://arxiv.org/abs/2203.01955) [hep-ph].
- [189] G. B. Gelmini and M. Roncadelli. “Left-Handed Neutrino Mass Scale and Spontaneously Broken Lepton Number”. In: *Phys. Lett. B* 99 (1981), pp. 411–415. DOI: [10.1016/0370-2693\(81\)90559-1](https://doi.org/10.1016/0370-2693(81)90559-1).
- [190] Y. Chikashige, Rabindra N. Mohapatra, and R. D. Peccei. “Are There Real Goldstone Bosons Associated with Broken Lepton Number?” In: *Phys. Lett. B* 98 (1981), pp. 265–268. DOI: [10.1016/0370-2693\(81\)90011-3](https://doi.org/10.1016/0370-2693(81)90011-3).
- [191] C. S. Aulakh and Rabindra N. Mohapatra. “Neutrino as the Supersymmetric Partner of the Majoron”. In: *Phys. Lett. B* 119 (1982), pp. 136–140. DOI: [10.1016/0370-2693\(82\)90262-3](https://doi.org/10.1016/0370-2693(82)90262-3).
- [192] André De Gouvêa et al. “Dodelson-Widrow Mechanism in the Presence of Self-Interacting Neutrinos”. In: *Phys. Rev. Lett.* 124.8 (2020), p. 081802. DOI: [10.1103/PhysRevLett.124.081802](https://doi.org/10.1103/PhysRevLett.124.081802). arXiv: [1910.04901](https://arxiv.org/abs/1910.04901) [hep-ph].
- [193] Kevin J. Kelly et al. “Origin of sterile neutrino dark matter via secret neutrino interactions with vector bosons”. In: *Phys. Rev. D* 101.11 (2020), p. 115031. DOI: [10.1103/PhysRevD.101.115031](https://doi.org/10.1103/PhysRevD.101.115031). arXiv: [2005.03681](https://arxiv.org/abs/2005.03681) [hep-ph].
- [194] Carlos Chichiri et al. “Cosmological Dependence of Sterile Neutrino Dark Matter With Self-Interacting Neutrinos”. In: (Nov. 2021). arXiv: [2111.04087](https://arxiv.org/abs/2111.04087) [hep-ph].
- [195] Lachlan Lancaster et al. “A tale of two modes: Neutrino free-streaming in the early universe”. In: *JCAP* 07 (2017), p. 033. DOI: [10.1088/1475-7516/2017/07/033](https://doi.org/10.1088/1475-7516/2017/07/033). arXiv: [1704.06657](https://arxiv.org/abs/1704.06657) [astro-ph.CO].
- [196] Christina D. Kreisch, Francis-Yan Cyr-Racine, and Olivier Doré. “Neutrino puzzle: Anomalies, interactions, and cosmological tensions”. In: *Phys. Rev. D* 101.12 (2020), p. 123505. DOI: [10.1103/PhysRevD.101.123505](https://doi.org/10.1103/PhysRevD.101.123505). arXiv: [1902.00534](https://arxiv.org/abs/1902.00534) [astro-ph.CO].
- [197] Shouvik Roy Choudhury, Steen Hannestad, and Thomas Tram. “Updated constraints on massive neutrino self-interactions from cosmology in light of the H_0 tension”. In: *JCAP* 03 (2021), p. 084. DOI: [10.1088/1475-7516/2021/03/084](https://doi.org/10.1088/1475-7516/2021/03/084). arXiv: [2012.07519](https://arxiv.org/abs/2012.07519) [astro-ph.CO].
- [198] Anirban Das and Subhjit Ghosh. “Flavor-specific interaction favors strong neutrino self-coupling in the early universe”. In: *JCAP* 07 (2021), p. 038. DOI: [10.1088/1475-7516/2021/07/038](https://doi.org/10.1088/1475-7516/2021/07/038). arXiv: [2011.12315](https://arxiv.org/abs/2011.12315) [astro-ph.CO].
- [199] Miguel Escudero et al. “Cosmology with A Very Light $L_\mu - L_\tau$ Gauge Boson”. In: *JHEP* 03 (2019), p. 071. DOI: [10.1007/JHEP03\(2019\)071](https://doi.org/10.1007/JHEP03(2019)071). arXiv: [1901.02010](https://arxiv.org/abs/1901.02010) [hep-ph].
- [200] Ian Holst, Dan Hooper, and Gordan Krnjaic. “Simplest and Most Predictive Model of Muon g-2 and Thermal Dark Matter”. In: *Phys. Rev. Lett.* 128.14 (2022), p. 141802. DOI: [10.1103/PhysRevLett.128.141802](https://doi.org/10.1103/PhysRevLett.128.141802). arXiv: [2107.09067](https://arxiv.org/abs/2107.09067) [hep-ph].

- [201] Rodolfo Capdevilla et al. “Systematically testing singlet models for $(g - 2)_\mu$ ”. In: *JHEP* 04 (2022), p. 129. DOI: [10.1007/JHEP04\(2022\)129](https://doi.org/10.1007/JHEP04(2022)129). arXiv: [2112.08377](https://arxiv.org/abs/2112.08377) [hep-ph].
- [202] *Neutrino Non-Standard Interactions: A Status Report*. Vol. 2. 2019, p. 001. DOI: [10.21468/SciPostPhysProc.2.001](https://doi.org/10.21468/SciPostPhysProc.2.001). arXiv: [1907.00991](https://arxiv.org/abs/1907.00991) [hep-ph].
- [203] Edward W. Kolb and Michael S. Turner. “Supernova SN 1987a and the Secret Interactions of Neutrinos”. In: *Phys. Rev. D* 36 (1987), p. 2895. DOI: [10.1103/PhysRevD.36.2895](https://doi.org/10.1103/PhysRevD.36.2895).
- [204] Anirban Das, Amol Dighe, and Manibrata Sen. “New effects of non-standard self-interactions of neutrinos in a supernova”. In: *JCAP* 05 (2017), p. 051. DOI: [10.1088/1475-7516/2017/05/051](https://doi.org/10.1088/1475-7516/2017/05/051). arXiv: [1705.00468](https://arxiv.org/abs/1705.00468) [hep-ph].
- [205] Amol Dighe and Manibrata Sen. “Nonstandard neutrino self-interactions in a supernova and fast flavor conversions”. In: *Phys. Rev. D* 97.4 (2018), p. 043011. DOI: [10.1103/PhysRevD.97.043011](https://doi.org/10.1103/PhysRevD.97.043011). arXiv: [1709.06858](https://arxiv.org/abs/1709.06858) [hep-ph].
- [206] Minjie Lei, Noah Steinberg, and James D. Wells. “Probing Non-Standard Neutrino Interactions with Supernova Neutrinos at Hyper-K”. In: *JHEP* 01 (2020), p. 179. DOI: [10.1007/JHEP01\(2020\)179](https://doi.org/10.1007/JHEP01(2020)179). arXiv: [1907.01059](https://arxiv.org/abs/1907.01059) [hep-ph].
- [207] Shashank Shalgar, Irene Tamborra, and Mauricio Bustamante. “Core-collapse supernovae stymie secret neutrino interactions”. In: *Phys. Rev. D* 103.12 (2021), p. 123008. DOI: [10.1103/PhysRevD.103.123008](https://doi.org/10.1103/PhysRevD.103.123008). arXiv: [1912.09115](https://arxiv.org/abs/1912.09115) [astro-ph.HE].
- [208] Kenny C. Y. Ng and John F. Beacom. “Cosmic neutrino cascades from secret neutrino interactions”. In: *Phys. Rev. D* 90.6 (2014). [Erratum: *Phys.Rev.D* 90, 089904 (2014)], p. 065035. DOI: [10.1103/PhysRevD.90.065035](https://doi.org/10.1103/PhysRevD.90.065035). arXiv: [1404.2288](https://arxiv.org/abs/1404.2288) [astro-ph.HE].
- [209] Ian M. Shoemaker and Kohta Murase. “Probing BSM Neutrino Physics with Flavor and Spectral Distortions: Prospects for Future High-Energy Neutrino Telescopes”. In: *Phys. Rev. D* 93.8 (2016), p. 085004. DOI: [10.1103/PhysRevD.93.085004](https://doi.org/10.1103/PhysRevD.93.085004). arXiv: [1512.07228](https://arxiv.org/abs/1512.07228) [astro-ph.HE].
- [210] Kunihto Ioka and Kohta Murase. “IceCube PeV–EeV neutrinos and secret interactions of neutrinos”. In: *PTEP* 2014.6 (2014), 061E01. DOI: [10.1093/ptep/ptu090](https://doi.org/10.1093/ptep/ptu090). arXiv: [1404.2279](https://arxiv.org/abs/1404.2279) [astro-ph.HE].
- [211] Mauricio Bustamante et al. “Bounds on secret neutrino interactions from high-energy astrophysical neutrinos”. In: *Phys. Rev. D* 101.12 (2020), p. 123024. DOI: [10.1103/PhysRevD.101.123024](https://doi.org/10.1103/PhysRevD.101.123024). arXiv: [2001.04994](https://arxiv.org/abs/2001.04994) [astro-ph.HE].
- [212] Kevin J. Kelly and Pedro A. N. Machado. “Multimessenger Astronomy and New Neutrino Physics”. In: *JCAP* 10 (2018), p. 048. DOI: [10.1088/1475-7516/2018/10/048](https://doi.org/10.1088/1475-7516/2018/10/048). arXiv: [1808.02889](https://arxiv.org/abs/1808.02889) [hep-ph].
- [213] Maria Archidiacono and Steen Hannestad. “Updated constraints on non-standard neutrino interactions from Planck”. In: *JCAP* 07 (2014), p. 046. DOI: [10.1088/1475-7516/2014/07/046](https://doi.org/10.1088/1475-7516/2014/07/046). arXiv: [1311.3873](https://arxiv.org/abs/1311.3873) [astro-ph.CO].
- [214] Francesco Forastieri et al. “Cosmic microwave background constraints on secret interactions among sterile neutrinos”. In: *JCAP* 07 (2017), p. 038. DOI: [10.1088/1475-7516/2017/07/038](https://doi.org/10.1088/1475-7516/2017/07/038). arXiv: [1704.00626](https://arxiv.org/abs/1704.00626) [astro-ph.CO].
- [215] Guo-yuan Huang, Tommy Ohlsson, and Shun Zhou. “Observational Constraints on Secret Neutrino Interactions from Big Bang Nucleosynthesis”. In: *Phys. Rev. D* 97.7 (2018), p. 075009. DOI: [10.1103/PhysRevD.97.075009](https://doi.org/10.1103/PhysRevD.97.075009). arXiv: [1712.04792](https://arxiv.org/abs/1712.04792) [hep-ph].

- [216] Pouya Bakhti and Yasaman Farzan. “Constraining secret gauge interactions of neutrinos by meson decays”. In: *Phys. Rev. D* 95.9 (2017), p. 095008. DOI: [10.1103/PhysRevD.95.095008](https://doi.org/10.1103/PhysRevD.95.095008). arXiv: [1702.04187](https://arxiv.org/abs/1702.04187) [hep-ph].
- [217] Frank F. Deppisch et al. “Neutrino Self-Interactions and Double Beta Decay”. In: *Phys. Rev. D* 102.5 (2020), p. 051701. DOI: [10.1103/PhysRevD.102.051701](https://doi.org/10.1103/PhysRevD.102.051701). arXiv: [2004.11919](https://arxiv.org/abs/2004.11919) [hep-ph].
- [218] Mikhail S. Bilenky, Samoil M. Bilenky, and A. Santamaria. “Invisible width of the Z boson and ‘secret’ neutrino-neutrino interactions”. In: *Phys. Lett. B* 301 (1993), pp. 287–291. DOI: [10.1016/0370-2693\(93\)90703-K](https://doi.org/10.1016/0370-2693(93)90703-K).
- [219] Mikhail S. Bilenky and Arcadi Santamaria. “‘Secret’ neutrino interactions”. In: *Neutrino Mixing: Meeting in Honor of Samoil Bilenky’s 70th Birthday*. Aug. 1999, pp. 50–61. arXiv: [hep-ph/9908272](https://arxiv.org/abs/hep-ph/9908272).
- [220] Vedran Brdar et al. “Revisiting neutrino self-interaction constraints from Z and τ decays”. In: *Phys. Rev. D* 101.11 (2020), p. 115001. DOI: [10.1103/PhysRevD.101.115001](https://doi.org/10.1103/PhysRevD.101.115001). arXiv: [2003.05339](https://arxiv.org/abs/2003.05339) [hep-ph].
- [221] M. Paraskevas. “Dirac and Majorana Feynman Rules with four-fermions”. In: (Feb. 2018). arXiv: [1802.02657](https://arxiv.org/abs/1802.02657) [hep-ph].
- [222] Palash B. Pal. “Dirac, Majorana and Weyl fermions”. In: *Am. J. Phys.* 79 (2011), pp. 485–498. DOI: [10.1119/1.3549729](https://doi.org/10.1119/1.3549729). arXiv: [1006.1718](https://arxiv.org/abs/1006.1718) [hep-ph].
- [223] Ansgar Denner et al. “Feynman rules for fermion number violating interactions”. In: *Nucl. Phys. B* 387 (1992), pp. 467–481. DOI: [10.1016/0550-3213\(92\)90169-C](https://doi.org/10.1016/0550-3213(92)90169-C).
- [224] R. Mertig, M. Bohm, and Ansgar Denner. “FEYN CALC: Computer algebraic calculation of Feynman amplitudes”. In: *Comput. Phys. Commun.* 64 (1991), pp. 345–359. DOI: [10.1016/0010-4655\(91\)90130-D](https://doi.org/10.1016/0010-4655(91)90130-D).
- [225] Vladyslav Shtabovenko, Rolf Mertig, and Frederik Orellana. “New Developments in FeynCalc 9.0”. In: *Comput. Phys. Commun.* 207 (2016), pp. 432–444. DOI: [10.1016/j.cpc.2016.06.008](https://doi.org/10.1016/j.cpc.2016.06.008). arXiv: [1601.01167](https://arxiv.org/abs/1601.01167) [hep-ph].
- [226] Vladyslav Shtabovenko, Rolf Mertig, and Frederik Orellana. “FeynCalc 9.3: New features and improvements”. In: *Comput. Phys. Commun.* 256 (2020), p. 107478. DOI: [10.1016/j.cpc.2020.107478](https://doi.org/10.1016/j.cpc.2020.107478). arXiv: [2001.04407](https://arxiv.org/abs/2001.04407) [hep-ph].
- [227] Juan Carlos D’Olivo, Jose F. Nieves, and Manuel Torres. “Finite temperature corrections to the effective potential of neutrinos in a medium”. In: *Phys. Rev. D* 46 (1992), pp. 1172–1179. DOI: [10.1103/PhysRevD.46.1172](https://doi.org/10.1103/PhysRevD.46.1172).
- [228] Alexey Boyarsky et al. “Lyman-alpha constraints on warm and on warm-plus-cold dark matter models”. In: *JCAP* 05 (2009), p. 012. DOI: [10.1088/1475-7516/2009/05/012](https://doi.org/10.1088/1475-7516/2009/05/012). arXiv: [0812.0010](https://arxiv.org/abs/0812.0010) [astro-ph].
- [229] Lucas Johns and George M. Fuller. “Self-interacting sterile neutrino dark matter: the heavy-mediator case”. In: *Phys. Rev. D* 100.2 (2019), p. 023533. DOI: [10.1103/PhysRevD.100.023533](https://doi.org/10.1103/PhysRevD.100.023533). arXiv: [1903.08296](https://arxiv.org/abs/1903.08296) [hep-ph].
- [230] Sho Iwamoto, Károly Sella, and Zoltán Trócsányi. “Sterile neutrino dark matter in a U(1) extension of the standard model”. In: *JCAP* 01.01 (2022), p. 035. DOI: [10.1088/1475-7516/2022/01/035](https://doi.org/10.1088/1475-7516/2022/01/035). arXiv: [2104.11248](https://arxiv.org/abs/2104.11248) [hep-ph].
- [231] Ioana A. Zelko et al. “Constraints on sterile neutrino models from strong gravitational lensing, Milky Way satellites, and Lyman- α forest”. In: (May 2022). arXiv: [2205.09777](https://arxiv.org/abs/2205.09777) [hep-ph].
- [232] David Griffiths. *Introduction to elementary particles*. 2008. ISBN: 978-3-527-40601-2.

- [233] Dirk Notzold and Georg Raffelt. "Neutrino Dispersion at Finite Temperature and Density". In: *Nucl. Phys. B* 307 (1988), pp. 924–936. DOI: [10.1016/0550-3213\(88\)90113-7](https://doi.org/10.1016/0550-3213(88)90113-7).